City Research Online

City St George's, University of London

Citation: Agnew, B. (1981). A theoretical and experimental investigation of the combustion process in a spark ignition internal combustion engine. (Unpublished Doctoral thesis, The City University)

This is the accepted version of the paper.

This version of the publication may differ from the final published version. To cite this item please consult the publisher's version.

Permanent repository link: https://openaccess.city.ac.uk/id/eprint/34306/

Copyright and Reuse: Copyright and Moral Rights remain with the author(s) and/or copyright holders. Copies of full items can be used for personal research or study, educational, or not-for-profit purposes without prior permission or charge, unless otherwise indicated, provided that the authors, title and full bibliographic details are credited, a hyperlink and/or URL is given for the original metadata page and the content is not changed in any way. For full details of reuse please refer to City Research Online policy.

City Research Online: http://openaccess.city.ac.uk/ publications@citystgeorges.ac.uk

T
585

A THEORETICAL AND EXPERIMENTAL INVESTIGATION OF THE COMBUSTION PROCESS IN A SPARK IGNITION INTERNAL COMBUSTION ENGINE

submitted
as PhD thesis
by

Brian Agnew
Department of Mechanical Engineering
The City University, London EC1

April 1981

CONTENTS

		Page
Introduction		16
Chapter 1	Literature Survey	19
	Introduction	19
	1.1 Cyclical Variation	19
	1.2 Combustion Modelling	23
	1.3 Heat Transfer	28
	1.4 NOx Formation in Internal Combustion Engines	29
	1.5 Unburnt Hydrocarbon Formation	33
	References	37
Chapter 2	Description of Equipment	46
	Introduction	46
	2.1 The CFR Experimental Engine	46
	2.1.1 The Multihole Cylinder	47
	2.1.2 The Engine Cooling System	47
	2.1.3 The Ignition System	55
	2.1.4 The Carburation and Air Intake System	55
	2.1.5 The Dynamometer Control Unit	57
	2.2 Combustion Chamber Pressure Measurement	57
	2.3 The Combustion Interval Meter	60
	2.3.1 Principle of Operation	61
	2.3.2 Functional Operation	63
	2.3.3 Operating Notes	65
	2.4 The Crank Angle Indicator and TDC Indicator	65
	2.5 The Piston and Piston Temperature Measuring Equipment	67
	2.5.1 The Internittent Contact Measuring Technique	68
	2.5.2 Calibration of the Measuring System	72
	2.6 The Combustion Chamber Surface Thermocouples	80
	2.7 The Exhaust Gas Analysis Equipment	85
	2.7.1 The Sampling System	85
	2.7.2 The Nitric Oxide Analyser	85
	2.7.3 The Carbon Monoxide and Hydrocarbon Analysers	88
	References	91
Chapter 3	Experimental Procedure	92
	Introduction	92
	3.1 The Ellison Starting Preocedure	92
	3.2 Setting the Mixture Strength	93
	3.3 Setting the Spark Advance	93
	3.4 Setting the Compression Ratio	94
	3.5 Setting Up the Gas Analysis Equipment	94
	3.6 Examination of the Cyclical Variation of the Engine Rotational Speed and the Ignition Timing	94

3.7 Examination of the Flame Propagation Speed with the Combustion Interval Meter 95
3.8 Examination of the Apparent Flame Speed and Combustion Phenomena 95
References 100

Chapter 4 Experimental Results 101
Introduction 101
4.1 Cyclical Variation of the Engine Rotational Speed and the Ignition Timing 101
4.2 Development of the Expanding Flame Front 106
4.3 Piston and Cylinder Wall Temperature 106
4.4 Cylinder Pressure Diagrams 106
4.5 Exhaust Emissions 106

Chapter 5 Mathematical Analysis 138
Introduction 138
5.1 The Thermodynamic Model 140
5.2 Prediction of the Turbulent Flame Speed 147
5.3 Calculation of the Equilibrium Concentrations of the Combustion Products 159
5.3.1 Formulation of the Initial Equations 159
5.3.2 Curve Fitting of Equilibrium Constants 165
5.4 Determination of the Surface Area of the Flame Front and of the Piston and Cylinder Surfaces Exposed to the Burnt Charge 166
5.4.1 Flame Front Surface Area 166
5.4.2 Piston Surface Area or Cylinder Head Surface Area 169
5.4.3 Cylinder Wall Surface Area 171
5.5 Calculation of the Volume of the Burnt Charge 175
References 176

Chapter 6 Analysis of the Experimental Results 180
Introduction 180
6.1 The Development of the Expanding Flame Front 180
6.2 Cyclical Variation of the Flame Travel Time 181
6.3 Cyclical Variation of the Apparent Flame Velocity 197
6.4 Analysis of the Cylinder Pressure Data 200
6.5 Flame Front Shape and Thickness 205
6.6 The Effect of Flame Thickness on Apparent Flame Speed 206
References 207

Chapter 7 Cycle Synthesis 208
Introduction 208
7.1 The Mathematical Model 208
7.1.1 The Solution Procedure 212
7.2 The Formation of Nitric Oxide 217
7.3 Hydrocarbon Quench Layer Thickness 215
7.4 Heat Transfer 219
7.5 Mass Burning Rate 220
7.6 Results of the Cycle Synthesis 221
References 230

Chapter 8 Discussion of the Theoretical and Experimental Results and Conclusions 232
Introduction 232
8.1 Flame Front Behaviour 232
8.2 Flame Speed Correlation 235
8.3 Emissions 238
8.4 Experimental Method 240
8.5 Conclusions 241

Appendix 1 Experimental Equipment 243
Introduction 243
A1.1 Measurement of the Combustion Chamber Pressure 243
A1.2 Properties of Transducers 243
A1.3 Effects of Transducer Installation Conditions on the Measurement of Pressure 247
A1.4 Investigations into the Limiting Values of the Aperture Ratios and the Length of the Connecting Pipe of the Pressure Transducer Holder 250
A1.5 Pressure Transducer Calibration 252
A1.6 Thermocouple Calibration 252
A1.7 Exhaust Gas Analysis Calibration 263
A1.8 List of Equipment 263
A1.9 Fuel Properties 263
References 269
Appendix 2 Computer Programs 271
Introduction 271
A2.1 Combustion Program 271
A2.2 Adiabatic Flame Temperature Program 272
A2.3 Cylinder and Flame Geometry Program 273

LIST OF TABLES

Table 2.1 Basic Dimensions of the CFR engine
Table 2.2 Penetration of Effect of Sinusoidally-Varying Surface Temperature
Table 2.3 Chemitox Analyser Specifications
Table 2.4 General Specification of the Model 20 Infra Red Gas Analyser
Table 3.1 Engine Operating Conditions for Examining the Cyclical Variations of the Ignition Timing and the Engine Rotational Speed
Table 3.2 Engine Operating Conditions for Examining the Flame Propagation Speed
Table 3.3 Engine Operating Conditions for Examining the Flame Speed and Combustion Phenomena
Table 4.1 Cyclical Variations of the Engine Roational Speed
Table 4.2 Cyclical Variations of the Ignition Timing Against TDC
Table 4.3 Flame Travel Time: Variation of Compression Ratio (Fuel Type:Benzene)
Table 4.4 Flame Travel Time: Variation of Equivalence Ratio (Fuel Type: Benzene)
Table 4.5 Flame Travel Time: Variation of Ignition Timing (Fuel Type: Benzene)
Table 4.6 Flame Travel Time: Variation of Equivalence Ratio (Fuel Type: Isooctane)
Table 4.7 Flame Travel Time: Variation of Ignition Timing (Fuel Type: Isooctane)
Table 4.8 Piston and Cylinder Wall Temperatures
Table 4.9 Piston and Cylinder Wall Temperatures
Table 5.1 Prediction of U_t for a Wrinkled Laminar Flame Model
Table 5.2 Turbulent Flame Model Predictions of U_t
Table 5.3 Values of Constants in Given Reactions
Table 5.4 Flame Front Radius When Indicated by Each Ion Gap
Table 6.1 Variation of Apparent Flame Velocity with Compression Ratio
Table 6.2 Variation of Apparent Flame Velocity with Equivalence Ratio
Table 6.3 Variation of Apparent Flame Velocity with Spark Timing
Table 6.4 Variation of Apparent Flame Velocity with Spark Timing
Table 6.5 Variation of Apparent Flame Velocity with Equivalence Ratio
Table 7.1 Values of Rate Constants and One-Way Equilibrium Reaction Rates for Extended Zeldovich Mechanism

Table 7.2 Quench Layer Parameters as a Function of Equivalence Ratio
Table A1.1 Properties and Dimensions of Some Transducers with High Natural Frequency (Values Quoted by Manufacturers)
Table A1.2 Temperature, Measured Output and True Output for Piston Thermocouples
Table A1.3 Temperature, Measured Output and True Output for Cylinder Head Thermocouples
Table A1.4 List of Experimental Equipment
Table A1.5 Fuel Properties

LIST OF FIGURES

Figure 2.1 Schematic Diagram of Test Bed Layout
Figure 2.2 The Test Bed
Figure 2.3 The Multiple Hole Cylinder Head: Vertical Cross-Section Showing Modifications and Position of Ionization Gaps
Figure 2.4 The Multiple Hole Cylinder Head: Horizontal Cross-Section Through Spark Plug
Figure 2.5 Combined 10mm Spark Plug Adaptor and Ion Gap
Figure 2.6 Schematic Diagram of the Engine Cooling System
Figure 2.7 The Calibration Curve of the Flow Meter
Figure 2.8 Schematic Diagram of the Air Inlet System
Figure 2.9 Schematic Diagram of the Cylinder Pressure Measuring System
Figure 2.10 Water-Cooled Mounting Adaptor for Quartz Pressure Transducer
Figure 2.11 Front View of Combustion Interval Meter
Figure 2.12 Block Diagram of the Combustion Interval Meter
Figure 2.13 Position of Thermocouples in the Piston Crown
Figure 2.14 Insertion of Thermocouples in Piston Crown
Figure 2.15 Thermocouple Leads Hanging Inside the Piston Skirt
Figure 2.16 Silver Steel Contacts at the Base of the Piston Skirt
Figure 2.17 Diagram of Machined Ring at Base of Piston Skirt
Figure 2.18 Berrilium-Copper Impact Spring Type Contacts
Figure 2.19 Hangers in the Crankcase Mouth
Figure 2.20 Modification of Sandwich Plate between Crankcase and Cylinder
Figure 2.21 Gland Set in Crankcase
Figure 2.22 Conventional Measuring System
Figure 2.23 Sectioned Drawing of the Thermocouple Head
Figure 2.24 Thermocouple and Plug Prior to Assembly
Figure 2.25 Thermocouple and Plugs Prior to Insertion in Cylinder Head Ports
Figure 2.26 Arrangement of Exhaust Gas Analysis Equipment
Figure 2.27 Schematic Diagram of the Gas Analysis Equipment
Figure 4.1 Variation of the Time required for one Engine Revolution
Figure 4.2 Variation of Ignition Timing Against TDC
Figure 4.3 Flame Travel Time: Variation in Compression Ratio (Fuel Type: Benzene)
Figure 4.4 Flame Travel Time: Variation of Equivalence Ratio (Fuel Type: Benzene)

Figure 4.5 Flame Travel Time: Variation of Ignition Timing (Fuel Type: Benzene)
Figure 4.6 Flame Travel Time: Variation of Equivalence Ratio (Fuel Type: Isooctane)
Figure 4.7 Flame Travel Time: Variation of Ignition Timing (Fuel Type: Isooctane)
Figure 4.8 Location of Thermocouples in Cylinder Head
Figure 4.9 Cylinder Pressure Diagram
Figure 4.10 "
Figure 4.11 "
Figure 4.12 "
Figure 4.13 "
Figure 4.14 "
Figure 4.15 "
Figure 4.16 "
Figure 4.17 "
Figure 4.18 "
Figure 4.19 Relationship Between Equivalence Ratio Spark Timing and Nitric Oxide Emissions
Figure 4.20 Relationship Between Equivalence Ratio Spark Timing and Hydrocarbon Emissions
Figure 4.21 Relationship Between Equivalence Ratio Spark Timing and Carbon Monoxide Emissions
Figure 5.1 Mass Fraction Burnt Against Volume Fraction Burnt for Several Equivalence Ratio (Fuel Type: Isooctane)
Figure 5.2 Variation of Mass Fraction Burnt with Crank Angle for Several Spark Timings (Fuel Type: Isooctane)
Figure 5.3 Variation of Mass Fraction Burnt with Crank Angle for Several Equivalence Ratios (Fuel Type: Isooctane)
Figure 5.4 Variation of Unburnt Charge Temperature with Crank Angle and Spark Timing
Figure 5.5 Variation of Burnt Charge Temperature with Crank Angle and Spark Timing
Figure 5.6 Reynolds Number Dependence of U_t/U_l
Figure 5.7 Variation of the Turbulence Intensity After Closing of the Intake Valve
Figure 5.8ab Effect of Temperature on the Laminar Flame Speed of Isooctane-Air Flows
Figure 5.9 Relationship Between V_t/V_l and the Turbulent Reynolds Number
Figure 5.10 Correlation Between V_t/V_l and the Turbulent Reynolds Number
Figure 5.11 Notation
Figure 5.12 Calculation of the Piston or Cylinder Head Surface Area
Figure 5.13 Relationship Between SAF, SAP, SAW, SAH and RR for Constant R

Figure 5.14 Relationship Between SAF and RR for Fixed Crank Angles
Figure 6.1 Variation of Flame Travel Time (Fuel Type: Benzene)
Figure 6.2 Variation of Flame Travel Time (Fuel Type: Isooctane)
Figure 6.3 Variation of the Flame Propagation Velocity (Fuel Type: Benzene)
Figure 6.4 Variation of the Flame Propagation Velocity (Fuel Type: Isooctane)
Figure 6.5 Variation of $\bar{V}$, σ and $\sigma/\bar{V}$ with Compression Ratio (Fuel Type: Benzene)
Figure 6.6 Variation of $\bar{V}$, σ and $\sigma/\bar{V}$ with Equivalence Ratio (Fuel Type: Benzene)
Figure 6.7 Variation of $\bar{V}$, σ and $\sigma/\bar{V}$ with θ (Fuel Type: Benzene)
Figure 6.8 Variation of $\bar{V}_f$, σ and $\sigma/\bar{V}_f$ with Spark Timing (Fuel Type: Isooctane)
Figure 6.9 Variation of $\bar{V}$, σ and $\sigma/\bar{V}$ with Equivalence Ratio (Fuel Type: Isooctane)
Figure 6.10 Relationship Between Mean Flame Velocity and Standard Deviation
Figure 6.11 Theoretical Total Turbulent Burning Velocity as Function of the Turbulence Intensity in Units of the Laminar Burning Velocity S
Figure 6.12 Relationship Between Cyclic Variation of Air-Fuel Ratio and the Apparent Flame Propagation Velocity
Figure 6.13 Comparison of Calculated and Measured Data of Flame Propagation Velocity
Figure 6.14 Cylinder Pressure Diagram
Figure 6.15 The Difference Between Measured and Predicted Flame Radius as Combustion Proceeds
Figure 7.1 Schematic Representation of the Hydrocarbon Quench Layer
Figure 7.2 The Effect of Changes of u' on the Mass Fraction Burnt
Figure 7.3 Cylinder Pressure Diagrams
Figure 7.4 Predicted Mass Fraction Burnt for Several Equivalence Ratios
Figure 7.5 Quench Layer Thickness for Various Engine Conditions
Figure 7.6 Burnt Gas Temperature Distribution
Figure 7.7 Predicted CO Concentration showing the Effect of Cyclical Variation of the Air-Fuel Ratio
Figure 7.8 Predicted Hydrocarbon Concentration
Figure 7.9 Predicted NO Concentration Showing the Effect of Cyclical Variation of the Air-Fuel Ratio
Figure A1.1 Water-Cooled Mounting Adaptor for Quartz Pressure Transducer
Figure A1.2 Calibration Curve of a Type XQL-080 Pressure Transducer Plotted for Different Operating Temperatures (Input voltage 5V)

Figure A1.3 Schematic Representation of the Surface Effect in Pressure Transducers (on the basis of an Arbitrary Local Pressure Distribution)
Figure A1.4 Order of Magnitude of the Pressure Fluctuation Resulting from Displacement Effect $(\Delta P/P)D$ and of the Change in Pressure resulting from Jet Expansion $(\Delta P/P)E$, as Functions of the Aperture ratio M (Symmetrical Rectangular Distribution)
Figure A1.5 Correction Curve for Thermocouple P_1
Figure A1.6 Correction Curve for Thermocouple P_2
Figure A1.7 Correction Curve for Thermocouple P_3
Figure A1.8 Correction Curve for Thermocouple P_4
Figure A1.9 Correction Curve for Thermocouple W_1
Figure A1.10 Correction Curve for Thermocouple W_2
Figure A1.11 Correction Curve for Thermocouple W_3
Figure A1.12 Correction Curve for Thermocouple W_4
Figure A1.13 Calibration Curve for the Chemitox Gas Analyser
Figure A1.14 Calibration Curve for the CO Gas Analyser
Figure A1.15 Calibration Curve for the Hexane Gas Analyser
Figure A2.1 Values of γ_b and σ_u Obtained by Fitting Straight Lines to Enthelpy Temperature Plots of Burnt and Unburnt Gas Mixtures Over the Temperature Range of Interest
Figure A2.2 Values of Difference in Intercept of Straight Line Fits to Enthalpy Temperature Plots (ab - au) of Burnt and Unburnt Gas Mixtures at T = 0°K
Figure A2.3 Molecular Weight of Burnt and Unburnt Isooctane-Air gas Mixtures
Figure A2.4 Mole Fraction Against Temperature and Pressure (N_2)
Figure A2.5 Mole Fraction Against Temperature and Pressure (H_2O)
Figure A2.6 Mole Fraction Against Temperature and Pressure (CO_2)
Figure A2.7 Mole Fraction Against Temperature and Pressure (O_2)
Figure A2.8 Mole Fraction Against Temperature and Pressure (CO)
Figure A2.9 Mole Fraction Against Temperature and Pressure (H_2)
Figure A2,10 Mole Fraction Against Temperature and Pressure (OH)
Figure A2.11 Mole Fraction Against Temperature and Pressure (NO)
Figure A2.12 Mole Fraction Against Temperature and Pressure (O)
Figure A2.13 Mole Fraction Against Temperature and Pressure (H)
Figure A2.14 Mole Fraction Against Temperature and Pressure (N)

ACKNOWLEDGEMENT

The author wished to thank his supervisor, Mr Brian Hayward for his insight and assistance throughout the project. The support of Mr Bert Davies and Mr Joe Heaffey was invaluable during the experimental phases of the work. Acknowledgement is also due to the SRC and The City University, which jointly funded the work.

Brian Agnew
April 1980

DECLARATION

The University Librarian may, at his discretion, allow this thesis to be copied, in whole, or in part, without further reference to the author. This permission covers only single copies made for study purposes, subject to normal conditions of acknowledgement.

ABSTRACT

An experimental investigation into the development of the expanding flame front in the combustion chamber was carried out using a CFR variable compression engine. Statistical analysis of the results indicated that the cyclical variation of the flame travel time followed a random distribution, but that the flame propagation velocity had a normal distribution. The cyclical variation of the flame propagation velocity was shown to be caused by cyclical variation in the air-fuel ratio. The experimental results were used in conjunction with a mathematical model of the combustion process to derive a correlation between the flame propagation speed and the turbulent Reynolds number. The correlation took the form:

$$\frac{Vt}{Vl} = 0.324\left[0.021\,\frac{h_o \rho_u u'_e}{\mu}\left(\frac{Po}{P}\right)^{1.33}\right]^{0.73} - 4.581$$

The flame speed correlation was then used in a cycle synthesis to predict the mass burning rates of the charge. The model predicted successfully mass burning rates, cylinder pressures, temperature distribution in the burnt charge and exhaust emissions levels. The results suggested that turbulence was a secondary factor in flame propagation after the pre-propagation period, but may be more important at the inititation of the combustion. The experimental results indicated that cyclical variations in cylinder pressure are produced by post-flame reactions. The thickness of the flame front was found to be significant and flame propagation followed the successive self-ignition theory more closely than the wrinkled flame front model.

SYMBOLS

A	Area
a	height of cylinder head above spark plug centre line
b	height of spark plug centre line above piston crown
ab	constant defined in text
au	"
C	constant
C_p	Specific Heat at constant pressure
C_v	Specific Heat at constant volume
CR	Compression Ratio
e	Specific internal energy
E	Total Internal Energy
hp	clearance height = a + b
ho	clearance height at TDC
H	enthalpy
h	heat transfer coefficient
K	thermal conductivity
L	integral length scale, length
lc	con rod length
M	mass, Aperture ratio, Molecular weight
Nu	Nusselt number
N	Crank shaft speed RPM
P	Pressure
Pr	Prandtl number
Q	heat transfer
q	quench layer thickness
Rc	cylinder radius
Rf	flame radius measured
Rfc	flame radius calculated
Rfh	flame radius subtended on the cylinder head
Rfp	flame radius subtended on the piston crown
R	Specific gas constant
Re	Reynolds number
Re_λ	Turbulent Reynolds number
RR	flame ratio = Rf/Rc
SAF	surface area of the flame
SAW	cylinder wall surface exposed to the burnt charge
SAH	cylinder head surface exposed to the burnt charge
SAP	piston crown surface exposed to the burnt charge
S	crank throw
tf	flame thickness
T	temperature
T	mean flame travel time
u'	turbulence intensity
u"	flame generated turbulence
Up	mean piston speed
Vl	laminar flame speed
Vt	turbulent flame speed

V	volume
Vf	Mean flame velocity
x	mole fraction
α	mass fraction burned, angle subtended by the
β	flame front
γ	angle subtended by the flame front,
	ratio of the specific heats
ρ	density
τ	shear stress
ϕ	crank angle, angle subtended by the flame front
$\varnothing$	equivalence ratio, angle subtended by the flame front
ϵ	eddy diffusivity
σ	standard deviation
λ	Taylor microscale
μ	dynamic viscousity

Subscripts

b	burnt charge
u	unburnt charge
f	flame
g	gas
o	initial conditions
R	reference conditions
t	condition at time t
T	total

INTRODUCTION

The work reported here was sponsored by the Science Research Council and carried out at The City University between September 1974 and June 1977. It was a continuation of the university's interest in combustion phenomena in the spark ignition reciprocating internal combustion engine, and was stimulated by a surge of interest in atmospheric pollution and exhaust emissions.

The relationship between atmospheric pollution and exhaust emissions is now well-established. Motor vehicle exhaust emission standards relating to Carbon Monoxide, Hydrocarbons and Oxides of Nitrogen have now been enforced throughout North America and Europe. Motor vehicle manufacturers have adopted two different but related methods of emissions control. Initially, the exhaust gases were treated as they emerged from the engine into the exhaust pipe. Catalysts or thermal reactors were installed which reduced the levels of Carbon Monoxide and Hydrocarbons discharged in to the atmosphere. Attempts to reduce NO concentrations have been less successful. Inherent in the installation of an exhaust reactor unit is a reduction in the overall performance of the vehicle and an increase in the specific fuel consumption. The second approach examined the combustion process to determine, from theoretical considerations, the mechanisms generating the emissions, and thereby, to find a way of attacking the problem at its root. The work reported here falls into the second category.

Several mathematical models of the combustion process and power phase of the internal combustion engine have been developed. They serve as diagnostic tools, aid design, predict trends and produce more information than is normally available from experimentation. This latter aspect is particularly important as the need to understand the combustion process becomes more pressing.

Combustion modelling has taken a much simplified view of the very complex combustion process. The combustion chamber can be regarded as a chemical reactor in which a large number of simultaneous and sequential chemical reactions occur. The increase in pressure and temperature during the combustion phase produces pre-flame reactions. These include, low temperature pyrolysis, slow oxidation and cool flames. Reactions of the various species formed in the flame front continue in the post-flame gases. When the flame reaches a cold surface it is extinguished as the thermal energy lost reduces the gas temperature below that required for continued flame propagation. Consequently, reactions of the fuel and Oxygen at these points is incomplete. Mass transport from the low temperature regions to the burnt gases results from turbulence and is followed by pyrolysis of the Hydrocarbons in the Oxygen-deficient burnt gases. Conversely, exchange of the burnt gases from behind the flame front with the quench layer promotes partial oxidation of the Hydrocarbons in this area. Throughout the combustion process, large thermal gradients occur which the transport processes cannot equalise. As the chemical composition of the burnt charge is highly temperature-dependent, it follows that a spatial variation in the composition of the exhaust gases will also occur.

Most models have been based on empirical or semi-empirical relationships. The lack of fundamental data about such phenomena as charge mixing, mass burning rates, heat transfer, cyclical variations and so on, creates weaknesses in these models.

This work was both an experimental and a theoretical study of combustion in a spark ignition engine. It addressed two major issues. The first was the effect of engine operating conditions on cyclical variations in flame propagation rates, and the second, the question of mass burning rates and turbulent flame speed.

The cyclical variations in flame speed were found to be strongly related to variations in the fuel-air equivalence ratio. The combustion models based upon mean cycle data are shown to be in error in cases where the variable of interest is not a linear

function of equivalence ratio. The flame propagation velocity was found to be correlated with the laminar flame speed and the turbulent Reynolds number of the unburnt charge. This correlation draws an analogy between internal combustion engine work and simple burner theory, allows prediction of mass burning rates based on well-established combustion data and readily calculable physical properties of the unburnt charge. The role of turbulence in controlling mass burning rates and emission fractions is examined.

The experimentation was carried out on a fully-instrumented CFR research engine, using a combustion interval meter developed at The City University for this research.

CHAPTER 1 LITERATURE SURVEY

INTRODUCTION

This chapter is a detailed review of the combustion phenomena in a spark ignition engine with particular reference to cyclical variations and combustion modelling. The scope of the review ranges from the constant pressure bomb work of Stevens in 1927 to the measurement of exhaust emissions in 1973 and is divided into several sub-sections. The first sub-section is entitled Cyclical Variation and the remaining sub-sections are Combustion Modelling, Heat Transfer, NO Formation, and Unburnt Hydrocarbon Formation. This chapter is not intended to be an exhaustive review of the work conducted in this field but it explains the current state of the art in internal combustion engine work and provides the basis and context for the remainder of this work.

1.1 CYCLICAL VARIATION

It is now well established that the progression of the flame front across the combustion chamber has a marked influence on engine performance. Early studies of flame movement in closed vessels of various kinds consisting of constant pressure bombs and constant volume bombs (Ref 1.1 - 1.10) yielded useful information that could be related to the internal combustion engine cycle. This information was later verified and extended by photographic studies of flame development (Ref 1.11 - 1.14) across the combustion chamber. The results of these studies showed amongst others that under conditions of normal combustion the general movement of the flame front remains consistent. Ignition is followed first by a period of slow burning and then by a gradual increase in burning rate. At a point approximately 10% of the distance across the combustion chamber, the flame front reaches a maximum speed. In then continues at this maximum speed to a point approximately 90% of the distance across the combustion chamber. From here on, the speed decreases rapidly until combustion is complete.

The relationships between the flame speed and several operating variables were established at this time. The average flame speed was found to increase with an increase in fuel/air ratio up to that required for maximum power. From this point decrease in flame speed will result from further increases in the fuel/air ratio. Increases in the initial combustion chamber pressure and small scale turbulence will increase the flame speed but the reverse will occur with an increase in the initial temperature or the proportion of residual gas present in the combustion chamber. Increases in charge temperature are generally expected to increase flame speed but with constant inlet and exhaust pressures an increase in inlet air temperature will cause a decrease in the mass of charge drawn into the combustion chamber per cycle. Since the pressure of the residual gas remains constant and its temperature decreases there will be a slightly larger weight of residuals in the combustion chamber. Thus as inlet air temperature is increased there will be an increase in the proportion of exhaust gases in the fresh charge. Due to its greater dilution and higher temperature, the fresh charge will expand less when burned, and compression of the unburned gases by the advancing flame front will not proceed as fast or as far as with a cooler charge. Thus, the rise in inlet temperature causes not only an increase in the dilution but also a decrease in the average pressure of the charge during the combustion process which more than offsets any increase in flame speed which may result from increased charge temperature.

Having established the basic variable dependencies further examination of the combustion process centred around the cycle by cycle variation or cyclic dispersion that occurs even with a well regulated engine. This has been examined by many workers who have studied the properties of individual combustion cycles. In their studies of knocking characteristics of fuels, Warren (1.15) and Curry (1.16), have shown that fast burns produce the highest and earliest maximum pressure; slow flame speeds reduce the engine power and represent limitations on performance with weak mixtures. The weak mixture limit was also found to be poorly defined, there being a wide region in which the number of ineffective cycles

prevents effective running. Also the cyclical variation of flame speed can produce speeds as fast as those in rich mixtures. Summarising the general conclusion of the previous works it can be seen that the variations are not due alone to fuel/air ratio variations and are not due to variations in the ignition timing, the type of spark, or the spark energy. The variations are related to the mean flame speed such that fast burning fuels have less cycle by cycle variations than slow burning fuels. The implications of these findings are that there are other factors affecting flame speed and cycle by cycle variations in an internal combustion engine.

An attempt to evaluate statistically the cycle by cycle combustion variations was made by Patterson (1.17) who examined pressure variations from a sample of 2000 consecutive cycles from a single cylinder engine and also from an eight cylinder engine. His results indicated that a major cause of cyclical variations was the mixture velocity variations that exist within the cylinder at or near the spark plug at ignition. Patterson suggested also that a better understanding of the combustion problem could result in reductions in exhaust emissions by eliminating cycles which burn the charge incompletely.

These velocity gradients affect the combustion rate through wrinkling and distortion of the flame front. A possible mechanism for this was suggested through the enlarging of the surface area of the flame front increasing the rate of burning of the charge. Bolt and Harrington (1.18) extended this work of Patterson, concentrating on the effect of mixture motion upon the combustion process within a constant volume cylindrical bomb. The charge motion generated with their equipment had a variable mean velocity with a fluctuating velocity of about constant magnitude superimposed upon it over the whole mean velocity range. They concluded that the observed combustion variations were due mainly to variations in the mean mixture velocity. Increased mixture velocity was seen to extend the linear limit air/fuel ratio towards richer mixtures and affect greatly the rate of pressure rise particularly when using weak mixtures.

Cole and Mirsky (1.19) in their study of cycle to cycle combustion rate variations attributed the effect to two factors. The first was increased mixture velocity which, they suggested, had a direct linear relationship with the rate of pressure rise in the combustion bomb. The second mechanism listed as a major cause of the pressure rate increase was direct distortion of the flame front area. The increase in flame front area was obtained from Schlieren photographs based upon an assumed two dimensional shape of the flame front. Their results showed that the average increase in flame area above that of a quiescent charge accounted for approximately 60% of the increase in pressure rate. The remainder was due to relative increases in mixture density and burning velocity. In conclusion they suggested a model of flame propagation. Central to this model is the hypothesis that the stretching or shearing of the flame front increases the reaction zone and the turbulent transport of unburnt reactants species into the burnt reactants. This extrapolation of their results to an Internal Combustion Engine suggests that the variation in mixture velocity in the vicinity of the developing flame front could be a major cause of cycle by cycle variations. Control of the velocity variation in the vicinity of the spark plug would possibly reduce cycle by cycle variations. Mori and Yamazaki (1.20) extended this idea and produced a relationship between the standard deviation of the flame velocity and the mean flame velocity in a C.F.R. engine. As the standard deviation is the R.M.S. value about the mean it is mathematically analogous to the intensity of turbulence. A comparison of the analytical relationships of Karlovitz (1.21) with the work of Mori and Yamazaki indicates that the intensity of turbulence is very small in a C.F.R. engine. Unfortunately, their data only suggest a relationship. The direct evidence of the effect of mixture motion and its variation on combustion and its variation in engines was not available. Further studies by Winsor and Patterson (1.22) using hot wire anemometers was used to determine the relationship between combustion variations and the mixture velocity. They argued that the sensitivity of a developing flame front to turbulent disturbances was related to the

relative size of the disturbances and the flame front radius. Their measurements indicated that the eddy size in the C.F.R. engine is approximately 0.1 in.(2.5 mm) larger than the flame kernel in the initial developmental period. They postulated a model based upon flame front sensitivity to eddy size during the development stage at which point the disturbances leading to cyclic variation occur. After the development phase the flame front radius was larger than the eddies that now only disturb the flame front locally. The average flame speed at this point was dependent upon the average turbulent velocity in the mixture. Their results showed an increased relationship between the burn time variations and mean flame speed in agreement with the work of other authors.

Subsequent work by Ma (1.23) has looked at cyclical variations in terms of 'combustion quality', with referenc to exhaust emissions and lean burns. Initially a relationship between cycle variations and engine performance was shown to exist but was of poor correlation. The statistical parameters used, such as the mean and deviation of the flame arrival distribution, were inadequate to effect a prominent feature of the cyclic variations. Consequently the concept of combustion quality was devised. Defining the Combustion Quality Ratio, C.Q.R., as (intense burn cycles %)/(normal burn cycles) it was found that this parameter was valid for a wide range of engine parameters such as air/fuel ratio, spark timing and mixture turbulence and also give a fair evaluation of the relative contribution of a burn to the overall thermal efficiency of the engine. A correlation with I.S.F.C. was observed. This paper points to the possibility of the introduction of new parameters to examine engine performance and a new approach in combustion process control.

1.2 COMBUSTION MODELLING

Combustion modelling of internal combustion engines has been more complex in the last twenty years with the development of the digital computer and the increased demands made upon the engine designer in the fields of economy and emissions control. The lack

of sound experimental data and the instrumentation to obtain this data has restricted the detail of the models. The processes of vaporization, diffusion, flame development etc. which are an important part of the combustion process at each point location in the combustion chamber are not fully understood, even in environments more hospitable than the internal combustion engine. Thus, the models have generally been developed using data obtained from other sources such as the flow in pipes, constant volume combustion and constant pressure combustion experiments. The current lack of knowledge therefore precludes precise prediction. However, models based upon past experience and reasonable mathematical simulations of the real process predict effects that can be checked on a development engine.

The process of modelling has followed two distinct paths. The first, based upon the first law of thermodynamics, uses simulations limited to the overall thermodynamic process through the first law energy balance or basic engine design parameters to predict combustion phenomena. These models do not provide the fine details of spatial resolution of state variables and as such are not useful as detailed design tools.

The second approach adopts a highly specified multi-dimensional model whose success lies in modelling combustion phenomena to examine the complex interaction of numerous variables. Attempts to describe the momentum transport properties of turbulent flames without knowledge of the turbulent structure itself leads to several difficulties. Initially, experimental evidence is required to replace the unknowns surrounding the turbulent structure. The assumption that the effect of turbulence is to increase the transport coefficient is wrong in that the turbulent transport phenomena are not properties of the fluid and its thermodynamic state alone. The physical configuration of the fluid is of equal importance. More useful perhaps is the approach which solves the conservation equations by assuming that each dependent variable can be expressed as the sum of two terms, the stationary component and the fluctuating component. Additional experimental evidence is

required to describe the system fully. Thus, the larger scale models meet with the same difficulties as the first law thermodynamic models with regard to lack of physical understanding.

Past workers have adopted various simplifications to account for the many unsolved problems that exist in constructing an accurate combustion model. These methods are listed below:

1) Constant volume models (1.24)
2) Mass burning rates determined from photographic observations (1.25)
3) Mass burning rates determined from pressure time data (1.26)
4) Mass burning rates determined from arbitrary relationships (1.27)
5) Mass burning rates determined from assured flame profile and experimentally determined flame velocity (1.28)
6) The use of flame propagation theory to determine energy release rates (1.29)

Of the more recent methods that of Phillips and Orman (1.30) is notable as marking the advent of the digital computer to this problem: Phillips and Orman utilised the thermal theory of Mallard and le Chatelier (1.31) modified to account for the effects of turbulence. This is a particularly useful model to use as the flame propagation rate is dependent upon the physical properties of the unburnt reactant and of the products. Whilst being the simplest to use of the major flame propagation theories this model gives results similar to the more complicated thermal model of Semenov (1.32). The propagation of the flame front across the combustion chamber as predicted by this model was in reasonable agreement with experimental observations predicting trends and illustrating quantitative changes. The complexity of the problem with respect to the effect of pressure on the flame propagation justified the adoption of the simpler expression of flame speed.

This approach has been adopted by several other notable workers. Annand (1.33) established an approximate expression for laminar flame speed and multiplied this by an arbitrary factor to account for the increase due to turbulence. Lucas and James (1.34) and Benson, Annand and Baruah (1.35) have also used this approach. There are, however, serious short comings with this technique. The phenomenological effects within the combustion chamber, such as ignition delay and variation of the turbulence intensity are poorly represented.

An alternative approach is to model the turbulent flame propagation in turbulent transport terms. Turbulence models based on solving differential equations for turbulence energy and length scale necessitate the introduction of several empirical constants. In some cases these can be taken as functions of other physical properties after introducing some empirical constants. These constants apply to basic physical properties and should have a wider range of application than empirical constants based upon a particular combustion system. Bracco and Sirignano (1.36 and 1.37) used a one-dimensional model of a turbulent flame front with equal diffusivity for heat and mass transfer. The intensity and scale of turbulence were related to the gas and motor velocities and to the local motor housing clearances. The turbulent diffusivity was taken to be made up of two components; the first due to the relative motion of motor and housing and the second decaying exponentially according to a characteristic time particular to the inlet port dimensions, due to the inlet flow. An extension of this approach was adopted by Bellen and Sirignano (1.29) who suggested a simplified expression based upon the previous work but extended in its generality to account for the insufficient information governing the decay of the turbulent eddies generated in the intake process. Although acceptable as a first approach this model was insensitive to ignition timing effects and the equivalence ratio trends were unsatisfactory. Blizard and Keck (1.38) modelled the turbulent flame propagation as the entrainment of discrete eddies with an assumed exponential distribution of the burning times of the entrained eddies. This

burning law was not rigorously devised but was introduced as a convenient analytical form that incorporated the basic features of turbulent combustion. The Blizard and Keck model was extended by Tabaczynski (1.39) who postulated a detailed structure for individual eddies together with a technique for calculating the time required to burn an individual eddy. This model predicted the trends in ignition delay and combustion duration and therefore in a sense justified the intuition and licence used in its formulation.

Considerable thought has been given to the problem of flame propagation in spark ignition internal combustion engines by Samaga and Murthy (1.40 to 1.43). In this model the linear burning velocity was calculated from Semenov's (1.32) thermal model and was augmented for engine turbulence through an empirical function of the engine Reynolds parameter, assuming a wrinkled flame model. The turbulence flame velocity thus utilised was then corrected for transportation due to the expansion of the burning gases. The theory was strongly dependent upon constants obtained experimentally on a single cylinder variable compression ratio research engine. The results of the work were generally disappointing, there being poor agreement between the mass burned as predicted from the model and that computed from measured pressure data. Ignition delay was poorly represented and predictions of overall concentration of exhaust emissions were unreliable. Also the generality of the model was limited due to its dependence upon empirical constants.

An expression of the burned mass can be obtained from Lavoie and Heywood (1.44 and 1.45) from purely thermodynamic considerations. They assumed an infinitely thin flame compressing the charge isentropically thus neglecting the effects of heat transfer to the combustion chamber walls and variable chemical reactions during the combustion process. Initial calculations of the burned mass fraction did not reach unity, but decreased possibly as a result of regeneration due to the heat transfer accounted for in the cylinder pressure data. These data were used in the calculations but ignored in the model. Subsequent development of the model (1.46 and 1.47) took into account the effects of heat transfer and per-

formance losses whilst retaining the perfect gas relationship of isentropic compression.

Although the more recent models are showing good agreement with the experimental data there are still several unresolved questions to be answered before they become a widely applicable design tool.

The heat transfer mechanism and the effects this has on the formation of hydrocarbon and NOx emissions is not clearly understood. The exact rule and mechanism of turbulence in the intake and combustion systems needs to be studied to determine the relationship between these factors and the geometrical design of the engine. This would also throw light on the validity or otherwise of the concept of mean cycles, and repeatability in internal combustion engines.

1.3 HEAT TRANSFER

Heat transfer in the internal combustion engine has been a topic of considerable interest. An understanding of the heat transfer to the engine cooling system and the thermal loading of components has stimulated a great deal of research.

Overall heat transfer coefficients for the piston crown and the cylinder liner were proposed by Pflaum (1.48) as an extension of the work of Eichelberg (1.49) to account for advances in design and specific performance of engine units. The above papers and others were critically analysed by Annand (1.50) who pointed out that the previous work failed to meet several requirements including dimensional consistency. The correlations thus produced apply strictly to overall heat transfer coefficients, other expressions of the same general form have been used to estimate heat transfer in cycle modelling. Krieger and Borman (1.51) have used the Eichelberg formula in calculating approximate heat release for internal combustion engines; and Danieli, Ferguson, Heywood and Keck (1.47) used a similar formula suggested by Woschni (1.52) primarily because the expected Reynolds number dependence was displayed and instantaneous heat transfer rates were not required. However, it is the instant-

aneous heat transfer coefficient that is required in detailed combustion models. Important factors that were ignored in obtaining the overall heat transfer coefficient play an important role in the combustion process. The build up of boundary layers or hydrocarbon quench layers and the effect this has on heat release and NO concentrations in the burnt charge has generally been ignored. Also spatial variations in heat transfer coefficient have not been taken into account. Blumberg and Kummer (1.53) have pointed out that if heat were drawn from the bulk gases unrealistically low values were obtained for NO levels. It is possible therefore that the heat loss is restricted to a thin hydrocarbon boundary layer whilst the bulk charge remains adiabatic at a higher temperature than would be predicted from the uniform temperature case.

The exact form of the heat transfer mechanism and the effect this has on hydrocarbon formation is however unclear, this being an area in which further work is required.

1.4 NOx FORMATION IN INTERNAL COMBUSTION ENGINES

A great deal of work has been done to establish the mechanism of the formation of Nitric Oxide in internal combustion engines. Initial studies concentrated upon establishing correlations between Nitric Oxide production and engine operating parameters (1.54 - 1.61). From such studies it was established that modifications to the engine operating conditions that change the combustion temperature or the concentration of oxygen in the burnt charge affected the nitric oxide concentration. The peak combustion temperature was found to be a prime factor in establishing NO concentrations rather than the equilibrium temperatures at the exhaust discharge condition.

Consideration of the non equilibrium concentrations of NO has lead to the development of several mechanisms for the formation of NO in the combustion chamber. It is now established that the NO formed from reactions of N_2 with Oxygen is found via the extended Zeldovich mechanism:

$$O + N_2 \rightleftharpoons NO + N \quad \ldots (1)$$

$$N + O_2 \rightleftharpoons NO + O \quad \ldots (2)$$

$$N + OH \rightleftharpoons NO + H \quad \ldots (3)$$

Reaction 3 was suggested by Lavoie and Blumberg (1.61) for near stoichiometric and fuel rich mixtures. These reactions are relatively slow, and so the formation and decomposition of NO depend to a large extent upon both high temperatures and the residence time at the higher temperatures.

The simplest approximation for computation of NO kinetics is that of the C.H.O. equilibrium. In this it is assumed that the time required to achieve equilibrium of NO concentrations is much greater than the time required to obtain equilibrium for the other constituents in the combustion products. The concentration of all the species and the temperature of the products being calculated from an equilibrium basis with NO excluded from the species concentrations.

Newhall and Starkman (1.58) using an extended Zeldovich mechanism predicted immediate freezing of the assumed equilibrium composition at the peak temperature and pressure for the homogeneous gases. Measured NO concentrations were considerably in excess of equilibrium concentrations and little decomposition of NO during the expansion stroke was observed. In conclusion they suggested that the average or bulk peak temperature was an inadequate representation of the state giving rise to the maximum equilibrium NO concentrations. They suggested that calculations of maximum equilibrium NO must be instead based on a distribution in time and space of local peak temperature states. Eyzat and Guibat (1.59) examined the formation process taking account of the possibility that the formation of NO could be rate limited thus preventing the formation of peak equilibrium levels particularly in weak mixtures. Unfortunately, they linked their kinetic model to a well mixed homogeneous mixture using the mean bulk temperature in calculating the NO concentrations. They also pointed to the significance of the heat release rate in determining NO concentrations.

Lavoie, Heywood and Keck (1.44) compiled a more complete kinetic model with an unmixed thermodynamic model. The charge was assumed to burn in discrete elements that remained unmixed as the burned gases were compressed and expanded. Using spectroscopic techniques to follow NO formation in the burned gases in the cylinder it was observed that NO concentrations are rate-controlled in the burned gases behind the flame front and freeze early during the expansion stroke. Measurements made at different locations in the combustion chamber showed that a substantial temperature gradient and hence Nitric Oxide concentration exists across the combustion chamber as predicted by the model.

Blumberg and Kummer (1.53) extended the fundamental work of Lavoie, Heywood and Keck (1.44) by incorporating it into a general thermodynamic analysis of an engine cycle. They then obtained quantitive predictions of the NO emission concentrations as a function of several variables including fuel type, equivalence ratio, humidity, E.G.R., R.P.M., compression ratio, charge inlet conditions and engine design parameters. They did not, however, consider heat losses in the cycle simulation but in an addendum to their work they suggested that uniform cooling of the burnt charge does not take place during combustion but that much of the gas behaves adiabatically with the layers adjacent to the wall absorbing a large fraction of the heat loss. They suggested that a reduction of 20% of the NO concentration could be expected due to the small drop in peak pressure and temperature of the adiabatic core.

In a later paper Blumberg (1.60) applied this model to a stratified charge engine in which the charge was sub-divided into discrete elements maintaining their integrity throughout the portion of the cycle during which the NO reactions are active. At a point in the expansion where all the elements of the burned charge were at a sufficiently low temperature so as to ensure freezing of the NO reactions the element was mixed and the burned charge expanded as a uniform mixture to the exhaust conditions. Heat transfer was also ignored in this paper. Lavoie and Blumberg (1.61) provided a test of the computer model of Blumberg by comparing its predictions with

experimental data from a single cylinder Ford PROCO engine. They concluded that the Blumberg model if modified to account for flame formed NO for rich and lean engine operation and wherever NO concentrations were less than 100 ppm, provided a good quantitative picture of NO formation. Further improvements in the quantitative accuracy would, however, require consideration of heat transfer effects and a better estimate of flame formed NO. The model over-predicted NO concentrations by a factor of 2.

Annand (1.62) questioned the simplifications used by previous workers in calculating the high non-equilibrium concentrations found in exhaust gases. These simplifications were:-

1) Neglecting reactions involving N_2O
2) Assuming quasi-equilibrium values of N and N_2O
3) Neglecting the reaction $N + OH \rightleftharpoons NO + H$
4) Neglecting that part of the departure from equilibrium in the burned gases which results from the slow recombination, during expansion, of atomic hydrogen, atomic oxygen and the hydroxyl radical, the outcome of which is the survival of excess carbon monoxide in the exhaust.

His work indicated that the departure of CO from equilibrium was insignificant in the formation of NO in spark ignition engines. The quasi steady approximation of N and N_2O is satisfactory at engine conditions. The reaction $N + OH \rightleftharpoons NO + H$ cannot be disregarded without appreciable error especially in rich mixtures and, finally, the exclusion of N_2O reactions produces a very small underestimation of NO.

The large errors in calculating the percentage concentration of NO in exhaust gases, particularly in fuel rich flames, lead to the fundamental assumption of the validity of the extended Zeldovich mechanism being questioned as the correct and only mechanism of NO formation. Fenimore (1.63) suggested that the flame did not follow the $N_2 - O_2 - NO$ system but that 'prompt NO' is formed in the primary reaction zone involving reactions with the hydrocarbon fuel such as $CH + N_2 \rightleftharpoons HCN + N$ and $C_2 + N_2 \rightleftharpoons 2CN$. The N atoms then form nitric oxide through the Zeldovich mechanism. The possibility exists that the quickly formed NO might be a significant but not major part of the total.

A radical overshoot model developed by Homer and Sutton (1.64) showed that a significant part of NO is formed very early in the flame as a result of the overshoot of oxygen atom concentrations above the equilibrium level. The extension of this radical overshoot model to a variety of combustion systems would require a knowledge of the extent of the radical overshoot in the corresponding flames. In many practical combustion systems, where the gas temperature is known only to within 100°K the detail of this approach may be unwarranted, and the far simpler equilibrium oxygen atom model will suffice. Undoubtedly there are radical overshoots in some hydrocarbon flames and they will contribute to the rate of NO formation very early in the flames, as suggested by Homer, Jenkins and Sutton (1.65). They could form part of the 'prompt NO' reported by Fenimore but not all, since the amount of 'prompt NO' was shown to be greater at high pressures, whilst the effect of any radical overshoot would decrease as pressure increased.

Potential modifications to the reaction mechanism to account for the formation of NO are therefore limited by the absence of fundamental combustion data from within the combustion chamber. However, it can be said that heat transfer will have an effect on the NO concentrations and it may, therefore, be unrealistic to examine the various fluid dynamic and thermodynamic mechanisms occurring simultaneously in the combustion chamber in isolation. Danieli, Ferguson, Heywood and Keck (1.46 - 1.47) have made an initial approach, integrating heat transfer, hydrocarbon formation and NO formation into a combined model. This model lacks detail and leaves room for development.

1.5 UNBURNT HYDROCARBON FORMATION

It is now generally accepted that the unburnt hydrocarbon emissions present in the exhaust gases of spark ignition engines are due to the quenching of the flame at the cylinder and piston surfaces and in piston ring and spark plug recesses. The quenched hydrocarbons are swept from the walls and undergo mixing with the burnt

charge with subsequent oxidation. The models proposed to date of quenching in engines have treated the formulation of a quench layer thickness largely empirically with data obtained using parallel plates. This approach is fundamentally incomplete as factors such as turbulence and species diffusion must also play a part in the quenching process.

The fundamental work of Daniel (1.66) based on Friedman and Johnston (1.67) on the quenching coefficient established the principles upon which subsequent theories of hydrocarbon quenching were based. Experimental evidence indicated that the quench distance calculated from burner data at the same temperature and pressure was in agreement with that observed in an internal combustion engine. The observed quench distances were of the right order of magnitude to account for all of the unburnt hydrocarbons found in the exhaust gases. This was in contrast with the previously held view that pockets of partially reacted mixture passed through the highly turbulent flame front, as in Wentworth and Daniel (1.68). This theory was more thoroughly examined by Gottenberg, Olson and Best (1.69) with experiments closely approximating engine combustion in which they could study the effects of varying surface-to-volume ratio and turbulence level. A direct linear relationship was obtained between the surface/volume ratio of a combustion chamber and the total concentration of unreacted hydrocarbons in the combustion products. A direct linear relationship was also found to exist between a representative measured quench distance and the quantity of unreacted hydrocarbons in the combustion products. Hydrocarbon concentrations decreased as the overall reaction rate increased. A theoretical analysis of hydrocarbon concentrations in combustion products has been presented by Agnew (1.70). Comparisons between the simple quench theory and experimental results were inconsistent suggesting a modification to the simple quench theory. More consistent results were obtained when the pressure dependence of the quenching distance was revised to accommodate the high pressures encountered in a constant volume process. The unburned hydrocarbons produced in or near quench layers, it was suggested, react during the post-flame reaction process such that the concentrations of hydrocarbons in the combustion products is signifi-

cantly lower than that predicted by quench theory alone. The effectiveness of these post-flame reactions depend upon the temperature/time history of the combustion chamber gases subsequent to flame extinction. The implication is that a large displacement low compression ratio engine would produce an exhaust with an unburned hydrocarbon concentration lower than that of a small displacement high compression ratio engine. Daniel (1.71) outlined a much more complex model, which included the effects of in-cylinder diffusion and the burn up of both the quench layer and ring crevice hydrocarbons, blow by, rate of combustion, variable fraction of hydrocarbons exhausted and exhaust port burn up.

The model was instructive in pointing out the general complexity of the hydrocarbon emission process and in identifying probable quantitative effects of the many physical phenomena involved. Unfortunately, most of the parameters defining the model were not based on fundamental data but were obtained by means of a multi-variable fitting technique which matched predicted results to a limited matrix of data points for a given engine. Regarding wall-quenching hydrocarbons however, the calculations were based on the two-plate data of Friedman and Johnston (1.67). The results were generally similar to those of Agnew (1.70) in that calculated in-cylinder hydrocarbon concentrations were always higher than exhaust levels by an amount which was greatest under lean conditions.

Other factors such as surface temperature and surface finish have been shown to have an influence on hydrocarbon emissions. Wentworth (1.72) studied the effect of variable wall temperature on an engine run at a constant load. Hydrocarbon concentrations were shown to decrease by a factor of 2, half of which was attributed to the increase in wall temperature and the remainder being due to oxidation of the quench layer during the expansion and exhaust stroke. The mechanism of the removal of the quench layer from the combustion chamber surfaces has been studied by several workers. Daniel and Wentworth (1.73) showed the presence of non-uniformities in the concentrations of the hydrocarbons in the exhaust gases. Tabaczynkski (1.74) proposed that the quench layer in the surfaces adjacent to the

exhaust ports is entrained in the blowby gases and leaves the cylinder. As the piston moves up the cylinder the effect of the moving wall is to impart a rolling motion to the quench layer that manifests itself as a scraping vortex. The size of this vortex at typical engine Reynolds number is several times the clearance height. Thus, towards the end of the exhaust stroke a major part of this hydrocarbon vortex exits the cylinder. The surface/volume ratio of the vortex has an effect on the oxidation of the hydrocarbons during the exhaust process. Hicks, Probstein and Keck (1.75) have developed an aerodynamic model of the entrainment of the quench layer during blowby and exhaust. The area from which the quench layer is swept is shown to be proportional to the cube root of the ratio of the quench layer thickness to the thickness of the viscous boundary layer. The hydrocarbon emissions were shown to be dependent upon the product of the hydrocarbon density at the time of quench, the quench area the the thickness of the quench layer.

The introduction of large scale organised turbulence in the combustion chamber as a means of reducing hydrocarbon emission concentrations has been suggested by Panduranga (1.76). At first sight it would appear that the turbulence should increase the hydrocarbon concentrations because of the more effective heat transfer enhancing wall quenching. However, the increase in quench thickness is more than offset by the decrease due to tangential turbulence.

The incorporation of the quench losses into a combustion model has been performed by Danieli, Ferguson, Heywood and Keck (1.47). In this model the quench layer thicknesses were based on exponents derived from Friedman and Johnson's (1.67) work and that of Green and Agnew (1.77). The model assumed that the mass quenched was independent of wall temperature and of turbulent scaling in the boundary layer. Although being over-simplified reasonable results were obtained and a pointer to the formation of a mathematical technique was given.

REFERENCES

1.1 STEVENS, F W
A Constant Pressure Bomb
NACA T R No 176. 1923

1.2 STEVENS, F W
The Gaseous Explosive Reaction: The Effect of Inert Gas
NACA T R No 280, 1927

1.3 STEVENS, F W
The Gaseous Explosive Reaction: A Study of the Kinetics of Composite Fuels
NACA T R No 305, 1928

1.4 STEVENS, F W
The Gaseous Explosive Reaction at Constant Pressure: The Reaction Order and Reaction Rate
NACA T R No 337, 1930

1.5 STEVENS, F W
The Gaseous Explosive Reaction: The Effect of Pressure on the Rate of Propagation of the Reaction Zone
NACA T R No 372, 1931

1.6 FIOCH, E F and KING, E R
The Effect of Water Vapour on Flame Velocities in Equivalent CO-O_2 Mixtures
NACA T R No 531. 1935

1.7 WOODBURN, C A, LEWIS, H A and GANBY, A T
The Nature of the Flame Movement in a Closed Cylinder
SAE Trans Part 1, 1921, vol 16

1.8 DUCHENE, M R
Contribution to the Study of Normal Burning in Gaseous Carbureted Mixtures
NACA T M Nos 547 and 548, 1930

1.9 DUCHENE, M R
Combustion of Gaseous Mixtures
NACA T M No 694, 1932

1.10 LEWIS, B and VON ELBE, G
Determination of the Speed of Flames and the Temperature Distribution in a Spherical Bomb, from Time-Pressure Explosive Records
Journal of Chemical Physics, May 1934, vol 2

1.11 WITHROW, L and BOYD, T A
Photographic Flame Studies in the Gasoline Engine
Industrial and Engineering Chemistry, 1931, vol 23

1.12 MARVIN, C F and BEST, R D
Flame Movement and Pressure Development in an Engine Cylinder
NACA T R No 399, 1931

1.13 SCHNAUFFER, K
Engine Cylinder Flame Propagation Studied by New Methods
SAE Trans, 1934

1.14 MARVIN, C F, WHARTON, T and ROEDER, P
Further Studies of Flame Movement and Pressure Development in an Engine Cylinder
NACA T R No 556, 1936

1.15 WARREN, J A and HINKAMP, J B
New Instrumentation For Engine Combustion Studies
SAE Trans, 1956, vol 64

1.16 CURRY, S
A Three-Dimensional Study of Flame Propagation in a Spark Ignition Engine
SAE Preprint 452B, 1962

1.17 PATTERSON, D J
Cylinder Pressure Variations: A Fundamental Combustion Problem
SAE Trans, 1967 vol 76 660129

1.18 BOLT, J A and HARRINGTON, D L
The Effects of Mixture Motion upon the Lean Limit and Combustion of Spark Ignitied Mixtures
SAE Trans, 1967 vol 76 670467

1.19 COLE, D E and MIRSKY, W
Mixture Motions - Its Effect on Pressure Rise in a Combustion Bomb. A New Look at Cyclic Variation
SAE Paper 680766, 1968

1.20 MORI, T and AMAZAKI, K
Variation of the Flame Propagation Time in a Spark Ignition Engine
Bull Jap Soc Mech Eng, 1970 vol 13 no 58

1.21 KARLOVITZ, B
AGARD: Selected Combustion Problems
Butterworth, 1954

1.22 WINSOR, R E and PATTERSON, D J
Mixture Turbulence - A Key to Cyclic Combustion Variation
SAE Paper 730086, 1973

1.23 MA, T H
The Effect of Cylinder Charge Mixture on Combustion
Proc Inst Mech Eng Conf on Combustion in Engines, 1975

1.24 BONAMY, S E
A Modified Constant Volume Fuel Air Cycle
Automobile Engineer Jan 1966

1.25 RASSWEILER, G M and WITHROW, C
Motion Pictures of Engine Flames Correlated with Pressure Cards
SAE Trans 1938, vol 33

1.26 MULLAR, G M, UYEHARA, O F and MYERS, P S
Practical Application of Engine Flame Temperature Measurements
SAE Trans, 1954 vol 62

1.27 WALKER, G
Effect of the Rate of Combustion on Gasoline Engine Performance
J Inst Fuel, Jun 1964

1.28 STRANGE, F M
An Analysis of Ideal Otto Cycle including the Effect of Heat Transfer, Finite Combustion Rates, Chemical Dissociation and Mechanical Losses
Proc SAE Automotive and Engineering Conf, 1963, Paper 633D

1.29 BELLEN, J R and SIRIGNANO, W A
Theory of Turbulent Flame Development and Nitric Oxide Formation in a Stratified Charge Internal Combustion Engine
Comb Sci & Tech, 1973, vol8

1.30 PHILLIPS, R A and ORMAN, P L
Simulation of Combustion in a Gasoline Engine Using a Digital Computer
Advances in Automobile Engineering, 1966

1.31 MALLARD, E and LE CHATELIER, H
Annales des Mines, 1883 4

1.32 SEMENOV, N
Theory of Normal Flame Propagation
NACA T N No 1026, 1942

1.33 ANNAND, W J D
A New Computational Model of Combustion in a Spark Ignition Engine
Proc Inst Mech Eng, 1970-71

1.34 LUCAS, G G and JAMES, E H
Computer Simulation of a Spark Ignition Engine
SAE Paper 730053, 1973

1.35 BENSON, R S, ANNAND, W J D and BARUAH, P C A
A Simulation Model including Intake and Exhaust System for a Single Cylinder Four Stroke Cycle Spark Ignition Engine
Inter J Mech Sci 1975, 17

1.36 BARCCO, F V and SIRIGNANO, W A
Theoretical Analysis of Wankel Engine Combustion
Comb Sci & Tech, 1973, vol 7

1.37 SIRIGNANO, W A
One Dimensional Analysis of Combustion in a Spark Ignition Engine
Comb Sci & Tech, 1973, vol7

1.38 BLIZARD, N C and KECK, J C
Experimental and Theoretical Investigation of a Turbulent Burning Model for Internal Combustion Engines
SAE Paper 740191, 1974

1.39 TABACZYNSKI, R J, FERGUSON, C R and RADHAKRISHNAN, K
A Turbulent Entrainment Model for Spark Ignition Combustion Engines
SAE Paper 770647, 1977

1.40 SAMAGA, B S, MURTHY, B S and NARAYANAMURTHI, R G
Flame Propagation in Spark Ignition Combustion Engines: A Mathematical Model
Indian J Tech, Nov 1974 vol 12

1.41 GAJENDRA BABU, M K and MURTHY, B S
Simulation and Evaluation of a Four Stroke Cylinder Spark Ignition Engine
SAE Paper 750687. 1975

1.42 SAMAGA, B S and MURTHY, B S
On the Problems of Predicting Burning Rates in a Spark Ignition Engine
SAE Paper 750688, 1975

1.43 SAMAGA, B S and MURTHY, B S
Investigations of a Turbulent Flame Propagation Model for Application for Combustion Prediction in the Spark Ignition Engine
SAE Paper 760758, 1976

1.44 LAVOIE, G A, HEYWOOD, J B and KECK, J C
Experimental and Theoretical Investigation of Turbulent Burning Model for Internal Combustion Engines
Comb Sci & Tech, 1970 vol 1

1.45 LAVOIE, G A, HEYWOOD, J B and KECK, J C
Experimental and Theoretical Study of Nitric Oxide Formation in Internal Combustion Engines
Comb Sci & Tech, 1970 vol 1

1.46 DANIELI, G A, FERGUSON, C R, HEYWOOD, J B and KECK, J C
Predicting the Emissions and Performance Characteristics of a Wankel Engine
SAE Paper 740186, 1974

1.47 DANIELI, G A, FERGUSON, C R, HEYWOOD, J B and KECK, J C
Analysis of Performance Losses in a Wankel Engine
Proc Inst Mech Eng Conf on Combustion in Engines, July 1975

1.48 PFLAUM, W
Heat Transfer in Internal Combustion Engines
Proc Conf Internazionale di Termotecnica, Milano, Nov 1962

1.49 EICHELBERG, G
Some new old Investigations on Combustion Engine Problems
Engineering, 1939 vol 148

1.50 ANNAND, W J D
Heat Transfer in the Cylinder of Reciprocating Internal Combustion Engines
Proc Inst Mech Eng, 1963 vol 177 no 36

1.51 KRIEGER, R B and BORMAN, G L
The Computation of Apparent Heat Release for Internal Combustion Engines
ASME Paper 66-WA/DGP-4, 1966

1.52 WOSCHNI, G
A Universally Applicable Equation for the Instantaneous Heat Transfer Coefficient in the Internal Combustion Engine
SAE Trans, 1967 vol 76 Paper 670913

1.53 BLUMBERG, P N and KUMMER, J
Prediction of Nitric Oxide Formation in Spark Ignited Engines - An Analysis of Methods of Control
Comb Sci & Tech, 1971

1.54 AIRMAN, W R
Engine Speed and Load Effects on Charge Dilation and Nitric Oxide Emissions
SAE Paper 720256, 1972

1.55 FELT, A E and KRAUSE, S R
Effects of Compression Ratio Changes on Exhaust Emissions
SAE Paper 710831, 1971

1.56 BENSON, J D and STEBAR, R F
Effects of Charge Dilation on Nitric Oxide Emissions for a Single Cylinder Engine
SAE Paper 710008, 1971

1.57 WENTWORTH, J T
Effects of Combustion Chamber Shape and Spark Ignition Location on Exhaust Nitric Oxide and Hydrocarbon Emissions
SAE Paper 740529, 1974

1.58 NEWHALL, H K and STARKMAN, E S
Directs Spectroscopic Determination of Nitric Oxide In Reciprocating Engine Cylinders
SAE Paper 670122, 1967

1.59 EYZAT, P and GUIBET, J C
A new look at Nitrogen Oxide formation in Internal Combustion Engines
SAE Paper 680124, 1968

1.60 BLUMBERG, P N
Nitric Oxide Emissions from Stratified Charge Engines: Prediction and Control
Comb Sci & Tech, 1973 vol 8

1.61 LAVOIE, G A and BLUMBERG, P N
Measurements of NO Emissions from a Stratified Charge Engine: Comparison of Theory and Experiment
Comb Sci & Tech, 1973 vol 8

1.62 ANNAND, W J D
Effect of Simplifying Kinetic Assumptions in Calculating Nitric Oxide Formation in Spark Ignition Engines
Proc Inst Mech Eng, 1974 vol 188

1.63 FENIMORE, C P
Formation of Nitric Oxide in Premixed Hydrocarbon Flames
Proc 13th Symp (Int) on Combustion, 1971

1.64 HOMER, J B and SUTTON, M M
Nitric Oxide Formation and Radical Overshoot in Premixed Hydrogen Flames
Comb & Flame, 1973 vol 20

1.65 HOMER, J B, JENKINS, D R and SUTTON, M M
Kinetsics of NO Formation
Comb Sci & Tech, 1971

1.66 DANIEL, W A
Flame Quenching at the Walls of an Internal Combustion Engine
Proc 6th Symp (Int) on Combustion, 1956

1.67 FRIEDMAN, R and JOHNSTON, W C
The Wall Quenching of Laminar Propane Flames as a Function of Pressure, Temperature and Air-Fuel Ratio
J Appl Phys, 1950 vol 21

1.68 WENTWORTH, J T and DANIEL, W A
Flame Photographs of Light Load Combustion Point the Way to Reduction of Hydrocarbons in Exhaust Gases
Trans Soc Automotive Engineers. 1955

1.69 GOTTENBERG, W G, OLSON, D R and BEST, H W
Flame Quenching during High Pressure, High Turbulence Combustion
Comb & Flame, 1963 vol 7

1.70 AGNEW, J T
Unburned Hydrocarbons in Closed Vessel Explosions: Theory Versus Experiment. Application to Spark Ignition Engine Exhaust
SAE Paper 670125, 1967

1.71 DANIEL, W A
Why Engine Variables Affect Exhaust Hydrocarbon Emissions
SAE Paper 700108, 1970

1.72 WENTWORTH, J T
Effect of Combustion Chamber Surface Temperature on Exhaust Hydrocarbons Concentration
SAE Paper 710587, 1971

1.73 DANIEL, W A and WENTWORTH, J T
Vehicle Emissions
SAE Technical Progress Series No 6, 1964

1.74 TABACZYNSKI, R J, HEYWOOD, J B and KECK, J C
Time-resolved Measurement of Hydrocarbon Mass Flow Rate in the Exhaust of a Spark Ignition Engine
SAE Paper 720112, 1972

1.75 HICKS, R E, PROBSTEIN, R F and KECK, J C
A Model of Quench Layer Entrainment during Blow down and Exhaust of the Cylinder on an Internal Combustion Engine
SAE Paper 750009, 1975

1.76 PANDURANGA, V
Correct Turbulence: A Way to Reduce the Concentrations of Unburnt Hydrocarbons from Automotive Engines
Comb & Flame, 1972 vol 18

1.77 GREEN, K A and AGNEW, J T
Quenching Distances of Propane-Air Flows on a Constant Volume Bomb
Comb & Flame, 1970 vol 15

CHAPTER 2 DESCRIPTION OF EQUIPMENT

INTRODUCTION

The majority of the experimental equipment used was obtained from normal commercial sources being generally well known. The exception was the Combustion Interval Meter which was designed and built specifically for this research. Several modifications were also made to an otherwise standard CFR research engine to enable the development of the flame front within the combustion chamber to be examined.

The CFR engine has been a familiar instrument in laboratories for several decades. It was designed initially for knock rating of fuels and is now accepted universally as a standard piece of test equipment. The specific performance of the engine is low however and efficiency has been sacrificed for stability of running and reliability. The operating conditions in terms of crankshaft rotational speed, combustion duration time, specific power output etc. are not representative of currently produced commercial units, but it is generally accepted that the combustion process can be explored successfully with this machine. Indeed the free availability of a large amount of experimental data on fundamental aspects of I.C. engine work performed with this unit is a great asset. A basis of comparison exists with the CFR engine which would not be the case for any commercially available multicylinder engine.

The experimental equipment centred around the CFR engine was designed specifically to enable constant operating conditions to be maintained during the examination of the combustion process, and to allow rapid collection of data.

2.1 THE CFR EXPERIMENTAL ENGINE

A suitably instrumented CFR variable compression ratio engine was adapted for use in this series of experiments. This is a well

established basic research tool and is used in various forms as an international standard for the rating of petrol, aviation and diesel fuels. The basic dimensions of the engine are listed in Table 2.1. A schematic diagram of the test bed layout is shown in Figure 2.1. Figure 2.2 is a photograph of the testbed. The following describes only the details of the engine of particular importance to this work along with modifications made to the standard unit.

2.1.1 The Multihole Cylinder

The variable compression ratio cylinder used in this series of engines is of one piece, with a cast iron cylinder head. The valve operating mechanism is mounted on a carrier situated on the top of the cylinder head and is of such a design as to maintain constant valve clearance irrespective of the vertical position of the cylinder relative to the crankcase. The multihole cylinder as used in this study is shown in section in Figures 2.3 and 2.4. The sparking plug was situated in port A (Figure 2.3) in a brass insert also housing an ionisation gap (Figure 2.5). A second ionisation gap was situated in port D. The remaining ports, B, C, E and F were used to house thermocouples described in a later section. A piezo-electric pressure transducer mounted in a water cooled adaptor was located as shown in Figure 2.4. The design of the adaptor and the choice of the pressure transducer are discussed in Appendix 1.

Modifications were made to the cylinder head as shown in Figures 2.4 and 2.5 to facilitate the location of four ionisation gap transducers on a diameter running through the spark plug port. The design of the ionisation gaps has been developed in the Mechanical Engineering Department over several years. A full account of this work and the installation of the transducers in the cylinder head has been given by Ellison (2.1).

2.1.2 The Engine Cooling System

A water filled gravity return evaporative cooling system was used with this engine. The advantage of this arrangement is its

Compression ratio range		3.5:1 to 18:1
Bore		3.25
Stroke		4.5
Displacement		37.33
Valve port diameter		1.18
Connecting rod bearings	diameter	2.25
	length	1.625
Front main bearings	diameter	3.00
	length	1.969
Rear main bearings	diameter	3.00
	length	3.25
Gudgeon pin diameter		1.25
Connecting rod length centre to centre		10.00
Piston rings number		5
Exhaust pipe diameter		1.25
Weight of engine (pounds)		800

Units are inches unless otherwise specified

TABLE 2.1 BASIC DIMENSIONS OF THE CFR ENGINE

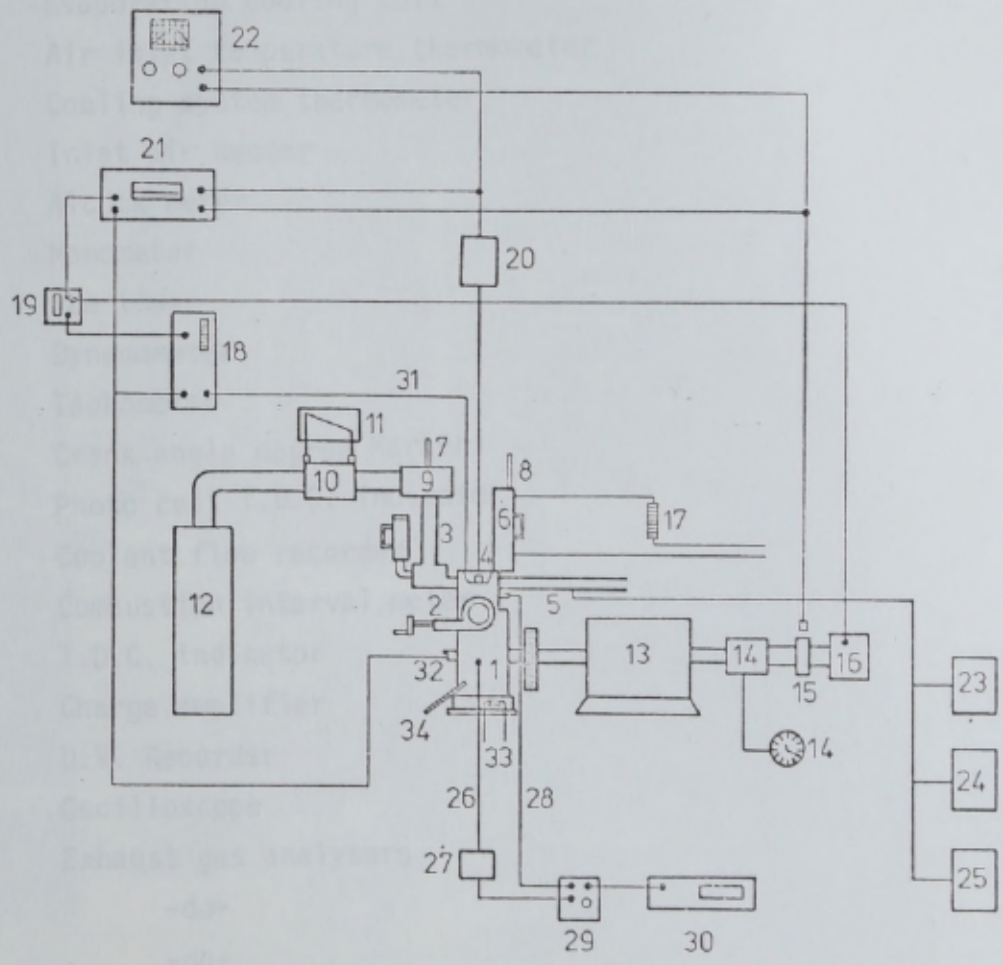

FIGURE 2.1 SCHEMATIC DIAGRAM OF TEST BED LAYOUT

KEY to FIGURE 2.1

1. CFR engine crank case
2. Compression control wheel
3. Carburettor inlet
4. Pressure transducer
5. Exhaust pipe
6. Evaporation cooling coil
7. Air inlet temperature thermometer
8. Cooling system thermometer
9. Inlet air heater
10. Alcock meter
11 Manometer
12 Ice tower
13. Dynamometer
14. Tachometer
15. Crank angle degree Marker
16. Photo cell T.D.C. indicator
17. Coolant flow recorder
18. Combustion interval meter
19. T.D.C. indicator
20. Charge amplifier
21. U.V. Recorder
22. Oscilloscope
23. Exhaust gas analysers
24. -do-
25. -do-
26. Piston thermocouples
27 Capacitor
28. Cylinder mean thermocouples
29. Selector switch
30. Digital volt meter
31. Ion gaps
32. Ignition pulse generator
33. Sump oil heater
34. Sump oil temperature indicator

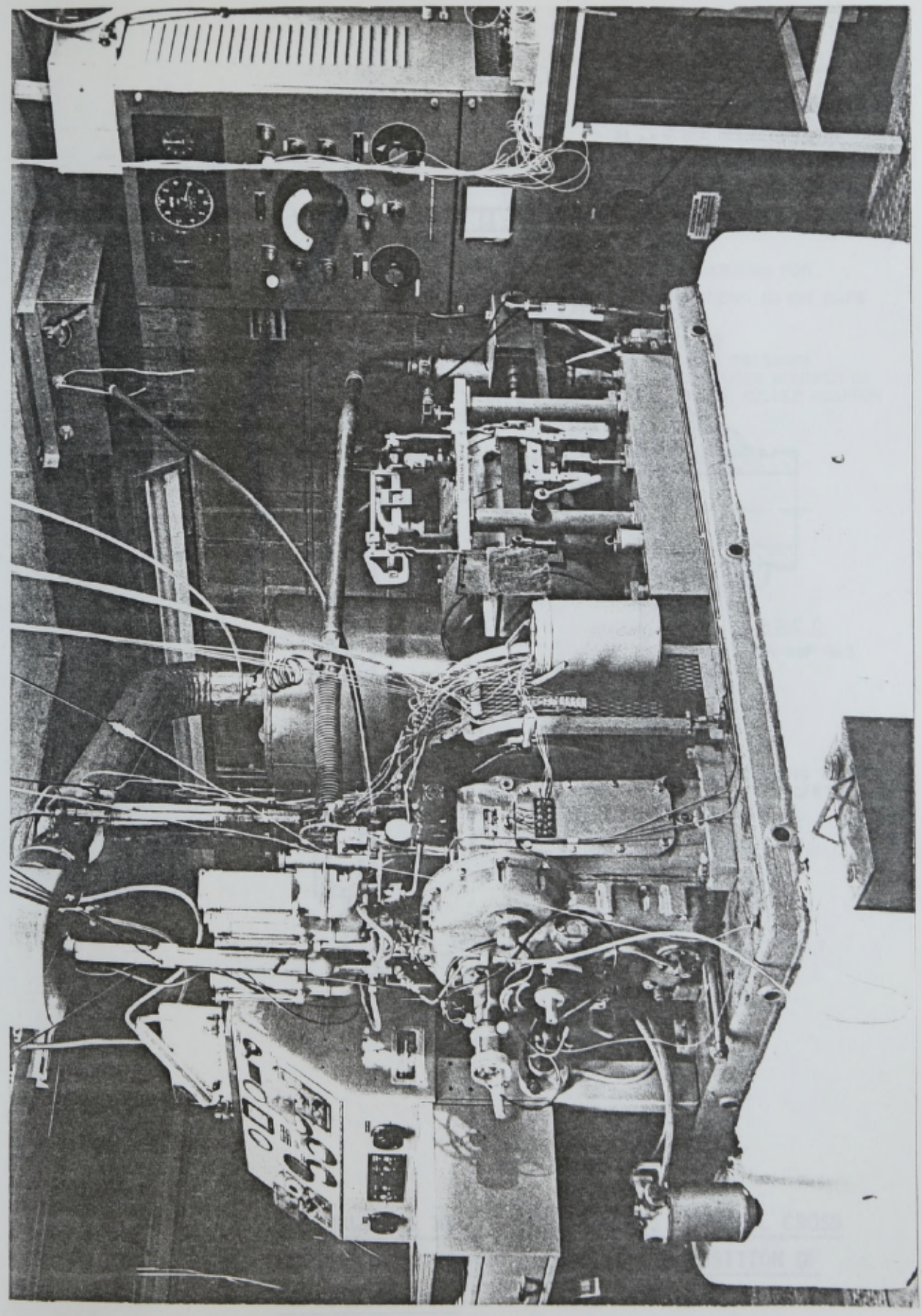

FIGURE 2.2 THE TEST BED

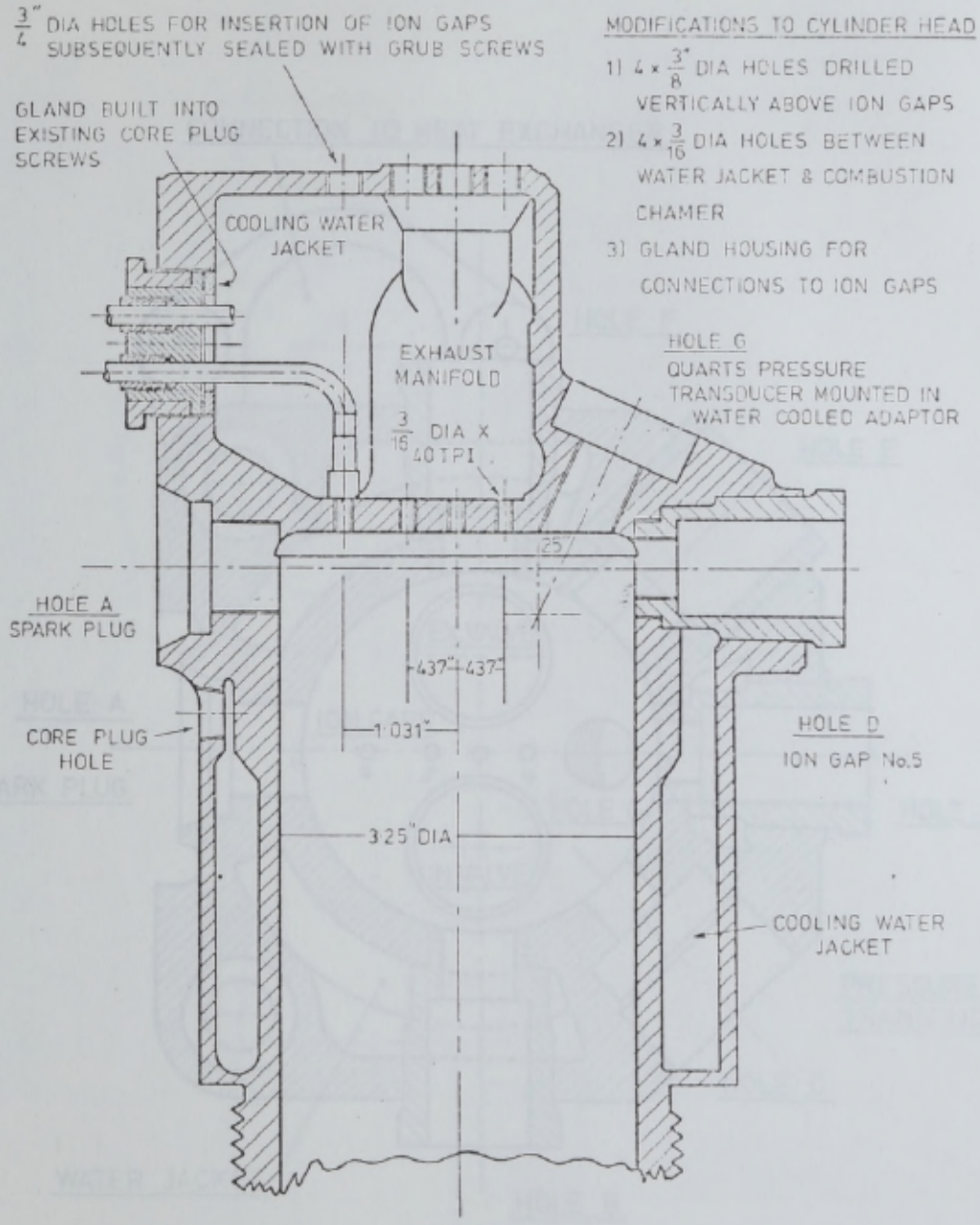

FIGURE 2.3 THE MULTIPLE HOLE CYLINDER HEAD: VERTICAL CROSS SECTION SHOWING MODIFICATIONS AND POSITION OF IONISATION GAPS

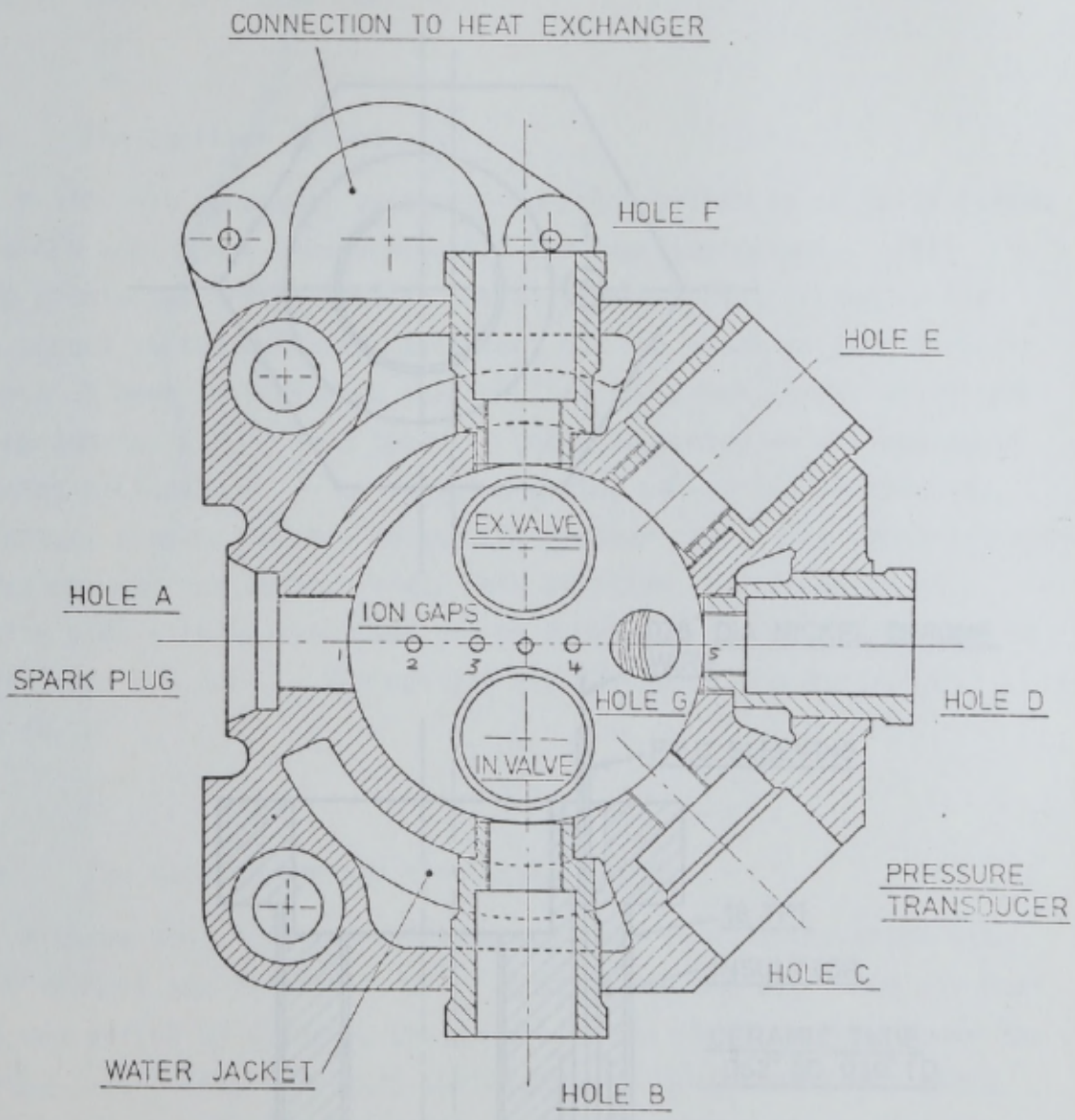

FIGURE 2.4 THE MULTIPLE HOLE CYLINDER HEAD: HORIZONTAL CROSS SECTION THROUGH SPARK PLUG

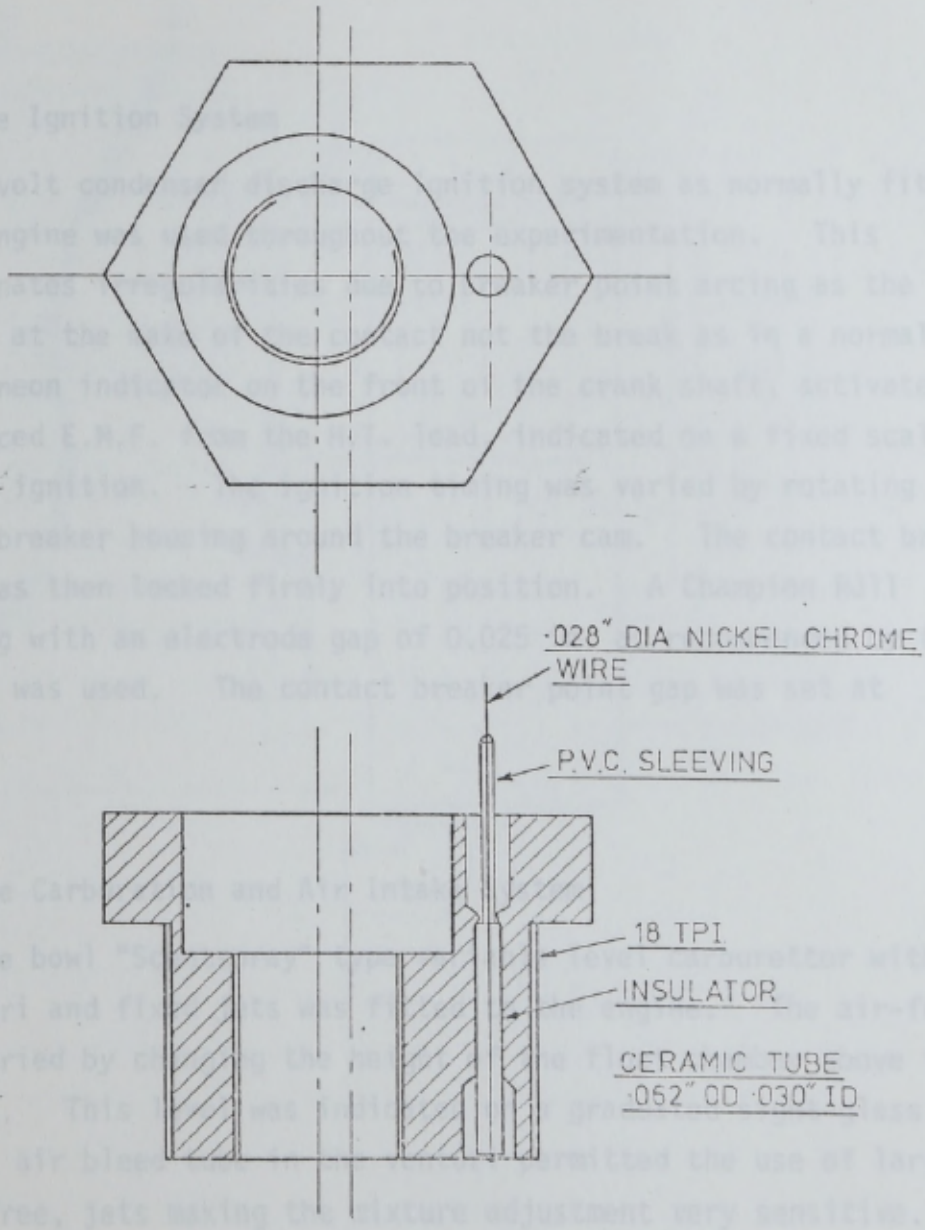

FIGURE 2.5 COMBINED 10mm SPARK PLUG ADAPTOR AND ION GAP

ability to maintain the cylinder head jacket temperature within very close limits irrespective of the operating conditions. The surge chamber and condenser unit were attached to the cylinder head. The mass flow rate and the temperature change of the cooling water used with this system was recorded. A schematic diagram of the cooling system is shown in Figure 2.6.

2.1.3 The Ignition System

A 110 volt condenser discharge ignition system as normally fitted to the CFR engine was used throughout the experimentation. This system eliminates irregularities due to breaker point arcing as the spark occurs at the make of the contact not the break as in a normal system. A neon indicator on the front of the crank shaft, activated from an induced E.M.F. from the H.T. lead, indicated on a fixed scale the point of ignition. The ignition timing was varied by rotating the contact breaker housing around the breaker cam. The contact breaker housing was then locked firmly into position. A Champion RJ11 sparking plug with an electrode gap of 0.025 in. as recommended by the manufacturer was used. The contact breaker point gap was set at 0.015 in.

2.1.4 The Carburation and Air Intake System

A three bowl "Scentspray" type variable level carburettor with single venturi and fixed jets was fitted to the engine. The air-fuel ratio was varied by changing the height of the float chamber above the metering jet. This level was indicated on a graduated sight glass. A horizontal air bleed tube in the venturi permitted the use of large size, clog free, jets making the mixture adjustment very sensitive.

An A.S.T.M. ice tower was installed upstream of the carburettor which saturated the air supply with a moisture content of 26 to 28 grains/lb. An Alcock viscous flow air meter was situated in the intake line between the ice tower and the surge tank mounted above the carburettor. The calibration curve of the flow meter is shown in

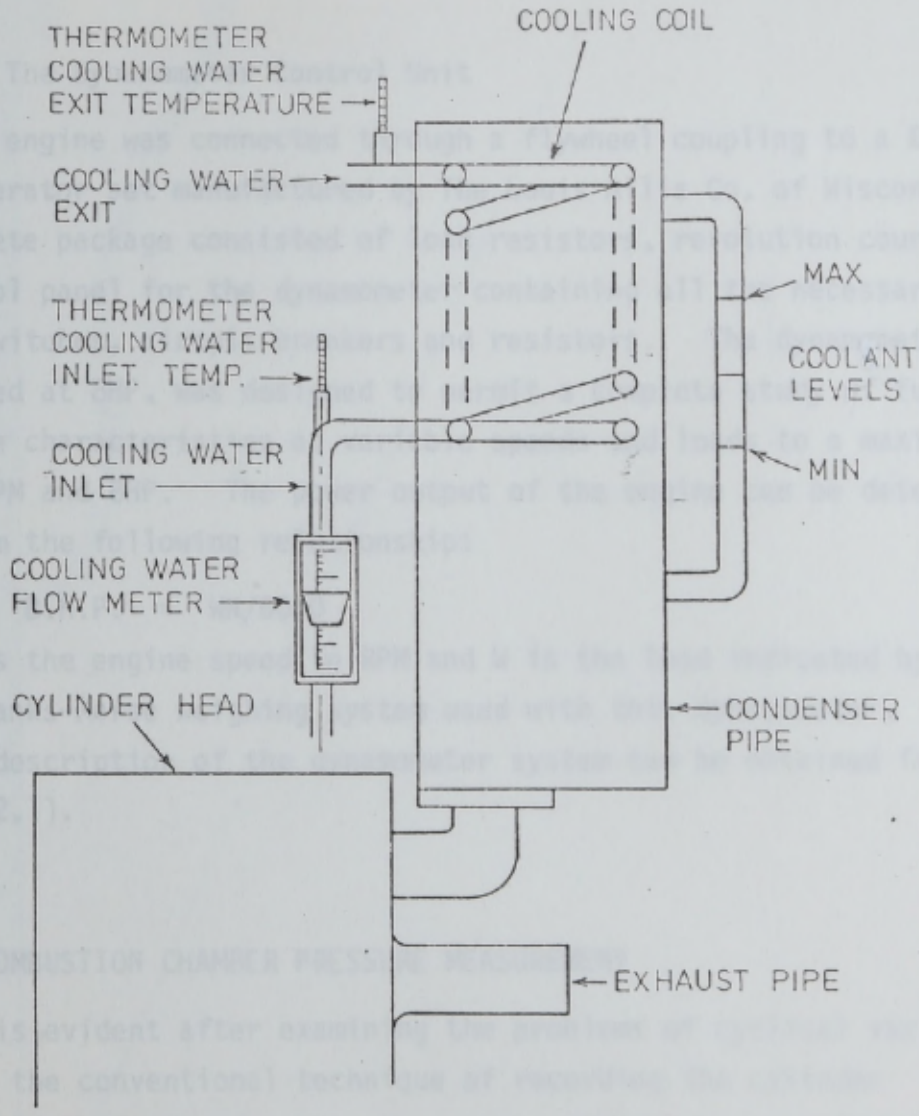

FIGURE 2.6 SCHEMATIC DIAGRAM OF THE ENGINE COOLING SYSTEM

Figure 2.7. A heater unit set into the surge tank and controlled from the main console was used to condition the air inlet temperature. A mercury in glass thermometer placed in the line between the surge tank and the carburettor indicated this air inlet temperature. A schematic diagram of the air intake system is shown in Figure 2.8.

2.1.5 The Dynamometer Control Unit

The engine was connected through a flywheel coupling to a D.C. motor generator set manufactured by The Louis Allis Co. of Wisconsin. The complete package consisted of load resistors, revolution counter and control panel for the dynamometer containing all the necessary meters, switches, circuit breakers and resistors. The dynamometer unit, rated at 8HP, was designed to permit a complete study of fuel and engine characteristics at variable speeds and loads to a maximum of 4000 RPM and 8HP. The power output of the engine can be determined from the following relationship:

$$B.H.P. = WN/6000$$

where N is the engine speed in RPM and W is the load indicated by the Fairbanks-Morse weighing system used with this dynamometer. A complete description of the dynamometer system can be obtained from Ellison (2.1).

2.2 COMBUSTION CHAMBER PRESSURE MEASUREMENT

It is evident after examining the problems of cyclical variations that the conventional technique of recording the cylinder pressure diagram on an oscilloscope screen obscures a significant cyclical pressure variation. It was decided therefore to record the pressure diagram on an ultra-violet recorder. The large trace thus obtained allowed a close examination of the variations and the relative fineness of the trace reduced the area of uncertainty. The traces obtained were to a base of crank angle degrees produced by a degree marker described in a later section. The remote control facility enabled the Bryans Southern series 70-430 U.V. recorder to

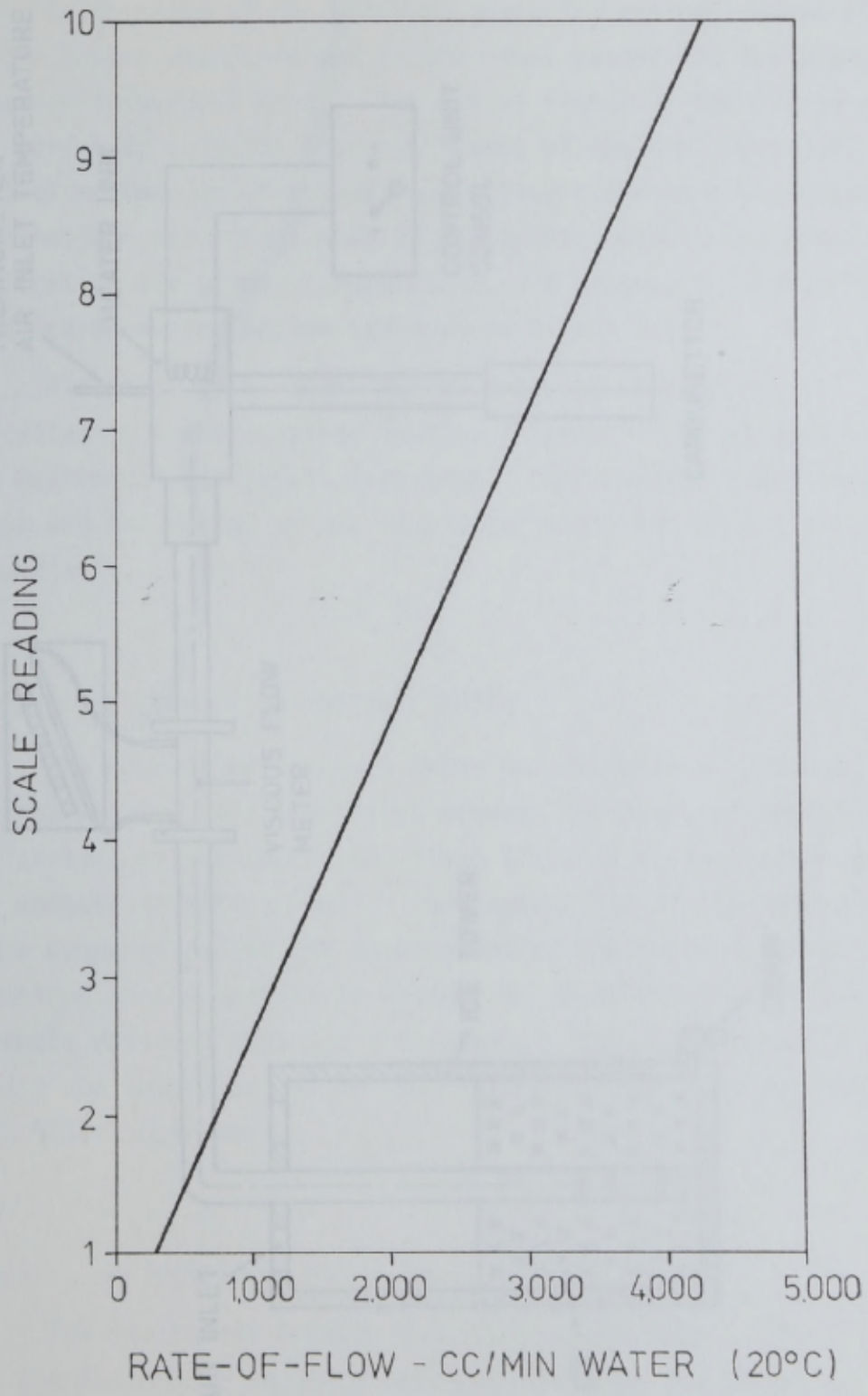

FIGURE 2.7 THE CALIBRATION CURVE OF THE FLOW METER

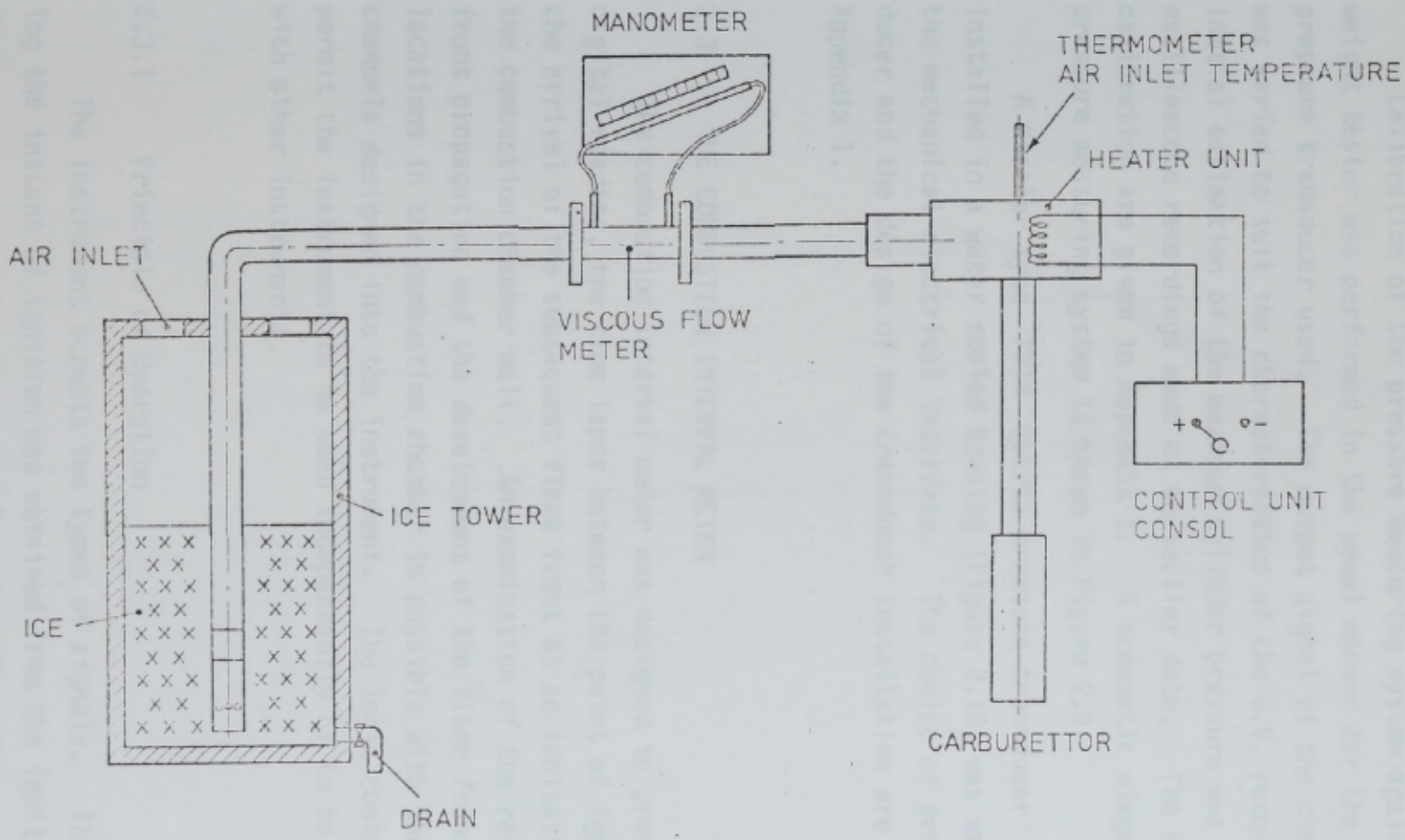

FIGURE 2.8 SCHEMATIC DIAGRAM OF THE AIR INLET SYSTEM

be used in conjunction with the combustion interval meter and the T.D.C. indicator.

Calibration of the pressure measuring system against a dead weight tester was performed in the usual manner for the piezo-electric pressure transducer used. The output signal of the charge amplifier was varied to suit the characteristics of the U.V. recorder. An initial estimation of the maximum cylinder pressure was obtained from oscilloscope recordings made at an earlier date. The details of the calibration are given in Appendix 1. A schematic diagram of the pressure measuring system is shown in Figure 2.9.

A Kistler type 701A quartz pressure transducer installed in a water cooled housing (Figure 2.10) was used to form the mechanical-electrical interface. The choice of pressure transducer and the design of the transducer installation are discussed in Appendix 1.

2.3 THE COMBUSTION INTERVAL METER

The combustion interval meter was designed to present, as a digital reading, the time lapse between the point of ignition and the arrival of the subsequent flame front at an ionisation gap set in the combustion chamber wall. An examination of the rate of flame front propagation and the development of the flame front at several locations in the combustion chamber is possible with the six input channels designed into the instrument. The logic controls also permit the instrument to be used independently or to be interfaced with other instruments.

2.3.1 Principle of Operation

The instrument accepts two types of signals. The first denoting the instant of ignition was obtained from the ignition system and the second registering the arrival of the flame front at a particular point in the combustion chamber was obtained from an ionisation gap. The basic pulse forms of these signals were modified in the instrument

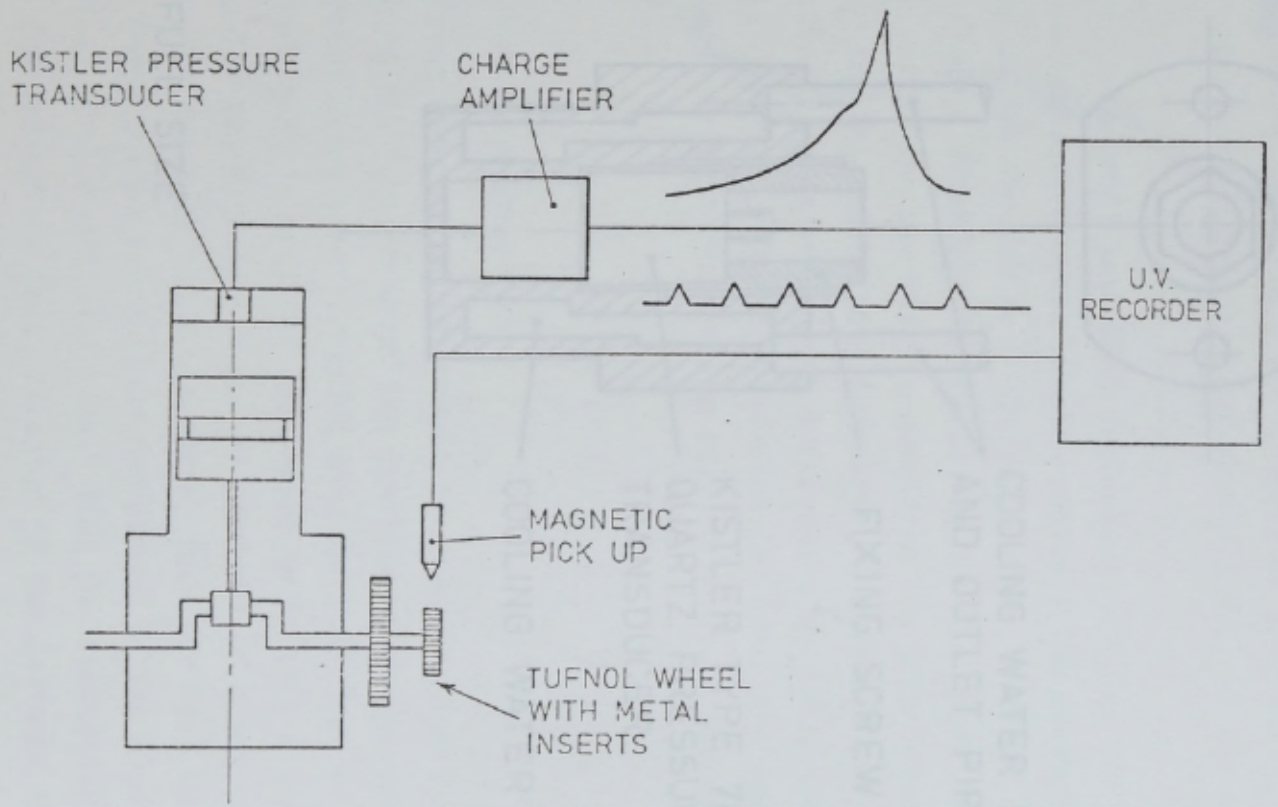

FIGURE 2.9 SCHEMATIC DIAGRAM OF THE CYLINDER PRESSURE MEASURING SYSTEM

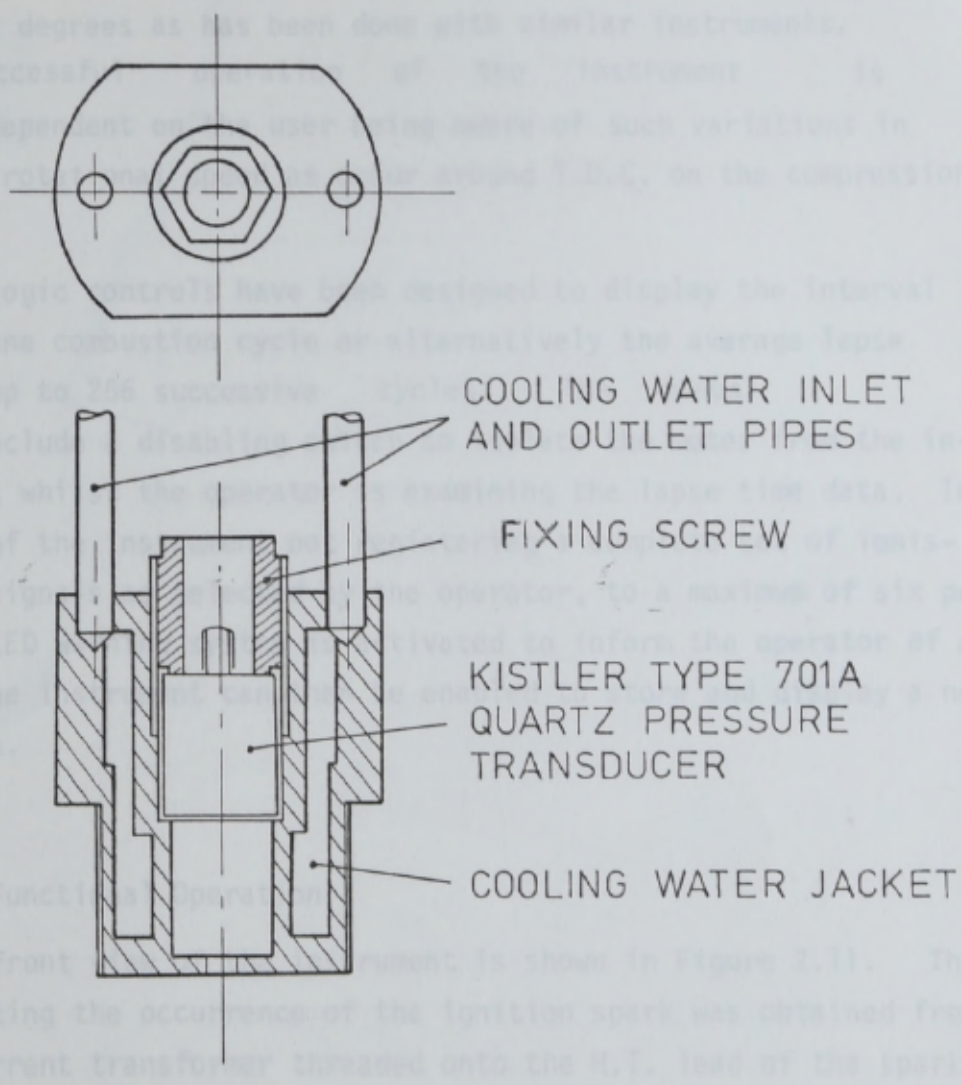

SCALE FULL SIZE

FIGURE 2.10 WATER COOLED MOUNTING ADAPTOR FOR QUARTZ PRESSURE TRANSDUCER

to square wave form, the leading edge of each corresponding to the point of interest. The time interval between the occurrence of the two leading edges thus represented the variable of interest. This time interval was displayed as real time rather than in terms of crank angle degrees as has been done with similar instruments. The successful operation of the instrument is therefore dependent on the user being aware of such variations in crankshaft rotational speed as occur around T.D.C. on the compression stroke.

The logic controls have been designed to display the interval times for one combustion cycle or alternatively the average lapse times for up to 256 successive cycles. The manual controls include a disabling switch to isolate the meter from the input signals whilst the operator is examining the lapse time data. In the event of the instrument not registering a complete set of ionisation gap signals as selected by the operator, to a maximum of six per cycle, an LED warning system is activated to inform the operator of an error. The instrument can then be enabled to store and display a new set of data.

2.3.2 Functional Operation

The front view of the instrument is shown in Figure 2.11. The signal marking the occurrence of the ignition spark was obtained from a small current transformer threaded onto the H.T. lead of the spark plug. This signal is modified and shaped to trigger a gating circuit controlling the registration of pulses produced by a crystal controlled oscillator into cascaded B.C.D. counters, four for each ionisation gap circuit. These pulses cease to be registered in the counter circuits at the arrival of a conditioned signal from the ionisation gap input channel. The ionisation gaps, situated in the cylinder head, were polarised by a steady potential 20 volts supplied from with the instrument. The lapse times are displayed on seven segment L.E.D. indicators driven from a B.C.D. decoder. The instrument was designed to record a pulse count of 9999 pulses but the least significant digit was not displayed as the uncertainty in calibration of the oscillator

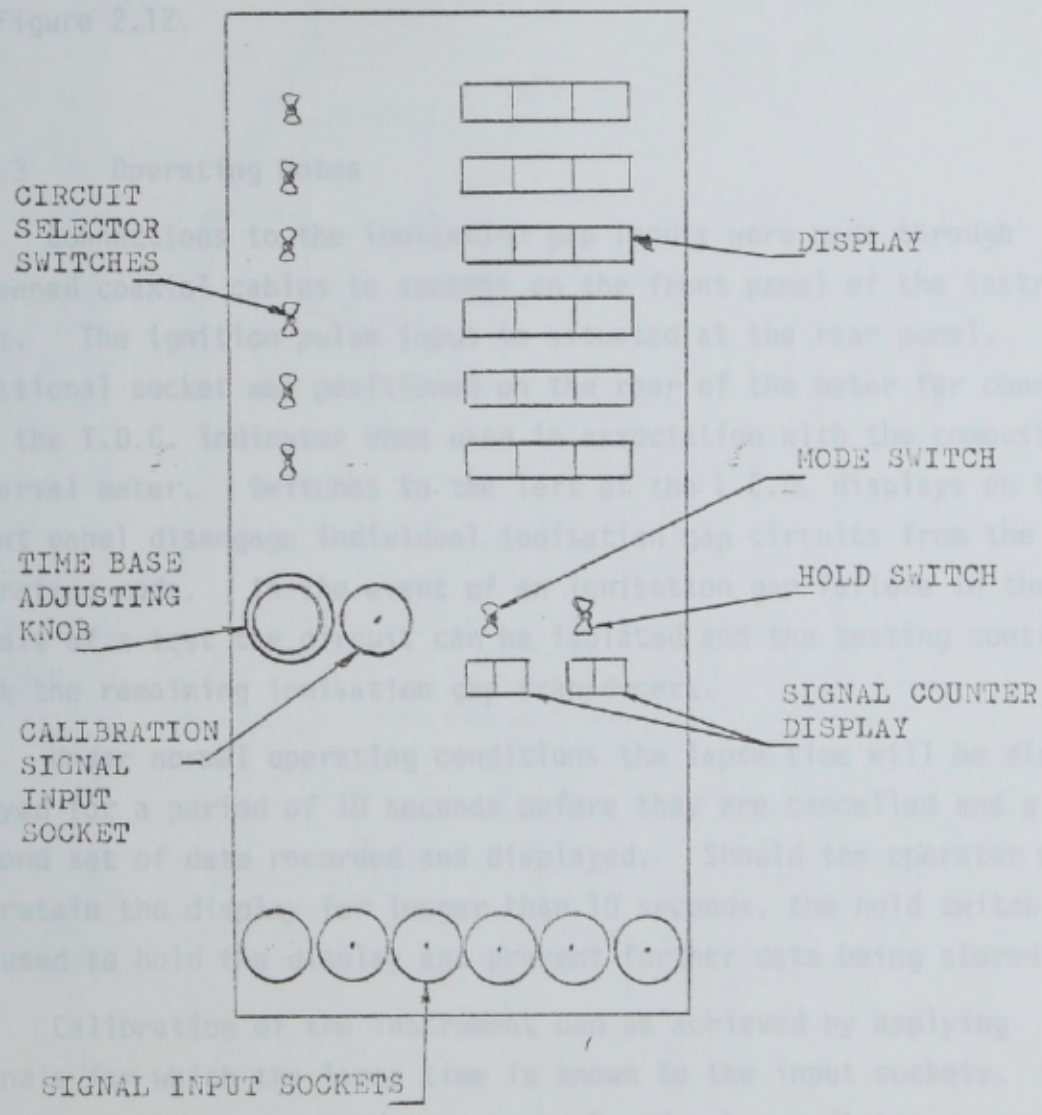

FIGURE 2.11 FRONT VIEW OF THE COMBUSTION INTERVAL METER

did not justify the inclusion of this count. The frequency of the oscillator was varied by adjusting a resistor set into the front of the instrument. Calibration was performed against a time mark generator or other suitable instrument.

The instrument is complete with its own inbuilt power supply operating off 230 volts AC. A block diagram of the meter is shown in Figure 2.12.

2.3.3 Operating Notes

Connections to the ionisation gap inputs were made through screened coaxial cables to sockets on the front panel of the instrument. The ignition pulse input is situated at the rear panel. An additional socket was positioned on the rear of the meter for connecting the T.D.C. indicator when used in association with the combustion interval meter. Switches to the left of the L.E.D. displays on the front panel disengage individual ionisation gap circuits from the operating mode. In the event of an ionisation gap failure in the middle of a test the circuit can be isolated and the testing continued with the remaining ionisation gap transducers.

Under normal operating conditions the lapse time will be displayed for a period of 10 seconds before they are cancelled and a second set of data recorded and displayed. Should the operator wish to retain the display for longer than 10 seconds, the hold switch can be used to hold the display and prevent further data being stored.

Calibration of the instrument can be achieved by applying signals for which the lapse time is known to the input sockets. Such signals can be derived from pickups placed a known distance apart and operated by a reference mark on a rotating disc or alternatively they can be derived from an electrical source.

2.4 THE CRANK ANGLE INDICATOR AND T.D.C. INDICATOR

The crank angle indicator was a proprietary unit manufactured by Southern Instruments Limited. It consisted essentially of a

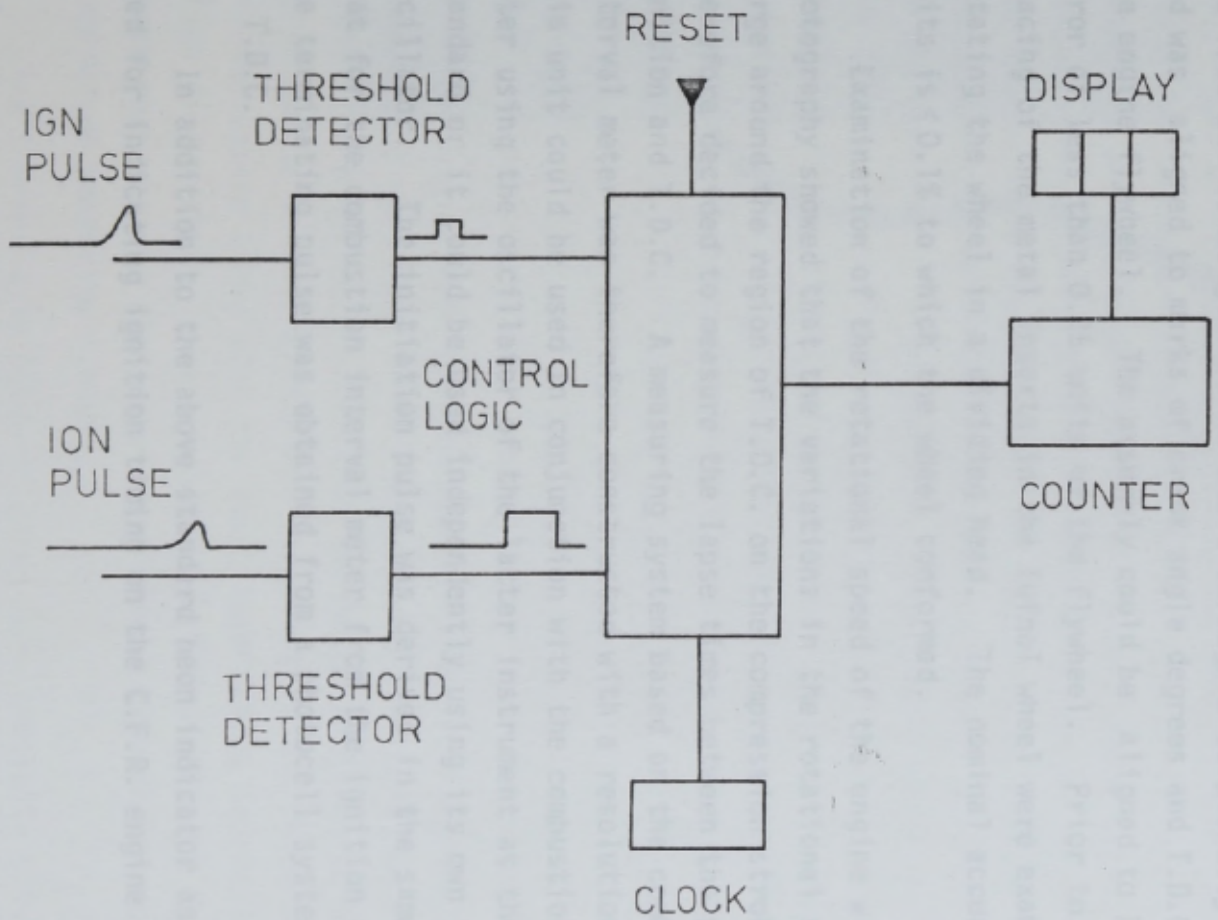

FIGURE 2.12 BLOCK DIAGRAM OF THE COMBUSTION INTERVAL METER

signal generator coupled to a signal conditioning and amplification unit. The output from the amplifier was a low voltage signal resembling an inverted V when viewed on an oscilloscope screen, with the centre of the V representing a datum point. The signals were produced by a magnetic pickup sensing strips of a ferrous material set into the circumference of a Tufnol wheel at 20° intervals. An extra three strips were inserted to produce a group of five strips at 10 intervals the centre one then representing T.D.C. The unit was connected to the free end of the dynamometer shaft through a torsionally stiff coupling and was aligned to marks of crank angle degrees and T.D.C. engraved on the engine flywheel. The assembly could be aligned to be within an error of less than 0.25 units of the flywheel. Prior to assembly the spacing of the metal inserts in the Tufnol wheel were examined by rotating the wheel in a dividing head. The nominal accuracy of these units is $< 0.1\%$ to which the wheel conformed.

Examination of the rotational speed of the engine with high speed photography showed that the variations in the rotational speed were large around the region of T.D.C. on the compression stroke. It was therefore decided to measure the lapse times between the point of ignition and T.D.C. A measuring system based on the combustion interval meter was therefore constructed with a resolution of 0.01 ms. This unit could be used in conjunction with the combustion interval meter using the oscillator of the latter instrument as the frequency standard or it could be used independently using its own internal oscillator. The initiation pulse was derived in the same way as that for the combustion interval meter from the ignition system and the terminating pulse was obtained from a photocell system triggered at T.D.C.

In addition to the above standard neon indicator as normally used for indicating ignition timing on the C.F.R. engine was retained.

2.5 THE PISTON AND PISTON TEMPERATURE MEASURING EQUIPMENT

The cast-iron piston had a fully floating gudgeon pin of 1.25in. diameter and was fitted with five compression rings. The top land of the piston was large compared with modern designs with a large

quench zone for the collection of unburnt fuel. The very adequate oil supply system and oil temperature control system coupled with the relatively low power output of the engine practically eliminated the possibility of overheating and subsequent breakdown of the piston.

A series of chrome/alumel thermocouples was installed in the piston crown on a diameter running from the spark plug (Figure 2.13). The problems of monitoring the piston temperature of an internal combustion engine has been the topic of much study (References 2.2 and 2.3). The difficulty of extracting the thermocouple signals from within the crankcase has been solved in several different ways, each having its own merits and demerits. A continuous signal could be obtained through the use of a radio-link system or the use of continuous thermocouple leads arranged on some form of linkage. The first mentioned method was disregarded because several channels were required and the problems of modulating the thermocouple signal on an RF carrier made the system unattractive. The possibility of an engine strip and rebuild, part way through the experimentation, due to fracture of one of several thermocouple leads precluded the use of the second method mentioned above and an intermittent contact system was adopted in this instance.

2.5.1 The Intermittent Contact Temperature Measuring Technique

The intermittent contact system for monitoring piston crown temperatures owes much of its development to BICERA and Ricardo and Co.Ltd. A brief account of this technique is given in Reference 2.3. The technique is essentially the insertion of the thermocouple bead into the piston crown with the leads terminating in resiliant contacts at the piston skirt. At around B.D.C. these contacts engage with impact contacts and thus complete a normal type of thermocouple temperature measuring circuit.

The thermocouple leads of 24swg were initially silver-soldered into conical housings (Figure 2.14) which in turn were inserted into a taper reemed hole in the piston crown with the leads hanging inside the piston skirt (Figure 2.15). The thermocouple leads were then run across the underside of the piston crown and down the skirt, being

FIGURE 2.13 POSITION OF THERMOCOUPLES IN THE PISTON CROWN

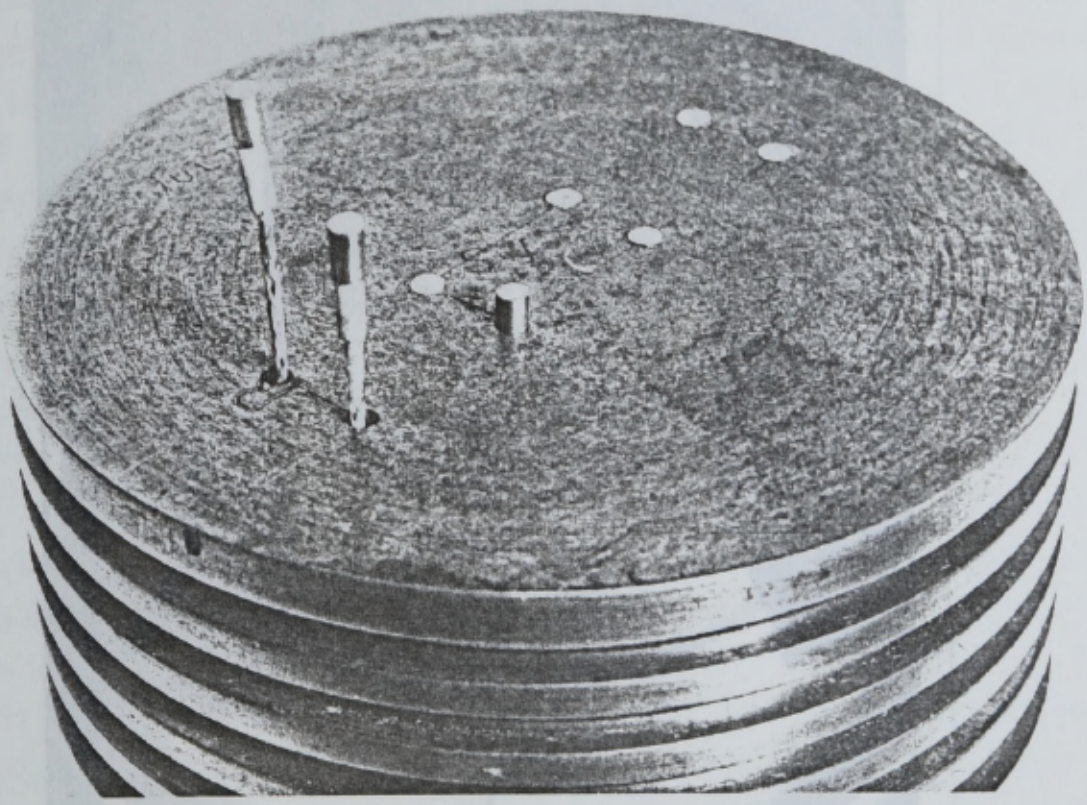

FIGURE 2.14 INSERTION OF THERMOCOUPLES IN PISTON CROWN

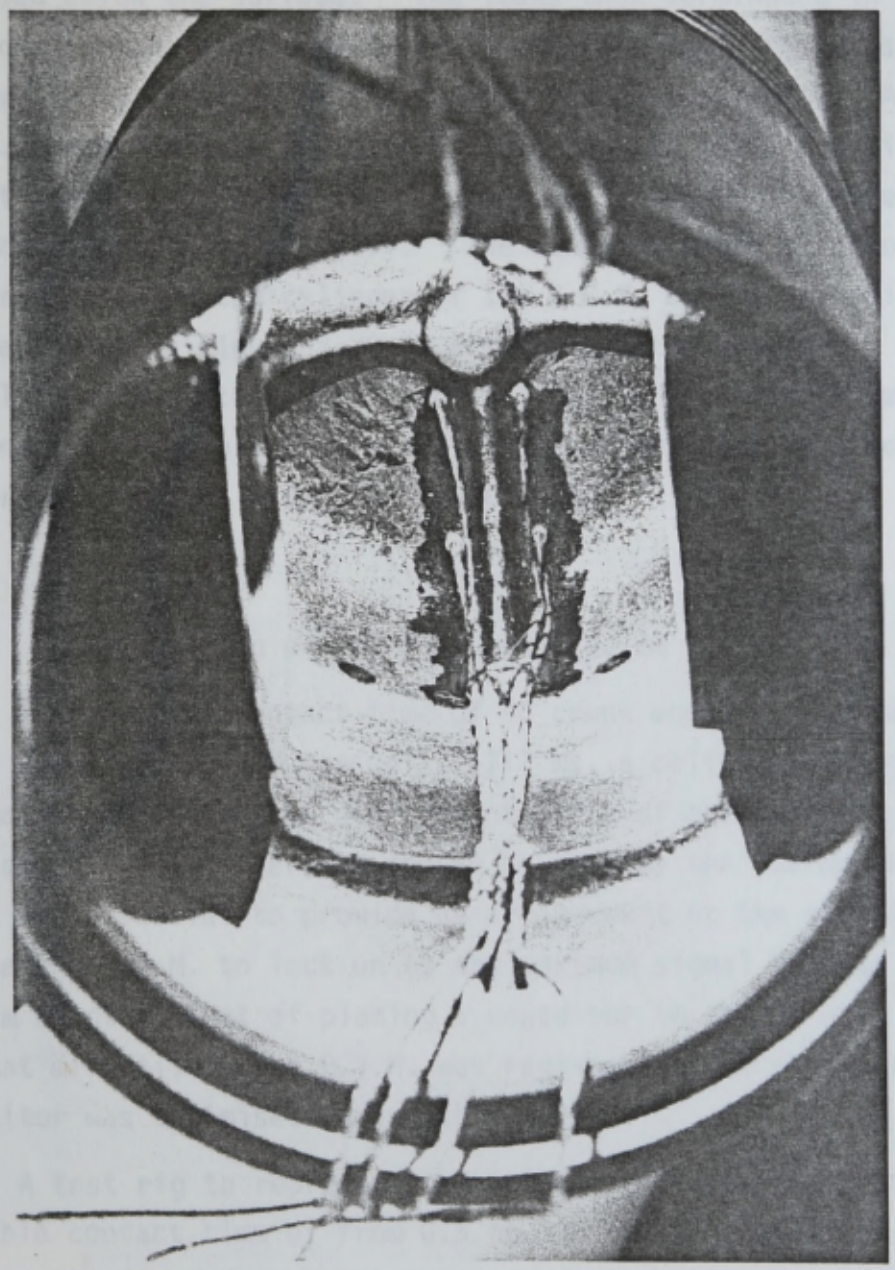

FIGURE 2.15 THERMOCOUPLE LEADS HANGING INSIDE THE PISTON SKIRT

secured with a strap located in one of the piston ring grooves and recessed below the surface. The leads then terminated in silver steel contacts (Figure 2.16) supported in but insulated from a machined ring (Figure 2.17) situated at the base of the piston skirt. At around B.D.C. these contacts are brought into contact with berrilium-copper impact spring type contacts (Figure 2.18) situated on hangers in the crankcase mouth (Figure 2.19). The sandwich plate positioned between the crankcase and the cylinder of the C.F.R. engine was slightly modified as shown in Figure 2.20 to accommodate the hangers. Chromal-alumel leads were then drawn from the spring contacts to emerge through a gland set (Figure 2.21) in the crankcase and then to a conventional measuring system as shown in Figure 2.22.

2.5.2 Calibration of the measuring system

As the total contact time of 40 crank angle degrees at a rotational speed of 900 RPM was only 0.711 ms. a calibration procedure was adopted to establish the overall integrity of the system. A solartron digital volt meter was chosen to display the thermocouple E.M.F. so it was essential to provide an arrangement at the signal input to enable the D.V.M. to lock on to the maximum signal voltage. The system adopted, that of placing a capacitor in series with the D.V.M. so that effectively the D.V.M. was registering the charge across the capacitor was optimised during this work.

A test rig to represent the intermittent contact system with a variable contact time of from 0.5 to 3.0 ms. was constructed and the calibration of a thermocouple connected to the contacts and thence a D.V.M. via the capacitor was compared with that of a normal thermocouple connected to the same D.V.M. at the same temperature. In both cases an ice junction was utilised. Various capacitors were used in the circuit, 10 μf being found to produce the maximum stability of the D.V.M. The calibration of the thermocouples in the piston was then performed with the piston inserted in a fluidised bed calibration bath against an NPL mercury in glass thermometer. An initial calibration was performed with the contacts of the test rig closed and then a series of points for several contact speeds were recorded. At higher

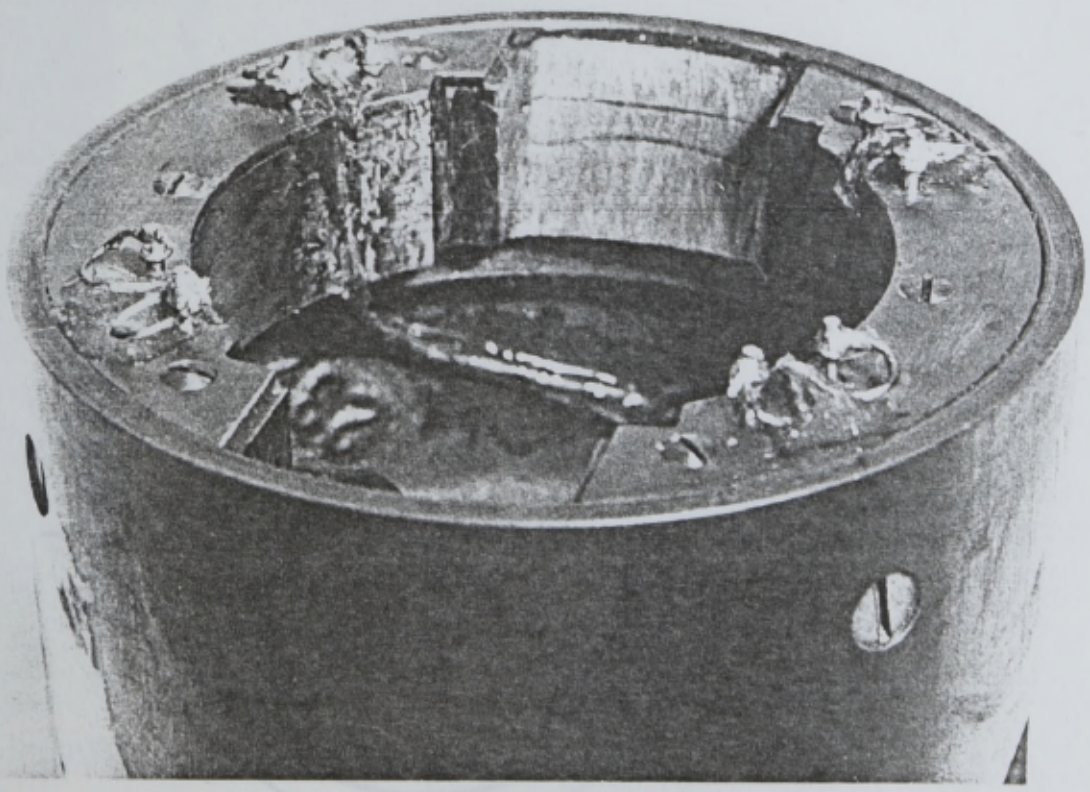

FIGURE 2.16 SILVER STEEL CONTACTS AT THE BASE OF THE PISTON SKIRT

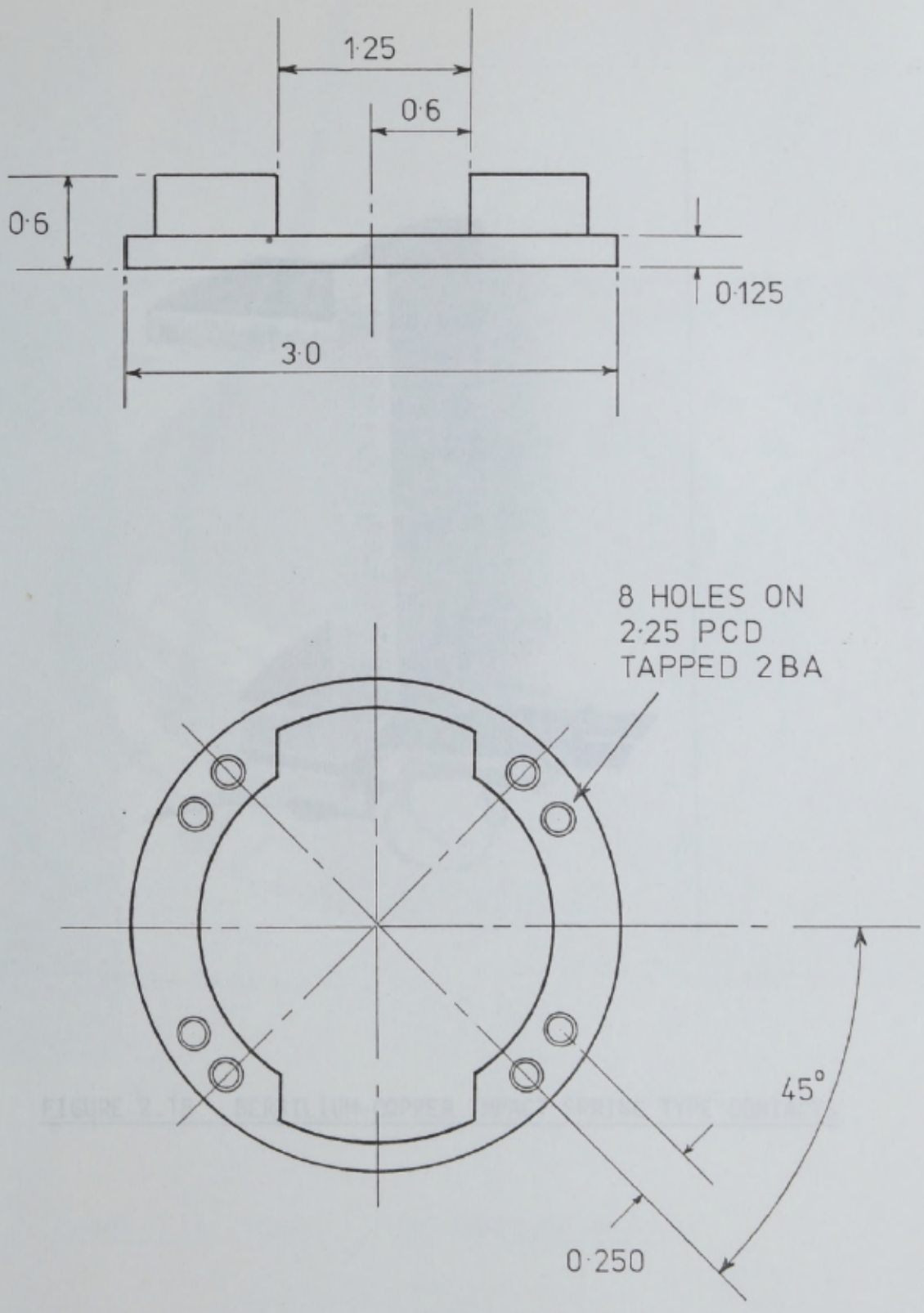

FIGURE 2.17 DIAGRAM OF MACHINED RING AT BASE OF PISTON SKIRT

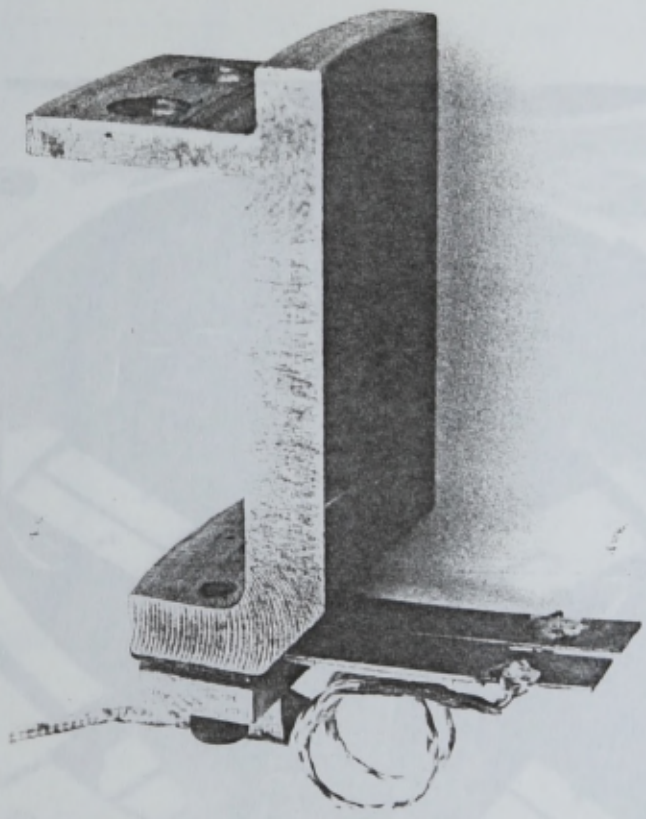

FIGURE 2.18 BERRILIUM-COPPER IMPACT SPRING TYPE CONTACTS

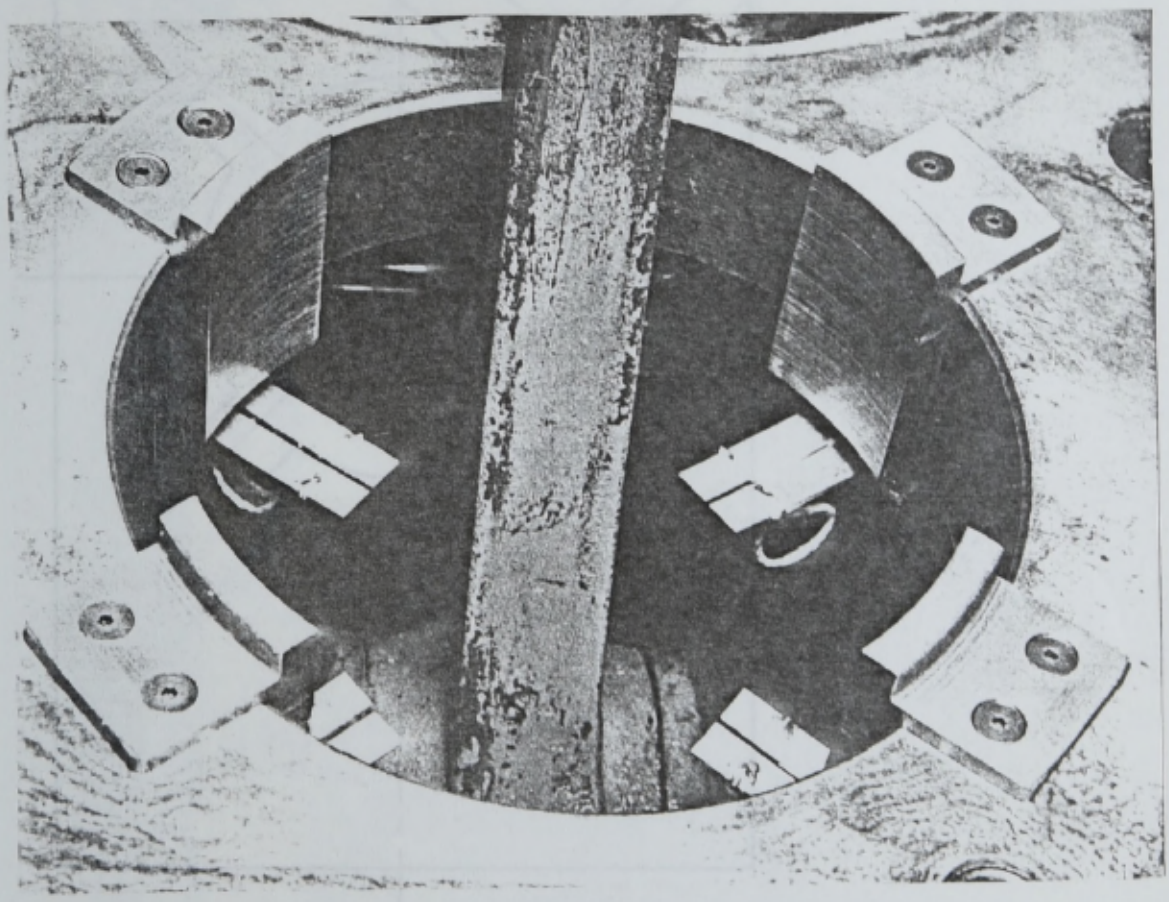

FIGURE 2.19 HANGERS IN THE CRANKCASE MOUTH

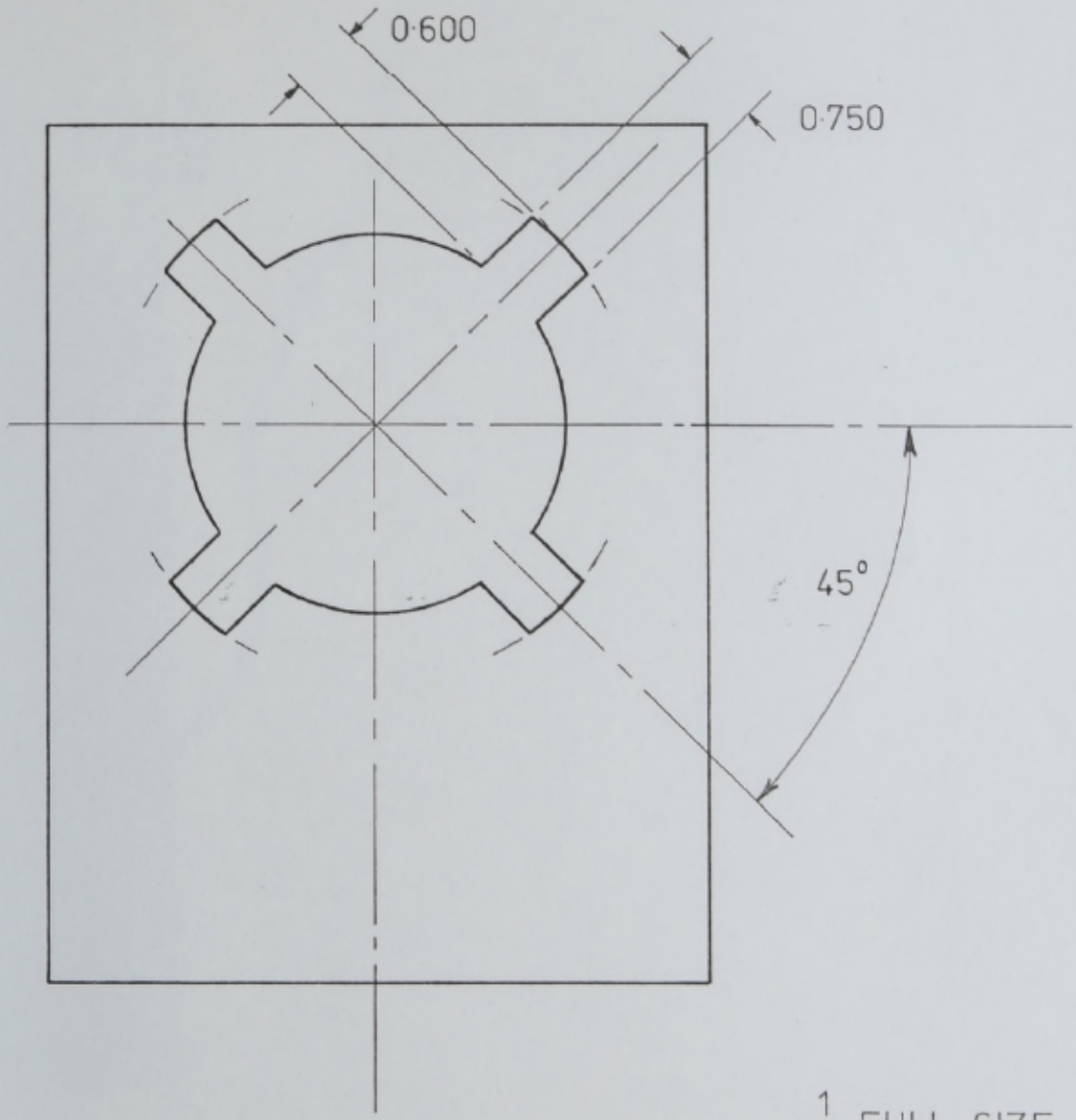

FIGURE 2.20 MODIFICATION OF SANDWICH PLATE BETWEEN CRANKCASE AND CYLINDER

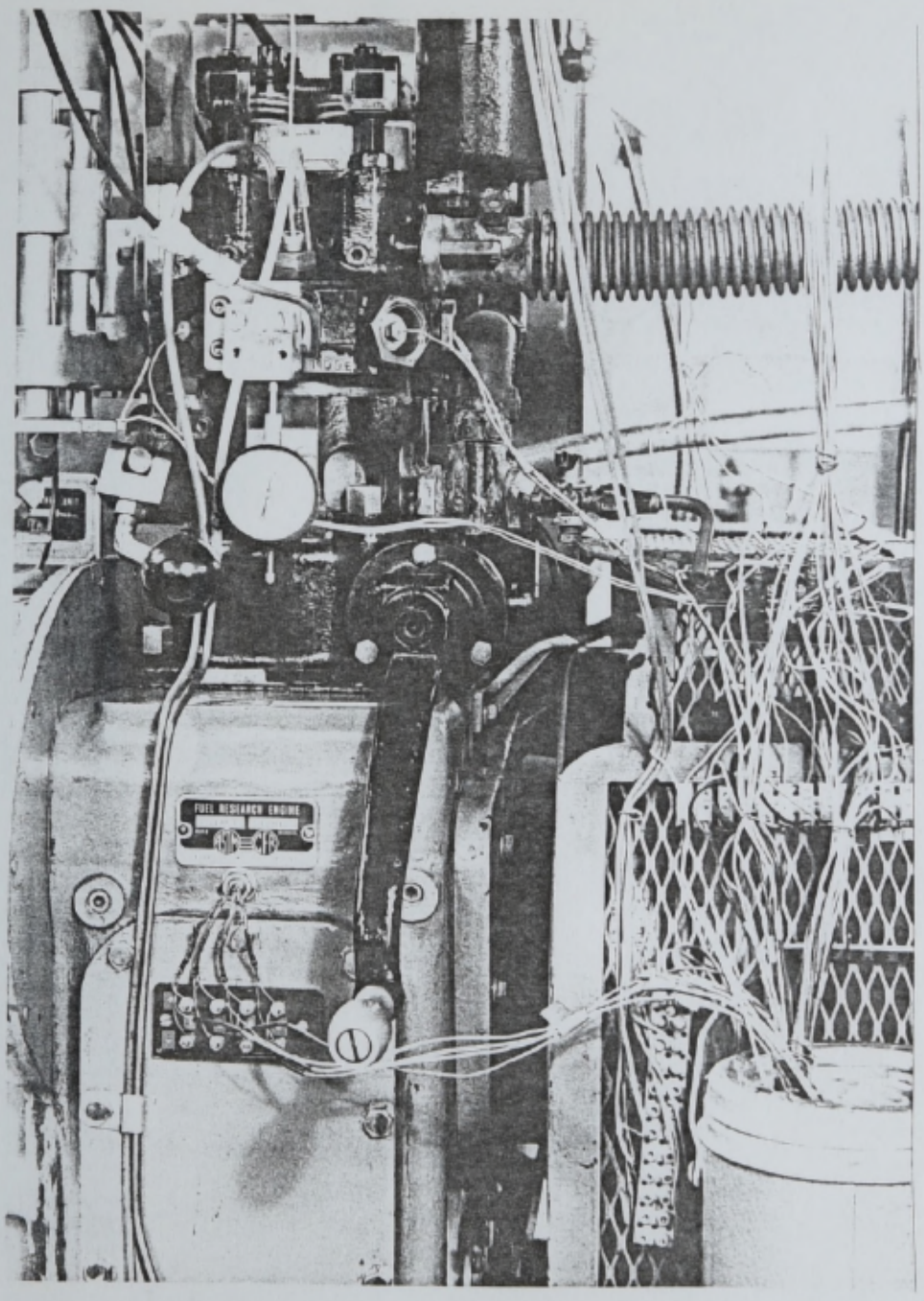

FIGURE 2.21 GLAND SET IN CRANKCASE

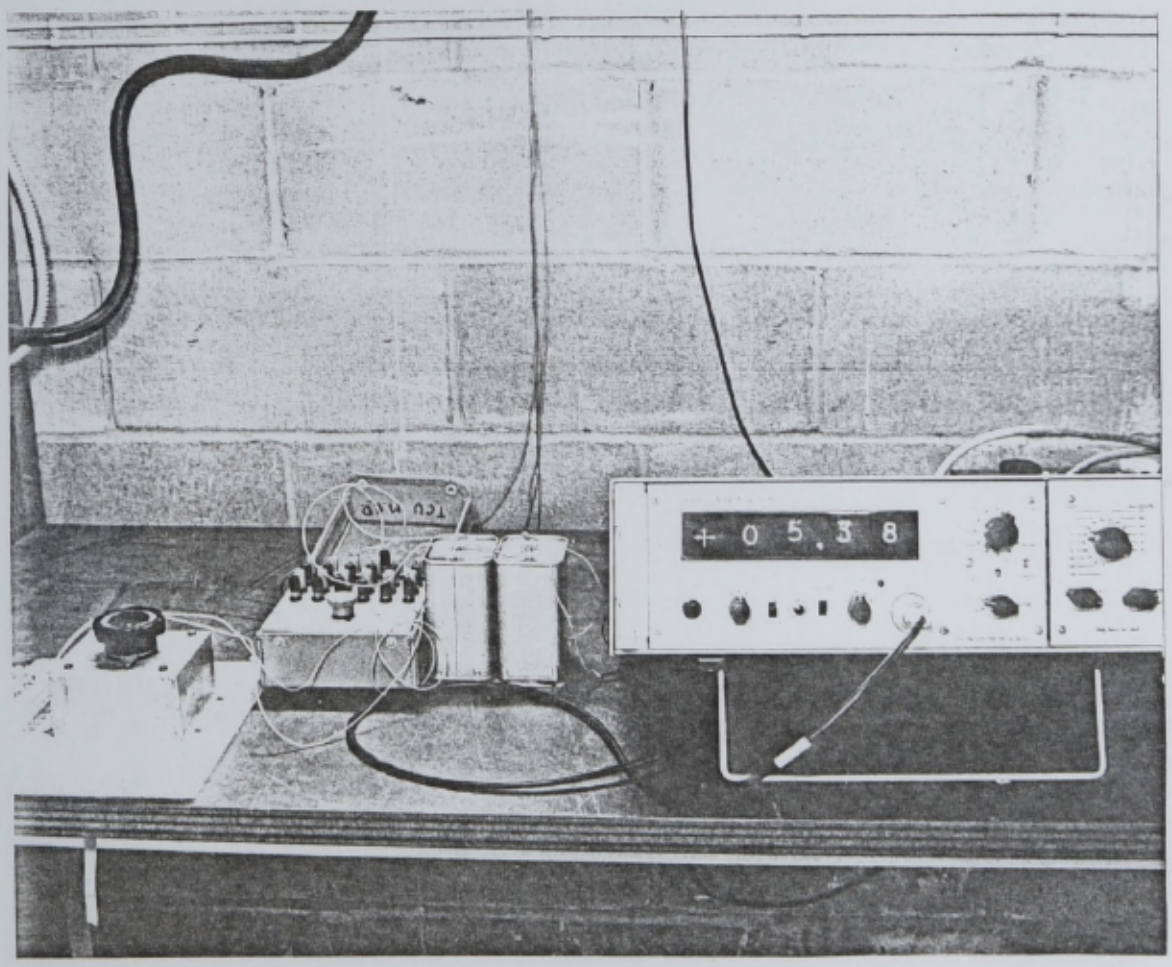

FIGURE 2.22 CONVENTIONAL THERMOCOUPLE MEASURING SYSTEM

speeds an upper limit was reached due to contact bounce. This is an inherent fault of the leaf spring type contacts that may be overcome with the adoption of contacts with a piano-key type of operation. The calibration curves of the piston thermocouples are shown in Appendix 1.

2.6 THE COMBUSTION CHAMBER SURFACE THERMOCOUPLES

Measurement of a combustion chamber surface temperature that is exposed to a rapidly varying temperature field is a severe problem. Uncertainty with regard to the exact location of a thermocouple bead can lead to large errors both in the amplitude of the temperature variation and the phase relationship of the temperature field and the thermocouple signal. Table 2.2 shows this clearly. An error in the location of the bead of 0.005 in. for example will reduce the amplitude of the temperature variation to only 14% of the value at the surface for a typical carbon steel cylinder head. In addition the presence of the thermocouple acting as a heat sink will also contribute to the level of uncertainty. As the wall temperature is considered to be a prime variable in the formation of hydrocarbon quench layers (Reference 2.4) and since heat transfer losses can effect engine power output it was decided to insert thermocouples into plugs situated in ports as shown in Figure 2.4.

The thermocouple heads were based on a design produced by the British Cast Iron Research Association and used by Knight (2.5). A sectioned drawing of the thermocouple head is shown in Figure 2.23. 24 swg wire chromel/alumel leads were silver soldered into supports and assembled into plugs, to be installed in the cylinder head ports, as shown in Figure 2.24. The combustion chamber face of the assembly was then machined to produce a flat surface at the flame face.

A conventional measuring system of cold junction, selector switch and digital indicator was used in the experimentation as shown schematically in Figure 2.22. The thermocouples were calibrated against an N.P.L. mercury thermometer in a fluidised bed calibration bath.

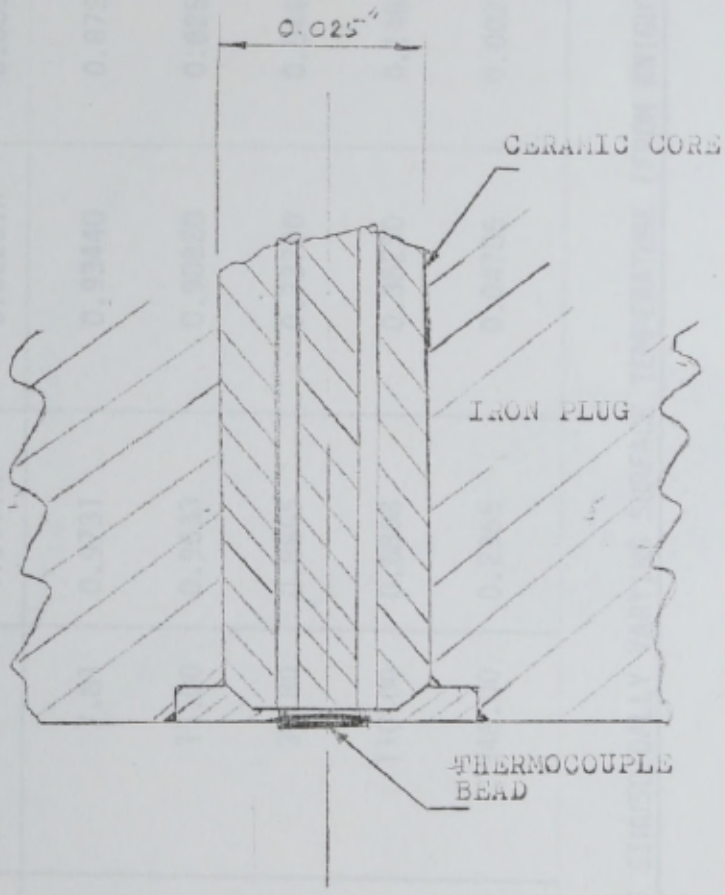

FIGURE 2.23 SECTIONED DRAWING OF THERMOCOUPLE HEAD

Frequency c/s	Period as Harmonic of four stroke cycle at 1000 RPM	Phase lag at depth 0.005in C.A. degrees	Ratio of amplitude at depth stated to amplitude at surface		
			0.001in	0.0025in	0.005in
5	0.6	7.81	0.9731	0.93440	0.872800
10	1.2	11.00	0.9633	0.90820	0.825000
100	12.0	34.80	0.8855	0.73790	0.544500
1000	120.0	110.00	0.6808	0.38230	0.146200
10000	1200.0	348.00	0.2965	0.04786	0.002291

TABLE 2.2 PREDICTION OF EFFECT OF SINUSOIDALLY VARYING SURFACE TEMPERATURE (FROM KNIGHT (2.5))

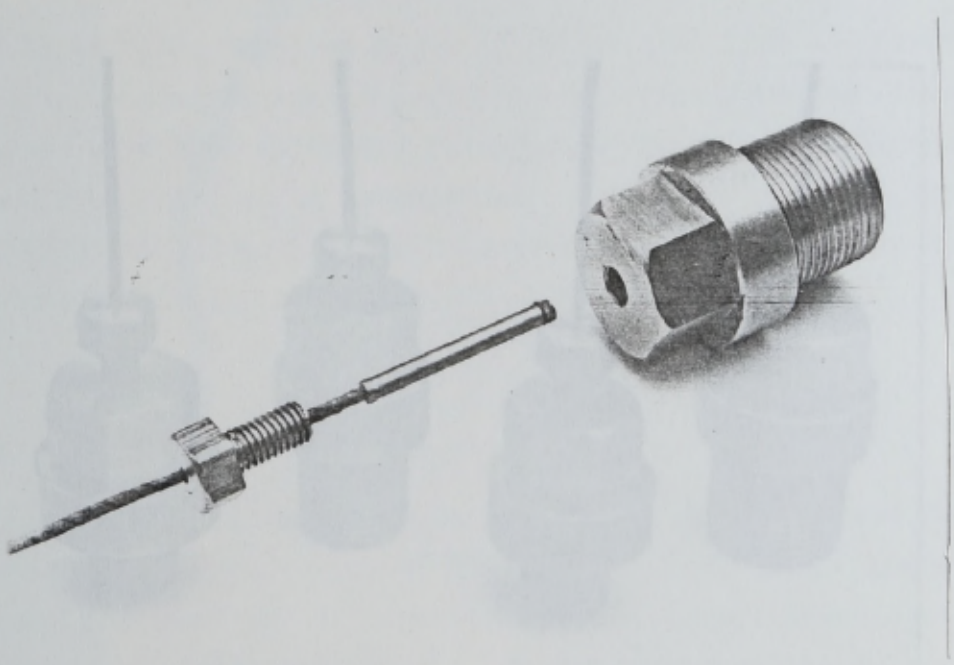

FIGURE 2.24 THERMOCOUPLE AND PLUG PRIOR TO ASSEMBLY

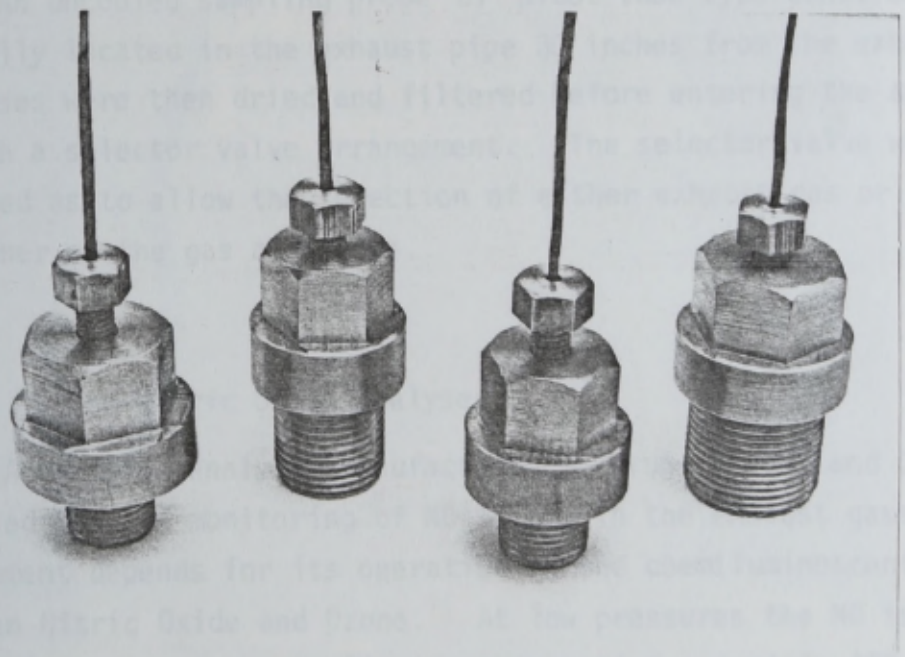

FIGURE 2.25 THERMOCOUPLES AND PLUGS PRIOR TO INSERTION IN CYLINDER HEAD PORTS

2.7 THE EXHAUST GAS ANALYSIS EQUIPMENT

Gas analysis equipment to monitor the time averaged concentrations of Carbon Monoxide, Hexane and Nitric Oxide in the exhaust gases was arranged as shown in Figures 2.26 and 2.27. In the absence of a British Standard relating to the sampling of exhaust gases the system was set up according to the manufacturer's advice and the accepted method used in the department.

2.7.1 The Sampling System

An uncooled sampling probe of pitot tube type construction was centrally located in the exhaust pipe 30 inches from the exhaust port. The gases were then dried and filtered before entering the analysers through a selector valve arrangement. The selector valve was so constructed as to allow the selection of either exhaust gas or span gas to either of the gas analysers.

2.7.2 The Nitric Oxide Analyser

A Chemitox analyser manufactured by Grub-Parsons and Co.Ltd. was used for the monitoring of NO levels in the exhaust gases. The instrument depends for its operation on the chemiluminescent reaction between Nitric Oxide and Ozone. At low pressures the NO is oxidised by Ozone to form Nitrogen Dioxide, NO_2. Approximately 10% of the resulting NO_2 is in an excited state; this excited NO_2 decays to the non-excited state by the emission of near infrared radiation. The intensity of the radiation is directly proportional to the amount of NO reacting with the ozone. The emitted radiation is detected by a photomultiplier. The signal is amplified and conditioned to produce an output proportional to the original NO concentration. In the instrument the low pressure is obtained by a rotary vacuum pump connected to the reaction chamber.

Calibration of the instrument is achieved by using pure Nitrogen as a zero gas after the stabilisation of the photomultiplier dark current level. The span was calibrated against a gas cylinder of

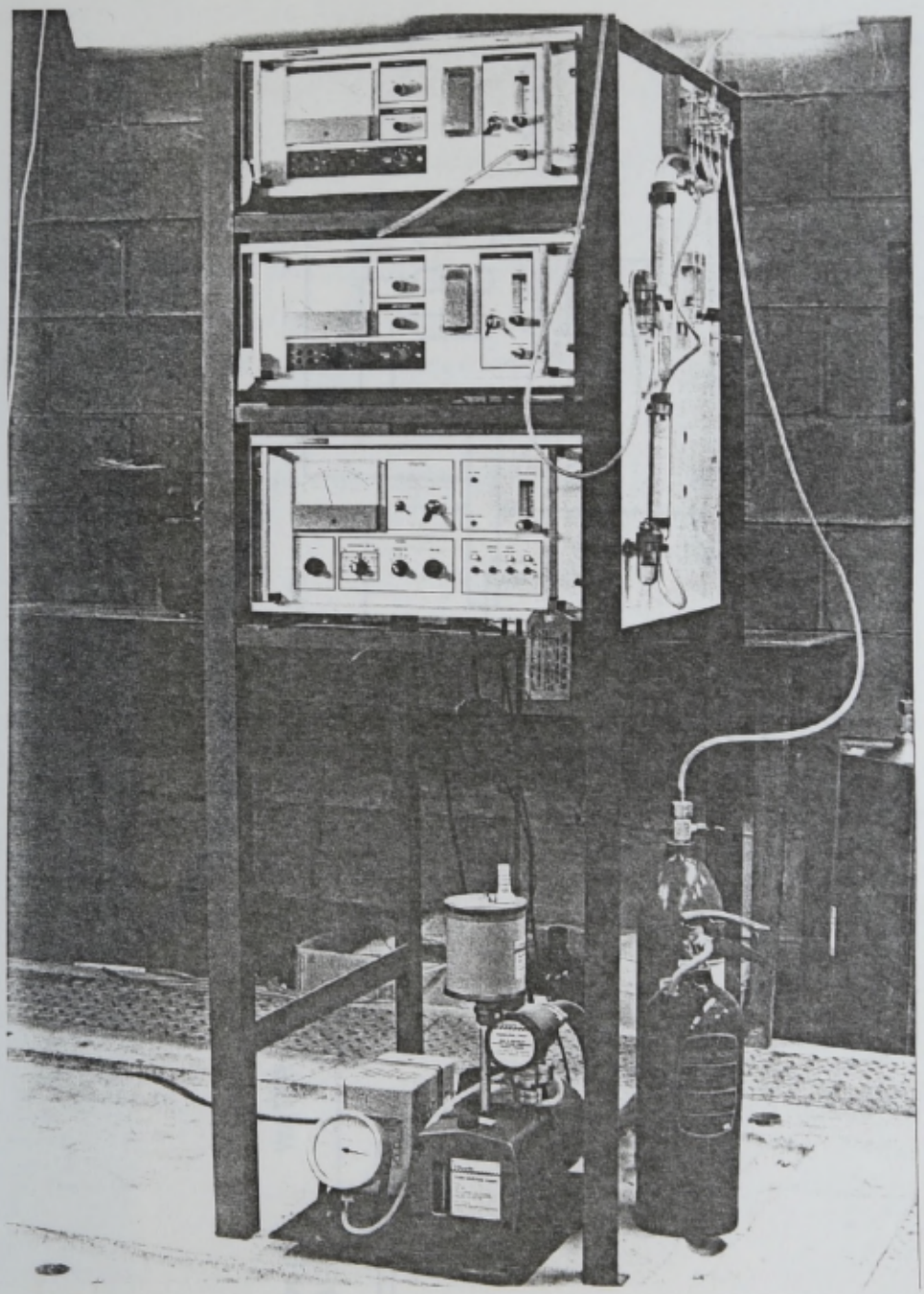

FIGURE 2.26 ARRANGEMENT OF EXHAUST GAS ANALYSIS EQUIPMENT

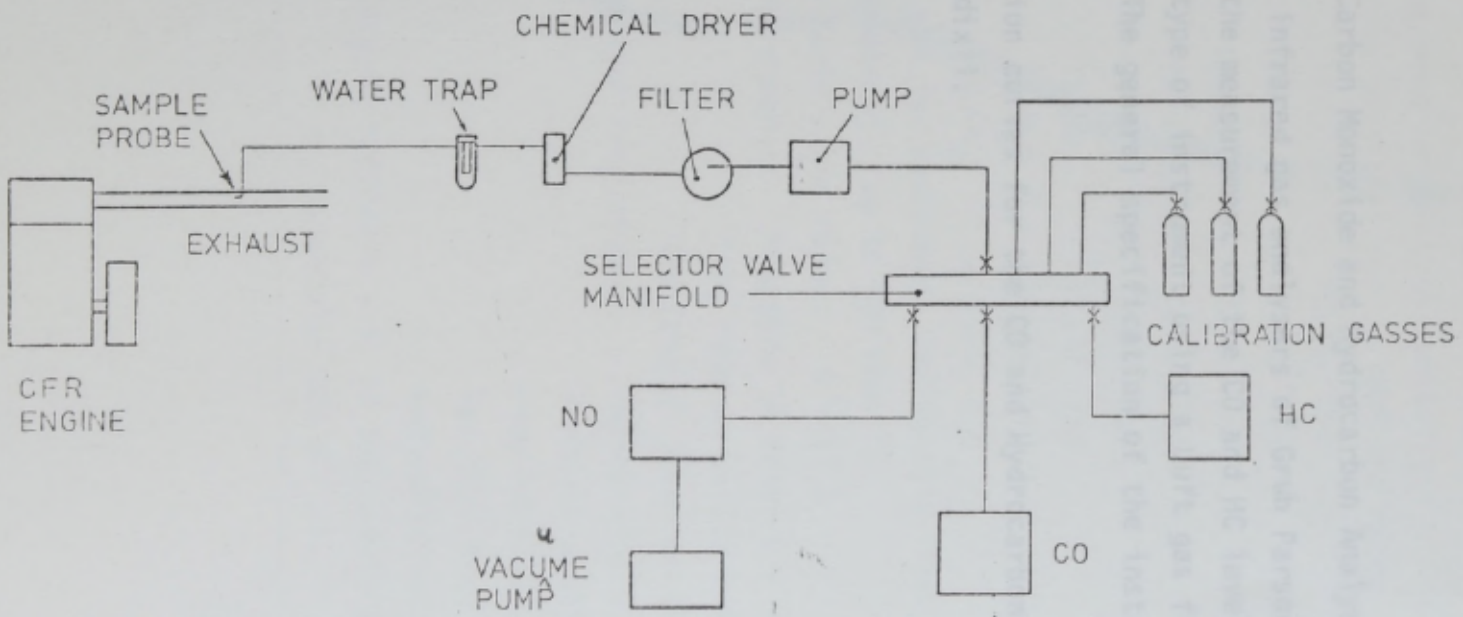

FIGURE 2.27 SCHEMATIC DIAGRAM OF THE GAS ANALYSIS EQUIPMENT

known concentration. The general specification of the Chemitox Analyser is shown in Table 2.3.

2.7.3 The Carbon Monoxide and Hydrocarbon Analysers

Model 20 infrared gas analysers of Grub Parsons manufacture were used for the measurement of the CO and HC levels in the exhaust gases. This type of instrument using a Luft gas filled detector is well known. The general specification of the instruments is listed in Table 2.4

Calibration curves for the CO and Hydrocarbon analysers are shown in Appendix 1.

* Converter Efficiency: 95% or better at 100 ppm NO/NO_2 in air at recommended oven temperature
* Accuracy of oven temperature indication: $\pm$ 5°C
* Typical cross sensitivities in 1000 ppm range:

1% CO	0.5% fsd
10% CO	1.0% fsd
15% CO_2	3.0% fsd
1% n-Hexane	0.6% fsd
3% H_2O	0.5% fsd
1% SO	12.0% fsd
1% N_2O	0.5% fsd
10% CH_4	3.0% fsd

* Output signal for recorder: adjustable from 0 to 100 mV DC
* Output impedance: up to 100 ohms
* Operating temperature range: 0 - 30°C
* Sample requirements: Pressure in range 0 - 10 psi
  Flow rate up to 2.5 L/min
  Gas free of large particles and desaturated
* Ozone generator requirements: Temperature 0 - 30°C
  Pressure within range 0 - 50 psi
  Flow rate 100 cc/min
  Gas dry, free of oil and particles and desaturated
* Power Supply: 220/240 volts, 50 Hz, single phase, approximately 1000 W

TABLE 2.3 CHEMITOX ANALYSER SPECIFICATIONS

Reproducibility	1% fsd
Stability	1% fsd (24 hours)
Linearity	1% high sensitivity
	2% (gain switch X3)
Speed of Response	4s (electrical time constant)
	20s to fsd
Sample Flow	1 - 1.5 L/min
Electrical Output	0 - 200 mV
	0 - 1 mA (to 1000 ohms)
Power Supply	110/120 V, 220/240 V, 10%
	50/60 Hz, approximately 50W

TABLE 2.4 GENERAL SPECIFICATION OF THE MODEL 20 INFRARED GAS ANALYSER

REFERENCES

2.1 ELLISON, R J
The Effect of Tetraethyl Lead on Flame Propagation in a Petrol Engine
M Phil Thesis, University of London, 1967

2.2 BROCK, E K and GLASSPOOLE, A J
The Thermal loading of Cylinder heads and pistons on Medium speed oil engines
Proc IMechE 1964-65 vol 179 Pt 3c Thermal Loading of Diesel Engines

2.3 RICARDO, H R and HEMPSON, J G G
The High Speed Internal Combustion Engine
Blackie & Son, 5th edition, 1972

2.4 HASKELL, W and LEGGATE, C
Exhaust Hydrocarbon Emissions from Gasoline Engines: Surface Phenomena
SAE Paper 720255, 1972

2.5 KNIGHT, B E
The Problem of Predicting Heat Transfer in Diesel Engines
Proc IMechE 1964-65, vol 179 Pt 3c Thermal Loading of Diesel Engines

CHAPTER 3 EXPERIMENTAL PROCEDURE

INTRODUCTION

There were two strands to the experimental work. Firstly, the relationship between the cyclical variations of the expanding flame front and the engine operating variables was examined, together with their effect on cylinder pressure development, using Benzine and isooctane fuels. Secondly, the apparent flame speed and its relationship with the laminar flame speed was examined. The information thus obtained was fed into a cycle synthesis to predict mass burning rates and emission formation. The experimental procedure adopted was chosen for its minimal effect on the variables under examination. The results obtained are therefore independent of the technique.

The difficulty of obtaining repeatable results from the CFR engine has been demonstrated by Ellison (3.1). Since this work has a wider scope than Ellison's, and in particular because the interdependence of the CFR system variables is uncertain, it was decided to monitor and maintain at fixed values piston crown temperature, cylinder surface temperature, cooling water temperature and flow rate. This minimised the effect of changes in these variables on the cyclical variations of flame propagation. These parameters were later used in the cycle synthesis routine.

In this chapter, the experimental method is outlined in two parts: the techniques used to obtain stable and repeatable running conditions in the engine, and the techniques used to produce experimental results.

3.1 THE ELLISON STARTING PROCEDURE

The work of Ellison highlighted the difficulty of obtaining consistent and repeatable running conditions with the CFR engine. Nevertheless, he developed a starting procedure which allowed the same running conditions to be produced day after day for speeds of either 600 or 900 RPM. The same technique was adopted here and is

as follows:

Step 1 Start the engine and run for 15 minutes at 900 RPM

Step 2 Adjust the speed to 1500 RPM and run for a further 15 minutes

Step 3 Adjust the speed to that required for the test conditions, set the mixture strength and ignition timing to the test conditions

Step 4 Adjust the sump oil temperature and the cooling water flow rate to obtain the required piston crown and cylinder head temperatures

Step 5 Allow to run at the stabilised conditions for at least 20 minutes before commencing the test

This starting technique was used prior to each day's running.

3.2 SETTING THE MIXTURE STRENGTH

The CFR engine is fitted with a multibowl scent spray carburettor system. The mixture strength is adjusted by varying the head of fuel relative to the jet. Large variation of the air-fuel ratio can be achieved by using jets of different sizes. The carburettor is fitted with a sight glass arrangement through which the level of the fuel can be observed. It is possible with a little care and practice to achieve fine adjustments to the air-fuel ratio. The ratio is determined by timing with a stop watch the time required for the engine to consume a given amount of fuel under steady conditions. The air flow was measured with a Alcock viscous flow meter in the inlet system.

3.3 SETTING THE SPARK ADVANCE

The CFR engine is equipped with a coil ignition system. The half time pinnion driving the contact breaker cam is situated at the front of the engine. A handle and clamp arrangement enclosing the points allows the points to be rotated about the cam to facilitate variation of the ignition timing. A neon flasher unit energised from the HT lead indicated on a graduated scale the ignition point.

3.4 SETTING THE COMPRESSION RATIO

The compression ratio can be adjusted by raising the cylinder and head assembly relative to the crank case. Turning a screw gear raises or lowers the cylinder which is normally clamped with a steel band. A micrometer head is used to measure cylinder travel. The micrometer is set up in the engine build at a specified reading for a specified compression ratio. The subsequent compression ratio can then be obtained from the CFR manual for specified micrometer setting.

3.5 SETTING UP THE GAS ANALYSIS EQUIPMENT

It was necessary to calibrate the gas analysis equipment prior to and at the end of each day's testing. The analysers were switched on at the beginning of the engine warm up period and were allowed to stabilise for an hour before attempting a calibration. The in line filter and water trap were cleared at the beginning of each test and the chemical dryer attached to each instrument was renewed as necessary. The gas analysers were calibrated according to the manufacturers' instructions, as outlined in the various handbooks, against full span and certified calibration gases.

3.6 EXAMINATION OF THE CYCLICAL VARIATION OF THE ENGINE ROTATIONAL SPEED AND THE IGNITION TIMING

The combustion interval meter used in this work displays as real time the interval between ignition point and the arrival of the flame front at the ion gap. As cyclical variation of the engine rotation and the point of ignition affect the combustion interval it was decided to examine both factors.

The combustion interval meter was used to measure the time taken for one revolution of the engine crank shaft by timing the interval between successive pulses from the TDC indicator under both motoring and firing conditions. High speed photography was also used to examine the motion of the graduated flywheel in both cases. In the test the compression ratio was raised from 5:1 to

10:1 and in the motoring test the ignition timing and spark advance were set for maximum power at 600 RPM.

The combustion interval meter was used to measure the cyclical variation of the ignition timing, by timing the interval between the point of ignition and TDC. These tests were performed under the same operating conditions as the previous tests. The operating conditions are listed in Table 3.1.

3.7 EXAMINATION OF THE FLAME PROPAGATION SPEED WITH THE COMBUSTION INTERVAL METER

The object of this part of the experimental phase was to examine the expanding flame front as it progressed across the combustion chamber. The presence of the flame front was detected by the ion gaps situated in the spark plug housing, across the cylinder head and in the port diametrically opposite the spark plug. The elapsed time between ignition and the arrival of the flame front at the ion gap was displayed by the combustion interval meter and then recorded. Five hundred samples of the flame propagation times were recorded for each engine setting in half an hour. Benzine and isooctane fuels were used in this test. As the test progressed and the results were analysed, cylinder pressure diagrams were taken in association with the combustion interval times. The UV recorder was triggered off by the combustion interval meter. A summary of the engine operating conditions used in these test is presented in Table 3.2.

3.8 EXAMINATION OF THE APPARENT FLAME SPEED AND COMBUSTION PHENOMENA

The object behind this series of tests was to obtain engine data from the combustion of isooctane fuel on which to base predictions of the behaviour of the flame front, and mass burning rates to be used in combustion modelling. These tests are similar to those described in Section 3.7, but were more detailed. The composition of the exhaust gas, in particular, the presence of unburnt hydrocarbons, CO and NO was examined using gas analysers. A larger sample of cylinder pressure diagrams was also used. The

	MOTORING	FIRING
* Fuel	-	Benzene
* Speed (RPM)	600	600
* CR	5,6,7,7.5,8,8.5	5,6,7,7.5,8,8.5
* Ignition Timing	-	Maximum power
* Equivalence Ratio	-	Maximum power
* Oil Temperature °C	46	46
* Evaporative Coolant Temp. °C	-	98
* Air Inlet Temperature °C	38	38

TABLE 3.1 ENGINE OPERATING CONDITIONS FOR EXAMINING THE CYCLICAL VARIATIONS OF THE IGNITION TIMING AND THE ENGINE ROTATIONAL SPEED

	BENZENE	ISOOCTANE
* Speed (RPM)	600	600
* CR	5,6,7,7.5,8,8.5	7
* Ignition Timing (BTDC)	10,15,21,25,30,35,40	10,15,20,24,30,40
* Equivalence Ratio	1.505, 1.420,1.220 1.100,1.015,0.938	1.460,1.350,1.250 1.120,0.952,0.860
* Oil Temperature °C	46	46
* Evaporative Coolant Temp °C	98.8	98.8
* Coolant Type	H_2O	H_2O
* Air inlet Temp °C	38	38

TABLE 3.2 ENGINE OPERATING CONDITIONS FOR EXAMINING THE FLAME PROPAGATION SPEED

apparent flame speed was recorded as in Section 3.7, for the range of operating conditions chosen. A summary of the engine operating conditions for this series of tests is presented in Table 3.3.

* Fuel	Isooctane
* Speed (RPM)	600
* CR	7
* Ignition Timing (BTDC)	40,30,20,15,10
* Equivalence Ratio	1.460,1.350,1.250 1.120, 0.952,0.860
* Oil Temperature °C	46
* Evaporative Coolant Temperature °C	98.8
* Coolant type	H_2O
* Air inlet Temp °C	38

TABLE 3.3 ENGINE OPERATING CONDITIONS FOR EXAMINING THE FLAME SPEED AND COMBUSTION PHENOMENA

REFERENCES

3.1 ELLISON, R J
The Effect of Tetraethyl Lead on Flame Propagation in a Petrol Engine
M Phil Thesis, University of London, 1967

CHAPTER 4 EXPERIMENTAL RESULTS

INTRODUCTION

The raw experimental data taken from the combustion interval meter have been analysed statistically using the University of London SPSS (Statistical Package for Social Scientists). The results shown here for this part of the work are the output from the statistical analysis. The emissions data and other steady state data are tabulated as raw data. For the sake of clarity, the data are displayed in tabular form, supported by a typical graphical representation of the variables of interest.

4.1 CYCLICAL VARIATION OF THE ENGINE ROTATIONAL SPEED AND THE IGNITION TIMING

The cyclical variation of the time required for one revolution of the engine crank shaft is shown in Table 4.1, for both motoring and firing cases (for operating conditions, see Table 3.1). Figure 4.1 shows, as a histogram, the frequency distribution for motoring and firing cases with a compression ratio of 6 at maximum power, ignition timing and equivalence ratio. The mean times and standard deviations of the times between the point of ignition and TDC are listed in Table 4.2. Figure 4.2 shows, as a histogram, the frequency distribution for a compression ratio of 6 at maximum power settings, of the data in Table 4.2.

The separation of the engine rotational speed into two distinct parts when firing is clearly shown. The reduction of the crank shaft speed during the intake and compression strokes and the increase during the expansion stroke is seen to be a function of compression ratio. The high speed photographic work verified these results.

COMPRESSION RATIO	MOTORING		FIRING			
			FIRST PEAK		SECOND PEAK	
	$\bar{T}$ msec	σ msec	$\bar{T}$ msec	σ msec	$\bar{T}$ msec	σ msec
5.0	100.	0.017	99.050	0.260	100.920	0.260
6.0	100.	0.017	99.074	0.270	100.926	0.270
7.0	100.	0.019	99.070	0.270	100.932	0.270
7.5	100.	0.020	99.063	0.270	100.938	0.270
8.0	100.	0.024	99.045	0.275	100.956	0.275
8.5	100.	0.029	99.030	0.280	100.900	0.280

ENGINE SPEED 600 RPM.

TABLE 4.1 CYCLICAL VARIATIONS OF THE ENGINE ROTATIONAL SPEED

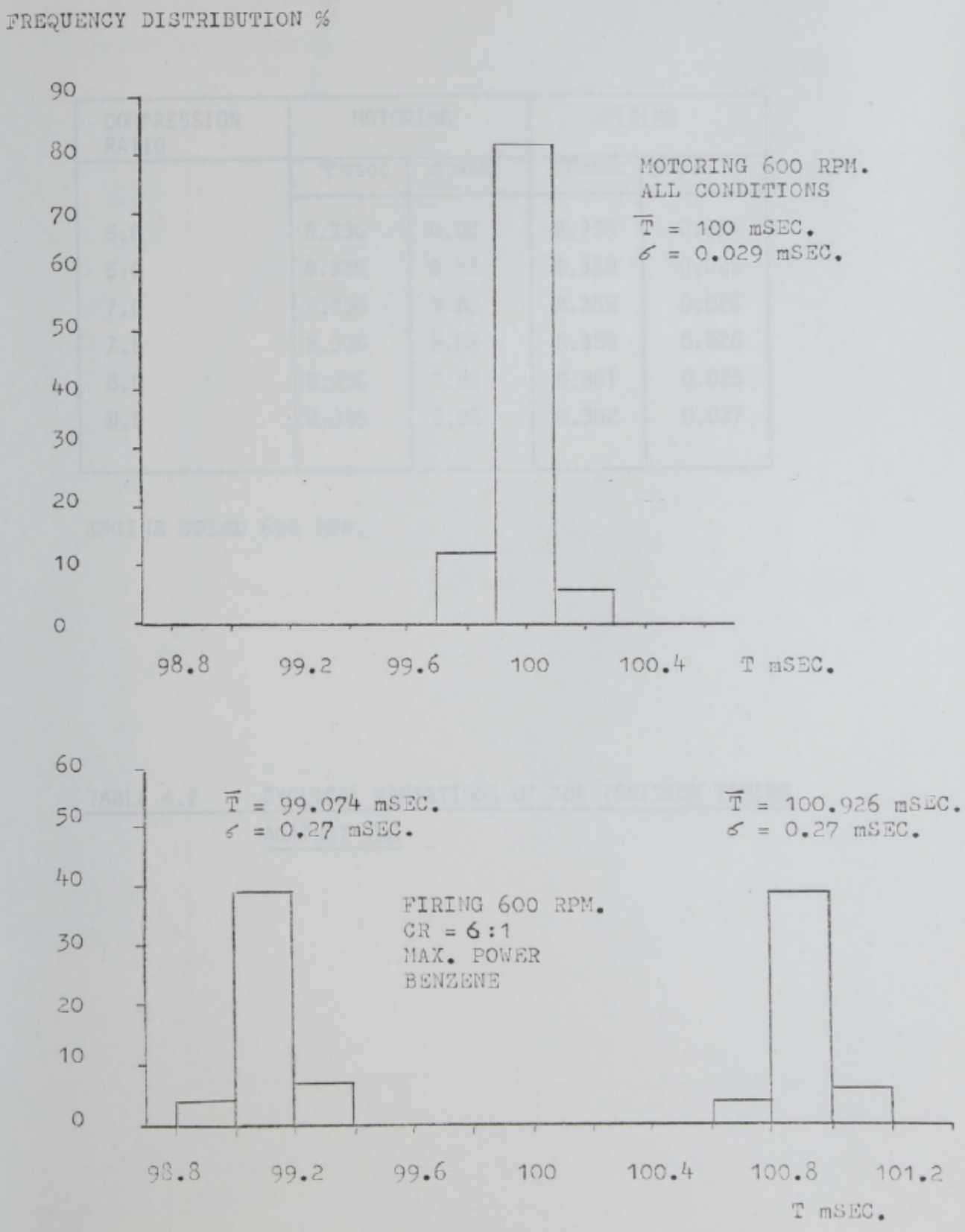

FIGURE 4.1 VARIATION OF THE TIME REQUIRED FOR ONE ENGINE REVOLUTION

COMPRESSION RATIO	MOTORING		FIRING	
	$\bar{\tau}$ msec	σ msec	$\bar{\tau}$ msec	σ msec
5.0	8.336	0.02	8.356	0.024
6.0	8.336	0.02	8.358	0.025
7.0	8.336	0.02	8.358	0.026
7.5	8.336	0.02	8.359	0.026
8.0	8.336	0.02	8.361	0.025
8.5	8.336	0.02	8.362	0.027

ENGINE SPEED 600 RPM.

TABLE 4.2 CYCLICAL VARIATIONS OF THE IGNITION TIMING AGAINST TDC

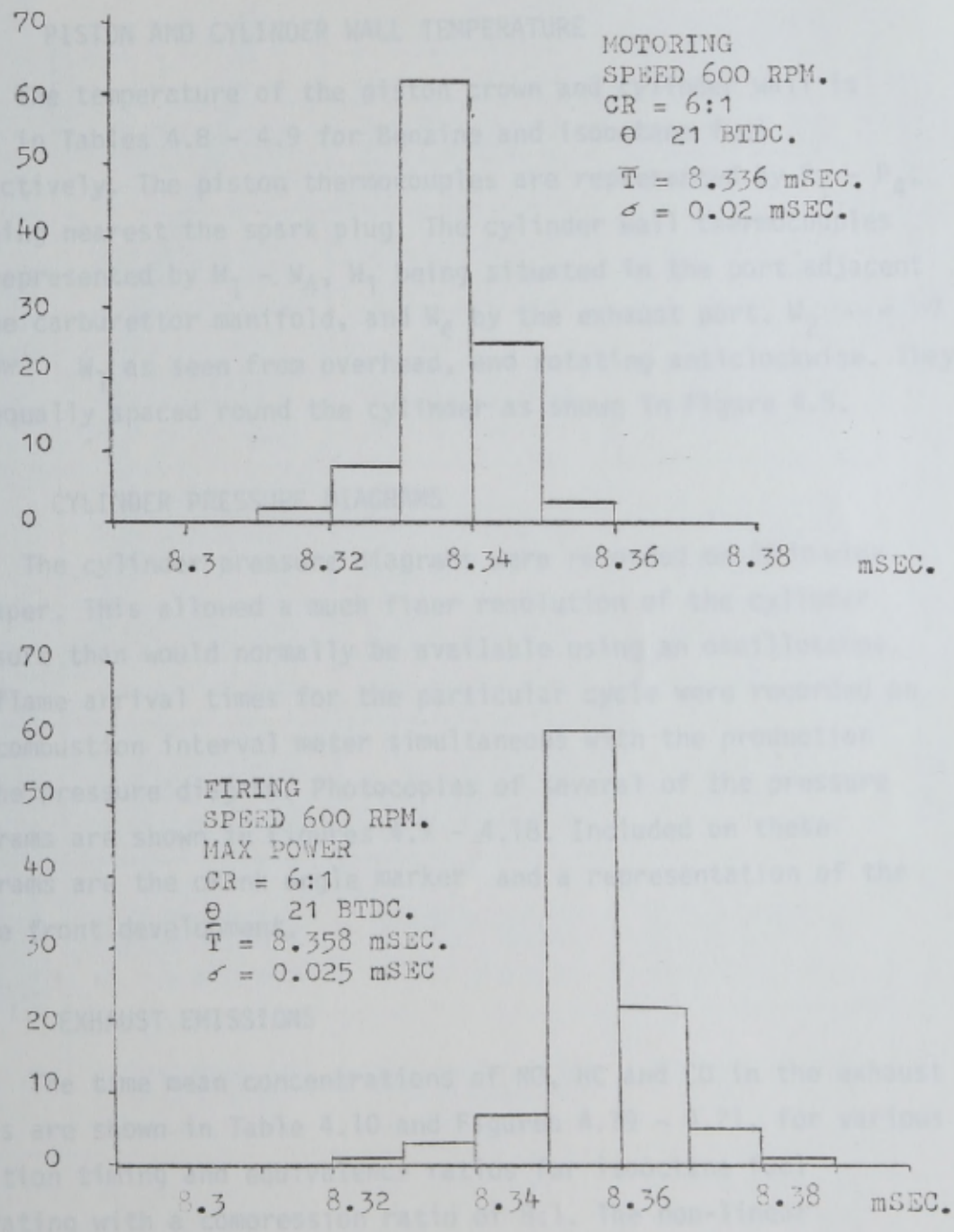

FIGURE 4.2 VARIATION OF IGNITION TIMING AGAINST TDC

4.2 DEVELOPMENT OF THE EXPANDING FLAME FRONT

The relationship between the mean flame travel time and the flame radius is shown in Tables 4.3 - 4.7 and Figures 4.3 - 4.7 for various engine conditions for both Benzine and isooctane fuels.

4.3 PISTON AND CYLINDER WALL TEMPERATURE

The temperature of the piston crown and cylinder wall is shown in Tables 4.8 - 4.9 for Benzine and isooctane fuel respectively. The piston thermocouples are represented by P_1 - P_4, P_1 being nearest the spark plug. The cylinder wall thermocouples are represented by W_1 - W_4, W_1 being situated in the port adjacent to the carburettor manifold, and W_4 by the exhaust port. W_2 and W_3 follow W_1 as seen from overhead, and rotating anticlockwise. They are equally spaced round the cylinder as shown in Figure 4.8.

4.4 CYLINDER PRESSURE DIAGRAMS

The cylinder pressure diagrams were recorded on 20 in wide UV paper. This allowed a much finer resolution of the cylinder pressure than would normally be available using an oscilloscope. The flame arrival times for the particular cycle were recorded on the combustion interval meter simultaneous with the production of the pressure diagram. Photocopies of several of the pressure diagrams are shown in Figures 4.9 - 4.18. Included on these diagrams are the crank angle marker and a representation of the flame front development.

4.5 EXHAUST EMISSIONS

The time mean concentrations of NO, HC and CO in the exhaust gases are shown in Table 4.10 and Figures 4.19 - 4.21, for various ignition timing and equivalence ratios for isooctane fuel operating with a compression ratio of 8:1. The non-linear relationship between the engine parameters and the NO concentration is clearly shown. The equivalent relationship for the other constituents is linear.

ION GAP	CR	MEAN	STD ERR	STD DEV	VAR	KUR	SKEW	MAX	MIN	0.95 CI
1	5.0	2.920	0.036	0.507	0.257	0.152	0.351	4.650	1.770	2.850 - 2.990
	6.0	2.550	0 028	0.393	0.154	0.019	0.557	3.670	1.620	2.501 - 2.610
	6.5	2.311	0.029	0.415	0.173	1.566	-1.395	2.790	1.070	2.250 - 2.369
	7.0	2.269	0.024	0.339	0.115	2.201	-0.350	3.180	0.680	2.220 - 2.316
	7.5	2.030	0.029	0.347	0.157	-0.046	0.610	3.700	1.800	1.981 - 2.088
	8.0	1.973	0.032	0.386	0.247	-0.410	-0.820	2.982	0.931	1.845 - 2.037
	8.5	1.737	0.045	0.640	0.410	-0.441	-0.972	2.670	0.510	1.648 - 1.825
2	5.0	4.320	0.040	0.572	0.327	-0.195	0.327	5.920	3.060	4.241 - 4.399
	6.0	3.556	0.034	0.477	0.228	-0.110	0.221	4.780	2.360	3.490 - 3.622
	6.5	3.362	0.028	0.400	0.160	-0.122	0.058	4.000	1.730	3.306 - 3.418
	7.0	3.253	0.031	0.443	0.196	-0.085	0.314	4.510	2.260	3.191 - 3.314
	7.5	3.012	0.041	0.563	0.317	0.995	0.633	4.550	1.480	2.930 - 3.094
	8.0	2.750	0.037	0.417	0.198	0.527	0.325	3.870	2.140	2.670 - 2.824
	8.5	2.792	0.022	0.315	0.100	0.549	0.496	3.900	2.060	2.794 - 2.836
3	5.0	6.713	0.050	0.719	0.517	-0.068	-0.118	8.580	4.670	6.613 - 6.812
	6.0	5.668	0.050	0.709	0.502	-0.419	0.215	7.850	4.210	5.570 - 5.760
	6.5	5.350	0.045	0.657	0.431	-0.164	-0.295	6.340	2.810	5.260 - 5.440
	7.0	5.177	0.042	0.592	0.351	-0.361	0.115	6.550	3.760	5.090 - 5.259
	7.5	4.950	0.056	0.755	0.570	0.135	0.273	8.330	4.120	4.838 - 5.062
	8.0	4.650	0.042	0.609	0.297	0.413	0.362	7.430	3.130	4.556 - 4.724
	8.5	4.603	0.031	0.440	0.195	0.518	0.431	6.150	3.590	4.542 - 4.664

TABLE 4.3 FLAME TRAVEL TIME: VARIATION OF COMPRESSION RATIO (FUEL TYPE:BENZENE)

ION GAP	CR	MEAN	STD ERR	STD DEV	VAR	KUR	SKEW	MAX	MIN	0.95 CI
4	5.0	7.911	0.061	0.864	0.746	0.414	0.272	10.360	5.500	7.790 - 8.030
	6.0	6.650	0.067	0.966	0.434	-0.302	0.180	8.920	3.740	6.516 - 6.784
	6.5	6.180	0.054	0.781	0.611	-0.190	-0.061	7.820	3.570	6.072 - 6.288
	7.0	6.157	0.048	0.683	0.466	0.024	0.343	8.150	4.560	6.063 - 6.252
	7.5	5.970	0.056	0.755	0.571	-0.139	0.143	7.810	3.890	5.858 - 6.082
	8.0	5.550	0.042	0.062	0.318	0.416	0.037	7.420	3.670	5.466 - 5.630
	8.5	5.510	0.037	0.534	0.285	0.745	0.028	7.270	3.550	5.436 - 5.584
5	5.0	9.693	0.059	0.841	0.707	-0.124	0.390	12.130	7.640	9.576 - 9.809
	6.0	8.736	0.080	1.162	1.351	-0.088	0.390	12.380	6.540	8.576 - 8.896
	6.5	8.270	0.064	0.931	0.867	-0.375	0.156	8.630	5.950	8.142 - 8.398
	7.0	7.950	0.056	0.797	0.635	-0.315	0.058	9.840	7.970	7.840 - 8.061
	7.5	7.500	0.075	1.014	1.029	-0.022	0.258	12.320	6.680	9.228 - 9.524
	8.0	6.950	0.056	0.721	0.673	-0.172	0.263	9.432	6.172	6.830 - 7.062
	8.5	6.634	0.048	0.690	0.476	-0.143	0.271	9.080	5.430	6.830 - 7.030

TABLE 4.3 (CONTINUED) θ = 21°BTDC ϕ = 1.1 N = 600 RPM T_{IN} = 38°C

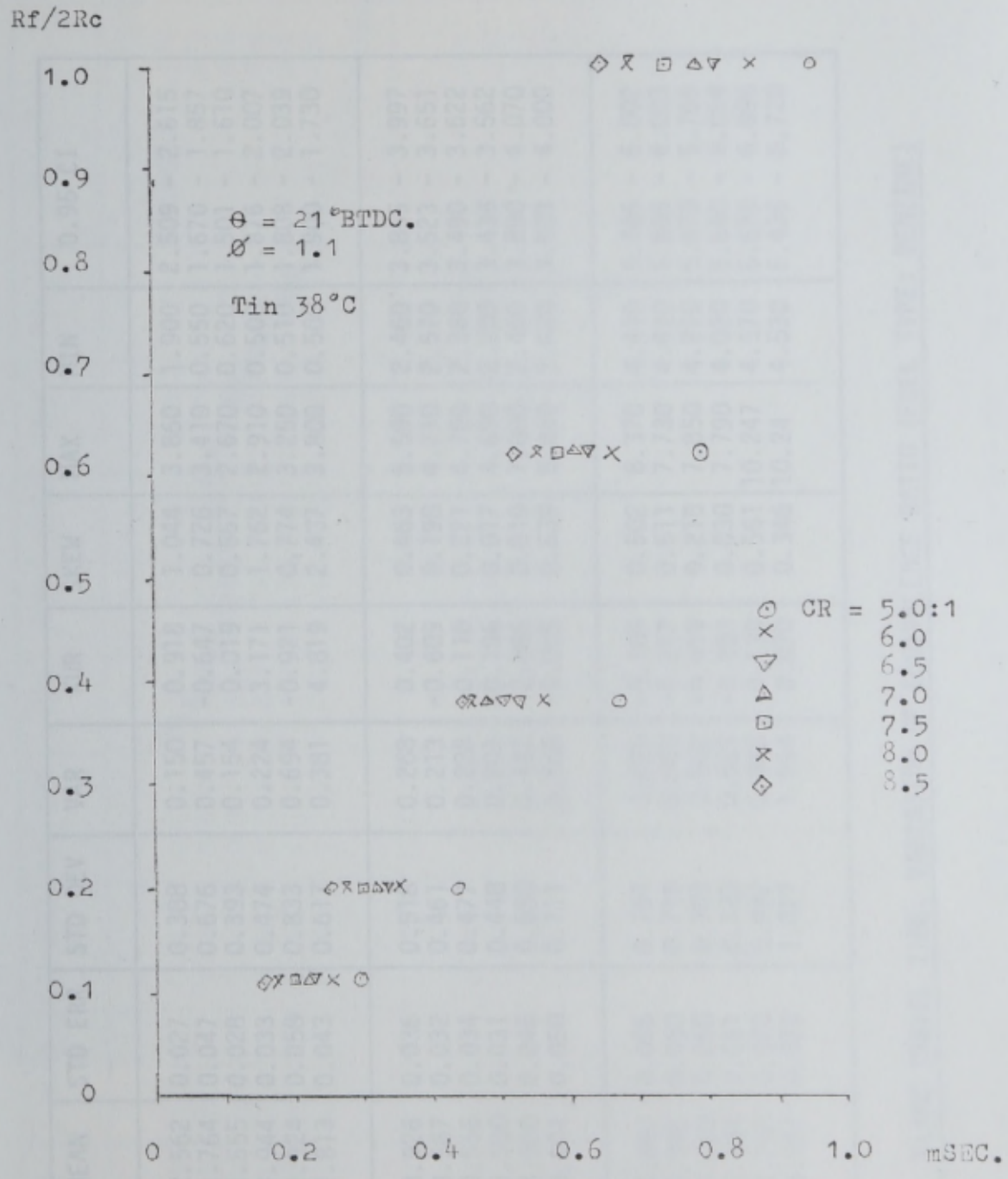

FIGURE 4.3 FLAME TRAVEL TIME: VARIATION IN COMPRESSION RATIO (FUEL TYPE: BENZENE)

ION GAP	Ø	MEAN	STD ERR	STD DEV	VAR	KUR	SKEW	MAX	MIN	0.95 CI
1	0.938	2.562	0.027	0.388	0.150	0.918	1.044	3.860	1.900	2.509 - 2.615
	1.015	1.764	0.047	0.676	0.457	-0.647	0.726	3.410	0.550	1.670 - 1.857
	1.100	1.555	0.028	0.393	0.154	0.019	0.557	2.670	0.620	1.501 - 1.610
	1.224	1.944	0.033	0.474	0.224	3.171	1.762	2.910	0.500	1.876 - 2.007
	1.420	1.924	0.058	0.833	0.694	-0.921	0.774	3.250	0.510	1.808 - 2.039
	1.505	1.813	0.043	0.617	0.381	4.819	2.437	3.800	0.500	1.900 - 1.730
2	0.938	3.926	0.036	0.518	0.268	0.402	0.463	5.590	2.460	3.855 - 3.997
	1.015	3.587	0.032	0.461	0.213	-0.609	0.198	4.710	2.570	3.523 - 3.651
	1.100	3.556	0.034	0.477	0.228	-0.110	0.221	4.780	2.360	3.490 - 3.622
	1.224	3.500	0.031	0.448	0.201	-0.196	0.017	4.690	2.200	3.438 - 3.562
	1.420	3.980	0.046	0.650	0.422	2.085	0.819	7.000	2.460	3.890 - 4.070
	1.505	3.901	0.050	0.711	0.505	-0.005	0.639	5.880	2.620	3.803 - 4.000
3	0.938	5.893	0.055	0.791	0.625	-0.105	0.502	8.370	4.410	5.785 - 6.002
	1.015	5.905	0.050	0.710	0.503	-0.217	0.511	7.730	4.410	5.806 - 6.003
	1.100	5.668	0.050	0.709	0.502	-0.419	0.215	7.850	4.210	5.570 - 5.766
	1.224	5.594	0.051	0.722	0.521	-0.283	0.030	7.790	4.020	5.840 - 6.054
	1.420	6.758	0.070	0.992	0.985	0.139	0.551	10.247	4.570	6.620 - 6.896
	1.505	6.587	0.072	1.027	1.054	0.070	0.346	10.24	4.530	6.436 - 6.720

TABLE 4.4 FLAME TRAVEL TIME: VARIATION OF EQUIVALENCE RATIO (FUEL TYPE: BENZENE)

ION GAP	Ø	MEAN	STD ERR	STD DEV	VAR	KUR	SKEW	MAX	MIN	0.95 CI
4	0.938	6.972	0.061	0.884	0.782	0.077	0.504	9.640	4.710	6.850 - 7.094
	1.015	6.959	0.054	0.842	0.709	-0.397	0.253	9.150	5.030	6.842 - 7.075
	1.100	6.691	0.058	0.827	0.685	-0.244	0.306	9.050	4.860	6.577 - 6.806
	1.224	7.167	0.064	0.913	0.833	0.247	0.348	9.940	4.890	7.041 - 7.294
	1.420	8.063	0.084	1.190	1.417	-0.152	0.454	11.640	5.500	7.899 - 8.228
	1.505	8.923	0.086	1.220	1.487	-0.185	0.282	11.670	5.350	8.754 - 9.092
5	0.938	8.968	0.076	1.0936	1.195	0.027	0.350	11.800	6.380	8.816 - 9.120
	1.015	8.928	0.066	0.9450	0.893	-0.453	0.012	11.290	6.890	8.797 - 9.059
	1.100	8.727	0.064	0.9060	0.822	-0.235	0.243	11.480	6.750	8.601 - 8.852
	1.224	9.492	0.074	1.0600	1.125	0.370	0.121	12.570	6.530	9.345 - 9.639
	1.420	10.474	0.093	1.3230	1.746	0.493	0.217	14.350	6.170	10.291 -10.670
	1.505	10.649	0.120	1.7140	2.938	-0.653	0.154	15.020	7.260	10.412 -10.887

TABLE 4.4 (CONTINUED) θ = 21 °BTDC T_{IN} = 38 °C N = 600 RPM CR = 6

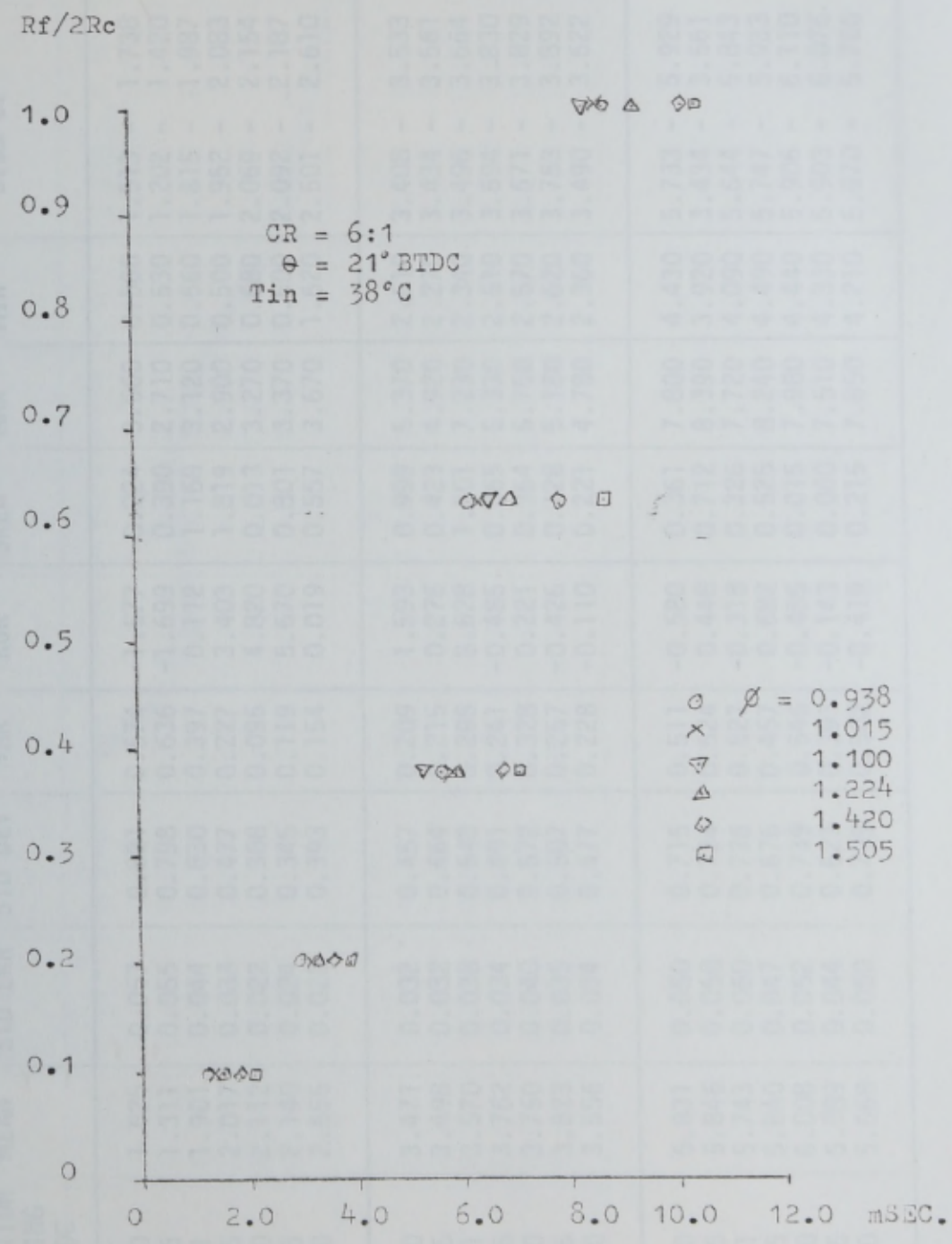

FIGURE 4.4 FLAME TRAVEL TIME: VARIATION OF EQUIVALENCE RATIO (FUEL TYPE: BENZENE)

ION GAP	IGNITION TIMING °BTDC	MEAN	STD ERR	STD DEV	VAR	KUR	SKEW	MAX	MIN	0.95 CI
1	10	1.625	0.057	0.821	0.674	-1.577	-0.224	3.660	0.500	1.513 - 1.738
	15	1.311	0.055	0.798	0.636	-1.699	0.390	2.710	0.530	1.202 - 1.420
	21	1.901	0.044	0.630	0.397	0.112	1.168	3.120	0.560	1.815 - 1.987
	25	2.017	0.033	0.477	0.227	3.403	1.819	2.900	0.500	1.952 - 2.083
	30	2.112	0.022	0.308	0.095	4.820	0.013	3.270	0.680	2.069 - 2.154
	35	2.140	0.024	0.345	0.119	5.670	0.801	3.370	0.600	2.092 - 2.187
	40	2.555	0.028	0.393	0.154	0.019	0.557	3.670	1.620	2.501 - 2.610
2	10	3.471	0.032	0.457	0.209	1.593	0.999	5.370	2.610	3.408 - 3.533
	15	3.498	0.032	0.464	0.215	0.276	0.423	4.920	2.270	3.434 - 3.561
	21	3.570	0.038	0.543	0.295	8.628	1.501	7.230	2.340	3.496 - 3.664
	25	3.762	0.034	0.491	0.241	-0.485	0.065	5.330	2.510	3.694 - 3.830
	30	3.750	0.040	0.572	0.328	0.221	0.364	5.750	2.570	3.671 - 3.829
	35	3.823	0.035	0.507	0.257	-0.426	0.128	5.180	2.620	3.753 - 3.892
	40	3.556	0.034	0.477	0.228	-0.110	0.221	4.780	2.360	3.490 - 3.622
3	10	5.831	0.050	0.715	0.511	-0.580	0.361	7.800	4.430	5.733 - 5.929
	15	5.846	0.050	0.724	0.524	0.448	0.712	8.390	3.920	3.434 - 3.561
	21	5.743	0.050	0.726	0.527	-0.318	0.326	7.720	4.090	5.644 - 5.843
	25	5.840	0.047	0.676	0.457	0.682	0.525	8.240	4.490	5.747 - 5.933
	30	6.008	0.052	0.739	0.546	-0.485	0.015	7.980	4.440	5.906 - 6.110
	35	5.989	0.044	0.627	0.393	-0.143	0.060	7.510	4.330	5.903 - 6.076
	40	5.668	0.050	0.709	0.502	-0.419	0.215	7.850	4.210	5.570 - 5.766

TABLE 4.5 FLAME TRAVEL TIME: VARIATION OF IGNITION TIMING (FUEL TYPE: BENZENE)

ION GAP	IGNITION TIMING	MEAN	STD ERR	STD DEV	VAR	KUR	SKEW	MAX	MIN	0.95 CI
4	10	6.852	0.057	0.818	0.668	-0.238	0.214	9.620	5.070	6.740 - 6.964
	15	6.857	0.057	0.824	0.678	-0.191	0.484	9.010	4.810	6.745 - 6.970
	21	6.705	0.061	0.881	0.776	2.856	0.460	8.780	2.020	6.585 - 6.826
	25	6.797	0.053	0.759	0.575	-0.469	0.315	8.750	5.290	6.692 - 6.901
	30	6.974	0.061	0.874	0.764	-0.162	0.187	9.550	5.070	6.853 - 7.094
	35	6.907	0.051	0.725	0.526	-0.436	0.122	8.610	5.120	6.880 - 7.007
	40	6.991	0.058	0.827	0.685	-0.299	0.306	9.050	4.860	6.880 - 7.111
5	10	8.398	0.067	0.962	0.925	-0.136	0.080	11.790	6.700	8.806 - 9.069
	15	8.739	0.065	0.934	0.871	0.221	0.046	11.050	5.630	8.611 - 8.867
	21	8.308	0.061	0.880	0.775	0.370	0.102	11.350	6.120	8.188 - 8.429
	25	8.179	0.053	0.764	0.584	0.670	0.193	10.520	5.480	8.074 - 8.284
	30	8.404	0.073	1.052	1.106	16.989	0.239	10.750	8.191	8.259 - 8.548
	35	8.318	0.053	0.755	0.570	-0.419	0.066	10.080	6.490	8.214 - 8.422
	40	8.727	0.064	0.906	0.822	-0.235	0.243	11.480	6.750	8.601 - 8.852

TABLE 4.5 (CONTINUED) CR = 6 N = 600 RPM Ø = 1.1 T_{IN} = 38°C

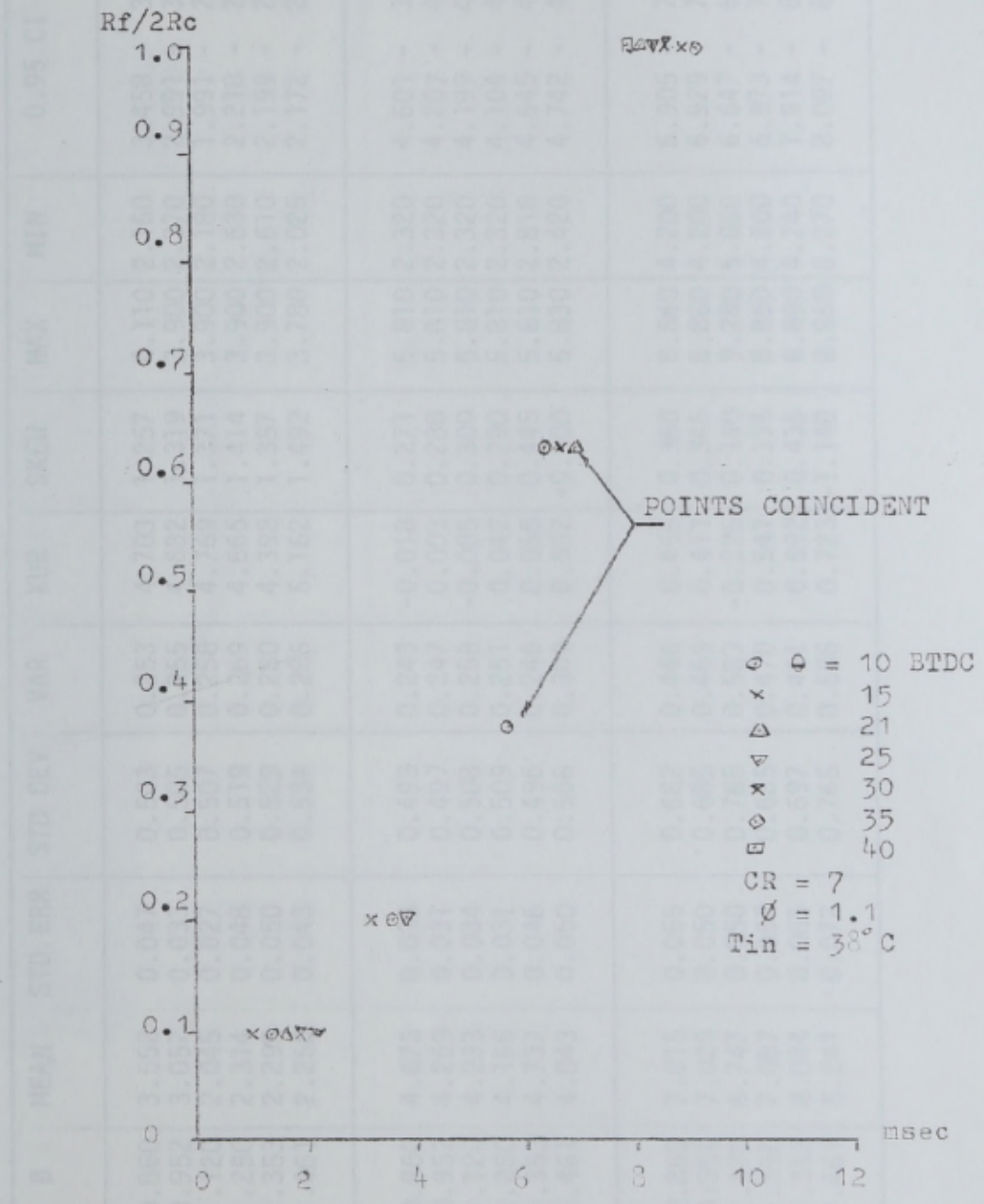

FIGURE 4.5 FLAME TRAVEL TIME: VARIATION OF IGNITION TIMING (FUEL TYPE: BENZINE)

ION GAP	Ø	MEAN	STD ERR	STD DEV	VAR	KUR	SKEW	MAX	MIN	0.95 CI
1	0.860	3.552	0.047	0.503	0.253	4.703	1.257	4.110	2.160	3.458 - 3.647
	0.952	3.057	0.033	0.505	0.255	4.632	1.319	3.900	2.370	2.991 - 3.123
	1.120	2.045	0.027	0.507	0.258	4.769	1.371	3.900	2.180	1.991 - 2.099
	1.250	2.314	0.048	0.519	0.269	4.665	1.414	3.900	2.630	2.218 - 2.410
	1.353	2.299	0.050	0.529	0.280	4.398	1.357	3.900	2.610	2.199 - 2.399
	1.461	2.258	0.043	0.534	0.285	5.162	1.492	3.780	2.025	2.172 - 2.341
2	0.860	4.673	0.036	0.493	0.243	-0.018	0.271	5.810	2.320	4.601 - 3.745
	0.952	4.269	0.031	0.497	0.247	0.003	0.288	5.810	2.320	4.207 - 4.331
	1.120	4.233	0.034	0.508	0.258	-0.005	0.300	5.810	2.320	4.199 - 4.302
	1.250	4.166	0.031	0.509	0.251	0.042	0.290	5.810	2.320	4.104 - 4.228
	1.353	4.737	0.046	0.496	0.246	0.056	0.445	5.810	2.810	4.645 - 4.829
	1.461	4.843	0.050	0.556	0.309	0.552	-0.600	5.830	2.420	4.742 - 4.941
3	0.860	7.015	0.055	0.682	0.466	0.455	0.360	8.860	4.200	6.905 - 7.120
	0.952	7.029	0.050	0.685	0.469	0.411	0.345	8.860	4.200	6.929 - 7.129
	1.120	6.747	0.050	0.765	0.583	-0.226	0.140	9.280	5.060	6.647 - 6.847
	1.250	7.087	0.057	0.685	0.470	0.547	0.335	8.860	4.200	6.973 - 7.201
	1.353	8.044	0.065	0.697	0.461	0.692	0.435	8.890	4.240	7.914 - 8.174
	1.461	8.241	0.072	0.765	0.586	0.723	-1.148	8.860	6.270	8.097 - 8.385

TABLE 4.6 FLAME TRAVEL TIME: VARIATION OF EQUIVALENCE RATIO (FUEL TYPE: ISOOCTANE)

ION GAP	Ø	MEAN	STD ERR	STD DEV	VAR	KUR	SKEW	MAX	MIN	0.95 CI
4	0.860	8.315	0.061	0.750	0.563	-0.216	0.119	9.280	5.060	8.193 - 8.437
	0.952	8.283	0.066	1.190	0.572	-0.252	1.045	11.640	5.500	7.899 - 8.228
	1.120	7.964	0.064	0.690	0.477	0.465	0.347	8.860	4.200	7.837 - 8.093
	1.250	8.531	0.073	0.761	0.579	-0.158	0.159	9.280	5.060	8.385 - 8.677
	1.353	9.598	0.087	0.741	0.549	-0.165	0.217	11.210	5.110	9.424 - 9.772
	1.461	10.618	0.123	0.836	0.698	0.172	1.631	11.220	8.370	10.372 - 10.864
5	0.860	10.107	0.075	0.891	0.793	-0.029	0.127	16.790	8.460	12.957 - 13.250
	0.952	13.008	0.063	0.893	0.797	-0.113	0.096	16.790	8.210	12.882 - 13.134
	1.120	12.769	0.076	0.900	0.809	-0.121	0.117	16.790	8.460	12.617 - 12.921
	1.250	13.680	0.083	0.889	0.790	-0.245	0.029	15.080	8.460	13.514 - 13.846
	1.353	15.440	0.094	0.884	0.781	-0.242	0.092	17.030	8.450	15.252 - 15.268
	1.461	15.657	0.120	1.075	1.115	-0.121	0.119	17.800	9.030	15.417 - 15.897

TABLE 4.6 (CONTINUED) CR = 7 N = 600 RPM θ = 24 °BTDC T_{IN} = 38°C

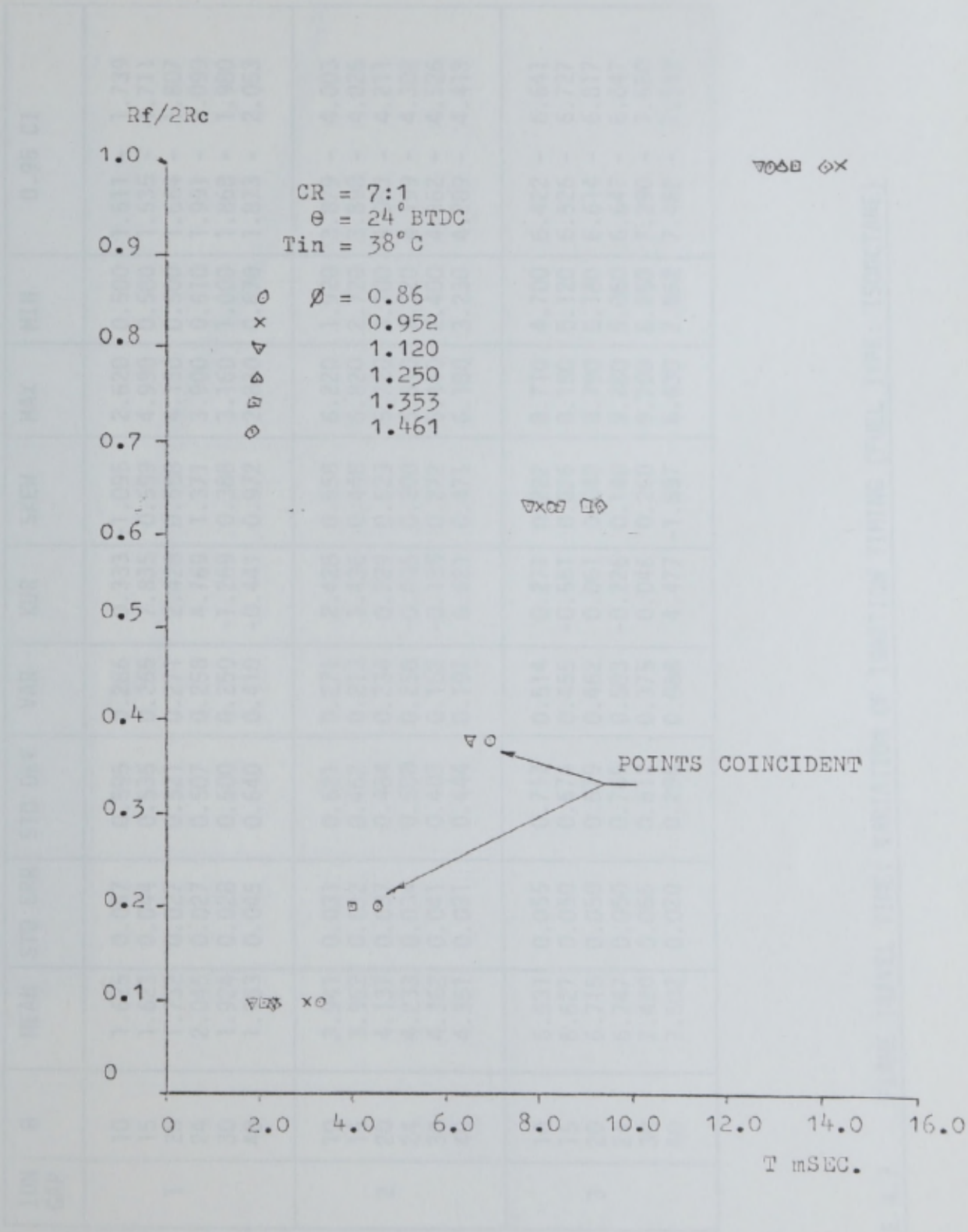

FIGURE 4.6 FLAME TRAVEL TIME: VARIATION OF EQUIVALENCE RATIO (FUEL TYPE: ISOOCTANE)

ION GAP	θ	MEAN	STD ERR	STD DEV	VAR	KUR	SKEW	MAX	MIN	0.95 CI
1	10	1.625	0.057	0.595	0.286	0.333	-1.095	2.620	0.500	1.511 - 1.739
	15	1.623	0.044	0.535	0.265	7.835	0.599	4.990	0.580	1.535 - 1.711
	20	1.732	0.027	0.521	0.271	2.428	0.558	4.150	0.500	1.664 - 1.807
	24	2.045	0.027	0.507	0.258	4.769	1.371	3.900	0.610	1.991 - 2.099
	30	1.924	0.028	0.500	0.250	-1.269	0.388	3.160	1.000	1.868 - 1.980
	40	1.963	0.045	0.640	0.410	-0.441	0.972	2.830	0.670	1.873 - 2.053
2	10	3.941	0.031	0.521	0.271	2.428	0.558	6.220	1.920	3.879 - 4.003
	15	3.962	0.032	0.462	0.213	1.436	0.448	5.820	2.720	3.898 - 4.026
	20	4.137	0.037	0.484	0.234	0.229	0.529	5.720	3.100	4.063 - 4.211
	24	4.233	0.034	0.508	0.258	-0.005	0.300	5.810	2.320	4.199 - 4.302
	30	4.362	0.041	0.403	0.162	-0.135	0.272	5.410	2.400	4.362 - 4.526
	40	4.351	0.031	0.444	0.197	0.621	0.471	6.180	3.230	4.289 - 4.413
3	10	6.531	0.055	0.717	0.514	0.271	0.222	8.710	4.700	6.422 - 6.641
	15	6.627	0.050	0.674	0.455	-0.551	0.075	8.150	5.120	6.526 - 6.727
	20	6.715	0.050	0.679	0.462	0.051	0.048	8.790	5.180	6.614 - 6.817
	24	6.747	0.050	0.765	0.583	-0.226	0.140	9.280	5.060	6.647 - 6.847
	30	7.420	0.065	0.612	0.375	0.046	0.250	9.700	6.250	7.290 - 7.550
	40	7.502	0.020	0.296	0.088	4.477	-1.897	6.630	7.862	7.462 - 7.542

TABLE 4.7 FLAME TRAVEL TIME: VARIATION OF IGNITION TIMING (FUEL TYPE: ISOOCTANE)

ION GAP	θ	MEAN	STD ERR	STD DEV	VAR	KUR	SKEW	MAX	MIN	0.95 CI
4	10	7.829	0.057	0.790	0.624	0.372	0.157	9.350	5.500	7.715 - 7.943
	15	7.831	0.061	0.778	0.605	-0.564	0.073	10.030	5.780	7.609 - 8.053
	20	7.854	0.064	0.690	0.477	0.465	0.347	8.860	4.200	7.837 - 8.093
	24	7.964	0.064	0.690	0.477	0.465	0.347	8.860	4.200	7.837 - 8.093
	30	7.990	0.051	0.605	0.367	-0.511	0.004	9.460	6.630	7.888 - 8.092
	40	8.004	0.064	0.931	0.867	-0.357	0.156	10.630	5.950	7.877 - 8.130
5	10	12.256	0.061	0.933	0.871	-0.047	0.057	14.600	9.340	12.134 - 12.378
	15	12.319	0.065	1.033	1.068	-0.414	0.019	15.160	9.890	11.989 - 12.449
	20	12.468	0.075	0.901	0.813	-0.121	0.117	13.790	8.460	12.619 - 12.721
	24	12.769	0.076	0.900	0.809	-0.121	0.117	13.790	8.460	12.617 - 12.921
	30	12.932	0.064	0.823	0.678	-0.013	0.499	15.270	10.890	12.804 - 13.060
	40	13.070	0.070	0.778	0.605	-0.564	0.073	14.630	11.560	12.930 - 13.210

TABLE 4.7 (CONTINUED) CR = 7 N = 600 RPM Ø = 1.12 T_{IN} = 38 °C

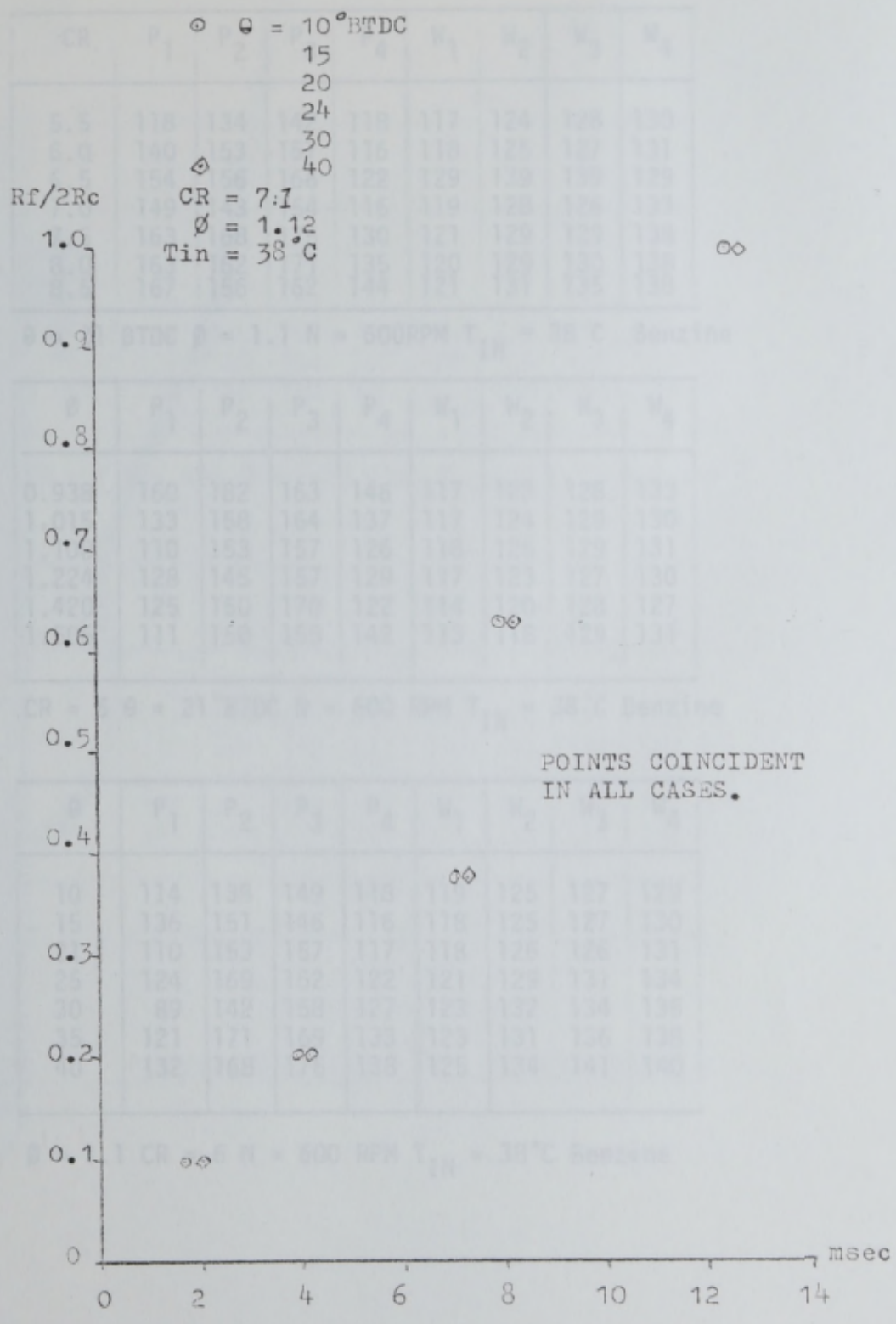

FIGURE 4.7 FLAME TRAVEL TIME: VARIATION OF IGNITION TIMING (FUEL TYPE: ISOOCTANE)

CR	P_1	P_2	P_3	P_4	W_1	W_2	W_3	W_4
5.5	118	134	142	118	117	124	128	130
6.0	140	153	157	116	118	125	127	131
6.5	154	156	166	122	129	139	139	129
7.0	149	143	154	116	119	128	126	133
7.5	163	168	175	130	121	129	129	138
8.0	163	162	171	135	120	129	130	138
8.5	167	156	162	144	121	131	135	138

θ = 21 BTDC ϕ = 1.1 N = 600RPM T_{IN} = 38 C Benzine

ϕ	P_1	P_2	P_3	P_4	W_1	W_2	W_3	W_4
0.938	160	182	163	146	117	123	128	133
1.015	133	158	164	137	117	124	129	130
1.100	110	153	157	126	118	125	129	131
1.224	128	145	157	129	117	123	127	130
1.420	125	150	170	122	114	120	128	127
1.505	111	150	155	142	113	118	129	131

CR = 6 θ = 21 BTDC N = 600 RPM T_{IN} = 38 C Benzine

θ	P_1	P_2	P_3	P_4	W_1	W_2	W_3	W_4
10	114	138	149	118	119	125	127	129
15	136	151	146	116	118	125	127	130
21	110	153	157	117	118	126	126	131
25	124	169	152	122	121	129	131	134
30	89	142	158	127	123	132	134	136
35	121	171	169	133	123	131	136	138
40	132	168	176	138	125	134	141	140

ϕ = 1.1 CR = 6 N = 600 RPM T_{IN} = 38°C Benzene

TABLE 4.8 PISTON AND CYLINDER WALL TEMPERATURES °C

Ø	P_1	P_2	P_3	P_4	W_1	W_2	W_3	W_4
0.860	152	160	163	142	117	124	128	130
0.950	144	147	142	145	118	125	127	131
1.120	143	144	141	146	118	125	128	130
1.250	124	146	157	130	121	128	129	132
1.353	132	150	154	135	120	125	129	130
1.461	128	148	150	136	123	130	130	129

CR = 7 N = 600 RPM θ=24°BTDC T_{IN}= 38°C Isooctane

θ	P_1	P_2	P_3	P_4	W_1	W_2	W_3	W_4
10	112	136	140	119	120	125	128	129
15	121	139	142	120	122	124	127	130
20	121	143	157	117	118	126	130	128
24	142	143	141	146	118	125	128	130
30	149	151	168	142	120	125	134	140
40	137	151	157	143	121	126	132	140

CR = 7 N = 600 RPM Ø = 1.12 T_{IN} = 38°C Isooctane

TABLE 4.9 PISTON AND CYLINDER WALL TEMPERATURES °C

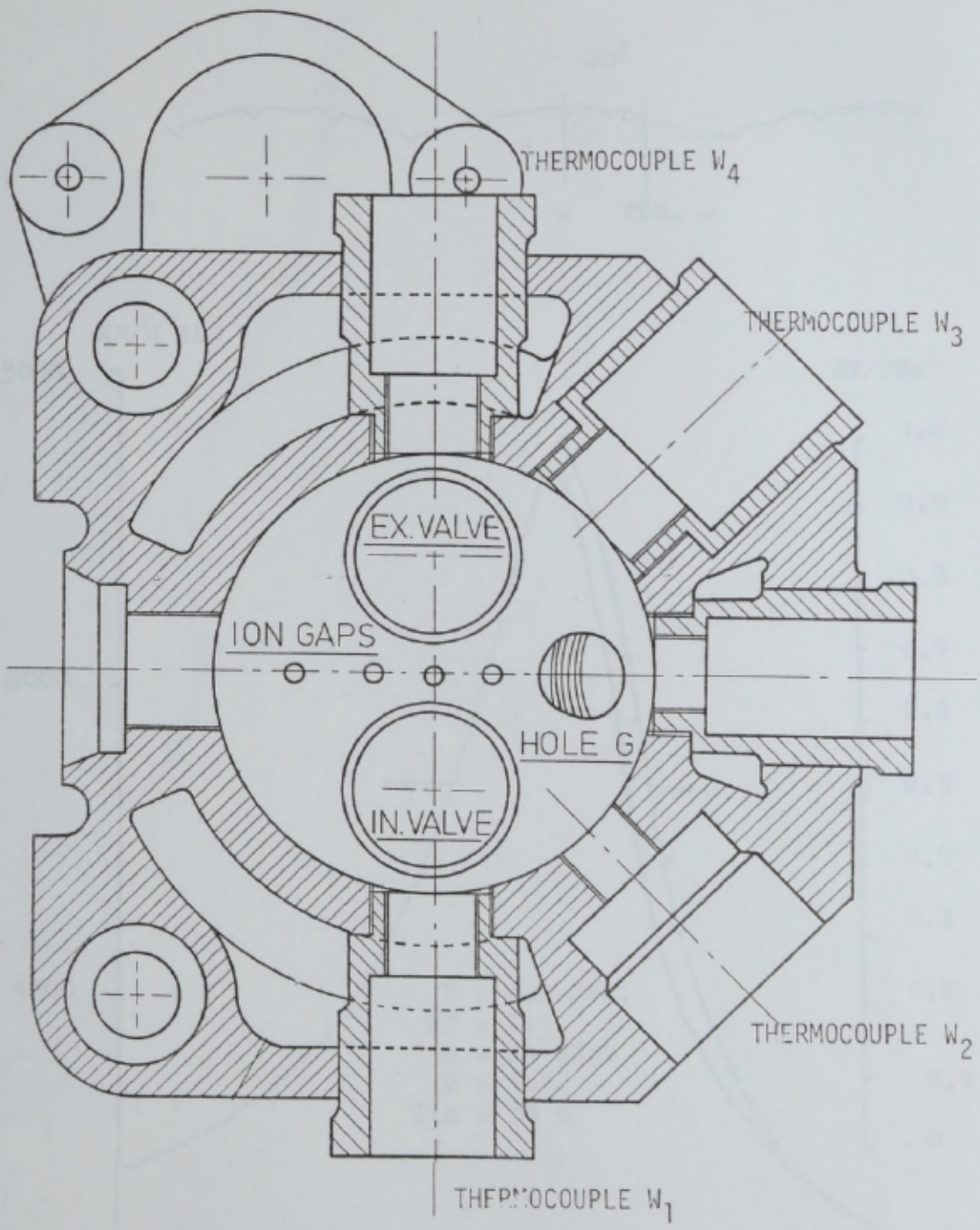

FIGURE 4.8 LOCATION OF THERMOCOUPLES IN CYLINDER HEAD

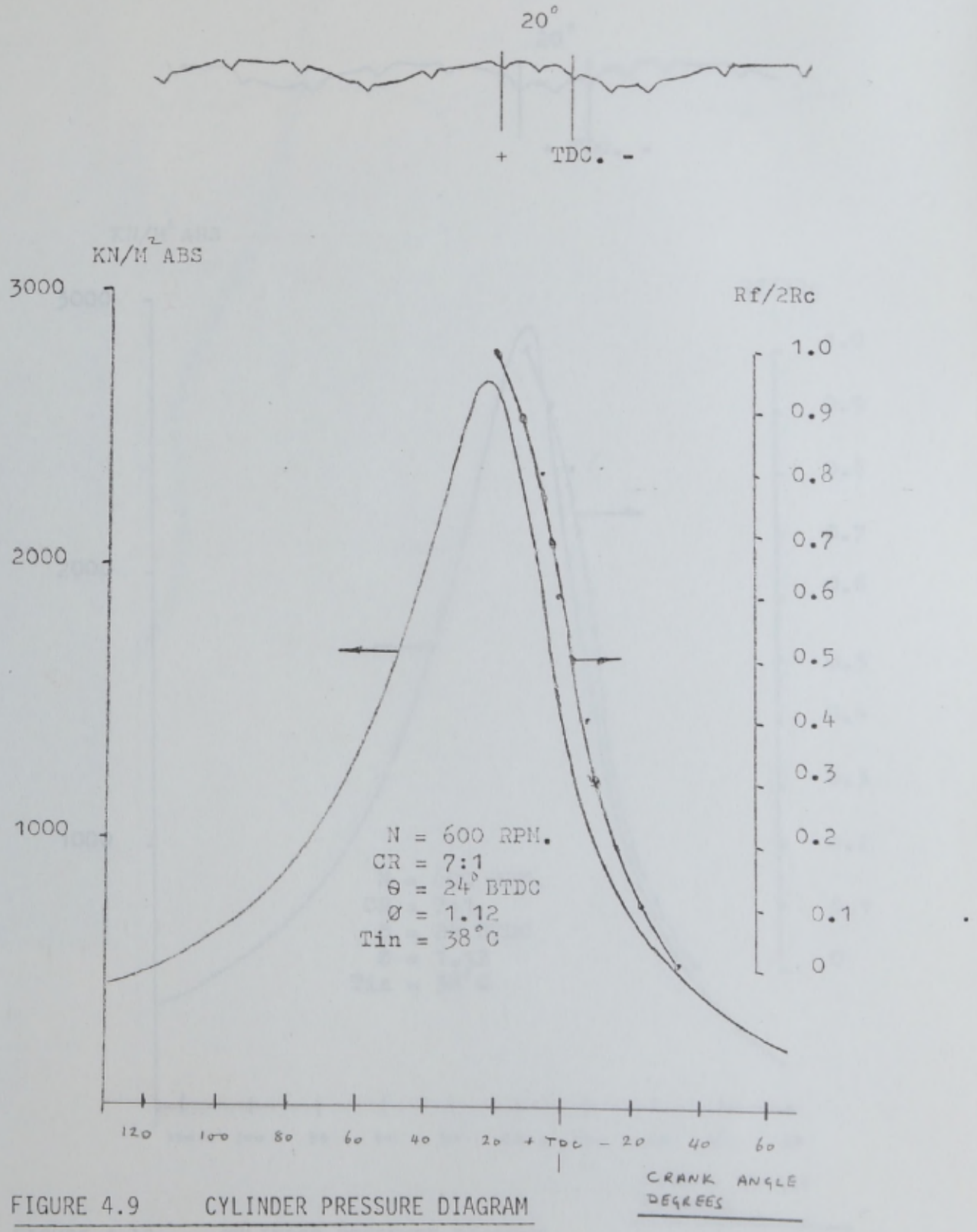

FIGURE 4.9 CYLINDER PRESSURE DIAGRAM

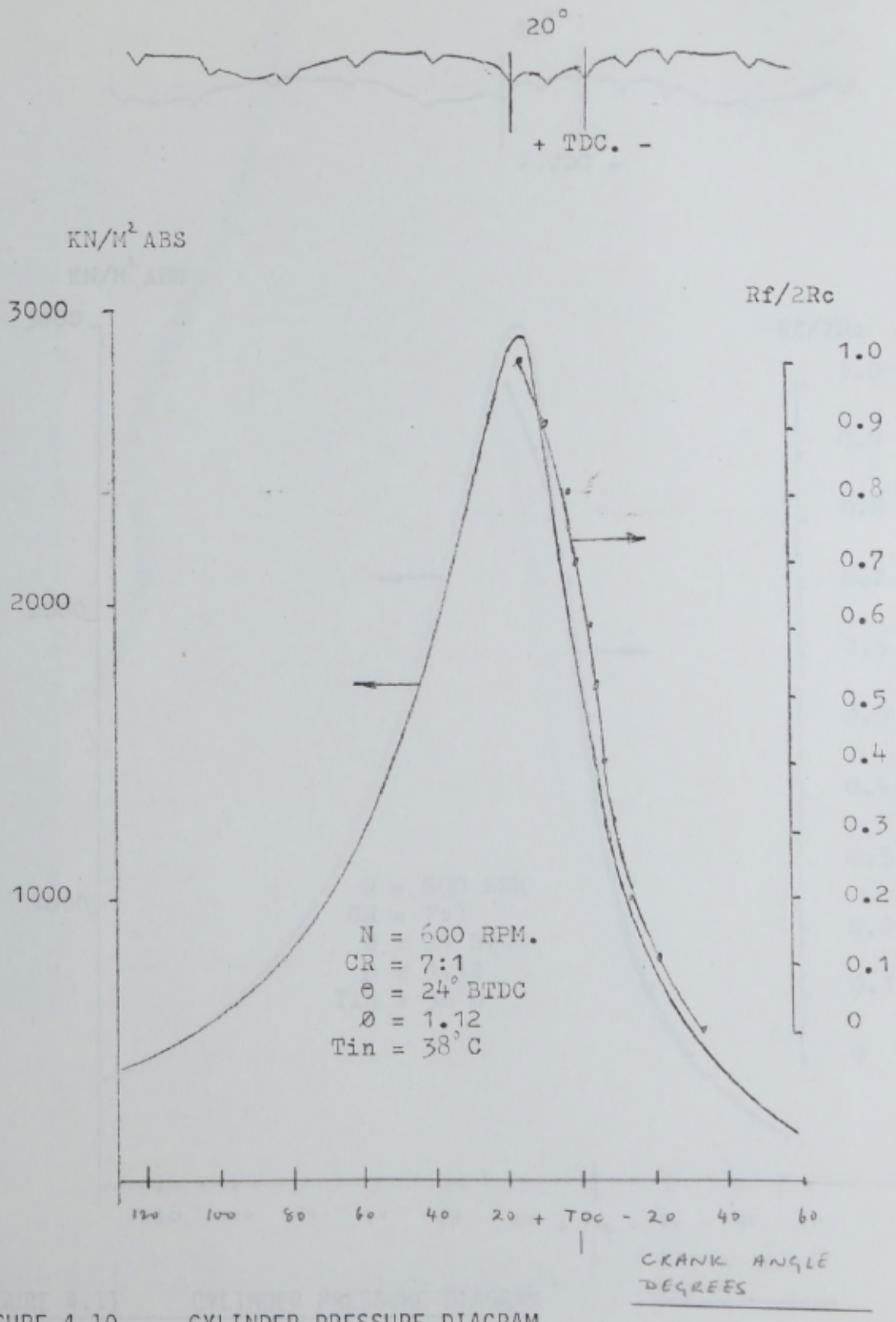

FIGURE 4.10 CYLINDER PRESSURE DIAGRAM

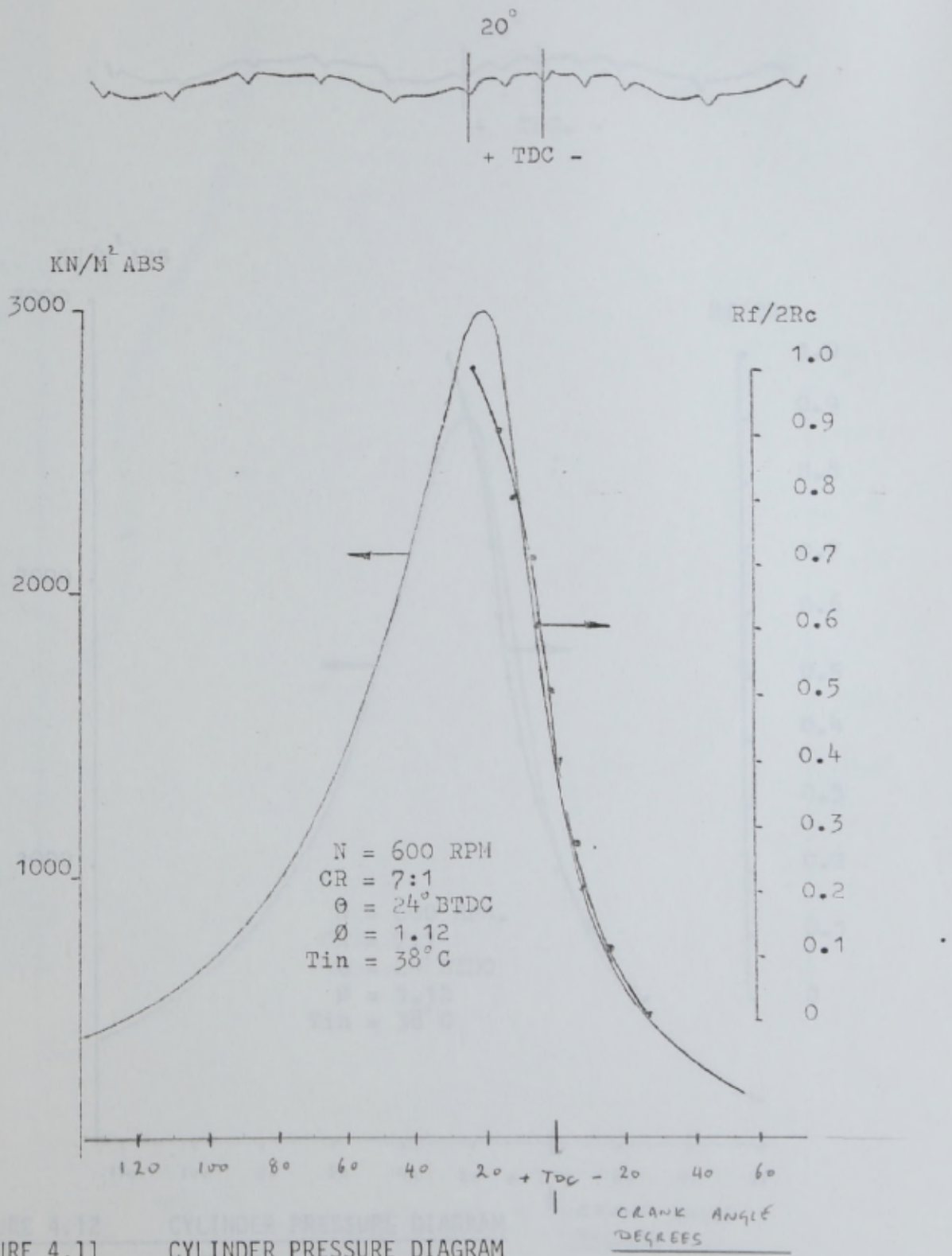

FIGURE 4.11 CYLINDER PRESSURE DIAGRAM

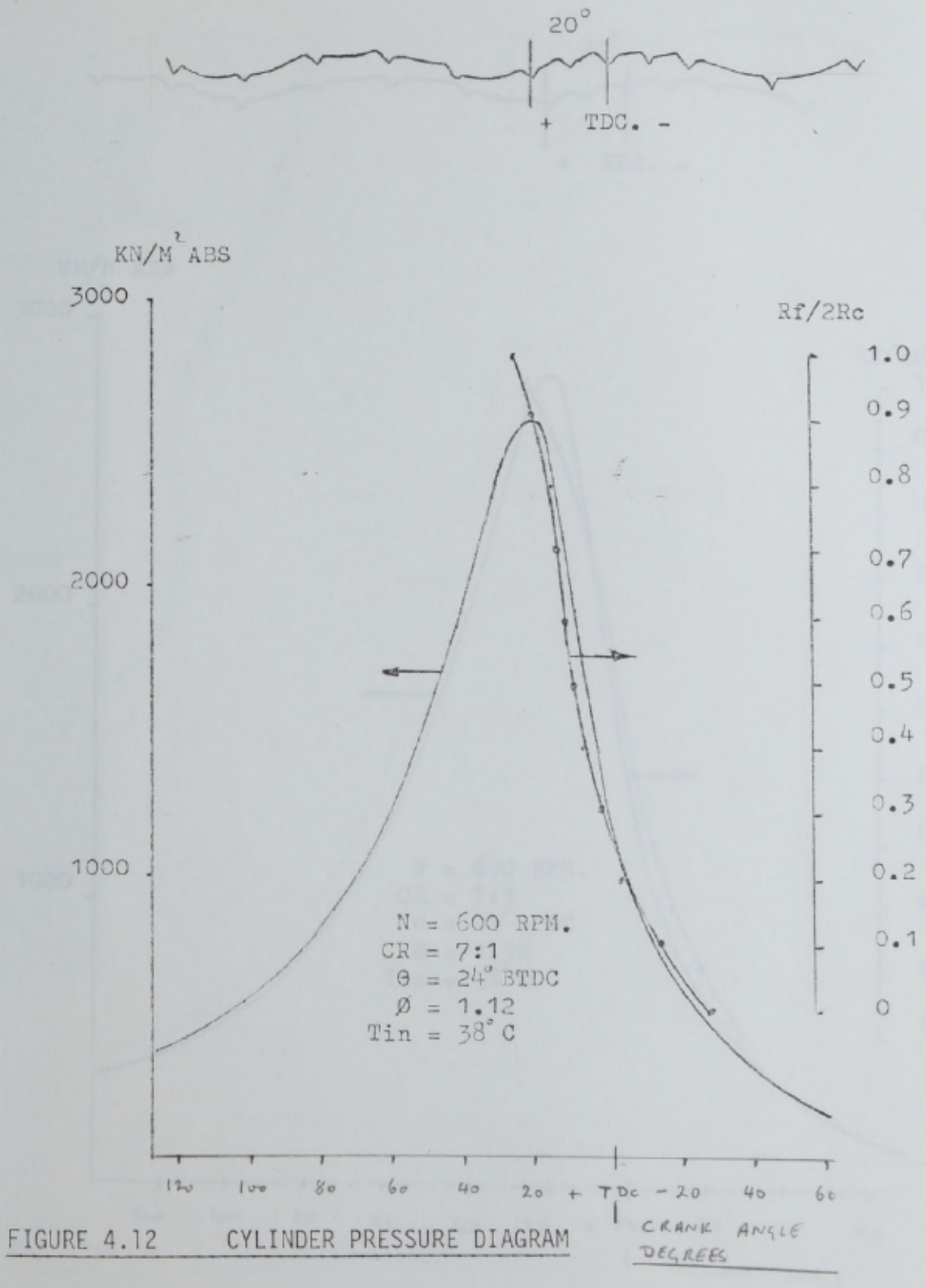

FIGURE 4.12 CYLINDER PRESSURE DIAGRAM

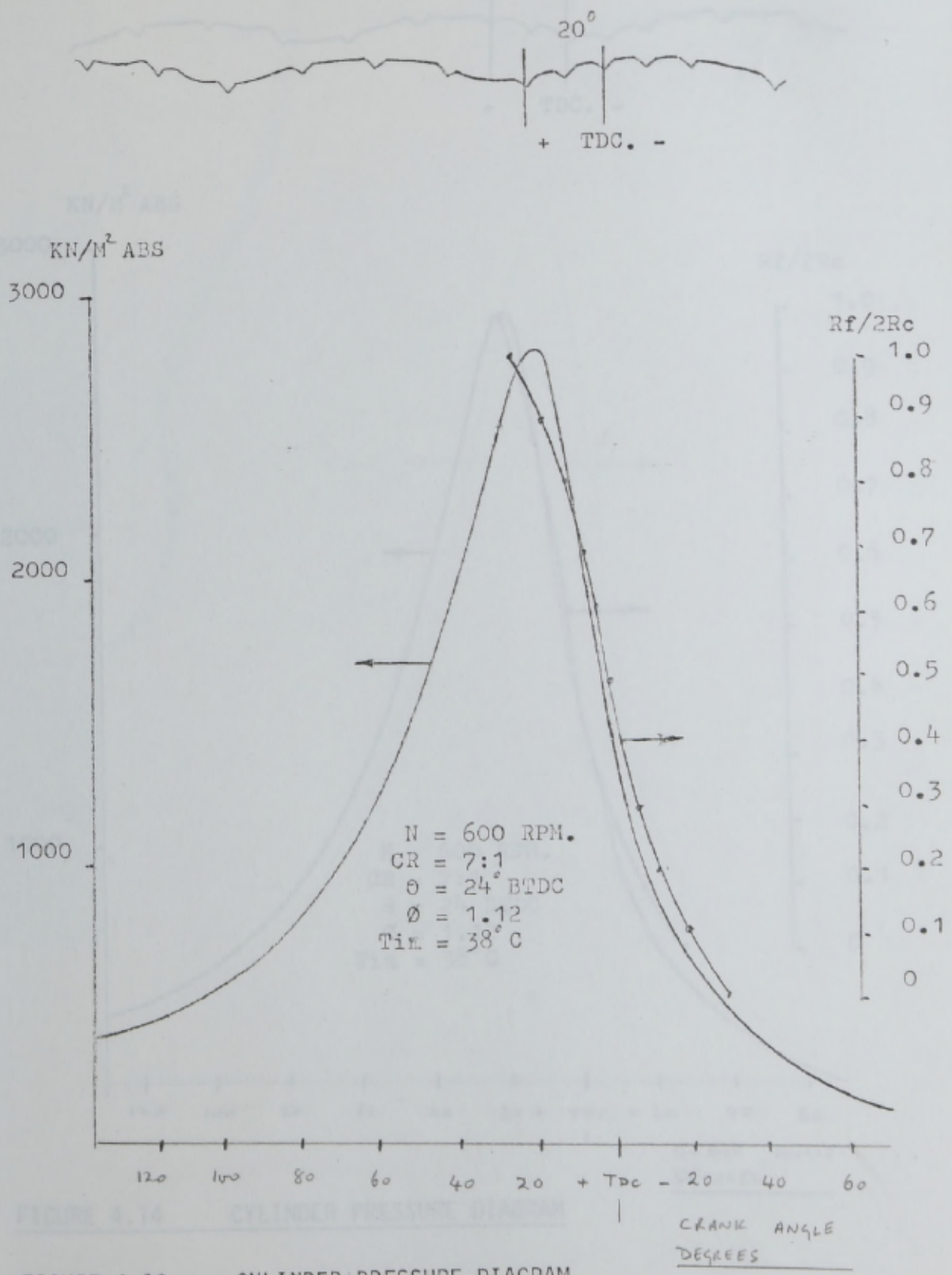

FIGURE 4.13 CYLINDER PRESSURE DIAGRAM

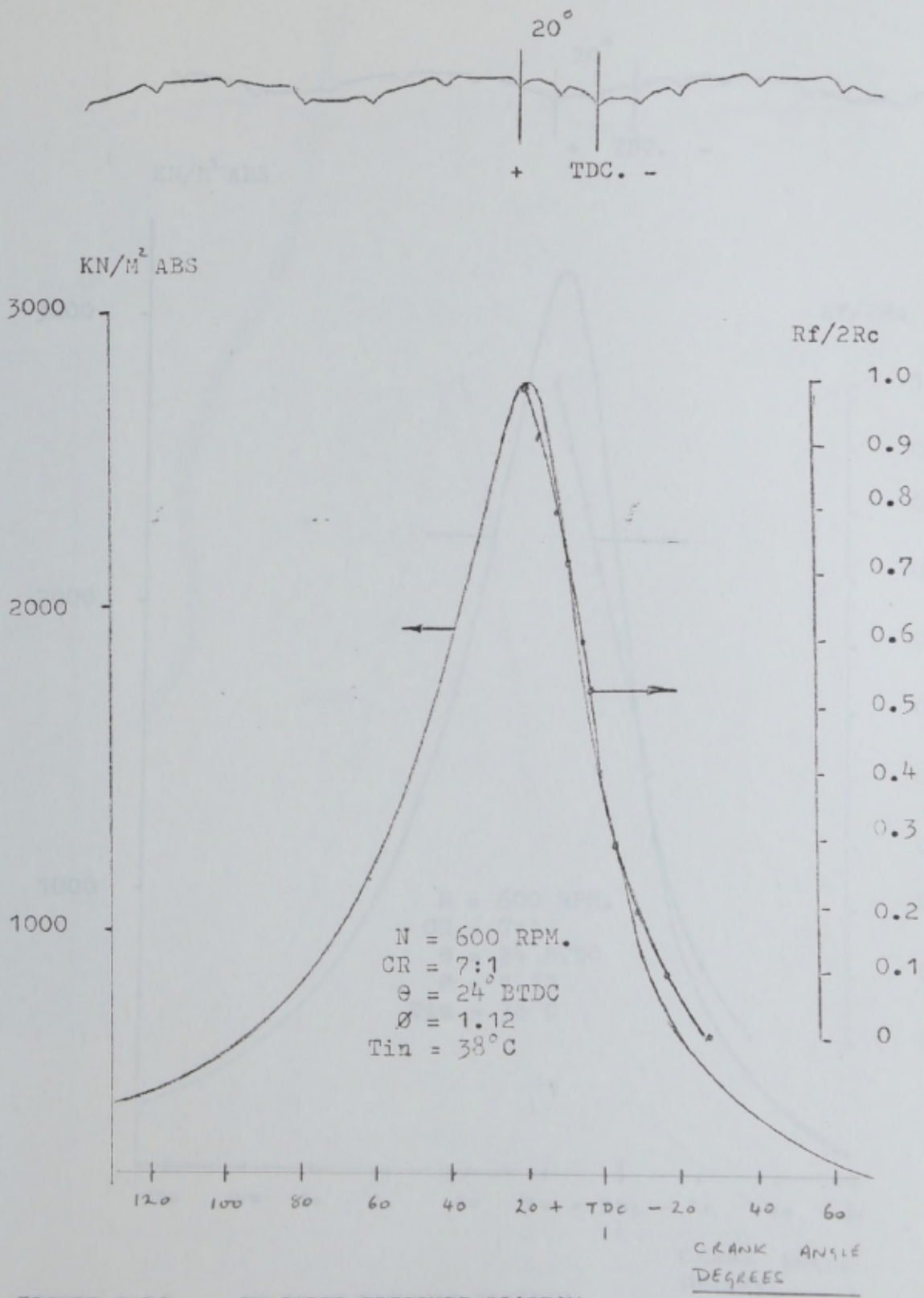

FIGURE 4.14 CYLINDER PRESSURE DIAGRAM

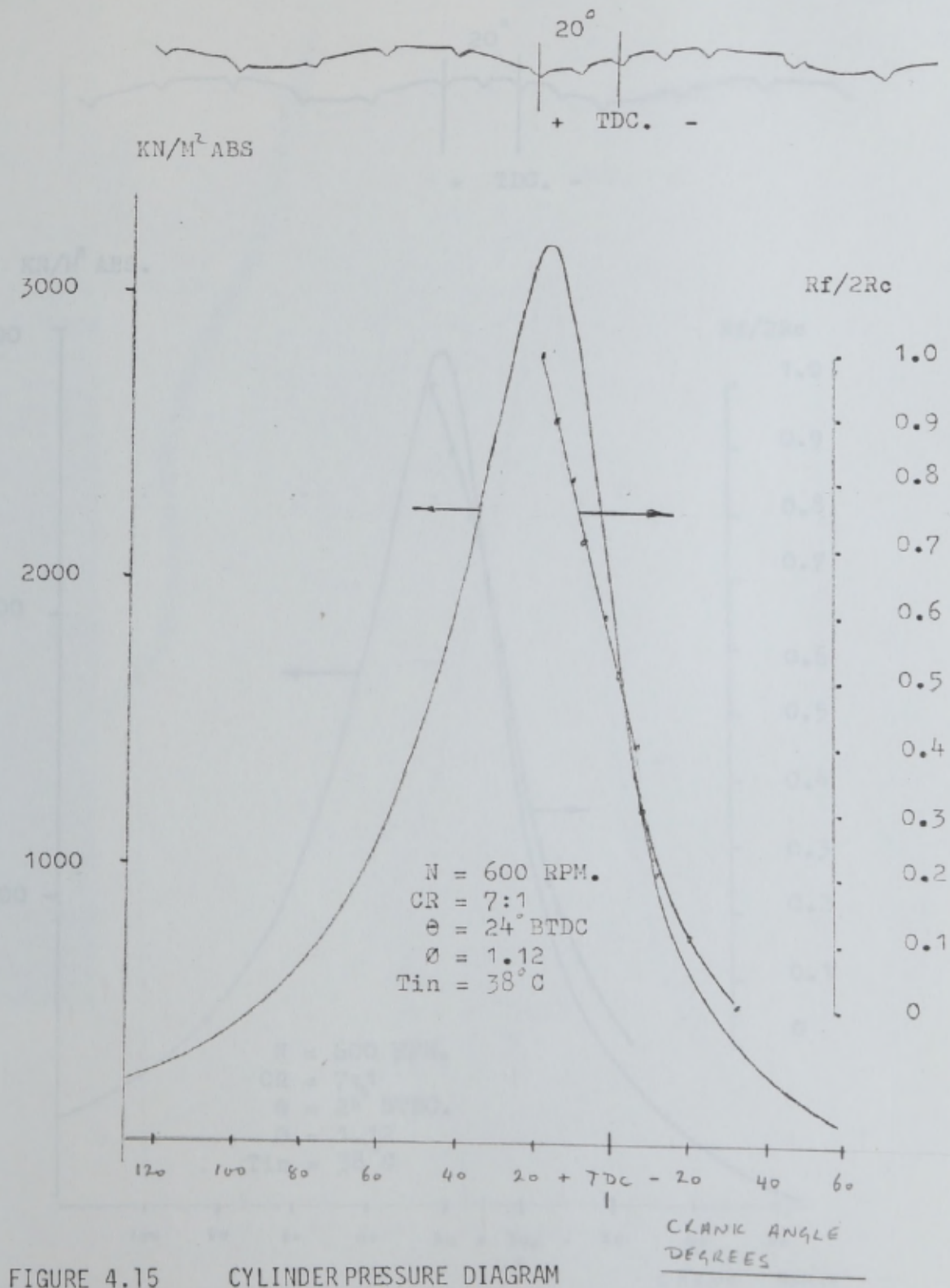

FIGURE 4.15 CYLINDER PRESSURE DIAGRAM

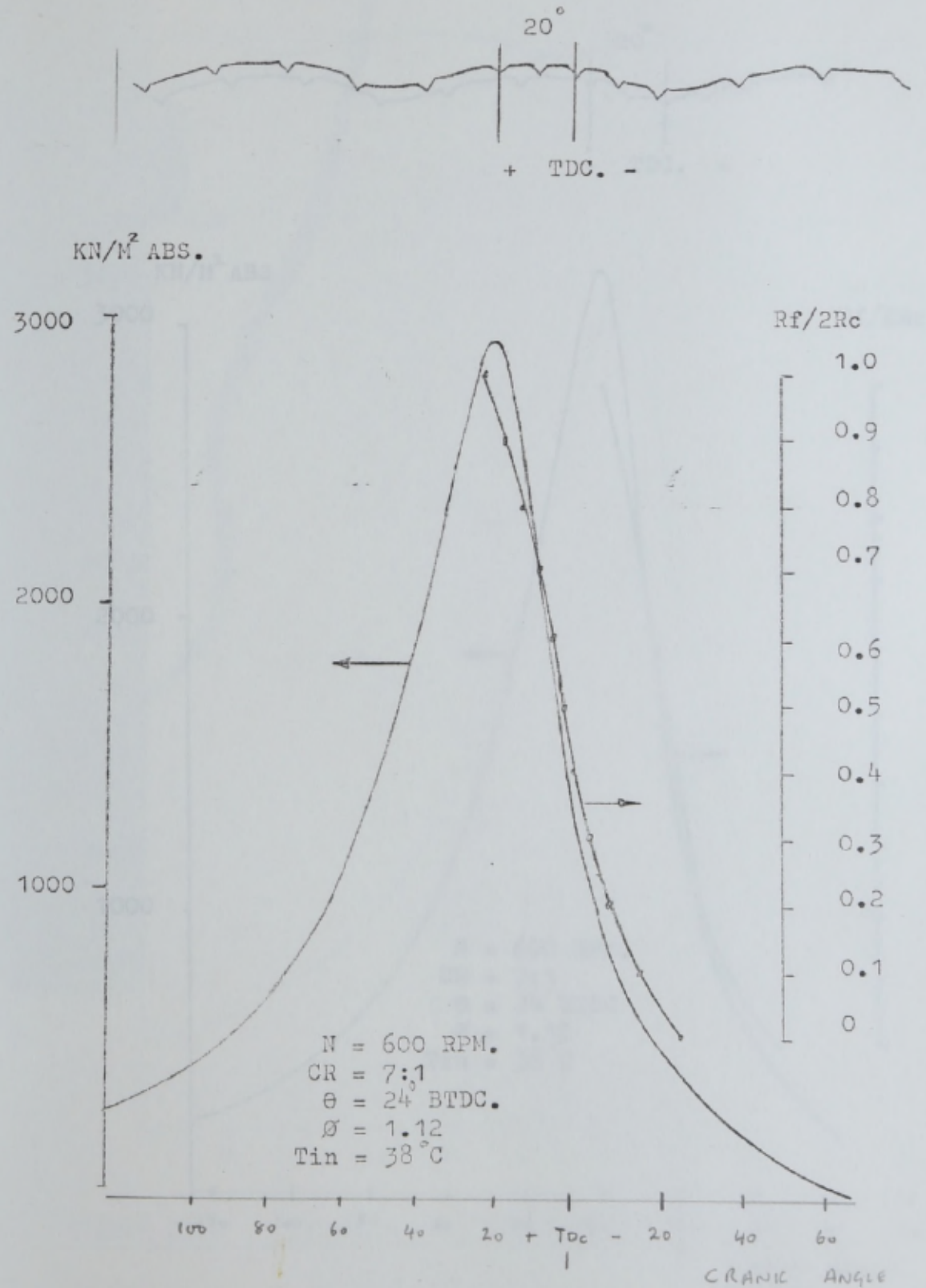

FIGURE 4.16 CYLINDER PRESSURE DIAGRAM

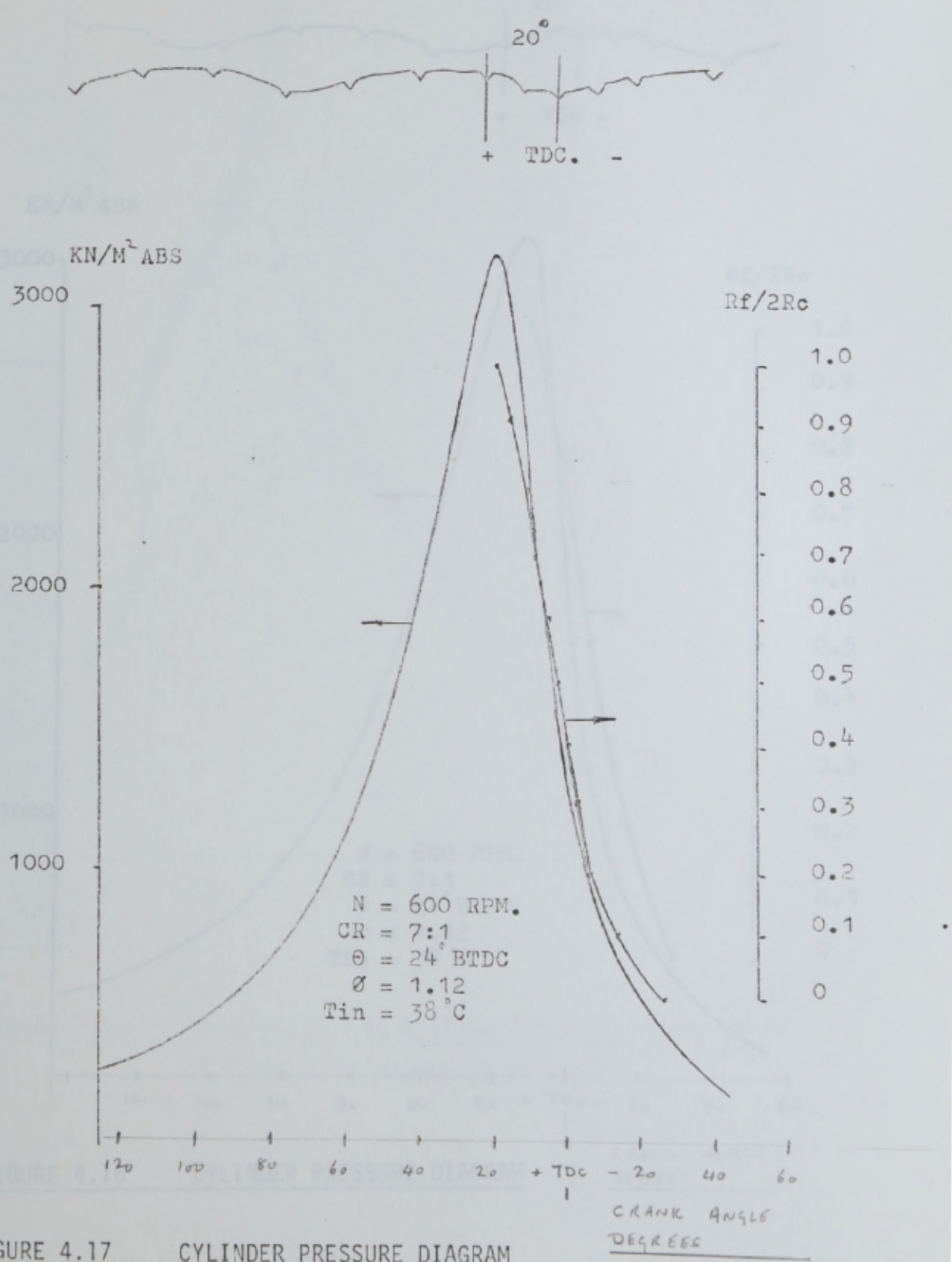

FIGURE 4.17 CYLINDER PRESSURE DIAGRAM

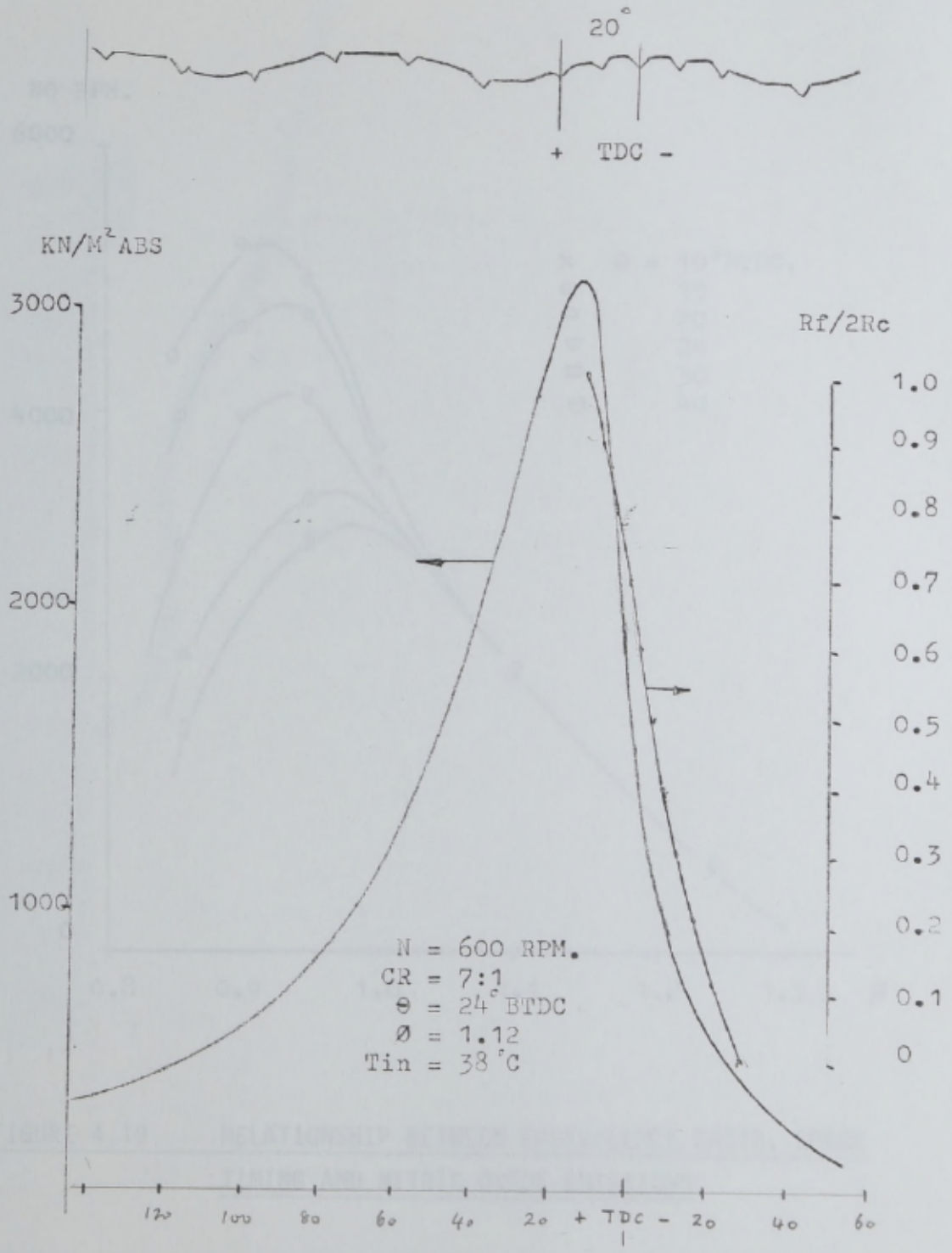

FIGURE 4.18 CYLINDER PRESSURE DIAGRAM

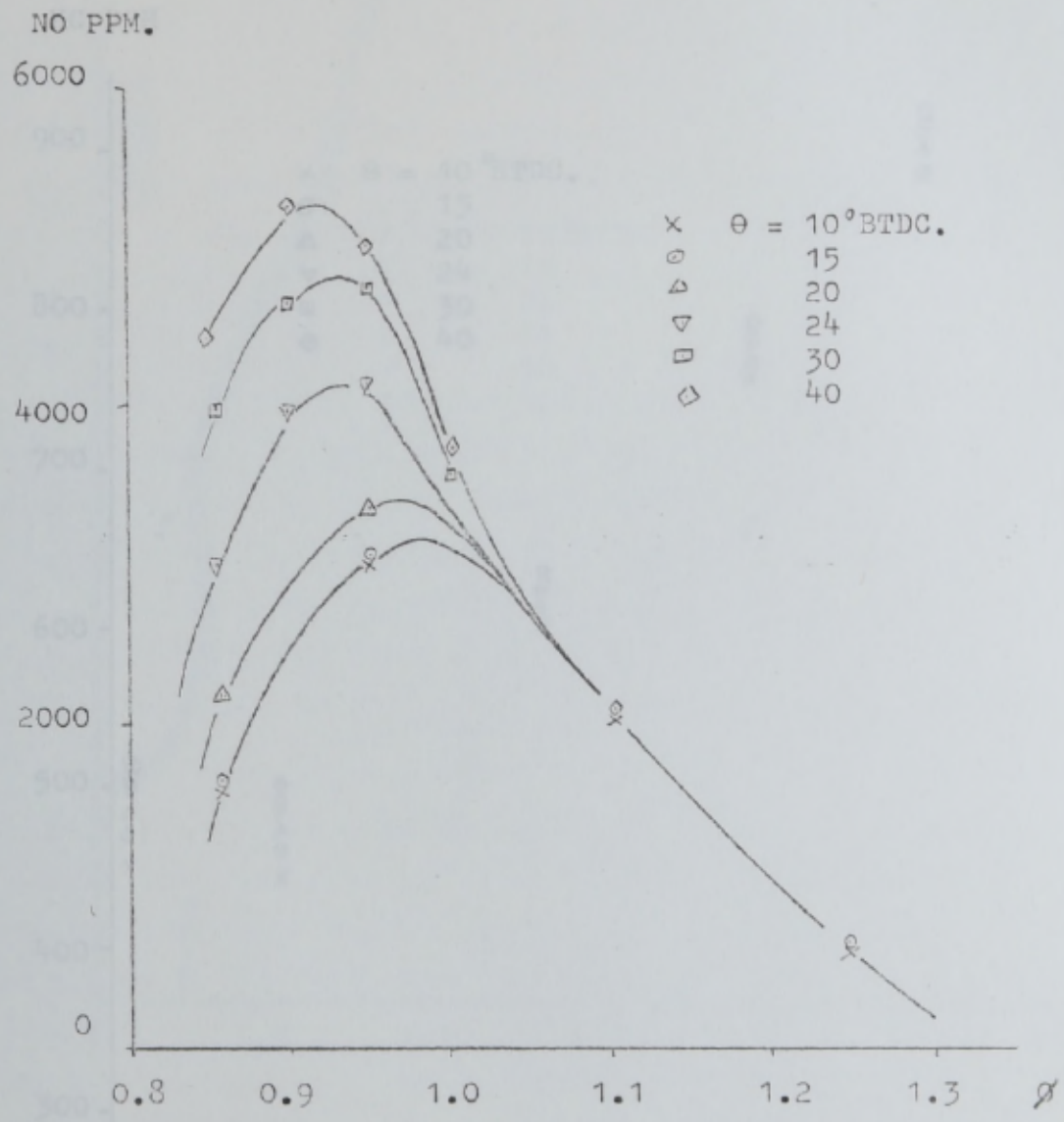

FIGURE 4.19 RELATIONSHIP BETWEEN EQUIVALENCE RATIO, SPARK TIMING AND NITRIC OXIDE EMISSIONS

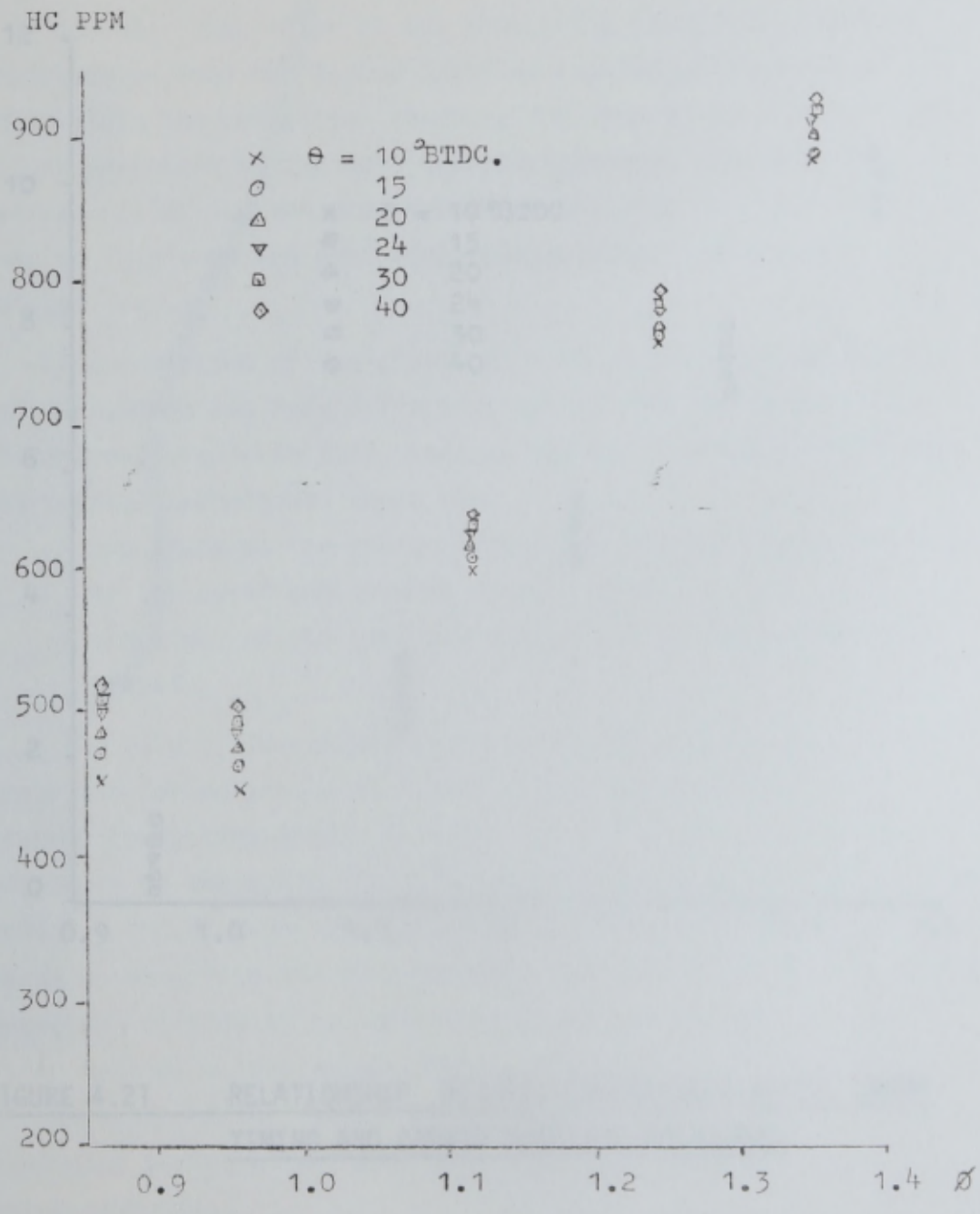

FIGURE 4.20 RELATIONSHIP BETWEEN EQUIVALENCE RATIO, SPARK TIMING AND HYDROCARBON EMISSIONS

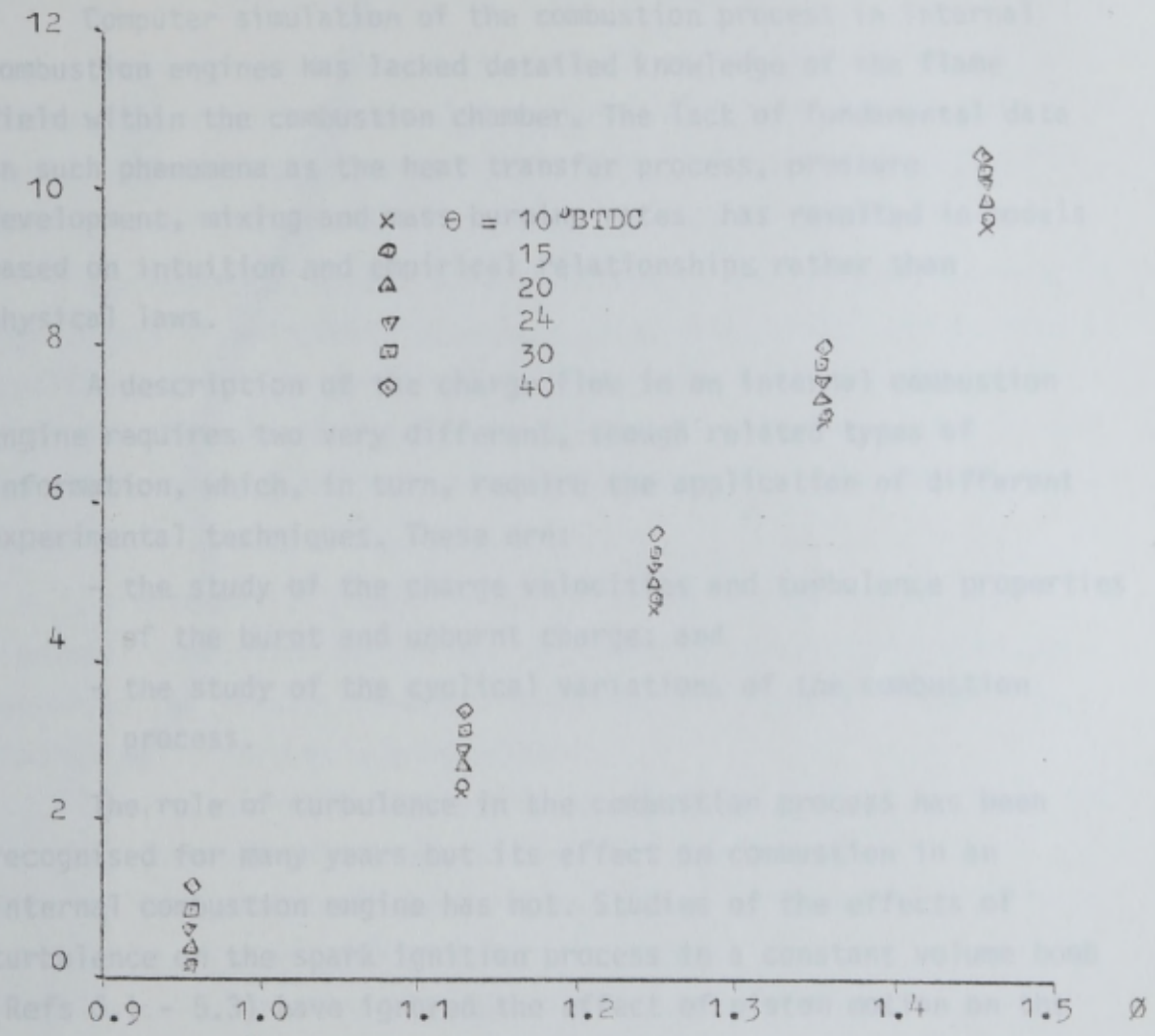

FIGURE 4.21 RELATIONSHIP BETWEEN EQUIVALENCE RATIO, SPARK TIMING AND CARBON MONOXIDE EMISSIONS

CHAPTER 5 MATHEMATICAL ANALYSIS

INTRODUCTION

Computer simulation of the combustion process in internal combustion engines has lacked detailed knowledge of the flame field within the combustion chamber. The lack of fundamental data on such phenomena as the heat transfer process, pressure development, mixing and mass burning rates has resulted in models based on intuition and empirical relationships rather than physical laws.

A description of the charge flow in an internal combustion engine requires two very different, though related types of information, which, in turn, require the application of different experimental techniques. These are:

- the study of the charge velocities and turbulence properties of the burnt and unburnt charge; and
- the study of the cyclical variations of the combustion process.

The role of turbulence in the combustion process has been recognised for many years but its effect on combustion in an internal combustion engine has not. Studies of the effects of turbulence on the spark ignition process in a constant volume bomb (Refs 5.1 - 5.3) have ignored the effect of piston motion on the charge burning rate and have produced conflicting conclusions. The conceptual difficulty in modelling a variable, heterogeneous system such as occurs in an engine, and the lack of experimental corroboration of the theory have hindered the process of developing stringent mathematical models of turbulence in IC engine combustion.

It has been suggested (Ref 5.4) that establishing correct levels of turbulence in the unburnt charge will reduce the extent of the cyclical variation of the combustion process. Others (Ref 5.5) have suggested that the cyclical variation is dependent on the initial period of flame development at the point of ignition.

However, the ignition process is dependent on several variables, including the ignition timing, and the air-fuel ratio, both of which exhibit their own cyclical variations in a normal running engine. In addition, the effect of flame-generated turbulence on the cyclical variations has not been considered.

The concentrations of the exhaust emissions of internal combustion engines are usually measured with instruments whose design and response characteristics are limited to indicating the mean emission concentrations taken over several engine cycles.

Mathematical models were developed as design tools to predict the levels of emissions in exhaust gases and do not take account of cyclical variations in the combustion process. Where emissions are a linear function of the cyclically-changing variable, this is of no consequence, but errors will occur where the relationship is non-linear.

A mathematical model to describe the combustion process in an internal combustion engine was developed in conjunction with the experimental results reported in Chapter 4. In this chapter, the following techniques are described:

- analysis of pressure data to derive mass burning rates and thermodynamic properties of the burnt charge;
- development of the turbulent flame speed correlation to be used to predict mass burning rates;
- calculation of the equilibrium concentrations of the combustion products; and
- determination of the geometric properties of the flame front and the combustion chamber.

A first law analysis of the reacting system in the combustion chamber is produced, to be compared with the mass burning rate predicted from an examination of burner theory. The equilibrium products of combustion are predicted using a program designed to deal with the gas phase productsof combustion of hydrocarbon fuels containing C, H, O and N atoms and air.

5.1 THE THERMODYNAMIC MODEL

Experimental cylinder pressure data are used to compute the mass burning rates. As a first approximation for establishing the turbulent combustion data, the burnt charge is assumed to be in chemical equilibrium. A thermodynamic energy balance on the burnt and unburnt system of ideal gases and the measured pressure traces provide all the information required for the burning rate computation.

The burnt and unburnt charges are assumed to be unmixed, with each section of uniform temperature. The pressure is taken to be uniform throughout the combustion chamber. It is therefore necessary to solve for 6 unknowns, that is, for each zone, the mass M, the volume V and the temperature T. This can be achieved from consideration of the following 6 equations, based on the equations of state, and mass and energy conservation.

Conservation of mass and volume gives:

$$\frac{dM_u}{dt} = -\frac{dM_b}{dt} \tag{1}$$

$$\frac{dV}{dt} = \frac{dV_u}{dt} + \frac{dV_b}{dt} \tag{2}$$

Assuming ideal gas conditions in both the burnt and unburnt charge, and taking R as a constant:

$$\frac{\dot{P}}{P} = \frac{\dot{T}_u}{T_u} + \frac{\dot{M}_u}{M_u} - \frac{\dot{V}_u}{V_u} \tag{3}$$

$$\frac{\dot{P}}{P} = \frac{\dot{T}_b}{T_b} + \frac{\dot{M}_b}{M_b} - \frac{\dot{V}_b}{V_b} \tag{4}$$

A first law analysis of 2 thermodynamically equilibrated systems gives:

$$\dot{M_u u_u} = -P\dot{V}_u + \Sigma Q_{ui} + H_u\dot{M}_u \tag{5}$$

$$\dot{M_b u_b} = -P\dot{V}_b + \Sigma Q_{bi} + H_b\dot{M}_b \tag{6}$$

The terms on the right hand side of the above equation represent work, heat exchange and mass exchange. The heat transfer terms were

summed over the surface of the piston, cylinder walls and cylinder head. The total heat transfer was computed from the following equation:

$$\sum Q_i = \sum h \left(T_i - T \right) A_i \qquad (7)$$

The heat transfer coefficient h was calculated using Sitkei's correlation (5.6) explained in Chapter 7. The wall temperatures were based on those measured in the experimental phase and the wall areas exposed to the burnt and unburnt charge, from the known geometry of the engine, assuming spherical flame front propagation.

Rearrangement of Equations 1 - 6 gave integratable functions of pressure for the unknowns in each zone.

$$\frac{dT_u}{dt} = \left[\frac{T_u}{P} \frac{dP}{P} + \sum Q_{ui} / \left[R_u (M - M_b) \right] \right] \Big/ \left(\frac{du}{dT_u} / \left(R_u + 1 \right) \right) \qquad (8)$$

$$\frac{dm_b}{dt} = \frac{\left\{ \left(M - M_b \right) R_u T_u - \frac{dP}{dt} V \right] \left(\frac{du_u}{dT_u} / \left(R_u + 1 \right) - P \frac{dV}{dt} \left[\frac{du_b}{dt} / R_b - \left(\frac{V_b}{V} + 1 \right) \right] \right\} + \sum Q_i}{\left(u_b - u_u \right) + \left(R_u T_u / R_b - T_b \right) \left(\frac{du_b}{dT_b} \right)} \qquad (9)$$

$$\frac{dV_b}{dt} = \left(V - V_b \right) \left[\frac{dM_b}{dt} \frac{1}{\left(M - M_b \right)} - \frac{1}{T_u} \frac{dT_u}{dt} + \frac{1}{P} \frac{dP}{dt} \right] + \frac{dV}{dt} \qquad (10)$$

$$T_b = \frac{P V_b}{R_b M_b} \qquad (11)$$

Equations 8 - 11 were integrated numerically using a fourth order Runge - Kutta technique. Thermodynamic properties of the burnt zone were determined by considering an equilibrium composition for the burnt fraction as shown in Appendix 2.

In order to initiate the computations it was assumed that 0.1% of the total mass in the cylinder burned instantaneously at the time of ignition. The adiabatic flame temperature was used to obtain the initial burnt volume. The results of the computation are presented in Figures 5.1 - 5.5 and discussed in Chapter 8.

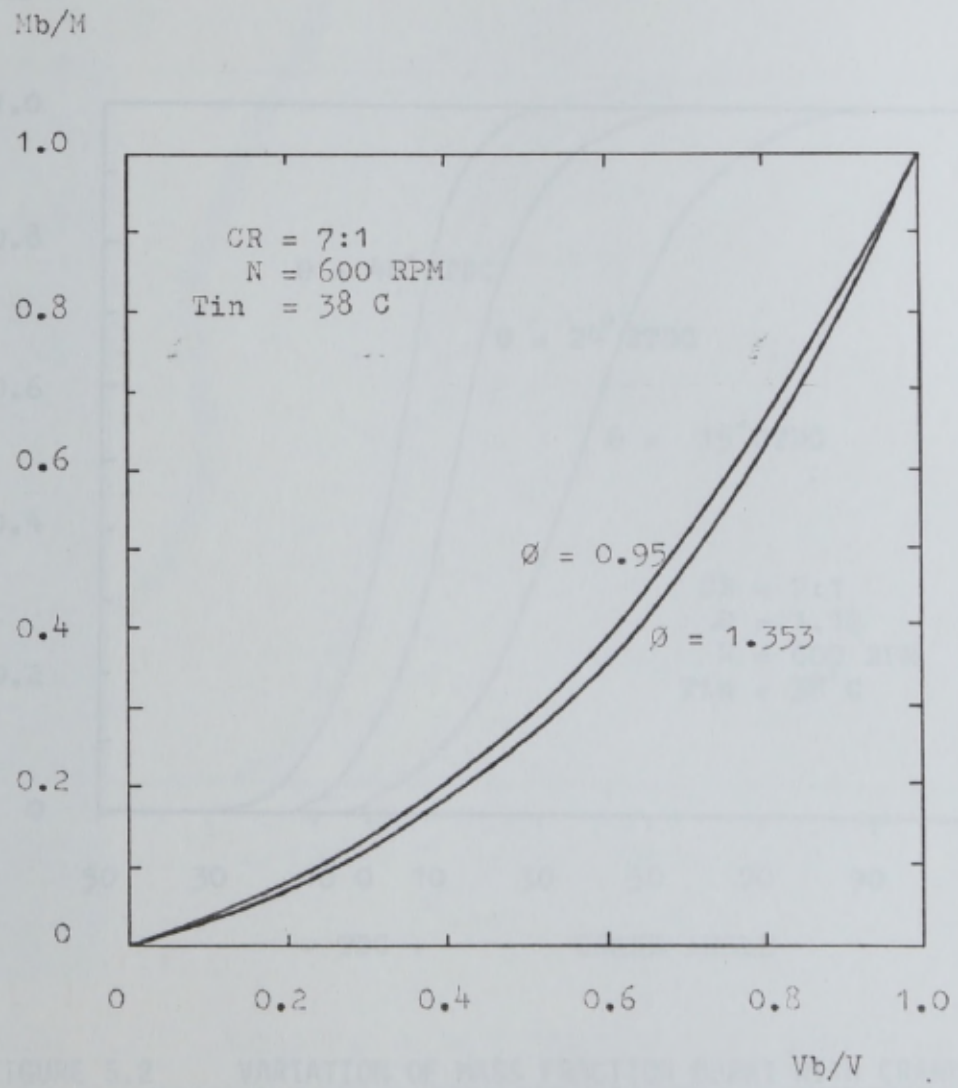

FIGURE 5.1 MASS FRACTION BURNT AGAINST VOLUME FRACTION BURNT FOR SEVERAL EQUIVALENCE RATIOS (FUEL TYPE: ISOOCTANE)

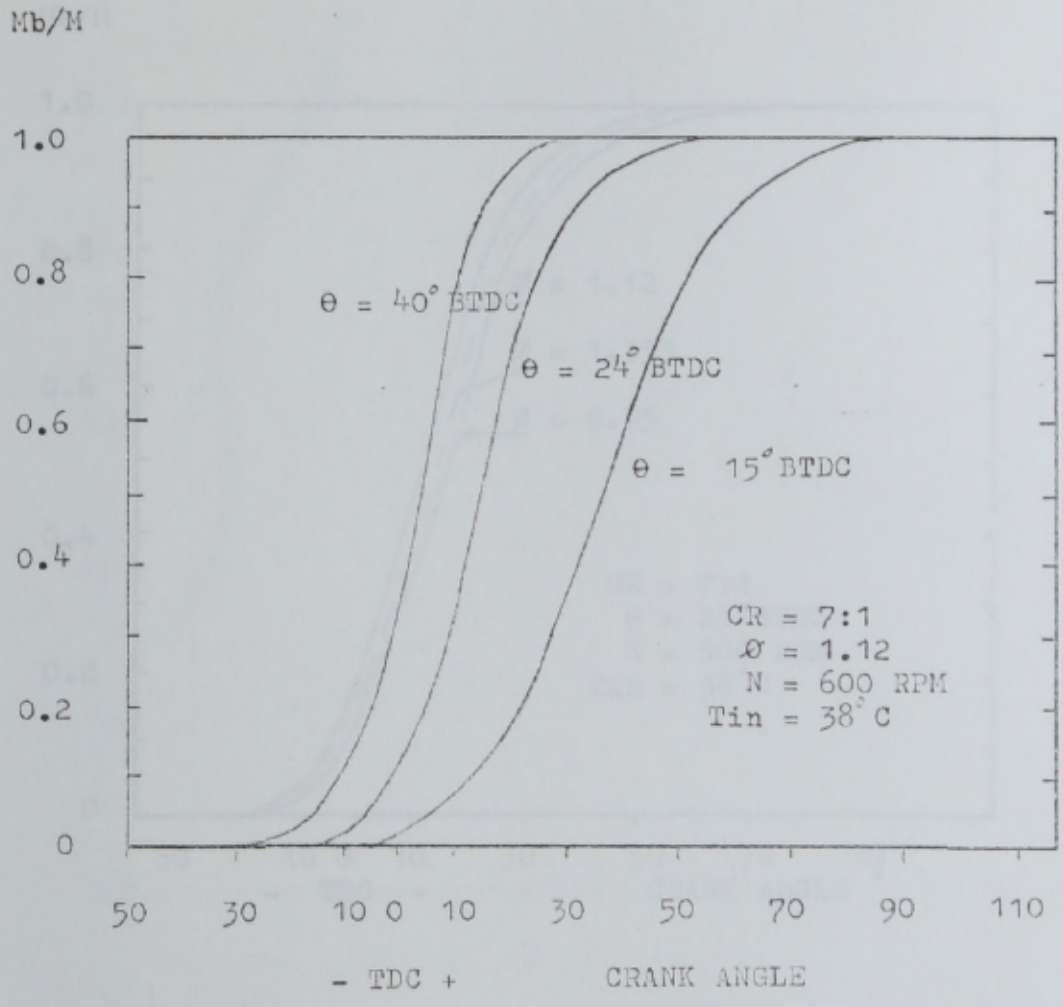

FIGURE 5.2 VARIATION OF MASS FRACTION BURNT WITH CRANK ANGLE FOR SEVERAL SPARK TIMINGS (FUEL TYPE: ISOOCTANE)

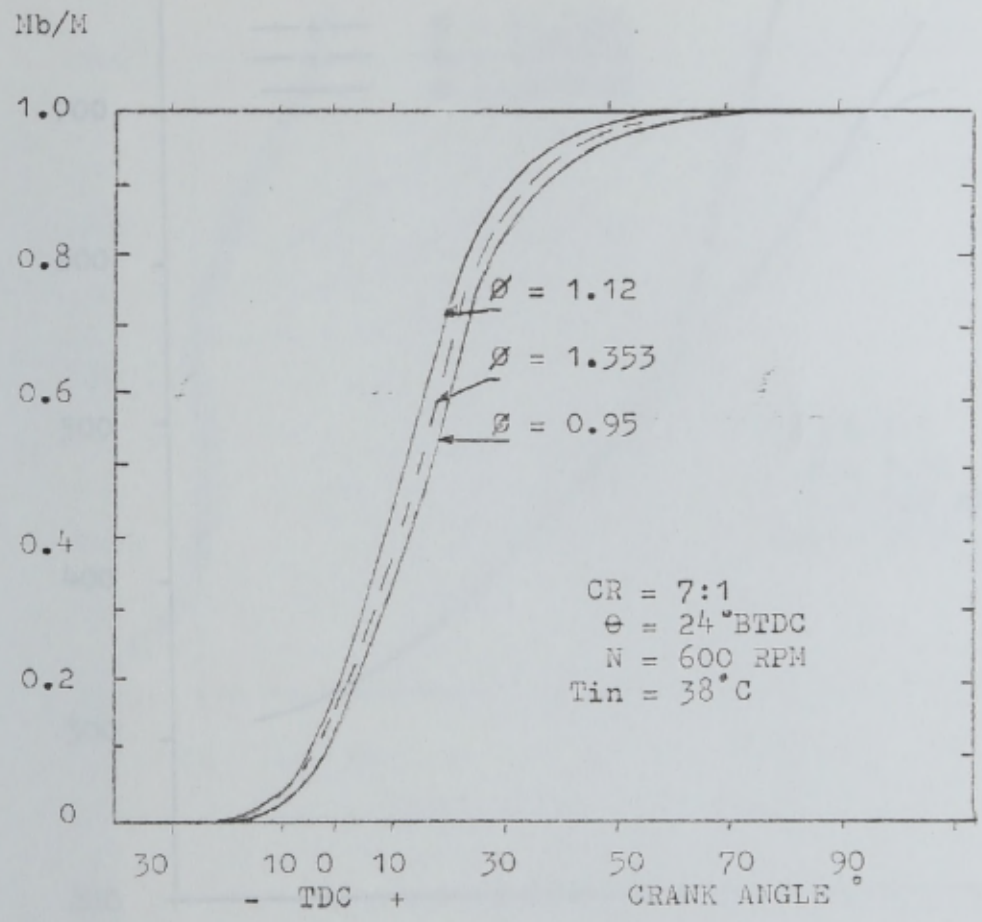

FIGURE 5.3 VARIATION OF MASS FRACTION BURNT WITH CRANK ANGLE FOR SEVERAL EQUIVALENCE RATIOS

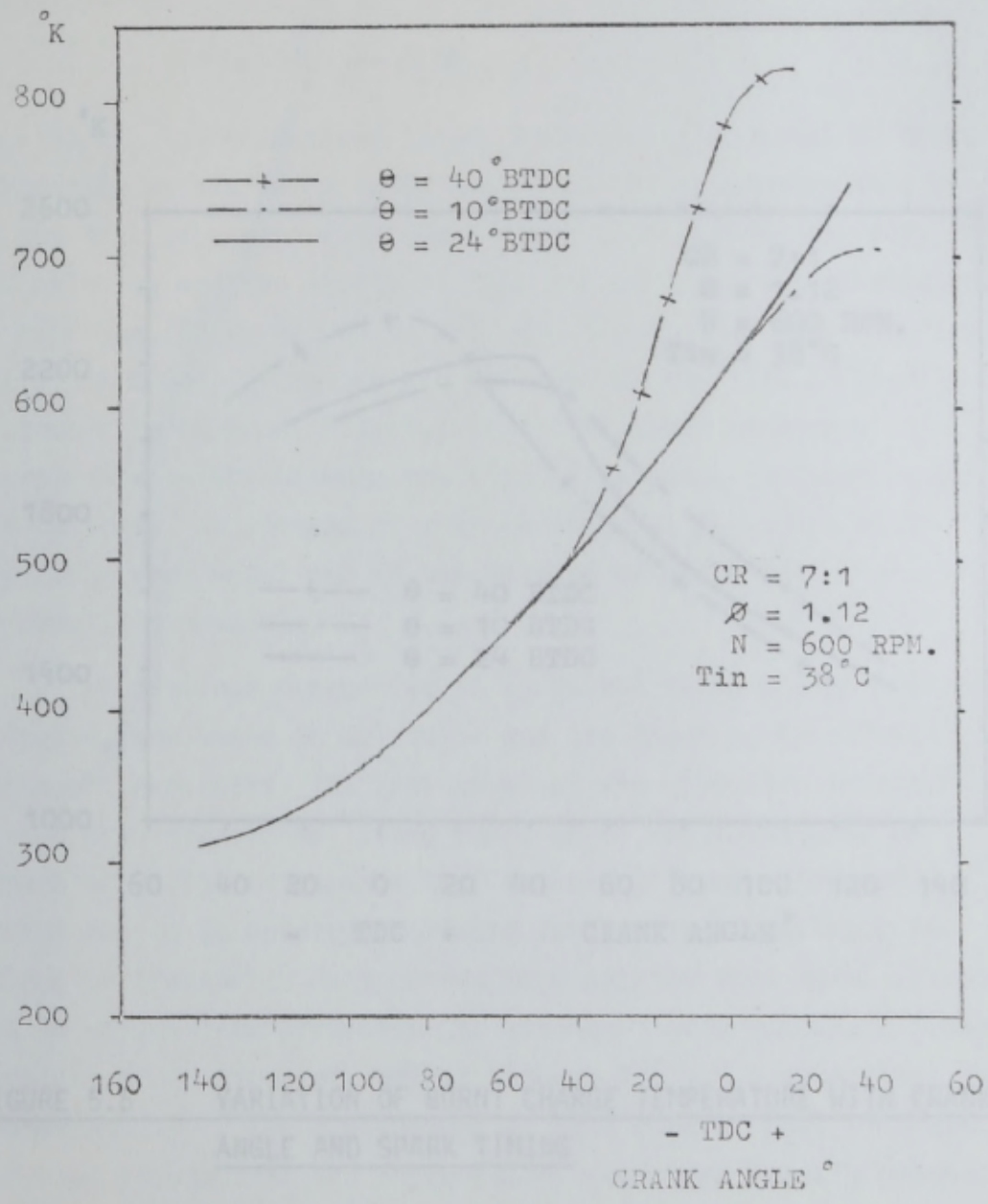

FIGURE 5.4 VARIATION OF UNBURNT CHARGE TEMPERATURE WITH CRANK ANGLE AND SPARK TIMING

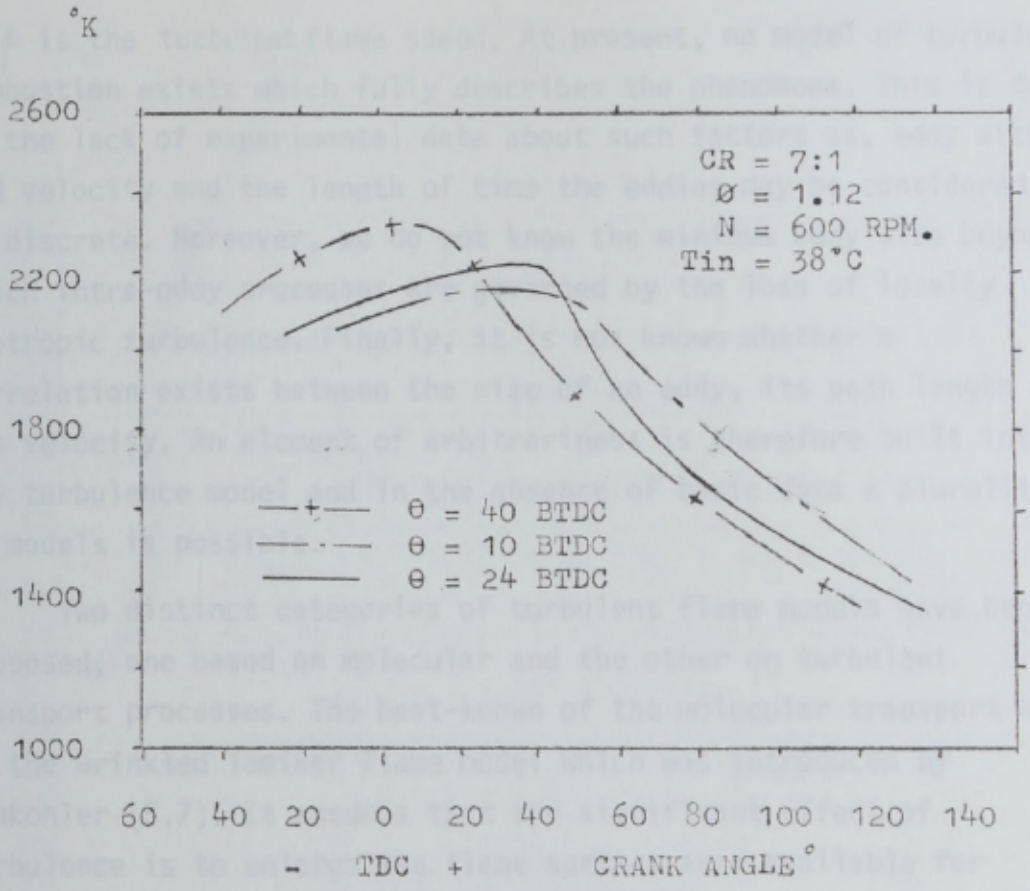

FIGURE 5.5 VARIATION OF BURNT CHARGE TEMPERATURE WITH CRANK ANGLE AND SPARK TIMING

5.2 PREDICTION OF THE TURBULENT FLAME SPEED

The calculation of the mass burning rate is closely related to the flame speed and the flame front area according to the relationship:

$$\dot{M}_b = \rho_u A_f V_f$$

V_f is the turbulent flame speed, At present, no model of turbulent combustion exists which fully describes the phenomena. This is due to the lack of experimental data about such factors as, eddy size and velocity and the length of time the eddies may be considered to be discrete. Moreover, we do not know the minimum eddy size beyond which intra-eddy processes are governed by the loss of locally isotropic turbulence. Finally, it is not known whether a correlation exists between the size of an eddy, its path length and its velocity. An element of arbitrariness is therefore built into any turbulence model and in the absence of basic data a plurality of models is possible.

Two distinct categories of turbulent flame models have been proposed, one based on molecular and the other on turbulent transport processes. The best-known of the molecular transport models is the wrinkled laminar flame model which was introduced by Damkohler (5.7). It assumes that the significant effect of turbulence is to enlarge the flame surface area available for molecular transport. Many others have adopted this model although it has no unique interpretation. It assumes that a turbulent flame consists of an array of laminar flames. Table 5.1 summarises the approaches to the development of this model. Most of these theories assume that the micro-scale l is significantly greater than the laminar flame thickness. This assumption implies that small-scale eddy transport over a distance less than l has no significant effect and the sole effect of turbulence lies in an increase in flame surface area due to the action of the large-scale eddies.

The various theoretical models based on turbulent, as opposed to molecular, transport processes are summarised in Table 5.2. The models fall into 2 main categories, with emphasis on

AUTHOR	REF	EQUATION FOR U_t
Damkohler	5.7	$\frac{V_t}{V_1} = 1 + \frac{U'}{V_1}$
Shchelkin	5.9	$\frac{V_t}{V_1} = (1 + \beta(U'/V_1)^2)^{\frac{1}{2}}$
Frank-Kamenetski	5.10	$V_t = (lU'/\nu)^{\frac{1}{2}}$
Leason	5.11	$\frac{V_t}{V_1} = (1 + (2U'/V_1)^2)^{\frac{1}{2}}$
Karlovitz	5.12	$V_t = V_1 + (2V_1U')^{\frac{1}{2}}$ For strong turbulence u' is increased by $U'' = V_1/\sqrt{3}\ (\rho_u/\rho_b - 1)$
Talantov	5.13	$\frac{V_t}{V_1} = \frac{T_b}{T_u} + \frac{2U'/V_1}{(\ln(1 + U'/V_1))^{\frac{1}{2}}}$
Karpov et al	5.8	$V_t = \frac{1}{2}U(1 + \rho_u/\rho_b)$ V_t = average eddy velocity U = eddy velocity
Tucker	5.14	$\frac{V_t}{V_1} = 1 + f(T_b/T_u)(U'/V_1)^2$
Richardson	5.15	$\frac{V_t}{V_1} = 1 + \frac{1}{2}\frac{U'}{1}$ $U' \ll V_1$ $\frac{V_t}{V_1} = 1 + \frac{V1}{2^{0.2}}(U'/V_1)^{0.8}$ $U' \gg V_1$

TABLE 5.1 PREDICTION OF V_t FOR A WRINKLED LAMINAR FLAME MODEL

AUTHOR	REF	EQUATION FOR U_t
Damkohler	5.7	$\frac{V_t}{V_1} = \left(\frac{\epsilon}{\lambda}\right)^{1/2} = \left(\frac{\lambda_t}{K}\right)$ where $\epsilon = \frac{\lambda_t}{c\rho} = 1U'$
Shchelkin	5.9	$\frac{V_t}{V_1} = \left(1 + \frac{\lambda_t}{K}\right)^{1/2}$
Delbourg	5.16	$\frac{V_t}{V_1} = c\left(1 + \frac{\lambda_t}{K}\right)$
Summerfield	5.17	$\frac{V_t}{V_1} = \frac{\epsilon}{\lambda} \frac{\delta c}{\delta t}$
Bhaduri	5.18	$\frac{V_t}{V_1} = \frac{V_1 K}{V \lambda_t}$ V flow velocity

TABLE 5.2 TURBULENT FLAME MODEL PREDICTIONS OF V_t

large and small scale eddy transport respectively. Karpov et al (5.8) have postulated a turbulent flame structure in which propagation is due to turbulent mixing of burnt and unburnt gas, followed by spontaneous ignition in which the rate of flame propagation is expressed as the ratio of the macro Lagrangian scale to the chemical reaction time. Damkohler (5.7) has suggested a turbulent transport model in which the molecular transport in laminar flows was influenced by turbulence when the Lagrangian scale L was less than the laminar flame thickness.

There are several incompatibilities between the flame models listed in Table 5.2 and the structure of turbulence. Large eddies usually have a long life and low convective velocity and are usually connected with a velocity similar to the mean charge velocity (Taylor (5.19)). Transport of large reacting eddies into the unburnt gas is unlikely. This however may be possible with small eddy motion for which there is some evidence of high velocity motion relative to the mean flow (Refs 5.20 - 5.22). Others have proposed turbulent burning models for internal combustion engines based on small scale propagation (Refs 5.23 - 5.25). The basis of these models is the formation of an eddy from both the hot and previously unreacted charge. If the life of the eddy is greater than the chemical induction time for the conditions, the reaction proceeds within the eddy until its decay. After the decay of this and similar eddies in partially reacted or unreacted charge, another generation of eddies is born and reaction is induced in them intitiated by the heat release, temperature rise and species formation in the original eddies. The life of a small eddy may be less than the chemical induction time. If such an eddy becomes a component of a succeeding, but hotter eddy, then flame propagation is possible. Although these models represent an important advance in the understanding of the turbulent structure in an internal combustion engine, the nature of the approximations made in their formulation and the form of the relationship for the mass burning rates which they produce, precludes their general applicability for performance work or cycle calculations. Consequently, Tabaczynski (5.26) simplified the model and formulated correlations between eddy burn time and the various turbulent parameters.

Since no comprehensive theory of turbulence can be applied, and simplified correlations have to be produced to permit use of the models, the production of a correlation between turbulent burning velocity and non-dimensional parameters is a sensible next step.

Summerfield et al (5.17, 5.27) developed a turbulent transport model similar to that of Damkohler (5.7) but with no restriction on the turbulence macroscale. If changes in chemical kinetics are small and turbulent transport predominates, a relationship can be obtained between V_t / V_l and ϵ/λ where ϵ is the eddy diffusivity. Spalding (5.28 - 5.29) has derived an expression for V_l with the turbulent transport coefficients replacing those of molecular transport. If thermal conductivity K is replaced by $\epsilon \rho C_p$ and if the turbulent Lewis number is unity then:

$$\frac{V_t}{V_l} = \left(\frac{\epsilon \rho_u C_p}{K}\right)^{1/2} = \left(\frac{\epsilon}{\lambda} P_r\right)^{1/2} \qquad (1)$$

Values of ϵ/λ cannot be obtained theoretically but they have been measured in several experimental studies. Correlation of the available experimental data (5.30) suggests that, for isotropic turbulence:

$$\frac{\epsilon}{\lambda} = 20.5\left(\frac{\rho \bar{u} \lambda}{\mu}\right) \qquad \text{for} \quad Re_\lambda > 100 \qquad (2)$$

Thus theoretical values of V_t / V_l can be obtained from Equations 1 and 2 for different values of turbulent Reynolds number. For constant Prandtl number, Equation 2 suggests that:

$$\frac{V_t}{V_l} = f\left(Re_\lambda\right)$$

The data of Karpov, Semenov and Sokolik (5.8 and 5.31) have been examined in terms of the above relationship. Data for combustion in constant volume spherical vessels with isotropic turbulence are shown in Figure 5.6. The Taylor microscale used to establish Figure 5.6 was determined from the isotropic relationship:

$$\frac{\lambda}{L} = \left(\frac{15 \bar{u} L}{\lambda}\right)^{1/2} \qquad (3)$$

taken from Frost and Moulden (5.32). Examination of Figure 5.6 shows the presence of a correlation of the form:

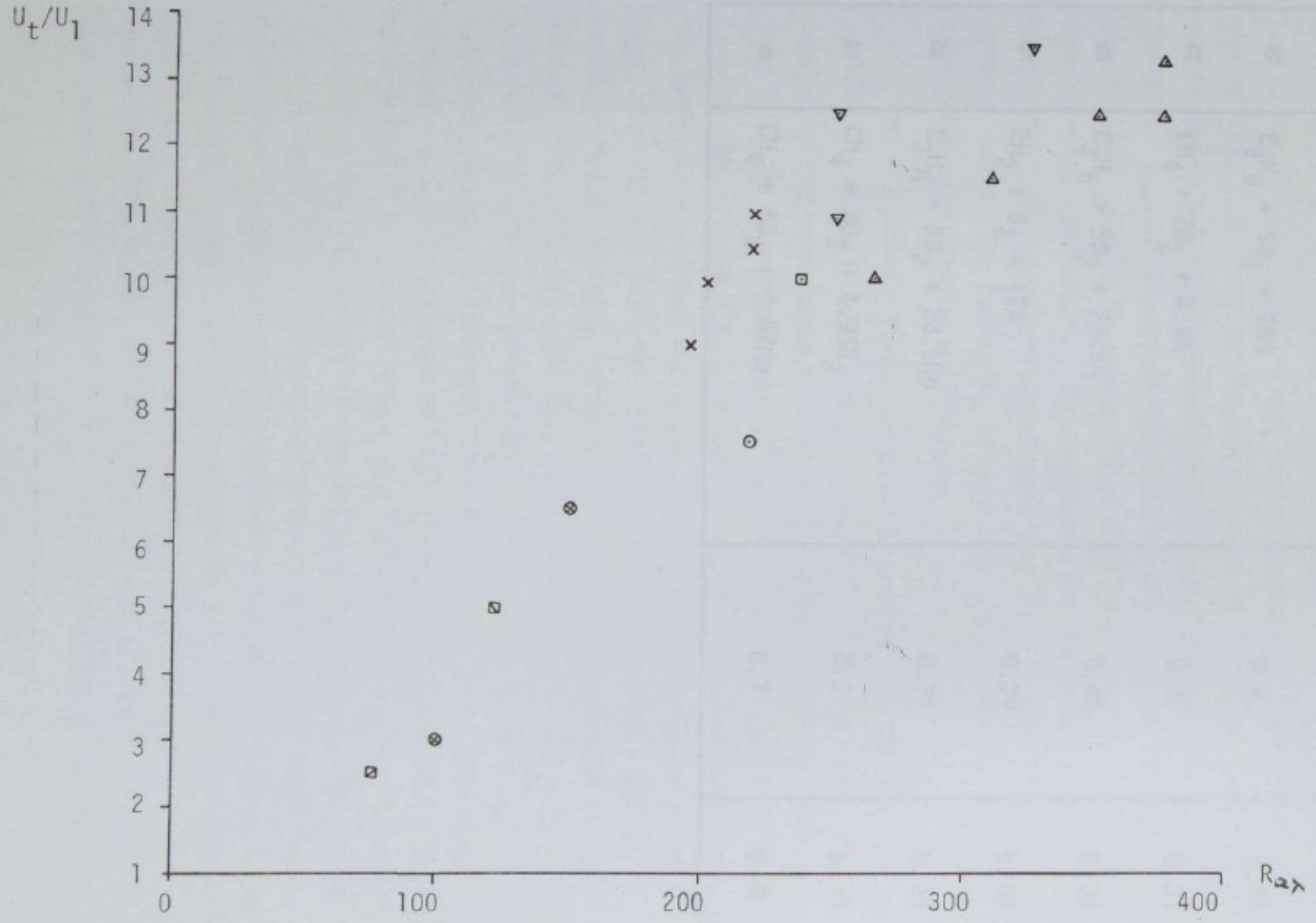

FIGURE 5.6 REYNOLDS NUMBER DEPENDENCE OF U_t/U_1 (FROM REFERENCES 5.8 AND 5.31)

KEY TO FIGURE 5.6

SYMBOL	MIXTURE	U_1 m/sec	REFERENCE
×	$C_3H_8 + 5O_2 + 18He$	1.4	5.31
⊙	$C_3H_8 + 5O_2 + 18A$	0.8	5.31
□	$CH_4 + 2O_2 + 4.9A$	0.7	5.31
△	$C_3H_8 + 5O_2 + 28.5A$	0.45	5.31
▽	$2H_2 + O_2 + 17A$	0.29	5.31
⋈	$C_3H_8 + 5O_2 + 28.5He$	0.74	5.31
⋈	$CH_4 + 2O_2 + 4.93N_2$	0.7	5.31
⊗	$CH_4 + 6O_2 + 9.07He$	0.7	5.8

$$\frac{V_t}{V_l} = A + B\,Re_\lambda^n \qquad (4)$$

The data displayed cover a wide range of fuel types and were obtained by interpretation of photographic evidence. The scatter of the points on the graph is not unsatisfactory in view of the errors that can occur in the measurement of burning velocities. It supports the suggested correlation between V_t/V_l and Re_λ and indicates its usefulness in determining the mass burning rates in an internal combustion engine. Thus Equation 4 is the basis of the mass burning rate model. The constants are to be determined from examination of the experimental data and the results of the thermodynamic model. The following assumptions are made in order to obtain the correlation coefficients.

The turbulence in the combustion chamber is taken to be small-scale and isotropic. The data of Semenov (5.33) are used to determine the turbulence intensity u' at the point of ignition (Figure 5.7). The assumption of isotropic turbulence is unlikely to be satisfied as the fluid is restricted by the solid boundaries of the combustion chamber where the eddy size is likely to be of the same order as the integral length scale. However, the influence of the mean motion quickly decreases for small eddies such that the motion is practically isotropic. Moreover, Kolmogorov (5.34) has suggested that at any given small sub-area, the motion can be regarded as totally isotropic. The integral length scale L is assumed to be proportional to the instantaneous chamber height h, according to the work of Tsuge et al (5.35) who showed, that for turbulence in closed vessels, an intially anisotropic turbulent field decayed to a condition for which the chamber dimensions controlled the turbulent macroscale. The turbulence intensity and the integral length scale are governed by the 'rapid distortion theory such that the angular momentum of the individual eddy is conserved. This produces changes in u' and L as the flame propagates across the combustion chamber according to Equation 5:

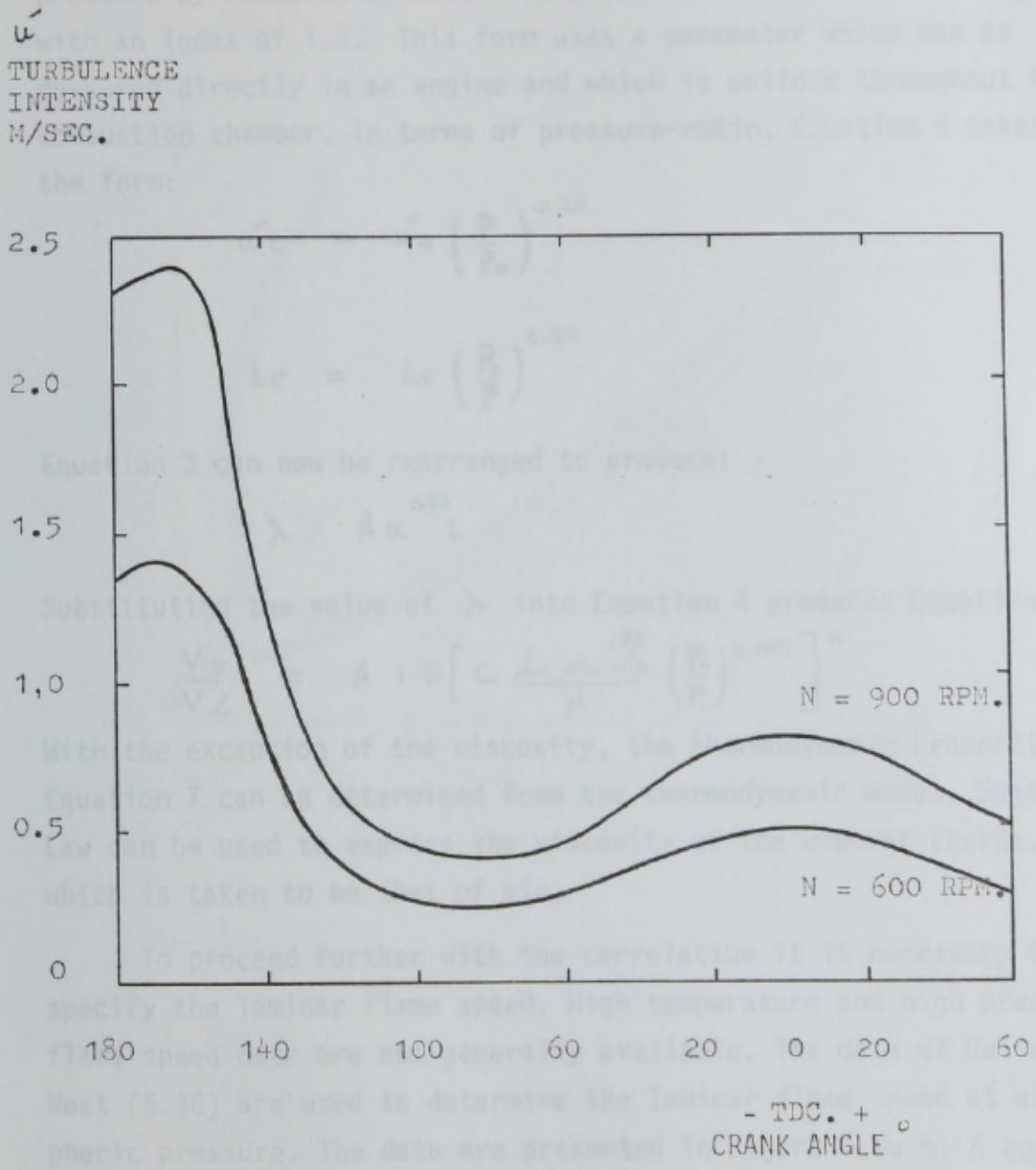

FIGURE 5.7 VARIATION OF THE TURBULENCE INTENSITY AFTER CLOSING OF THE INTAKE VALVE (FROM REFERENCE 5.33)

$$u't = u'_o \left(\rho_u/\rho_o\right)^{1/3}$$
$$L_t = L_o \left(\rho_o/\rho_u\right)^{1/3} \qquad (5)$$

Equation 5 can be expressed in terms of the combustion chamber pressure by assuming adiabatic compression of the unburnt charge with an index of 1.3. This form uses a parameter which can be measured directly in an engine and which is uniform throughout the combustion chamber. In terms of pressure-ratio, Equation 5 takes the form:

$$u't = u'_o \left(\frac{P}{P_o}\right)^{0.26}$$
$$L_t = L_o \left(\frac{P_o}{P}\right)^{0.26} \qquad (6)$$

Equation 3 can now be rearranged to produce:

$$\lambda = A u'^{0.33} L$$

Substituting the value of λ into Equation 4 produces Equation 7:

$$\frac{V_t}{V_l} = A + B\left[C \frac{l_o \rho_u u'^{1.33}_o}{\mu} \left(\frac{P_o}{P}\right)^{0.087}\right]^n \qquad (7)$$

With the exception of the viscosity, the thermodynamic properties in Equation 7 can be determined from the thermodynamic model. Sutherland's Law can be used to express the viscosity of the unburnt charge, which is taken to be that of air.

To proceed further with the correlation it is necessary to specify the laminar flame speed. High temperature and high pressure flame speed data are not generally available. The data of Heimel and West (5.36) are used to determine the laminar flame speed at atmospheric pressure. The data are presented in Figure 5.8a-b. A correction for pressure variations is made, following Fine (5.37), to the effect that:

$$u_p = u_R \left(\frac{P}{P_R}\right)^{0.3}$$

where R denotes the reference conditions.

Using the data provided by the mathematical analysis, the correlation parameters for Equation 7 were determined by iterating on the exponent n until the least squares fit was

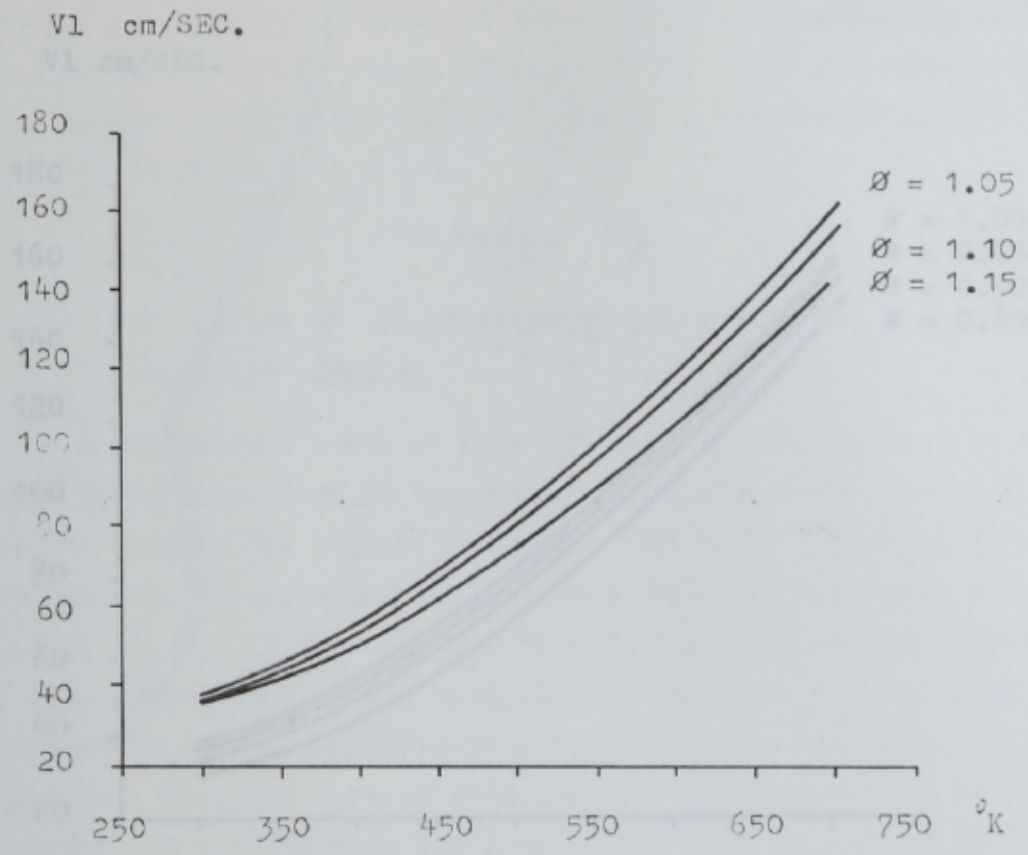

FIGURE 5.8a EFFECT OF TEMPERATURE ON THE LAMINAR FLAME SPEED OF ISOOCTANE-AIR FLOWS (FROM REFERENCE 5.36)

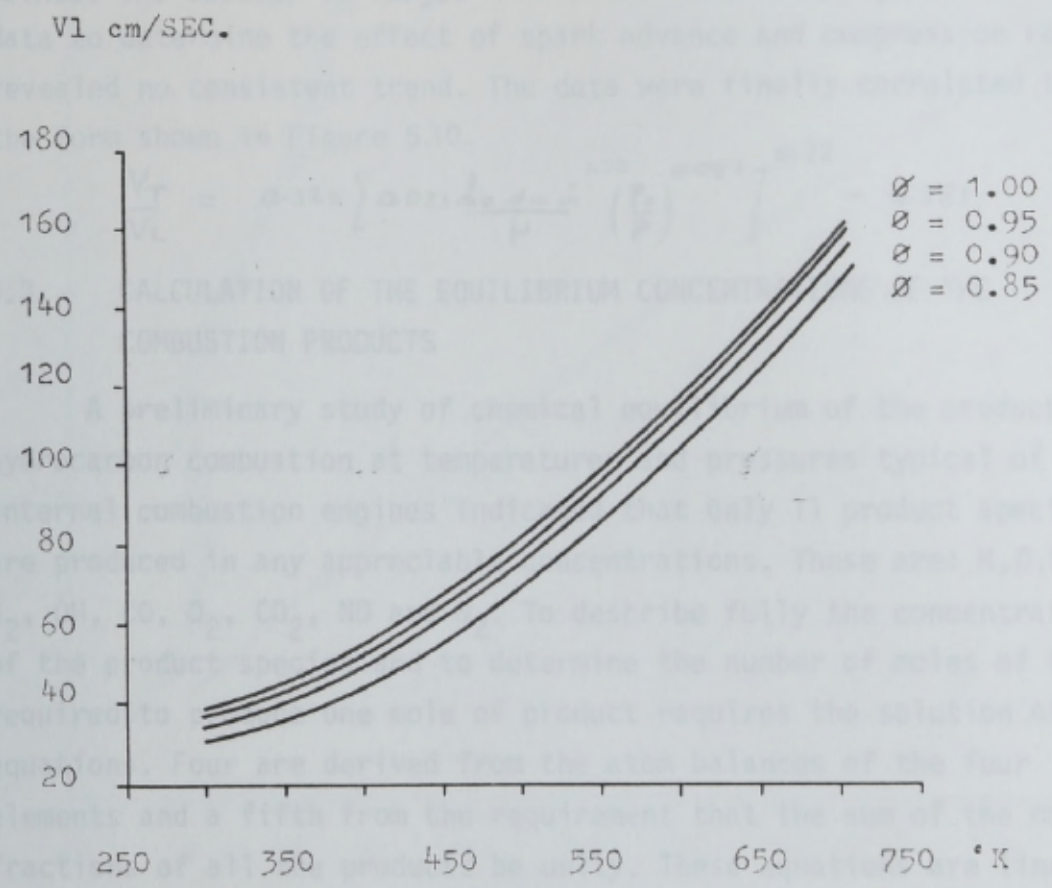

FIGURE 5.8b EFFECT OF TEMPERATURE ON THE LAMINAR FLAME SPEED OF ISOOCTANE-AIR FLOWS (FROM REFERENCE 5.36)

optimised by a minimum coefficient of variation CV and standard deviation σ. The best fit was found with Equation 8:

$$\frac{V_T}{V_L} = \left[0.021 \frac{l_0 \rho_a u^{1.33}}{\mu} \left(\frac{P_0}{P}\right)^{0.087}\right]^{0.73} \qquad (8)$$

This is shown in Figure 5.9 as a line through the experimental points. The scatter is large. A more detailed investigation of the data to determine the effect of spark advance and compression ratio revealed no consistent trend. The data were finally correlated to the form shown in Figure 5.10.

$$\frac{V_T}{V_L} = 0.324 \left[0.021 \frac{l_0 \rho_a u^{1.33}}{\mu} \left(\frac{P_0}{P}\right)^{0.087}\right]^{0.73} - 4.581.$$

5.3 CALCULATION OF THE EQUILIBRIUM CONCENTRATIONS OF THE COMBUSTION PRODUCTS

A preliminary study of chemical equilibrium of the products of hydrocarbon combustion at temperatures and pressures typical of internal combustion engines indicated that only 11 product species are produced in any appreciable concentrations. These are: H, O, N, H_2O, H_2, OH, CO, O_2, CO_2, NO and N_2. To describe fully the concentrations of the product species and to determine the number of moles of fuel required to produce one mole of product requires the solution of 12 equations. Four are derived from the atom balances of the four elements and a fifth from the requirement that the sum of the mole fractions of all the products be unity. These equations are linear. The remaining 7, the equilibrium constant equations are non-linear, some being cubic and others quadratic. The only practical way of solving such a system of equations is by successive approximations.

Many techniques are available for solution by successive approximations. As the preliminary study of 18 of the products of combustion using a matrix inversion technique highlighted the complexity of the problem, the criteria for selection of a technique were simplicity, speed and accuracy. The technique chosen is described below.

5.3.1 Formulation of the Initial Equations

If the fuel, in this case C_8H_{18}, is allowed to react with air at an equivalence ratio Ø, the resulting chemical reaction can be represented by the following equation (for isooctane):

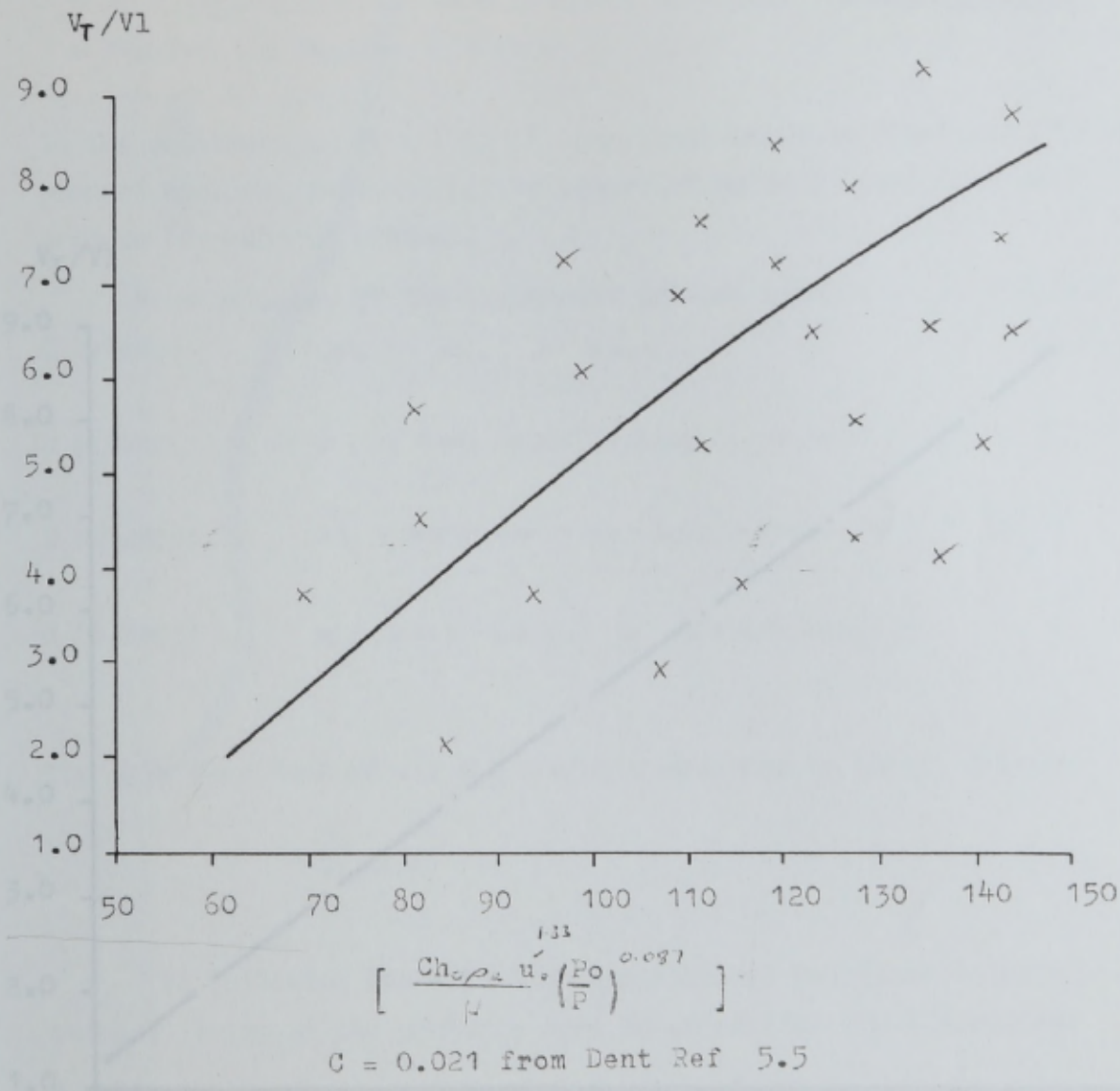

FIGURE 5.9 RELATIONSHIP BETWEEN V_t/V_1 AND THE TURBULENT REYNOLDS NUMBER

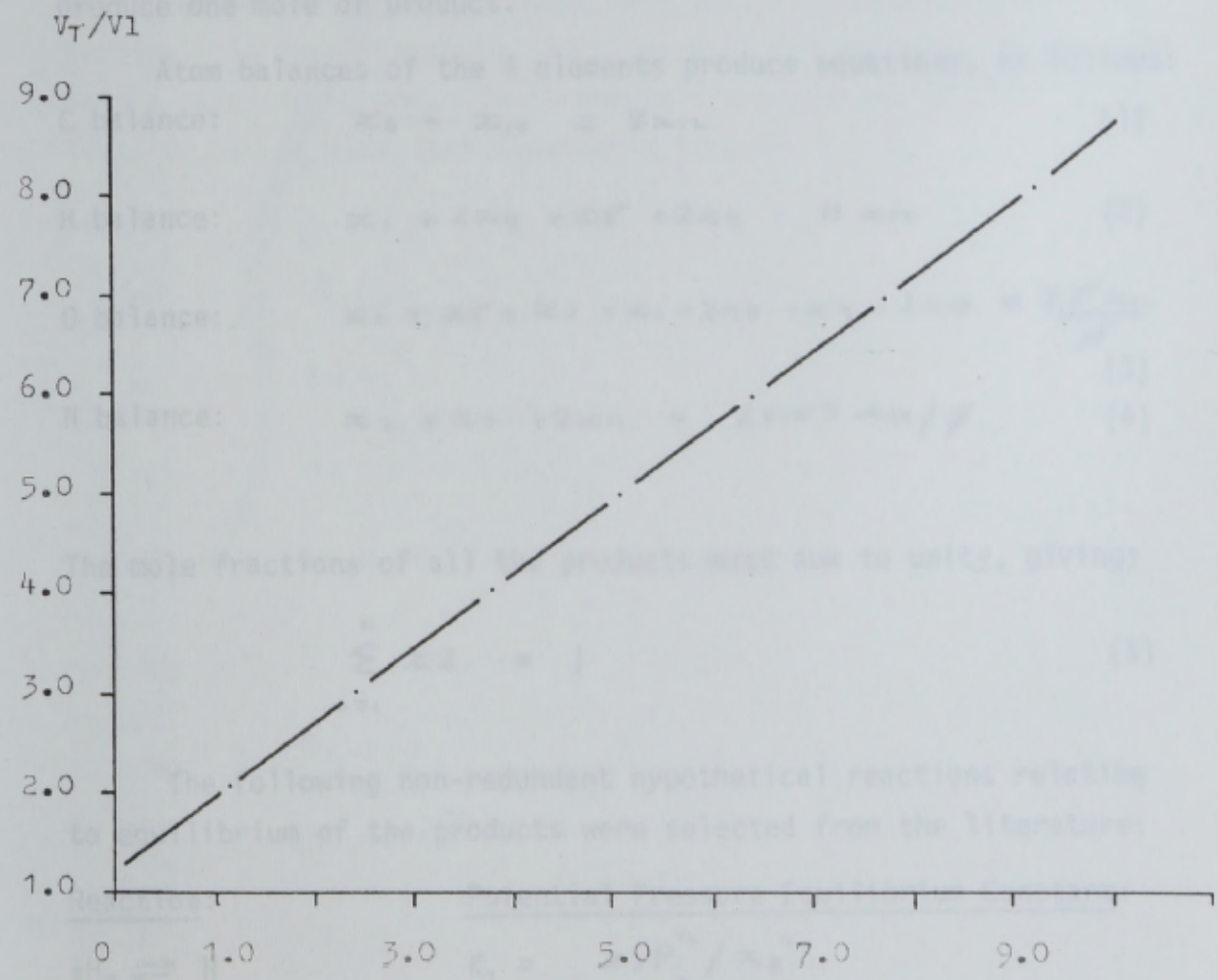

FIGURE 5.10 CORRELATION BETWEEN V_T/V_1 AND TURBULENT REYNOLDS NUMBER

$$x_{12}\left[C_8H_{18} + \frac{15}{2\phi}\left[O_2 + 3.7274\ N_2\right]\right] \longrightarrow$$

$$x_1 H + x_2 O + x_3 N + x_4 H_2 + x_5 OH + x_6 CO + x_7 NO + x_8 O_2 + x_9 H_2O + x_{10} CO_2 + x_{11} N_2$$

In the equation, x_i (i = 1 to 11) represent the mole fractions of the product species, and x_{12} is the number of moles of fuel that will produce one mole of product.

Atom balances of the 4 elements produce equations, as follows:

C balance: $x_6 + x_{10} = 8x_{12}$ (1)

H balance: $x_1 + 2x_4 + x_5 + 2x_9 = 18x_{12}$ (2)

O balance: $x_2 + x_5 + x_6 + x_7 + 2x_8 + x_9 + 2x_{10} = \frac{7.5x_{12}}{\phi}$ (3)

N balance: $x_3 + x_7 + 2x_{11} = 28.03x_{12}/\phi$ (4)

The mole fractions of all the products must sum to unity, giving:

$$\sum_{i=1}^{11} x_i = 1 \quad (5)$$

The following non-redundant hypothetical reactions relating to equilibrium of the products were selected from the literature:

Reaction:	Potential Pressure Equilibrium Constant:
$\frac{1}{2}H_2 \rightleftharpoons H$	$K_1 = x_1 P^{1/2} / x_4^{1/2}$
$\frac{1}{2}O_2 \rightleftharpoons O$	$K_2 = x_2 P^{1/2} / x_8^{1/2}$
$\frac{1}{2}N_2 \rightleftharpoons N$	$K_3 = x_3 P^{1/2} / x_{11}^{1/2}$
$\frac{1}{2}H_2 + \frac{1}{2}O_2 \rightleftharpoons OH$	$K_5 = x_5 / x_4^{1/2} x_8^{1/2}$
$\frac{1}{2}O_2 + \frac{1}{2}N_2 \rightleftharpoons NO$	$K_7 = x_7 / x_8^{1/2} x_{11}^{1/2}$
$H_2 + \frac{1}{2}O_2 \rightleftharpoons H_2O$	$K_9 = x_9 / x_4 x_8^{1/2} P^{1/2}$
$CO + \frac{1}{2}O_2 \rightleftharpoons CO_2$	$K_{10} = x_{10} / x_6 x_8^{1/2} P^{1/2}$

(6)

An initial estimate was made of the 4 chemical species most likely to be present in the highest concentrations in the final equilibrium mixture. The other products were then expressed in terms of the reaction coefficients and the mole fractions of these components. This precluded the possibility of computing the concentration of a relatively high concentration species through intermediates existing only in low concentrations. One drawback is that the technique requires knowledge of the final concentrations prior to the calculations. These data are, fortunately, generally available in the literature. This phase of the work is, in any case, only a means to an end. The products are expressed in terms of H_2, CO_2, O_2 and N_2 such that Equation 6 becomes:

$$
\begin{aligned}
x_1 &= A_1 x_4^{1/2} \\
x_2 &= A_2 x_8^{1/2} \\
x_3 &= A_3 x_{11}^{1/2} \\
x_5 &= A_5 x_4 x_8^{1/2} \\
x_7 &= A_7 x_8^{1/2} x_{11}^{1/2} \\
x_9 &= A_9 x_4 x_8^{1/2} \\
x_{10} &= A_{10} x_6 x_8^{1/2}
\end{aligned}
\qquad (7)
$$

where $A_1 = K_1 / P^{1/2}$
$A_2 = K_2 / P^{1/2}$
$A_3 = K_3 / P^{1/2}$
$A_5 = K_5$
$A_7 = K_7$
$A_9 = K_9 P^{1/2}$
$A_{10} = K_{10} P^{1/2}$

The above Equations can now be substituted into Equations 1 - 5 to form four non-linear equations in the four unknowns:

$$f_j(x_8, x_9, x_{10}, x_{11}) = 0 \qquad j = 1, 2, 3, 4 \qquad (8)$$

The equations were linearised by expansion around a known vector as a Taylor's series. If the solution of the equations is given by x_8, x_9, x_{10}, x_{11} and an initial estimate is $x_8^*, x_9^*, x_{10}^*, x_{11}^*$, then:

$$\Delta x_i = x_i - x_i^* \qquad i = 8, 9, 10, 11$$

Neglecting the partial derivatives of second and higher orders allows a set of linear equations with Δx_i as the approximate correction to be produced:

$$f_j + \frac{df_j}{dx_8}\Delta x_8 + \frac{df_j}{dx_9}\Delta x_9 + \frac{df_j}{dx_{10}}\Delta x_{10} + \frac{df_j}{dx_{11}}\Delta x_{11} = 0 \qquad (9)$$

where functions f_j and their partial derivatives are evaluated at the known vector. The equations were solved for $\Delta x_8, \Delta x_9, \Delta x_{10}$ and Δx_{11} using a Gaussian elimination method. The improved values were then:

$$x_{i_2} = x_{i_1} + \Delta x_i \qquad (10)$$

and these were used to evaluate the partial derivatives and functions. Further correction can then be calculated and applied until the relative changes in all the components are less than a specified value.

The method for solving Equations 8 is not self-starting and so either approximate values from a previous calculation or initial estimates must be used to initiate the procedure. Suitable initial values were produced using the following method. Let the product of combustion be limited to species H_2, CO, O_2, H_2O, CO_2 and N_2. The chemical reaction can then be represented by the following:

$$x_{12}\left[C_8H_{18} + \frac{15}{2\phi}\left[O_2 + 3.72N_2\right]\right] \rightarrow x_4H_2 + x_6CO + x_8O_2 + x_9H_2O + x_{10}CO_2 + x_{11}N_2 \qquad (11)$$

Using Equations 7, the atom balances become:

C balance: $$x_9 = \frac{9x_{12}}{1 + A_{10}x_8^{1/2}} \qquad (12)$$

H balance: $$x_4 = 9x_{12} / (1 + A_9 x_8^{1/2}) \quad (13)$$

N balance: $$x_{11} = 14.015\, x_{12} / \phi \quad (14)$$

O balance: $$x_6 + 2x_8 + x_9 + 2x_{10} = 7.5\, x_{12} / \phi \quad (15)$$

Substitution of values for x_6, x_9 and x_{10} into Equation 15 produces an equation in x_8 and x_{12} :

$$\frac{16A_{10}x_8^{1/2} + 9}{1 + A_{10}x_8^{1/2}} + \frac{9A_9 x_8^{1/2}}{1 + A_9 x_8} + \frac{2x_8}{x_{12}} = \frac{25}{\phi} \quad (16)$$

An initial estimate of x_{12} can be obtained from the requirement for the sum of the mole fractions of the products to be unity.

Substitution for $x_4, x_6, x_9, x_{10}, x_{11}$ in Equation 11, and rearrangement produces an equation for x_{12} :

$$x_{12} = \left[\frac{1 + A_6}{A_6 + x_8^{1/2}} \right] + \frac{x_8^{1/2}(1 + A_9)}{x_8 + A_9} + \frac{14.015}{\phi} \quad (17)$$

Substitution for x_{12} in Equation 16 produces an equation in the single unknown x_8 which can be solved by Newton's method. The other unknowns x_9, x_{10}, x_{11} can then be obtained directly, by substitution in Equations 12 - 14. The initial estimates can then be used to start the iterations of the main solution.

5.3.2 Curve Fitting of the Equilibrium Constants

The equilibrium constants were stored in the computer in polynomial form. The temperature range 600 K - 4000 K was chosen as a compromise between the high accuracy obtainable in a narrower range and the low accuracy in a wider range. The value of K predicted by the polynomials was compared with the original data in the JANAF thermo-chemical tables (2nd edition) and the error was found to be less than 0.0009. The original data were tabulated to the 3rd decimal place, and so there is an inherent uncertainty of 0.0005. The deviation was therefore considered to be insignificant.

The equilibrium constants were calculated using the relation:

$$\log K_p(\text{REACTION}) = \sum \log K_{p\,\text{FORMATION}}^{\text{PRODUCTS}} - \sum \log K_{p\,\text{FORMATION}}^{\text{REACTANTS}}$$

Klotz (5.38) suggested a functional relationship of the form:

$$\log K_p = A \ln\left(T + B/T + C + DT + ET^2\right)$$

where T is the absolute temperature and A, B, C, D and E are constants. A transformed temperature, T_R defined as 0.001T/9 where T is in R was used for the curve fitting. The constants are listed in Table 5.3.

The computer program used to calculate the equilibrium concentrations of the exhaust products is listed in Appendix 2. Examples of the output of the program are presented in graphical form, together with graphs showing the thermodynamic properties of the reactants and the combustion products.

5.4 DETERMINATION OF THE SURFACE AREA OF THE FLAME FRONT AND THE PISTON AND CYLINDER SURFACES EXPOSED TO THE BURNT CHARGE

5.4.1 Flame Front Surface Area

The flame is assumed to develop as an undistorted sphere, centred at the spark plug. The notation used in this sub-section is that used in Figure 5.11. The surface area of the flame front can be established by considering the intersection of a sphere and cylinder as, follows, for the general case of $R_f > a$ and $R_f > b$:

$$SAF = 2(\alpha + \beta) \int_0^{\alpha} R_f^2 \sin\theta \, d\theta$$

$$= 2(\alpha + \beta) R_f^2 (1 - \cos\theta)$$

$$= 2 R_c^2 RR^2 (\alpha + \beta)(1 - RR/2)$$

The above equation can be expressed as a fraction of the area of the cylinder by dividing by πR_c to produce:

$$SAF = \frac{2(\alpha + \beta)}{\pi} RR^2 (1 - RR/2)$$

REACTION	CONSTANT				
	A	B	C	D	E
$\frac{1}{2}H_2 \rightleftharpoons H$	0.43216800	-0.112464×10^{2}	0.267269×10	-0.745744×10^{-1}	0.242484×10^{-2}
$\frac{1}{2}O_2 \rightleftharpoons O$	0.31080500	-0.129540×10^{2}	0.321779×10	-0.738336×10^{-1}	0.344645×10^{-2}
$\frac{1}{2}N_2 \rightleftharpoons N$	0.38971600	-0.245828×10^{2}	0.314505×10	-0.963730×10^{-1}	0.585643×10^{-2}
$\frac{1}{2}O_2 + \frac{1}{2}H_2 \rightleftharpoons OH$	-0.14178400	-0.213308×10	0.853461	0.355015×10^{-1}	-0.310227×10^{-2}
$\frac{1}{2}N_2 + \frac{1}{2}O_2 \rightleftharpoons NO$	0.01508790	-0.470959×10	0.646096	0.272805×10^{-2}	0.154444×10^{-2}
$H_2 + \frac{1}{2}O_2 \rightleftharpoons H_2O$	-0.75263400	0.124210×10^{2}	-0.260286×10	0.259556	-0.162687×10^{-1}
$CO + \frac{1}{2}O_2 \rightleftharpoons CO_2$	0.00415302	0.148627×10^{2}	-0.475746×10	0.124699	-0.900227×10^{-2}

TABLE 5.3 VALUES OF CONSTANTS IN GIVEN REACTIONS

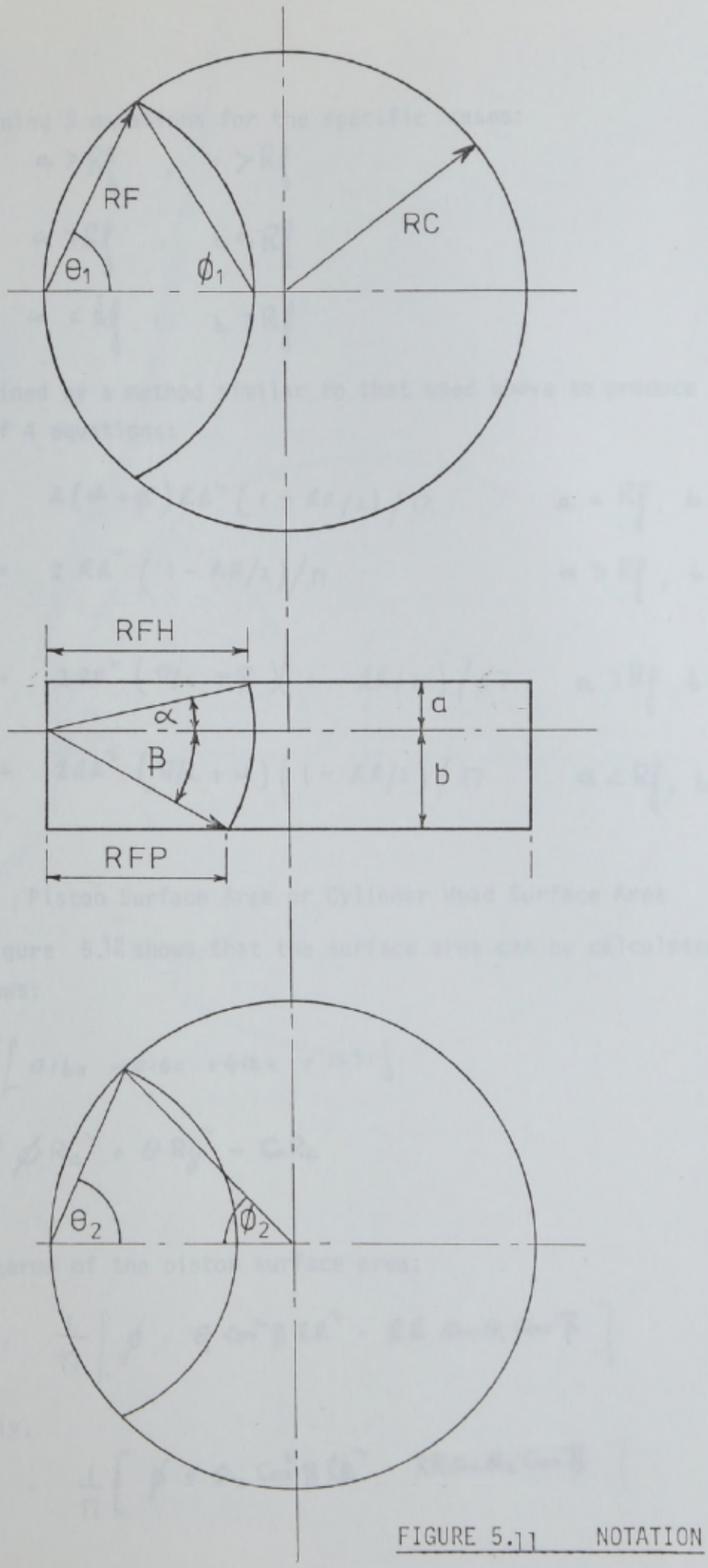

FIGURE 5.11 NOTATION

The remaining 3 equations for the specific cases:

Case 1: $a > Rf$, $b > Rf$

Case 2: $a > Rf$, $b < Rf$

Case 3: $a < Rf$, $b > Rf$

are obtained by a method similar to that used above to produce a family of 4 equations:

$$SAF_1 = 2(\alpha + \beta) RR^2 (1 - RR/2)/\pi \qquad a < Rf,\ b < Rf$$

$$SAF_2 = 2 RR^2 (1 - RR/2)/\pi \qquad a > Rf,\ b > Rf$$

$$SAF_3 = 2RR^2 (\pi/2 + \beta)(1 - RR/2)/\pi \qquad a > Rf,\ b < Rf$$

$$SAF_3 = 2RR^2 (\pi/2 + \alpha)(1 - RR/2)/\pi \qquad a < Rf,\ b > Rf$$

5.4.2 Piston Surface Area or Cylinder Head Surface Area

Figure 5.12 shows that the surface area can be calculated as follows:

$$A_{PF} = \{ 0160 + 0140 + 4124 + 1221 \}$$

$$= \phi R_c^2 + \theta Rf_p^2 - C_1 R_c$$

or, in terms of the piston surface area;

$$\frac{A_{PF}}{A_P} = \frac{1}{\pi} \left[\phi + \theta_1 \cos^2\beta\, RR^2 - RR \sin\theta_1 \cos\beta \right]$$

Similarly,

$$\frac{A_{HF}}{A_P} = \frac{1}{\pi} \left[\phi + \theta_2 \cos^2\beta\, RR^2 - RR \sin\theta_2 \cos\beta \right]$$

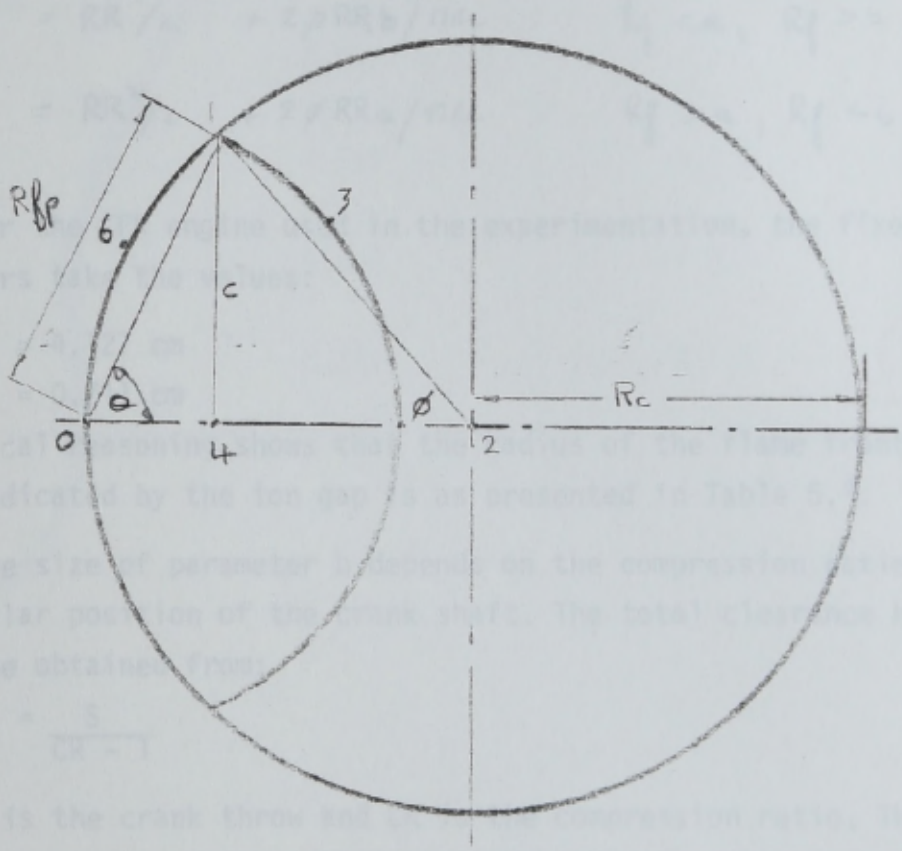

FIGURE 5.12 CALCULATION OF THE PISTON OR CYLINDER HEAD SURFACE AREA

5.4.3 Cylinder Wall Surface Area

There are 4 possible cases, depending on the relative sizes of a and b to R_F (see Figure 5.11). The results for each case are:

$$S_{aw} = 2\phi RR(a+b)/\pi R_c \qquad R_f > a,\ R_f > b$$

$$S_{aw} = RR\breve{} \qquad R_f < a,\ R_f < b$$

$$S_{aw} = RR\breve{}/2 + 2\phi RRb/\pi R_c \qquad R_f < a,\ R_f > b$$

$$S_{aw} = RR^2/2 + 2\phi RRa/\pi R_c \qquad R_f > a,\ R_f < b$$

For the CFR engine used in the experimentation, the fixed parameters take the values:

R_C = 4.127 cm
a = 0.711 cm

Geometrical reasoning shows that the radius of the flame front when it is indicated by the ion gap is as presented in Table 5.4.

The size of parameter b depends on the compression ratio and the angular position of the crank shaft. The total clearance height, h_o can be obtained from:

$$h_o = \frac{S}{CR - 1}$$

where S is the crank throw and CR is the compression ratio. The distance of the piston from TDC can be obtained from:

$$h_p = l_c\left[1 - \sqrt{1 - \frac{S^2 \sin^2\theta}{l_c^2}}\right] + S(1 - \cos\theta)$$

In this case, θ is the crank angle from TDC and l_c is the length of the connecting rod. Parameter b can then be expressed as:

$$b = (h_o + h_p) - a.$$

The behaviour of the flame front and the areas of the piston and cylinder wall surfaces can be seen in Figure 5.13 which shows the relationship between SAF, SAP, SAH, SAW and RR for constant value of R (= a/b) of 0.396. Figure 5.14 shows the relationship between SAF and RR for fixed crank angles of 10 , 20 , 30 and 40 °BTDC.

ION GAP NUMBER	RADIAL POSITION cm	FLAME FRONT RADIUS cm
1 (Spark Plug)	-	0.952
2	1.407	1.625
3	3.017	3.022
4	4.127	4.216
5	5.237	5.257
6	8.255	8.255

TABLE 5.4 FLAME FRONT RADIUS WHEN INDICATED BY EACH ION GAP

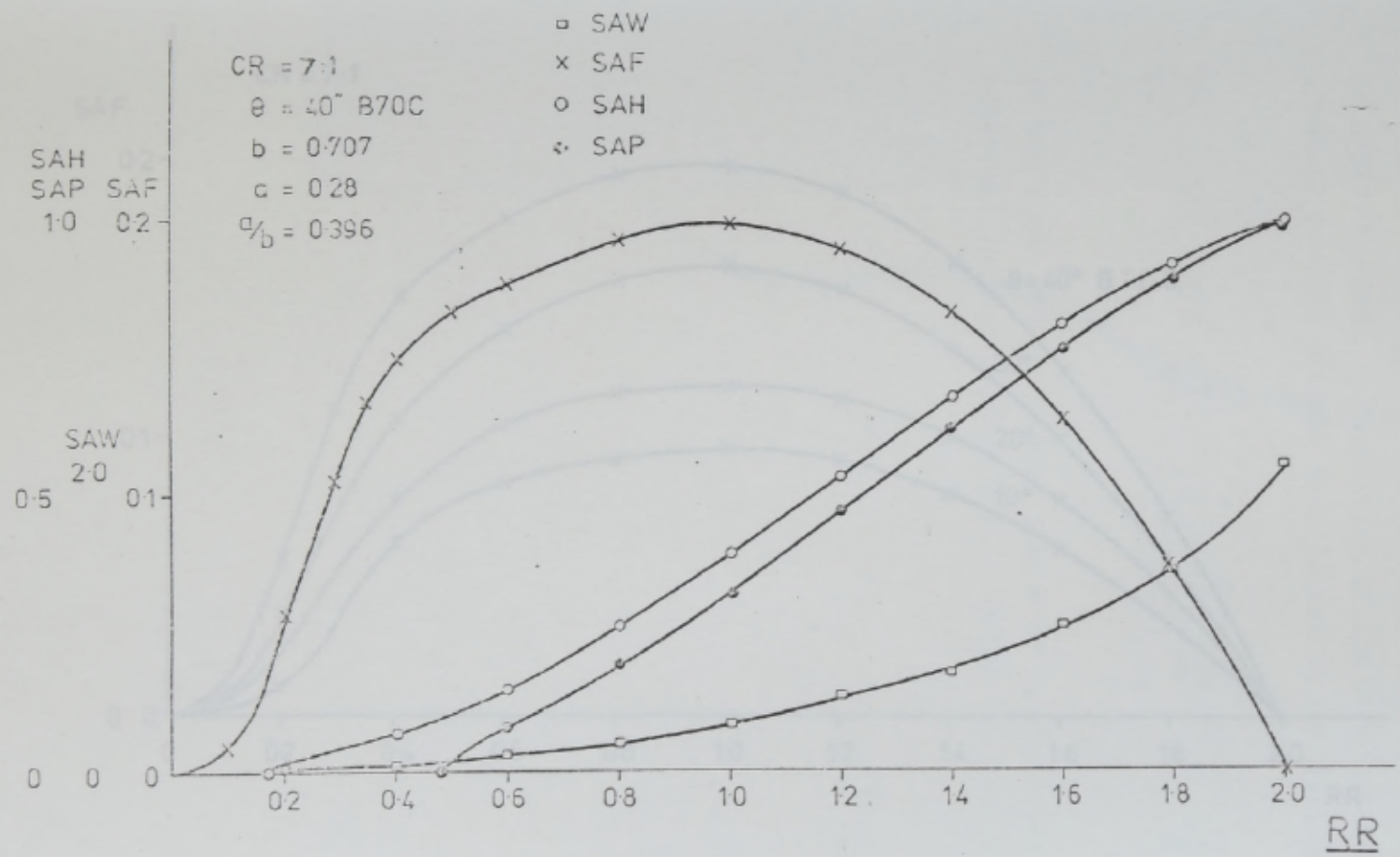

FIGURE 5.13 RELATIONSHIP BETWEEN SAF, SAP, SAW, SAH AND RR FOR CONSTANT R

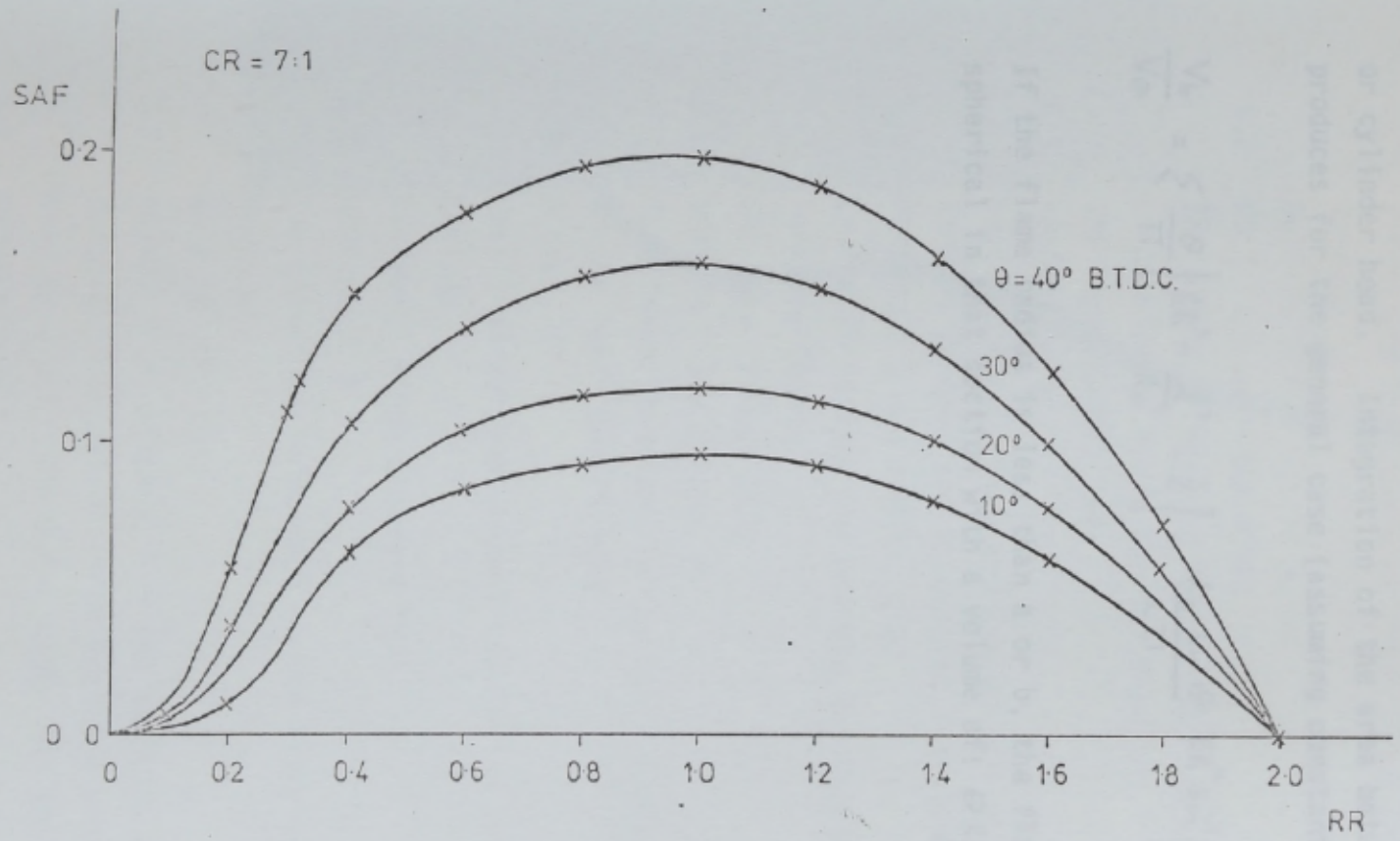

FIGURE 5.14 RELATIONSHIP BETWEEN SAF AND RR FOR FIXED CRANK ANGLES

5.5 CALCULATION OF THE VOLUME OF THE BURNT CHARGE

The volume of the burnt charge can be determined in a manner similar to that used in the calculation of the area of the piston or cylinder head. Integration of the area between heights a and b produces for the general case (assuming constant θ):

$$\frac{V_b}{V_\theta} = \sum \frac{\theta}{\pi}\left[RR^2 - \frac{l^2}{Rc^2} - 2\right] - \frac{Rc \sin\theta}{2\pi} RR \sin^{-1}\left(\frac{l}{Rf}\right) + \frac{\sin\theta}{2\pi}\left(\frac{l}{Rc}\right)\left(Rf^2 - l^2\right)^{1/2} + 1$$

If the flame radius is less than a or b, the flame is assumed to be spherical in that section with a volume of: $\theta Rf^3/3$

REFERENCES

5.1 OHIGASHI, S, HAMAMOTO, V and KIZIMA, A
Effects of Turbulence on Flame Propagation in Closed Vessels
Bull JSME 1971 vol 14 no 74

5.2 BOLT, J A and HARRINGTON, D L
The Effect of Mixture Motion Upon the Lean Limit and Combustion of Spark Ignited Mixtures
SAE Paper 670467 1967

5.3 SOKOLIK, A S
Self-ignition, Flame and Explosions in Gases
Israeli Program for Scientific Translations 1967

5.4 PETERS, B D and BORMAN, G L
Cyclic Variations and Average Burning Rates in a Spark Ignition Engine
SAE Paper 700064 1970

5.5 DENT, J C and SALAMA, N
Turbulence Structure in the Spark Ignition Engine
IMechE Paper C83/75 1976

5.6 SITKEI, G
Heat Transfer and Thermal Loading in Internal Combustion Engines
Akademiai Kiado Budapest 1974

5.7 DAMKOHLER, G
The Effect of Turbulence on the Flame Velocity of Gas Mixtures
NACA TM 1112 1947

5.8 KARPOV, V P, SEMENOV, E S and SOKOLIK, A S
Turbulent Combustion in an Enclosed Space
Proc Acad Sci USSR Phys - Chem Sec 128 871 1959

5.9 SHCHELKIN, K I
On Combustion in a Turbulent Flow
NACA T M 1110 1947

5.10 FRANK-KAMENETSKII, D A
Contribution to the Theory of Micro Diffusive Turbulent Combustion
Trudy Nauchno-Issledouatel' Skogo Instituta Oborongiz, 1946

5.11 LEASON, D B
Effect of Gaseous Additions on the Burning Velocity of Propane-Air Mixtures
Proc 4th Symp (Int) on Combustion, Cambridge, Mass. 1952

5.12 KARLOVITZ, B
AGARD: Selected Combustion Problems
Butterworth, London 1954

5.13 TALANATOV, A V
A Study of Combustion in Turbulent Flows
Trudy (8) NII MAP Oborongiz, 1955

5.14 TUCKER, M
Interaction of a Free Flame Front with a Turbulent Field
NACA T N 3407, 1955

5.15 RICHARDSON, J M
Mathematical Theory of Turbulent Flames
Proc Gas Dynamics Sym on Aerothermochemistry, 1956

5.16 DELBOURG, M P
Influence of Turbulence on the Mechanism of Gas Phase Combustion
Revue de l'Institut Francais du Petrole, 1949 vol 4

5.17 SUMMERFIELD, M
Turbulent Flows in Gases
Jet Propulsion, 1956 vol 26

5.18 BHADURI, D
Mechanisms of Flame Propagation
J Sci & Industrial Research, 1964 vol23

5.19 TAYLOR, G I
The Spectrum of Turbulence
Proc Royal Soc Seca, 1938

5.20 WILLS, J A B
On Corrective Velocities in Turbulent Shear Flows
J Fluid Mech, 1964 vol 20

5.21 FAVRE, A J
Review of Space-Time Correlations in Turbulent Fluids
J App Mech, 1965 vol 32E

5.22 POREH, M
Accelerations, Turbulent Trajectories amd Space-Time Correlations in Turbulent Shear Flow
Israel J Tech, 1968 vol 6

5.23 SIRIGNANO, W A
One-Dimensional Analysis of Combustion in a Spark Ignition Engine
Comb Sci & Tech, 1973 vol 7

5.24 BLIZARD, N C and KECK, J C
Experimental and Theoretical Investigation of Turbulent Burning Models for Internal Combustion Engine
SAE Paper 740191, 1974

5.25 BELLAN, J R and SIRIGNANO, W A
A Theory of Turbulent Flame Development and Nitric Oxide Formation in a Stratified Charge Internal Combustion Engine
Comb Sci & Tech, 1973 vol 8

5.26 TABACZYNSKI, R J, FERGUSON, C R and RADHAKRISHNAN,K
A Turbulent Entrainment Model for Spark Ignition Engine Combustion
SAE Paper 770647, 1977

5.27 SUMMERFIELD, M, REITER, S M, KEBELY, V and MASCOLD, R W
The Structure and Propagation Mechanism of Turbulent Flames at High Speed Flow
Jet Propulsion, 1955 vol 25

5.28 SPALDING, D B
One-Dimensional Laminar Flame Theory for Temperature-Explicit Reaction Rates
Comb & Flame, 1957 vol 1

5.29 SPALDING, D B
Predicting the Laminar Flame Speed in Gases with Temperature-Explicit Reaction Rates
Comb & Flame, 1957 vol 1

5.30 ABDEL-GAYED, R G and BRADLEY, D
Turbulence and Turbulent Flame Propagation: A Critical Appraisal
Comb & Flame, 1975 vol 24

5.31 SOKOLIK, A S , KARPOV, V P and SEMENOV, E S
Turbulent Combustion of Gases
Comb Expl and Shock Waves, 1967 vol 3

5.32 FROST, W and MOULDEN, T H
Handbook of Turbulence
Plenum Press, 1977

5.33 SEMENOV, E S
A Study of Turbulent Gas Motion in the Cylinder of a Piston Engine
Gorenie V Turbulentom Potoke p141-167
Moskva Izdatel'stud Akademii Nauk SSSR, 1959
NACA Tech Trans F 97, 1963

5.34 KOLMOGOROV, A N
Dissipation of Energy in Locally-Isotropic Turbulence
Doklady Acad Sci, USSR, 1941

5.35 TSUGE, M, KIDO, M and NOMIYAMAU, Y
Decay of Turbulence in Closed Vessel
Bull J S M E, 1973

5.36 HEIMEL, S and WEAST, R C
Effect of Initial Mixture Temperature on the Burning Velocity of Benzine-Air, nHeptane Air and Isooctane-Air Mixtures
Proc 6th Symp (Int) on Combustion, 1957

5.37 FINE, B
Effects of Pressure on Turbulent Burning Velocity
Comb & Flame, 1958 vol 2 no 2

5.38 KLOTZ, I
Introduction to Chemical Thermodynamics
W A Benjamin Co, New York, 1964

CHAPTER 6 ANALYSIS OF EXPERIMENTAL RESULTS

INTRODUCTION

The analysis of the experimental results serves a dual purpose. The first is that it indicates the repeatability of the tests and the correctness of the procedures adopted in the recording of the data. The second is that it produces factors to be used in the combustion modelling, and substantiates, or otherwise the assumptions made in its development.

6.1 THE DEVELOPMENT OF THE EXPANDING FLAME FRONT

Flame front development is an important variable in the combustion model. Statistical analysis of the progress of the flame front requires elucidation of the effects of other operating variables on either the flame propagation or the frame of reference against which the measurements are made. The relationships between the engine operating variables and the time after ignition for the flame front to reach a set point in the combustion chamber are shown in Figures 4.3 - 4.7. The data presented are consistent with other experimental results.

The engine variables likely to affect the frame of reference are the ignition timing and the rotational speed. Large cyclical variations in either of these factors will produce a corresponding effect in the combustion duration time. The cyclical variation of the ignition timing against the TDC indicator for motoring and firing conditions is shown in Figure 4.2. The standard deviation of 0.025 m sec was considered to indicate that ignition timing had a negligible effect on flame travel time. The variation in the time required for one engine revolution at motoring and firing is shown in Figure 4.1. The standard deviation ranged from 0.26 to 0.28 m sec at firing for the range of compression ratios under consideration was equivalent to 1/40 of that of the total flame time. The total varied between 1/9 and 1/15 of the time for one revolution and so the effect of speed variation on the period of flame travel was deemed small.

6.2 CYCLICAL VARIATION OF THE FLAME TRAVEL TIME

The cyclical variation of the flame front travel time for each of the cylinder head ion gaps is shown in Figures 6.1 - 6.2. The first shows the variation for Benzene, at compression ratio 6:1 and equivalence ratio 0.938. Figure 6.2 shows the variation for Isooctane fuel under the same conditions. The distribution is clearly not normal, but resembles that shown by the data of Harrow (6.1) and Ogasawara and Matsuda (6.2). The distribution pattern may therefore be typical for spark ignition engines.

However, in statistical analysis, normal distributions are easier to deal with, as their variation can be expressed in terms of their standard deviations, and so attempts were made to normalise the data. In time of flight measurement, it is customary to define the variable of interest as a velocity. In this case, if the apparent flame velocity is defined as L_n/t_f where L_n is the distance from the spark plug to the ion gap n, and the flame travel time data are examined in these terms, the distributions shown in Figures 6.1 - 6.2 become those in Figures 6.3 - 6.4 respectively. These may be regarded as normal distributions and it is possible to define from them the following parameters:

$\overline{V}_f$: mean flame velocity (mean of the apparent flame velocity)

$\overline{t}_f$: mean flame travel time $L_n/\overline{V}_f$.

The relationship between the mean flame velocity $\overline{V}_f$, the standard deviation σ and the coefficient of variation $\sigma/\overline{V}_f$, for several running parameters is shown in Figures 6.5 - 6.9. These figures are based on the data presented in Tables 6.1 - 6.5 respectively. As the standard deviation of the flame propagation velocity is the RMS of the deviation about the mean, it is mathematically analogous to the intensity of turbulence. This is shown to be practically constant in the CFR combustion chamber when expressed as a fraction of the mean flame velocity.

The relationship between σ and $\overline{V}_f$ for the end ion gaps is shown in Figure 6.10. The laminar burning velocity used to obtain this graph was calculated from the data of Heimel (6.3)

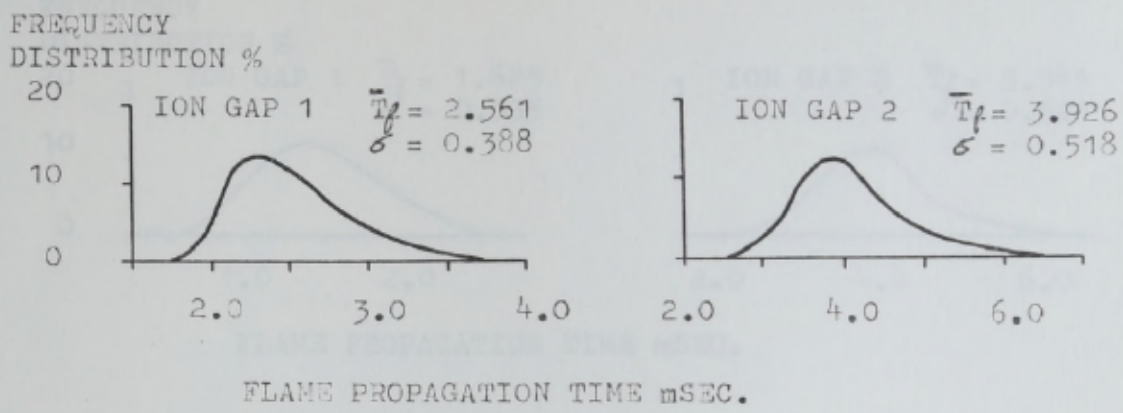

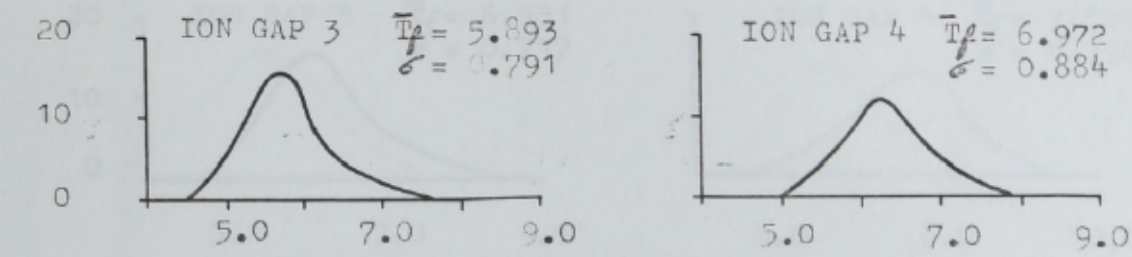

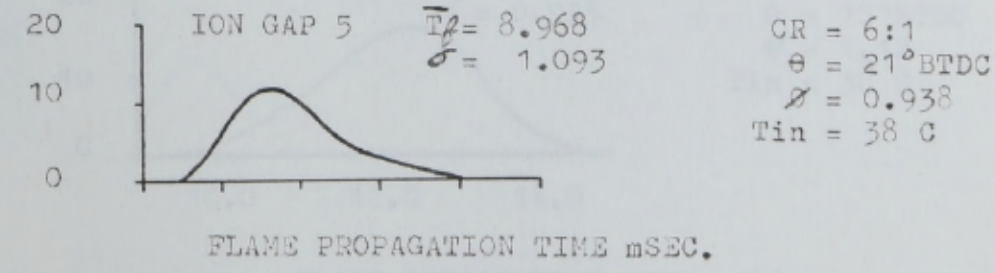

FIGURE 6.1 VARIATION OF FLAME TRAVEL TIME (FUEL TYPE: BENZENE)

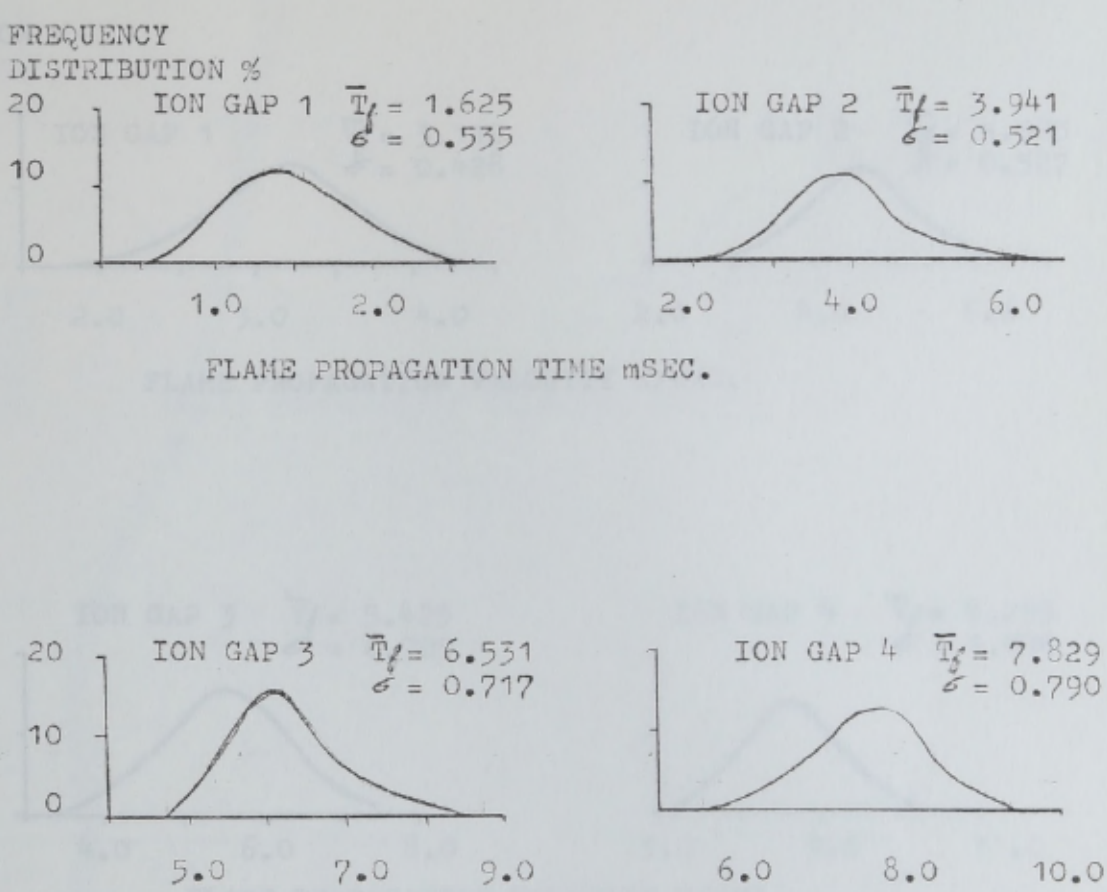

FIGURE 6.2 VARIATION OF FLAME TRAVEL TIME (FUEL TYPE: ISOOCTANE)

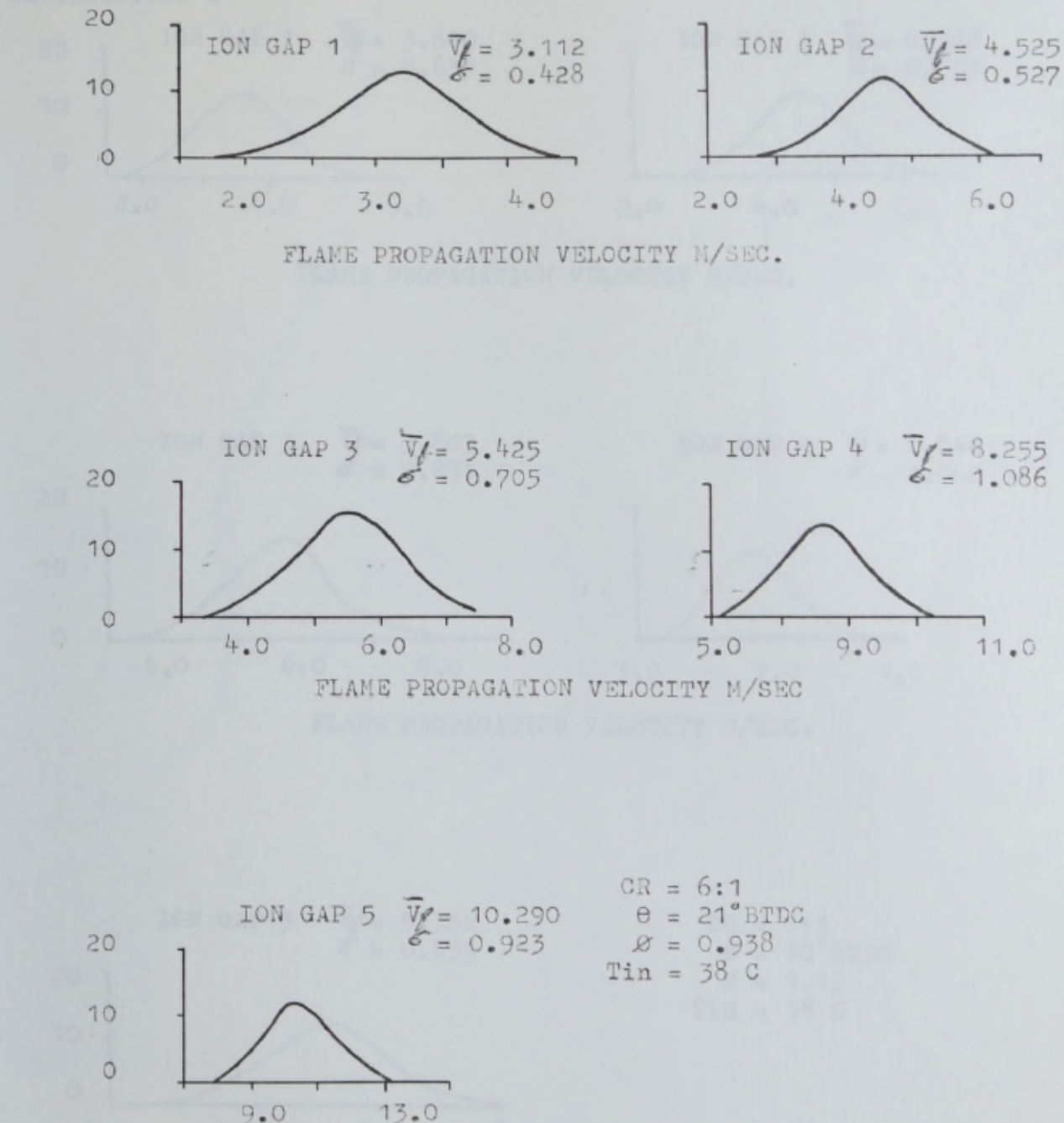

FIGURE 6.3 VARIATION OF THE FLAME PROPAGATION VELOCITY (FUEL TYPE: BENZENE)

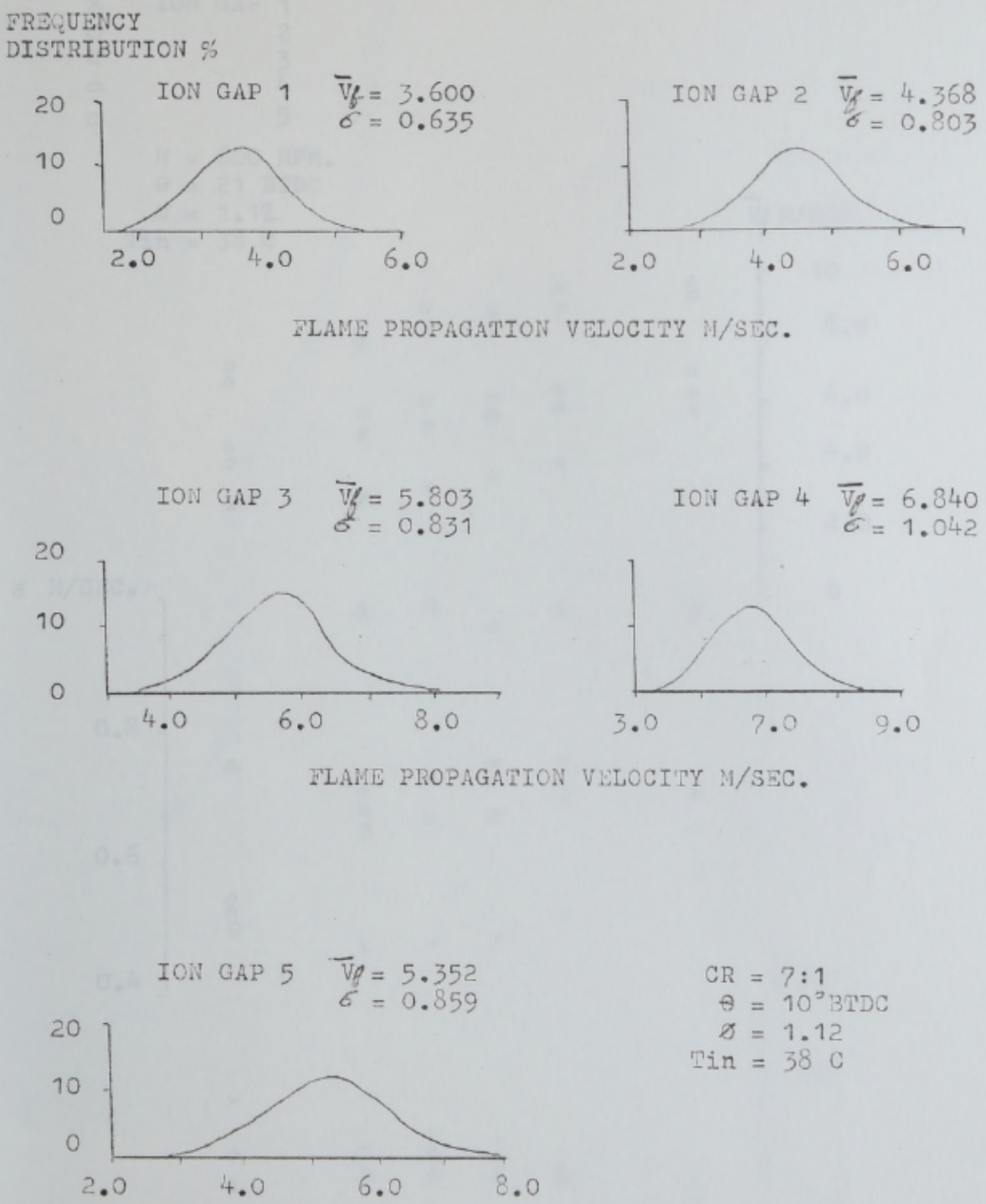

FIGURE 6.4 VARIATION OF THE FLAME PROPAGATION VELOCITY (FUEL TYPE: ISOOCTANE)

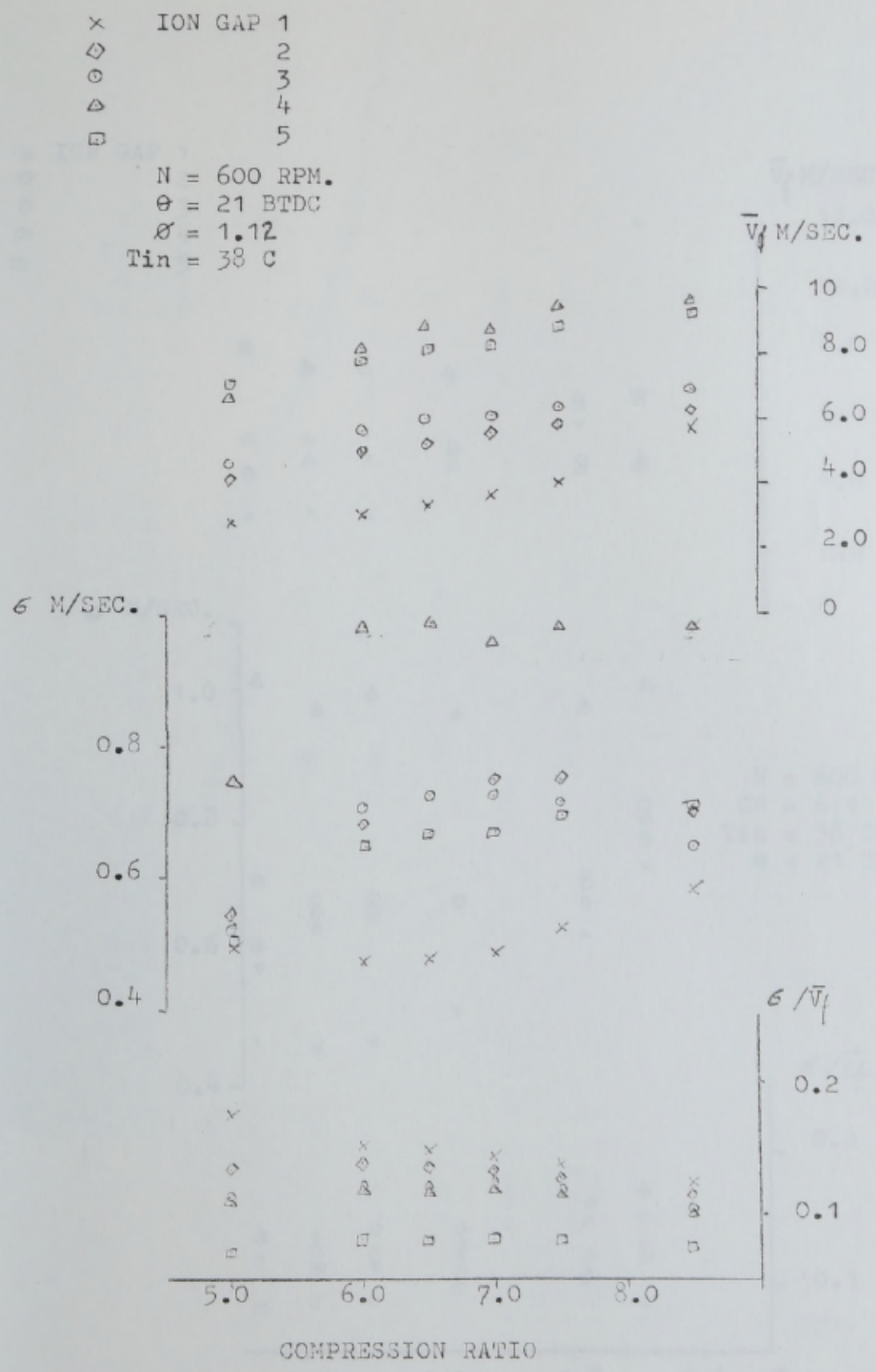

FIGURE 6.5 VARIATION OF $\bar{V}_f$, σ AND $\sigma/\bar{V}_f$ WITH COMPRESSION RATIO (FUEL TYPE: BENZENE)

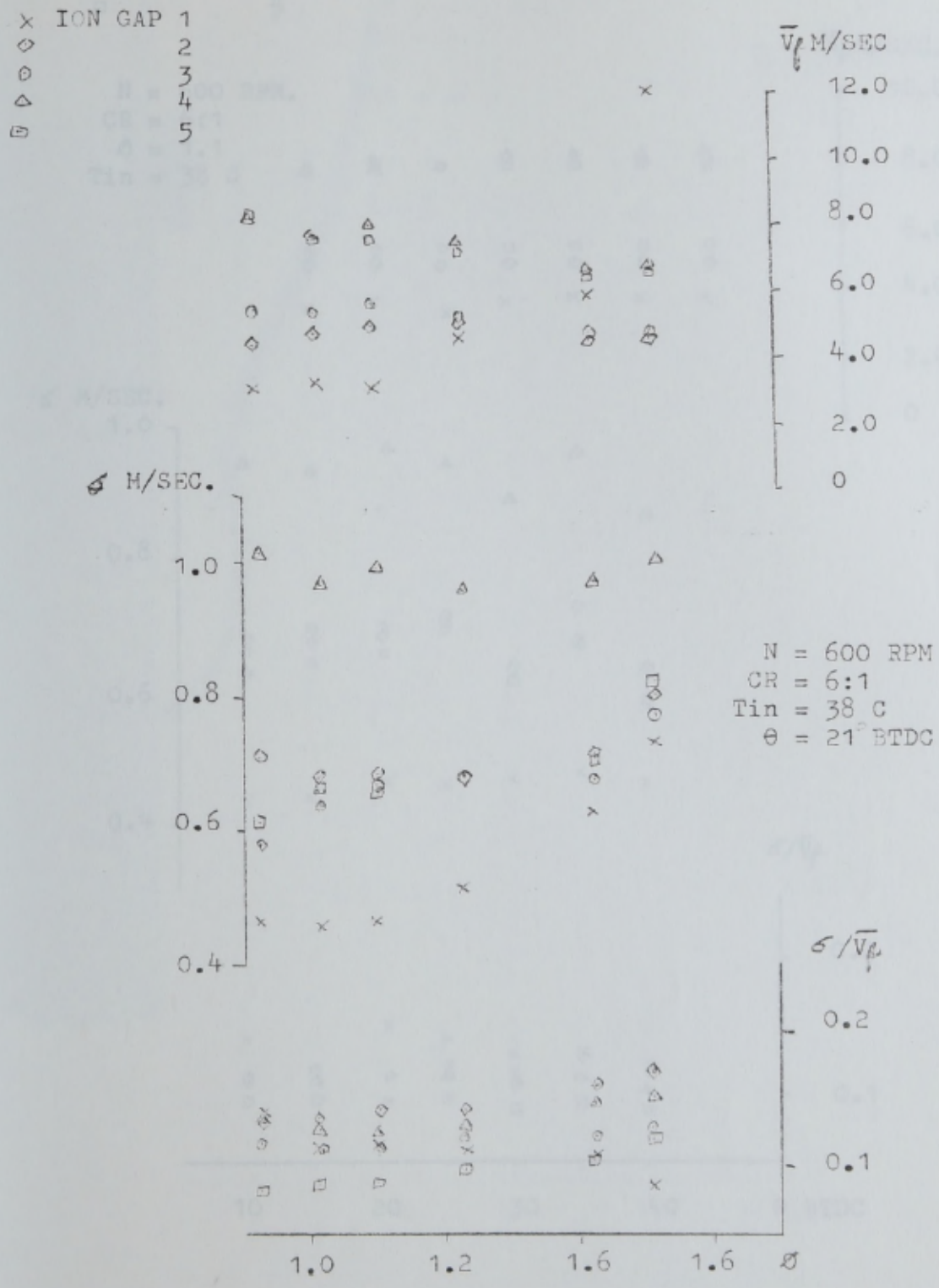

FIGURE 6.6 VARIATION OF $\bar{V}_f$, σ AND $\sigma/\bar{V}_f$ WITH EQUIVALENCE RATIO (FUEL TYPE: BENZENE)

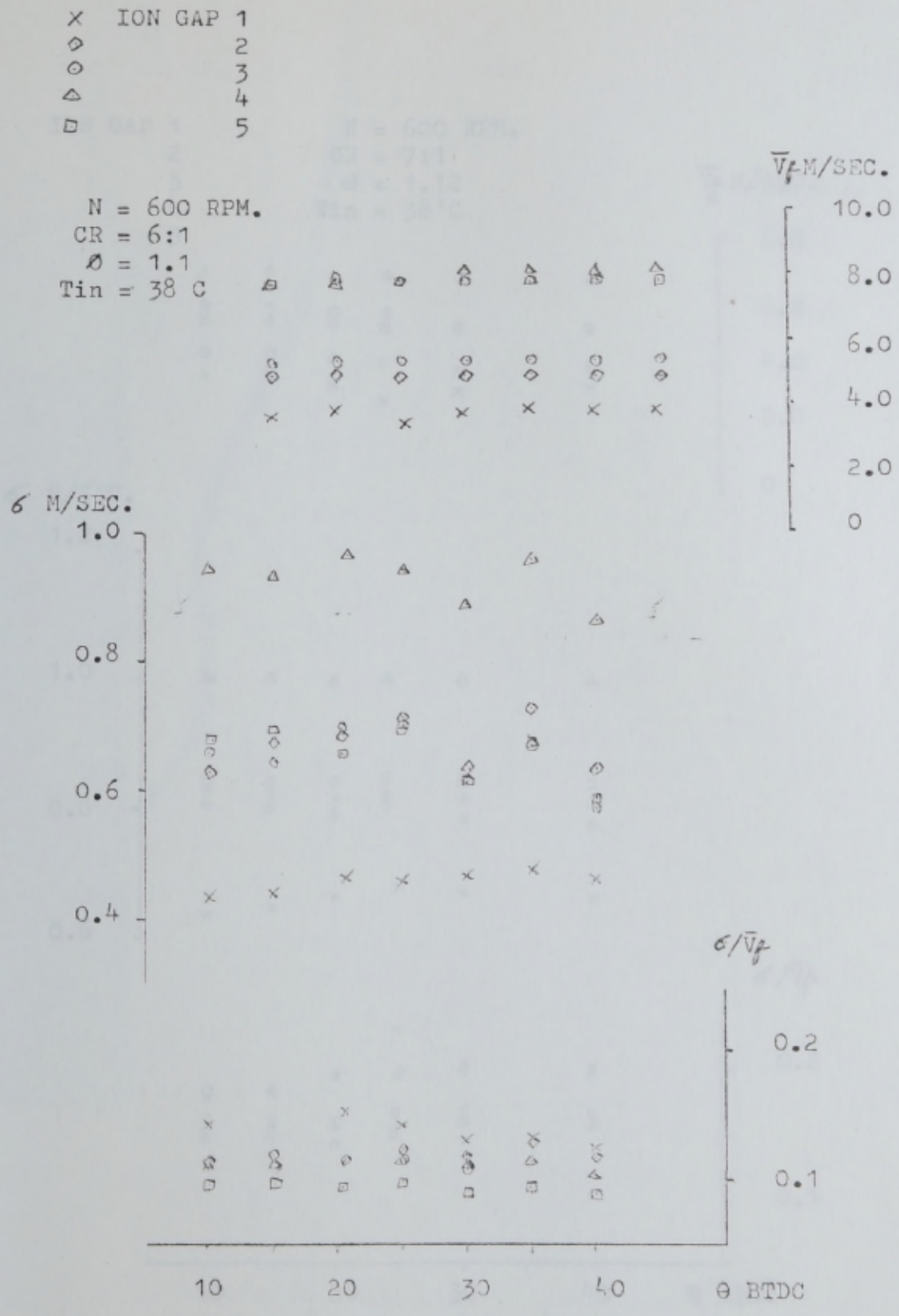

FIGURE 6.7 VARIATION OF $\bar{V}_f$, σ AND $\sigma/\bar{V}_f$ WITH θ
(FUEL TYPE: BENZENE)

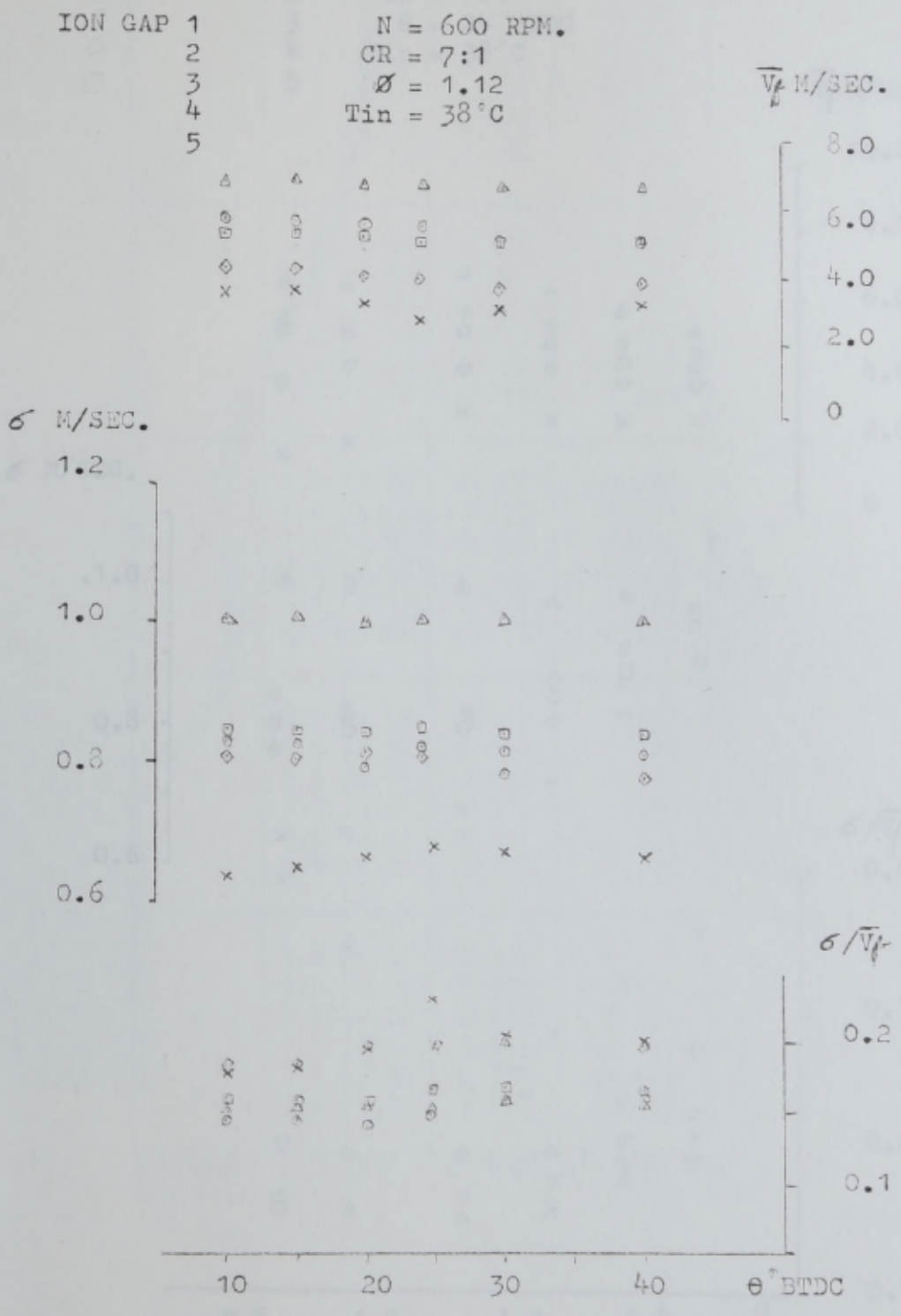

FIGURE 6.8 VARIATION OF $\overline{V_f}$, σ AND $\sigma/\overline{V_f}$ WITH SPARK TIMING (FUEL TYPE: ISOOCTANE)

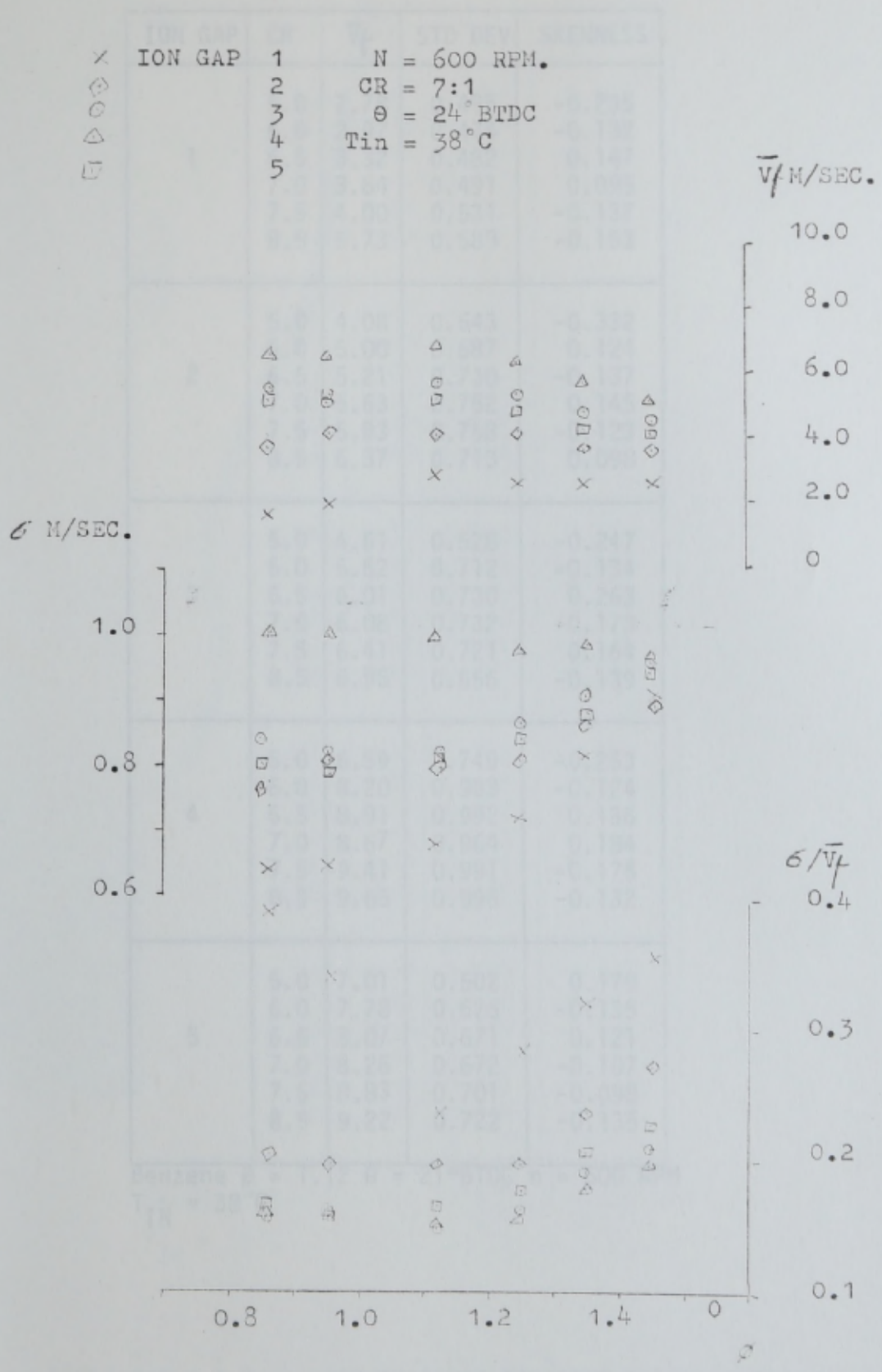

FIGURE 6.9 VARIATION OF $\bar{V}_f$, σ AND $\sigma/\bar{V}_f$ WITH EQUIVALENCE RATIO (FUEL TYPE: ISOOCTANE)

ION GAP	CR	$\bar{V}_f$	STD DEV	SKEWNESS
1	5.0	2.78	0.495	-0.235
	6.0	2.97	0.474	-0.132
	6.5	3.32	0.482	0.147
	7.0	3.64	0.491	0.095
	7.5	4.00	0.531	-0.137
	8.5	5.73	0.583	-0.153
2	5.0	4.08	0.543	-0.332
	6.0	5.00	0.687	0.124
	6.5	5.21	0.730	-0.137
	7.0	5.63	0.752	0.145
	7.5	5.83	0.758	-0.123
	8.5	6.37	0.713	0.098
3	5.0	4.61	0.528	-0.247
	6.0	5.62	0.712	-0.134
	6.5	6.01	0.730	0.263
	7.0	6.08	0.732	-0.173
	7.5	6.41	0.721	0.164
	8.5	6.95	0.656	-0.139
4	5.0	6.59	0.749	-0.253
	6.0	8.20	0.983	-0.124
	6.5	8.91	0.992	0.136
	7.0	8.67	0.964	0.184
	7.5	9.41	0.991	-0.175
	8.5	9.65	0.995	-0.132
5	5.0	7.01	0.502	0.179
	6.0	7.78	0.625	-0.135
	6.5	8.07	0.671	0.121
	7.0	8.26	0.672	-0.107
	7.5	8.83	0.701	-0.098
	8.5	9.22	0.722	-0.135

Benzene $\emptyset$ = 1.12 θ = 21°BTDC n = 600 RPM
T_{IN} = 38°C

TABLE 6.1 VARIATION OF APPARENT FLAME VELOCITY WITH COMPRESSION RATIO

ION GAP	Ø	V_f	STD DEV	SKEWNESS
1	0.938	3.12	0.462	-0.265
	1.015	3.23	0.458	0.352
	1.100	3.10	0.465	-0.132
	1.224	4.65	0.513	0.174
	1.412	5.84	0.628	-0.832
	1.505	12.00	0.727	0.109
2	0.938	4.51	0.575	0.136
	1.015	4.83	0.642	-0.253
	1.100	5.01	0.685	-0.124
	1.224	5.19	0.677	-0.934
	1.412	4.58	0.715	-0.873
	1.505	4.80	0.806	0.264
3	0.938	5.50	0.712	0.216
	1.015	5.42	0.635	-0.082
	1.100	5.65	0.655	0.134
	1.224	5.28	0.675	0.127
	1.412	4.81	0.681	-0.135
	1.505	4.80	0.775	0.098
4	0.938	8.18	1.100	-0.126
	1.015	7.81	0.968	0.103
	1.100	8.06	0.992	-0.127
	1.224	7.51	0.963	0.165
	1.412	6.72	0.974	-0.123
	1.505	6.81	1.042	0.725
5	0.938	8.12	0.612	0.201
	1.015	7.87	0.657	-0.357
	1.100	7.64	0.668	-0.135
	1.224	7.21	0.675	0.163
	1.412	6.41	0.707	-0.124
	1.505	6.58	0.822	-0.217

Benzene CR = 6:1 θ = 21°BTDC N = 600 RPM

T_{IN} = 38°C

TABLE 6.2 VARIATION OF APPARENT FLAME VELOCITY WITH EQUIVALENCE RATIO

ION GAP	θ	$\bar{V}_f$	STD DEV	SKEWNESS
1	10	3.60	0.432	0.097
	15	3.75	0.440	0.102
	21	3.39	0.465	-0.132
	25	3.75	0.463	0.112
	30	3.81	0.470	0.137
	35	3.81	0.481	-0.148
	40	3.80	0.463	0.012
2	10	4.96	0.629	0.095
	15	5.00	0.674	0.122
	21	4.98	0.682	0.124
	25	4.98	0.713	-0.098
	30	5.01	0.634	-0.129
	35	4.97	0.734	0.103
	40	4.93	0.636	0.162
3	10	5.21	0.660	0.186
	15	5.22	0.648	0.034
	21	5.41	0.701	-0.134
	25	5.38	0.699	0.085
	30	5.40	0.621	0.032
	35	5.39	0.677	0.183
	40	5.39	0.574	0.172
4	10	7.81	0.942	-0.037
	15	7.92	0.931	0.102
	21	7.92	0.967	-0.127
	25	8.18	0.942	0.107
	30	8.15	0.891	-0.236
	35	8.10	0.961	-0.123
	40	8.13	0.862	0.013
5	10	7.81	0.679	-0.152
	15	7.91	0.692	0.146
	21	7.92	0.656	-0.135
	25	7.91	0.705	0.104
	30	7.89	0.621	0.128
	35	7.93	0.677	-0.097
	40	7.95	0.591	0.082

N = 600 RPM CR = 6:1 Ø = 1.1 T_{IN} = 38°C
Benzene

TABLE 6.3 VARIATION OF APPARENT FLAME VELOCITY WITH SPARK TIMING

ION GAP	θ	$\bar{V}_f$	STD DEV	SKEWNESS
1	10	3.60	0.635	-0.263
	15	3.60	0.652	-0.173
	20	3.37	0.666	0.352
	24	2.86	0.680	-0.237
	30	3.04	0.673	0.867
	40	3.30	0.673	-0.123
2	10	4.37	0.803	0.182
	15	4.35	0.804	-0.263
	20	4.16	0.816	0.184
	24	4.03	0.800	-0.264
	30	3.94	0.789	0.328
	40	3.96	0.781	-0.128
3	10	5.80	0.831	-0.165
	15	5.72	0.828	0.247
	20	5.64	0.795	-0.112
	24	5.62	0.822	-0.238
	30	5.11	0.816	0.163
	40	5.05	0.811	-0.185
4	10	6.84	1.042	0.127
	15	6.83	1.041	-0.138
	20	6.73	1.028	0.268
	24	6.72	1.017	-0.127
	30	6.69	1.042	0.832
	40	6.68	1.026	-0.431
5	10	5.35	0.859	0.192
	15	5.33	0.844	-0.186
	20	5.26	0.841	-0.218
	24	5.14	0.852	-0.265
	30	5.07	0.842	0.143
	40	5.09	0.843	-0.167

CR = 7:1 N = 600 RPM ϕ = 1.12

T_{IN} = 38°C Isooctane

TABLE 6.4 VARIATION OF APPARENT FLAME VELOCITY WITH SPARK TIMING

ION GAP	ø	$\bar{V}_f$	STD DEV	SKEWNESS
1	0.860	1.647	0.640	-0.832
	0.952	1.914	0.645	-0.426
	1.120	2.861	0.680	-0.237
	1.250	2.528	0.721	0.153
	1.353	2.544	0.821	-0.127
	1.461	2.591	0.921	0.104
2	0.860	3.684	0.765	-0.243
	0.952	4.032	0.791	0.164
	1.120	4.029	0.800	-0.264
	1.250	4.132	0.814	0.372
	1.353	3.634	0.871	-0.416
	1.461	3.552	0.972	0.211
3	0.860	5.402	0.841	0.109
	0.952	5.392	0.822	0.237
	1.120	5.617	0.822	-0.238
	1.250	5.438	0.872	0.136
	1.353	4.711	0.912	0.621
	1.461	4.599	0.966	0.327
4	0.860	6.434	1.032	0.113
	0.952	6.459	1.058	0.214
	1.120	6.717	1.017	-0.127
	1.250	6.271	0.987	0.327
	1.353	5.574	0.992	-0.126
	1.461	5.030	0.978	0.124
5	0.860	5.012	0.811	0.312
	0.952	5.050	0.812	-0.228
	1.120	5.137	0.852	-0.265
	1.250	4.802	0.848	0.136
	1.353	4.255	0.883	-0.214
	1.461	4.196	0.963	0.347

Isooctane CR = 7, N = 600 RPM

θ = 24°BTDC T_{IN} = 38°C

TABLE 6.5 VARIATION OF APPARENT FLAME VELOCITY WITH EQUIVALENCE RATIO

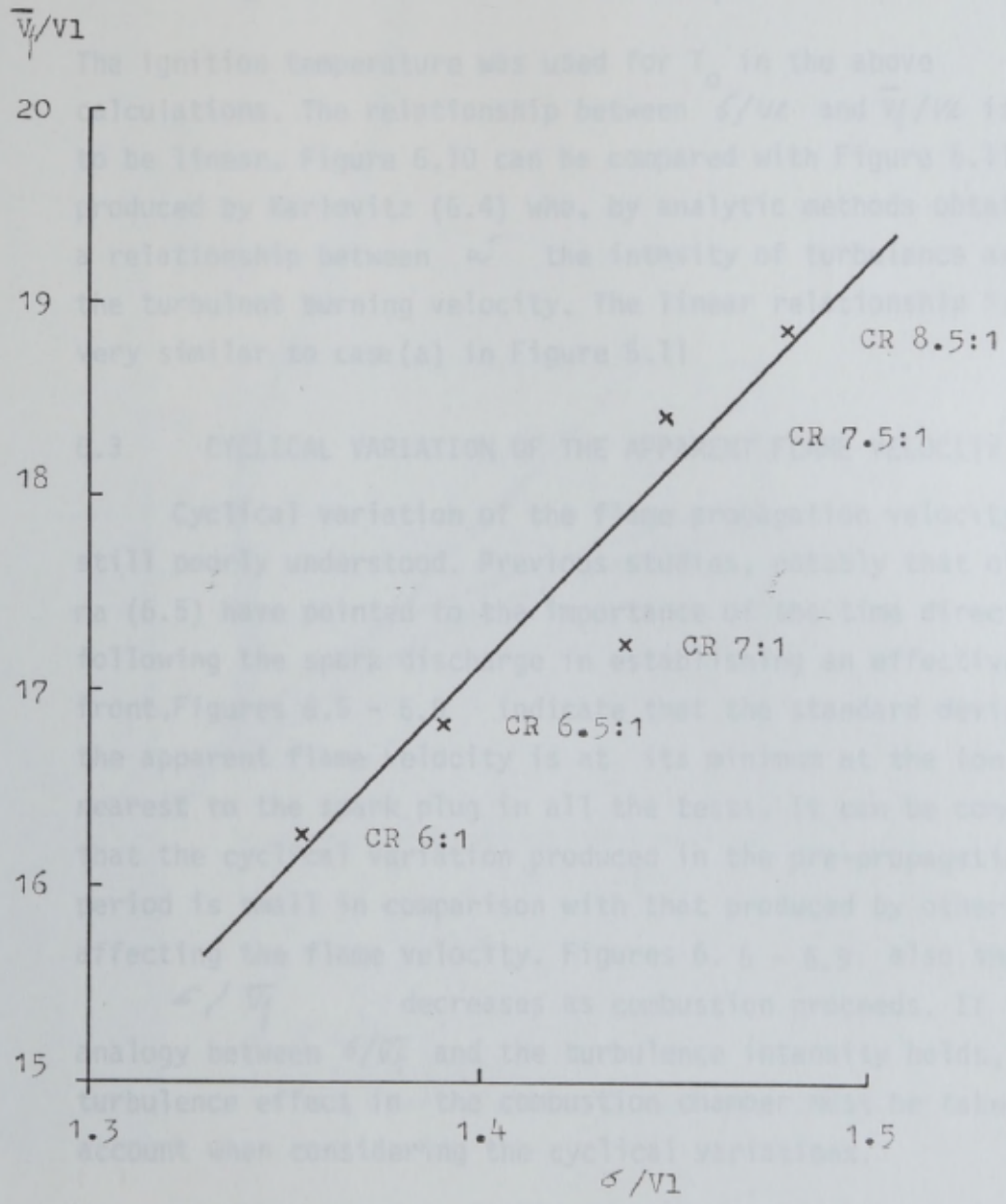

FIGURE 6.10 RELATIONSHIP BETWEEN MEAN FLAME VELOCITY AND STANDARD DEVIATION

whose equation for stoichiometric mixtures of Benzine is:

$$V_l = 30 + 7.910 \times 10^{-7} T_o^{2.92} \text{ cm/sec}$$

The ignition temperature was used for T_o in the above calculations. The relationship between σ/V_l and $\bar{V}_f/V_l$ is seen to be linear. Figure 6.10 can be compared with Figure 6.11, produced by Karlovitz (6.4) who, by analytic methods obtained a relationship between ω' the intnsity of turbulence and V_T the turbulent burning velocity. The linear relationship in 6.10 is very similar to case(a) in Figure 6.11

6.3 CYCLICAL VARIATION OF THE APPARENT FLAME VELOCITY

Cyclical variation of the flame propagation velocity is still poorly understood. Previous studies, notably that of Dent& Salama (6.5) have pointed to the importance of the time directly following the spark discharge in establishing an effective flame front.Figures 6.5 - 6.9 indicate that the standard deviation of the apparent flame velocity is at its minimum at the ion gap nearest to the spark plug in all the tests. It can be concluded that the cyclical variation produced in the pre-propagation period is small in comparison with that produced by other factors affecting the flame velocity. Figures 6. 5 - 6.9 also show that $\sigma/\bar{V}_f$ decreases as combustion proceeds. If the analogy between $\sigma/\bar{V}_f$ and the turbulence intensity holds, the turbulence effect in the combustion chamber must be taken into account when considering the cyclical variations.

In the remainder of this section, cyclical variation in flame propagation is explained using the effects of the fluctuation of mixture strength, and of turbulence in the unburnt charge.

The following assumptions are made in developing the argument. The cycle - to - cycle variation of the mixture follows a normal distribution. The pre-propagation period is included in the flame travel time or in the flame propagation velocity. The relationship between the flame propagation velocity and the equivalence ratio is linear, and the charge prior to ignition is homogeneous.

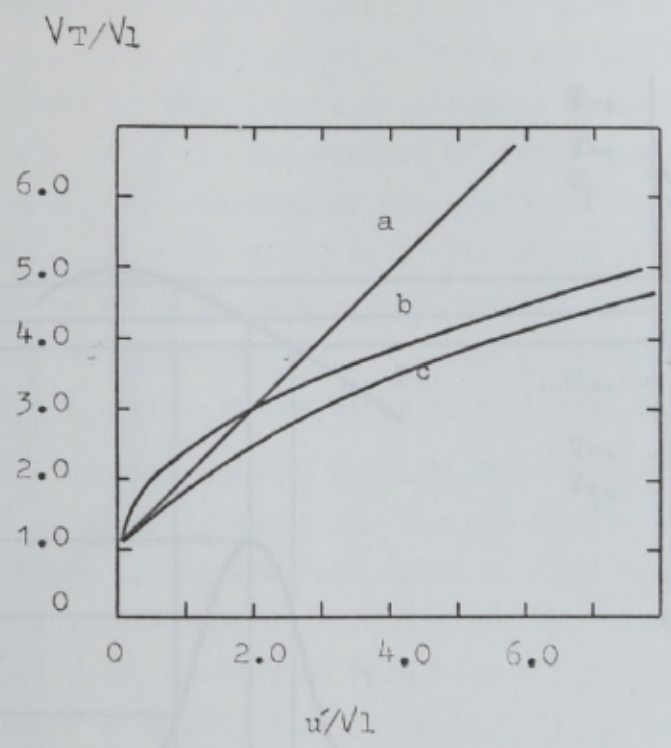

a, $T = V_l + u'$

b, $T = V_l + (2V_l u')^{1/2}$

c, $T = V_l + (2V_l u')^{1/2} (1 - V_l/u'(1 - \exp(-u'/V_l)))^{1/2}$

FIGURE 6.11 THEORETICAL TOTAL TURBULENT BURNING VELOCITY AS FUNCTION OF THE TURBULENCE INTENSITY IN UNITS OF THE LAMINAR BURNING VELOCITY V_l (FROM REFERENCE 6.4)

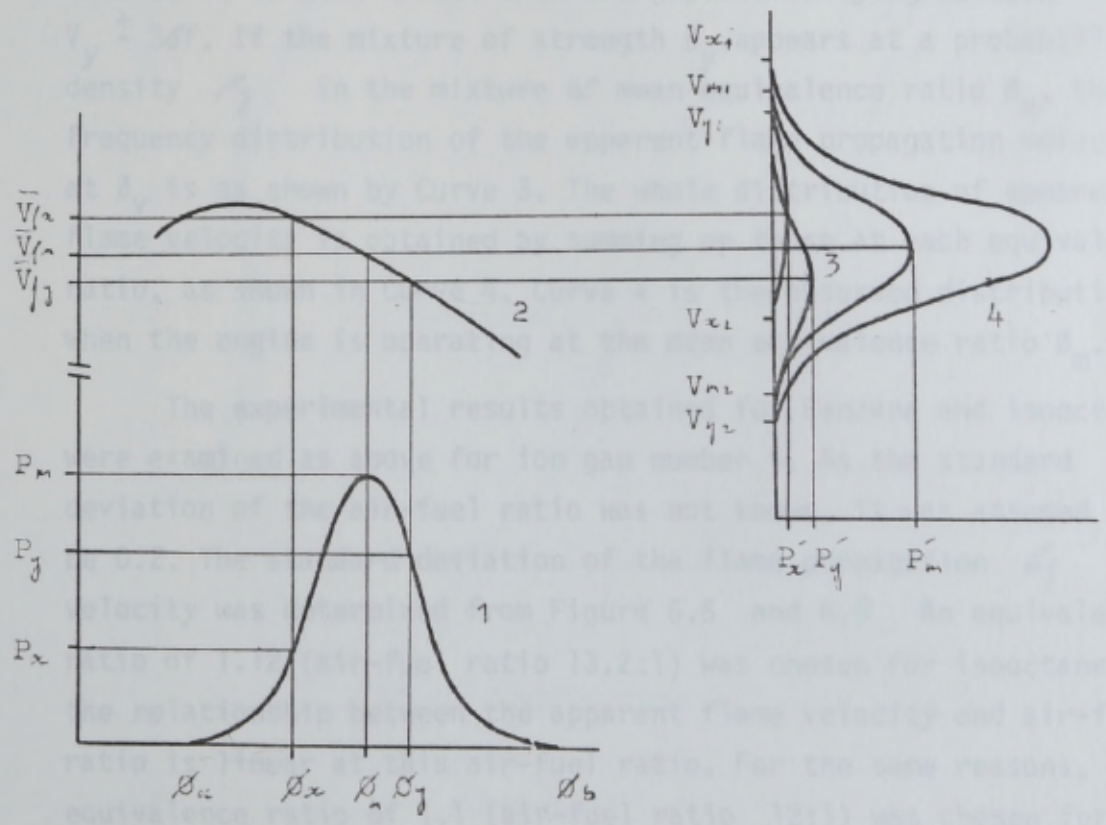

FIGURE 6.12 RELATIONSHIP BETWEEN CYCLIC VARIATION OF AIR-FUEL RATIO AND THE APPARENT FLAME PROPAGATION VELOCITY

The overall effect of cyclical variation on the flame propagation velocity can be determined as follows. If the engine is operating with a mean equivalence ratio Øm as in Figure 6.12, the cycle-by-cycle variation of equivalence ratio follows Curve 1. This curve is a normal distribution with its population lying between $Øm \pm 3\sigma_Ø$ For each equivalence ratio, the mean flame speed is given by Curve 2. At the equivalence ratio $Ø_y$, the flame propagation velocity varies with turbulence as shown in Curve 3. This curve is also normal with the population lying between $V_y \pm 3\sigma_f$. If the mixture of strength $Ø_y$ appears at a probability density P_y in the mixture of mean equivalence ratio $Ø_m$, the frequency distribution of the apparent flame propagation velocity at $Ø_y$ is as shown by Curve 3. The whole distribution of apparent flame velocity is obtained by summing up those at each equivalence ratio, as shown in Curve 4. Curve 4 is the observed distribution when the engine is operating at the mean equivalence ratio $Ø_m$.

The experimental results obtained for Benzene and Isooctane were examined as above for ion gap number 5. As the standard deviation of the air-fuel ratio was not known, it was assumed to be 0.2. The standard deviation of the flame propagation velocity was determined from Figure 6.6 and 6.9 An equivalence ratio of 1.12 (air-fuel ratio 13.2:1) was chosen for isooctane as the relationship between the apparent flame velocity and air-fuel ratio is linear at this air-fuel ratio. For the same reasons, an equivalence ratio of 1.1 (air-fuel ratio 12:1) was chosen for Benzene.

The results of the calculations are shown in Figure 6.13. The calculated results (solid lines) are in good agreement with the measured data (crosses) and the normal distribution (dots).

6.4 ANALYSIS OF THE CYLINDER PRESSURE DATA

In the second phase of the experimental work, the combustion interval meter was used, along with the UV recorder which produced cylinder pressure traces.

The conclusion of the analysis so far is that for a given

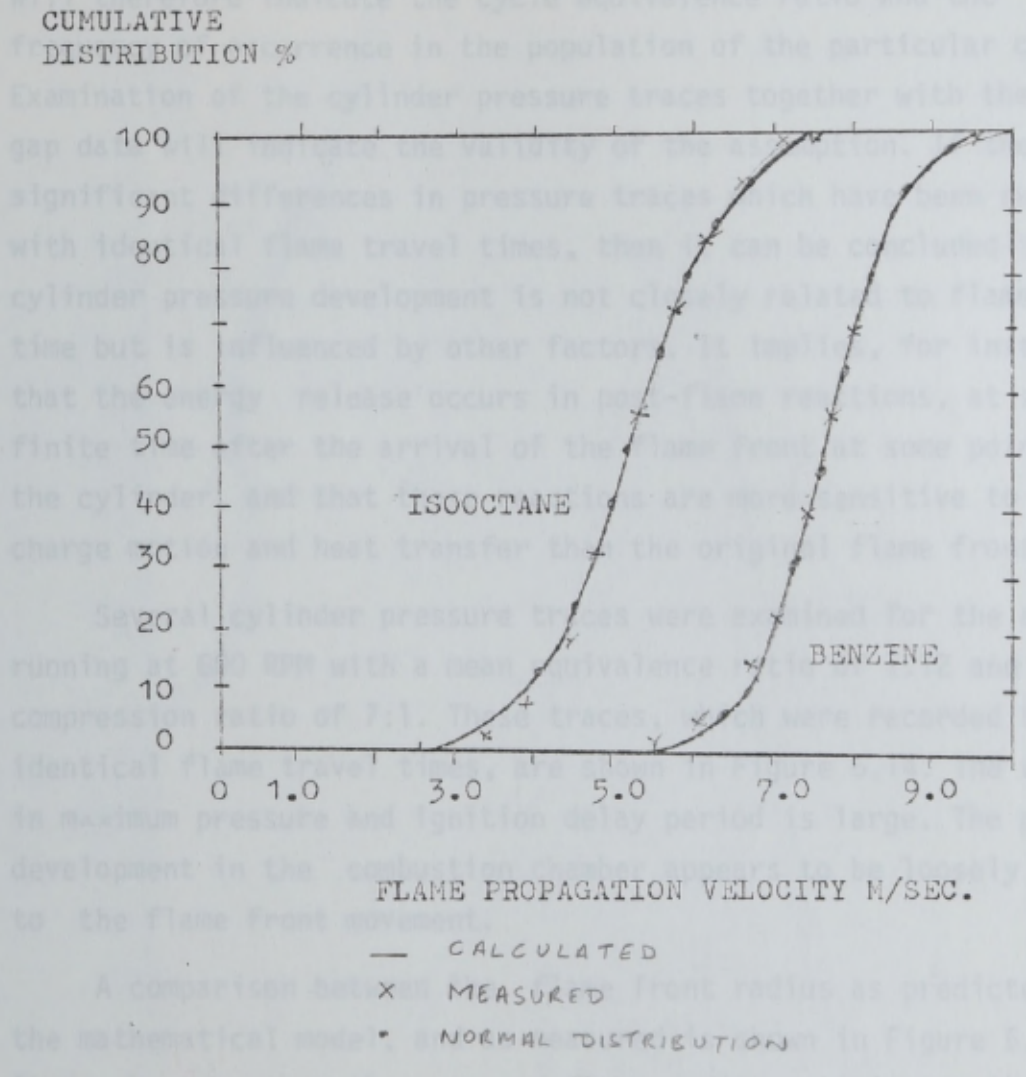

FIGURE 6.13 COMPARISON OF CALCULATED AND MEASURED DATA OF FLAME PROPAGATION VELOCITY

mean equivalence ratio setting on the carburettor, the equivalence ratio of a single cycle is specified by the flame travel time. Examination of the population distribution of the flame travel time will therefore indicate the cycle equivalence ratio and the frequency of occurrence in the population of the particular cycle. Examination of the cylinder pressure traces together with the ion gap data will indicate the validity of the assumption. If there are significant differences in pressure traces which have been recorded with identical flame travel times, then it can be concluded that cylinder pressure development is not closely related to flame travel time but is influenced by other factors. It implies, for instance, that the energy release occurs in post-flame reactions, at some finite time after the arrival of the flame front at some point in the cylinder, and that those reactions are more sensitive to charge motion and heat transfer than the original flame front.

Several cylinder pressure traces were examined for the engine running at 600 RPM with a mean equivalence ratio of 1.12 and a compression ratio of 7:1. These traces, which were recorded for identical flame travel times, are shown in Figure 6.14. The variation in maximum pressure and ignition delay period is large. The pressure development in the combustion chamber appears to be loosely related to the flame front movement.

A comparison between the flame front radius as predicted from the mathematical model, and as measured is shown in Figure 6.15. It can be seen that the measured flame radius anticipates the predicted radius over the entire range of flame propagation. It can therefore be suggested that the mechanism producing the cyclical variation in the cylinder pressure is a feature of post-flame reactions.

The effect of variation in the flame radius on mass burning rates is discussed in the next section.

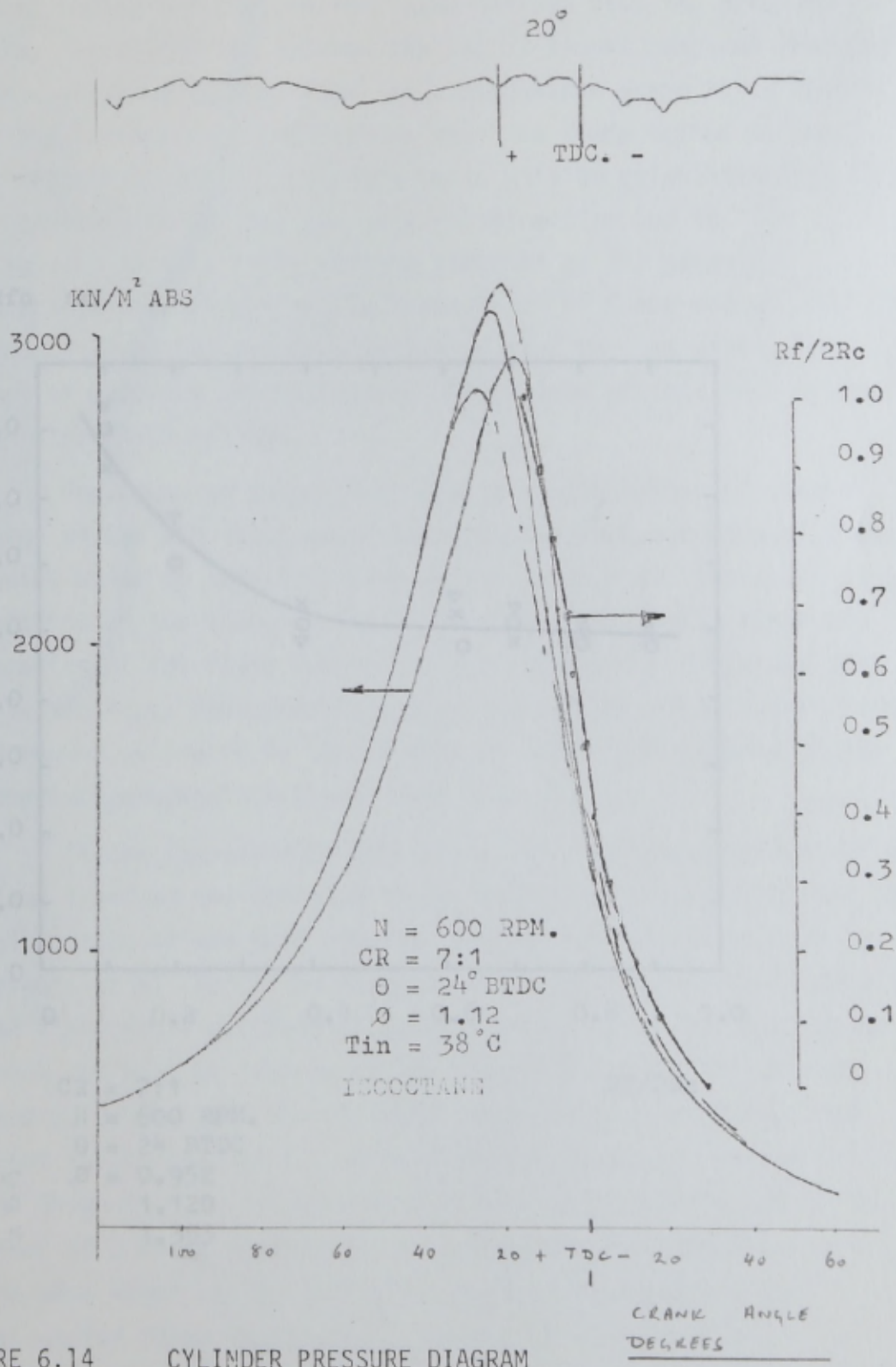

FIGURE 6.14 CYLINDER PRESSURE DIAGRAM

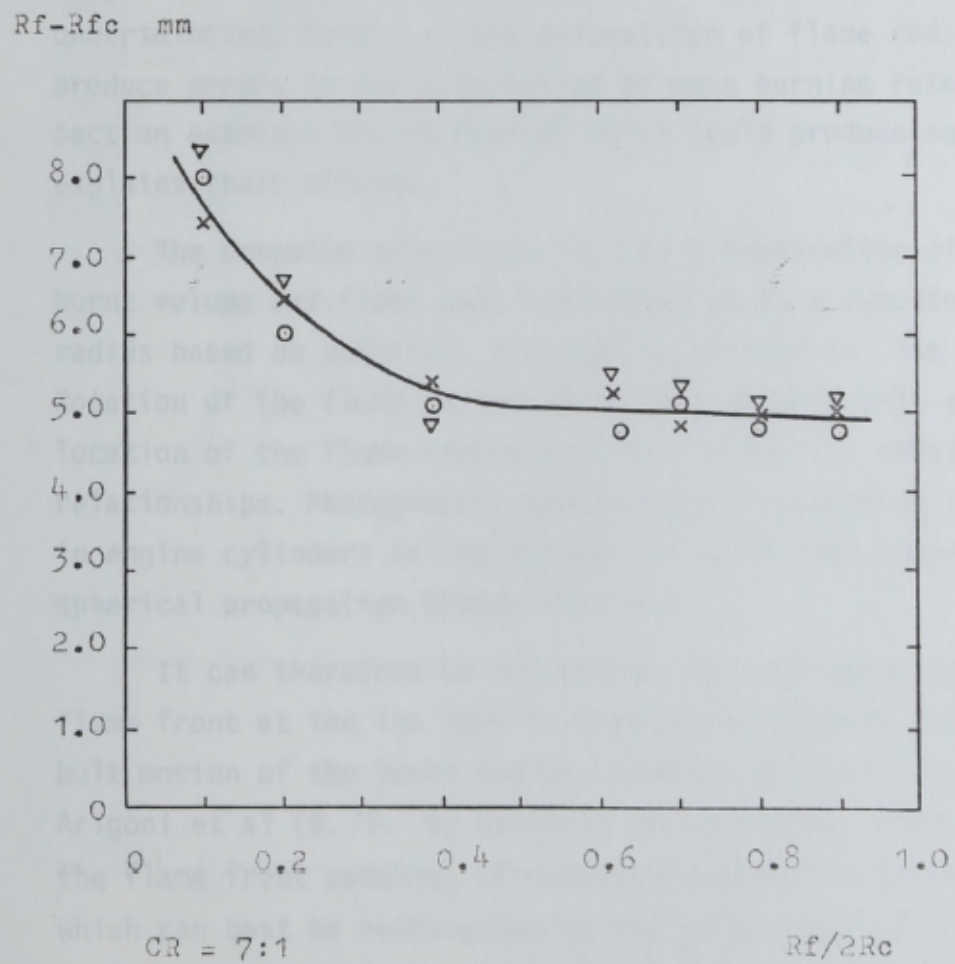

FIGURE 6.15 THE DIFFERENCE BETWEEN MEASURED AND PREDICTED FLAME RADIUS AS COMBUSTION PROCEEDS

6.5 FLAME FRONT SHAPE AND THICKNESS

It was shown in section 6.4 that the measured flame front radius anticipated the value derived from the pressure data. The difference between the two is almost constant throughout the combustion period. Thus, as a percentage error it is larger at the initiation of combustion when the flame radius is small. In Chapter 7, the mass burning rates will be calculated from flame propagation velocities and area relationships and so the diagnosed burning rates will be affected by any geometric uncertainties. Errors in the calcualtion of flame radius and shape produce errors in the calculation of mass burning rates. This section examines the mechanisms which could produce such errors and explains their affects.

The computed quantities involve a combination of chamber burnt volume and flame area relationships as a function of flame radius based on spherical propagation centred on the spark plug. Rotation of the flame in the combustion chamber will alter the location of the flame centre and thus change the effective area relationships. Photographic examination of expanding flame fronts in engine cylinders in the absence of swirl lend support to the spherical propagation theory (Ref 6.6).

It can therefore be considered that the early arrival of the flame front at the ion gaps is produced by factors other than the bulk motion of the burnt charge. Studies of flame structure by Arigoni et al (6.7). by analysis of ionization intensity show that the flame front consists of successive eddies of burning charge which can best be represented by the successive self-ignition theory, rather than the wrinkled flame front hypothesis. Flame front thicknesses of 2.5 mm have been measured by Winsor (6.8) and Ohigashi (6.9) measured turbulent flame thicknesses of the order of 8 mm in engine-like environments. This distance is of the same order as the difference between the measured and calculated flame front radius. This difference, 5.1 mm can be attributed to flame thickness, and this value will be used in Chapter 7.

6.6 THE EFFECT OF FLAME THICKNESS ON APPARENT FLAME SPEED

The influence of flame thickness on the calculation of flame speed can be approximated by the increase in the actual flame radius. The burning velocity is calculated from continuity in the flame as:

$$u_t = \frac{\dot{m}_b}{\rho_u A_f}$$

The calculated burning velocity is inversely proportional to the flame area. In the region where the flame area increases with radius, the effect of introducing flame thickness is to increase the flame area and thus decrease the flame speed, and vice versa. During the early stages of flame development, the curvature of the flame is at its largest and the ratio of entrained charge to burnt charge is at its highest. Thus the uncertainty in calculating u_t is largest in this zone. From Figure 6.15, the flame thickness can be approximated by the following expression:

$$t_f = 5.1 + 12\left(0.3 - \frac{R_F}{2R_c}\right) \quad ; \quad \frac{R_F}{2R_c} < 0.3$$

$$t_f = 5.1 \quad ; \quad \frac{R_F}{2R_c} \geq 0.3$$

in which the flame thickness is taken to be stabilised at 30% of the total flame travel distance.

REFERENCES

6.1 HARROW, G A, ORMAN, P L and TOFT, G B
The Effects of Engine Operating Variables on the Time of Flame Propagation in a Spark Ignition Engine
J Inst Petrol, 1963 vol 49 no 457

6.2 OGASAWARA, M and MATSUDA, K
An Experimental Study of the Flame Propagation Delay in a Spark Ignition Gasoline Engine
Bull JSME, 1967 vol 10

6.3 HEIMEL, S and WEAST, R C
Effect of Initial Mixture Temperature on the Burning Velocity of Benzine-Air, nHeptane Air and Isooctane-Air Mixtures
Proc 6th Symp (Int) on Combustion, 1957

6.4 KARLOVITZ, B
AGARD: Selected Combustion Problems
Butterworth, London, 1954

6.5 DENT, J C and SALAMA, N
Turbulent Structure in a Spark Ignition Engine
Proc Inst Mech Eng Conf on Combustion in Engines, Cranfield, 1975

6.6 SEMENOV, E S
Studies of Turbulent Gas Flow in Piston Engines
NACA Tch Trans F97, 1963

6.7 ARIGONI, V, CALVI, F, CORNETTI, G M and POZZI, U
Turbulent Flame Structure as Determined by Pressure Development and Ionization Intensity
SAE Paper 730088, 1973

6.8 WINSOR, R E and PATTERSON, D J
Mixture Turbulence - A Key to Cyclic Combustion Variation
SAE Paper 730086, 1973

6.9 OHIGASHI, Y, MAMAMOTO, Y and KIMIZA, A
Effect of Turbulence on Flame Propagation in Closed Vessels
Bull JSME, 1971 vol 14 no 74

CHAPTER 7 CYCLE SYNTHESIS

INTRODUCTION

The purpose of this chapter is to apply the flame propagation correlation and the equivalence ratio variation to the prediction of the indicated performance and exhaust emissions of a spark ignition engine. Cycle synthesis in internal combustion engines has been studied for several years and there exists a large number of models varying in accuracy of prediction and scope of applicability. Recent work has concentrated on attention to detail and modifications to existing models. The work reported here is no exception. The analysis is based on the work of Lavoie et al. (7.1) and Watfa et al. (7.2).

The following assumptions were made in developing the model. The high temperatures and pressures in the combustion chamber produce equilibrium concentrations of the majority of the product species in the flame (Ref. 7.3 - 7.4). However, allowance was made, through the use of an iterative procedure for the variation in the specific heat with temperature of the product species. The technique used in the analysis assumed perfect gas behaviour. The variation of the specific heats at low temperature is very small. The temperature profiles in the combustion chamber were calculated assuming a finite degree of mixing, to account for the different burning histories of each element, which produce a temperature gradient across the burnt charge.

This chapter also deals with the formation of Nitrogen Oxide and Hydrocarbon emissions, and heat transfer. The mass burning rates were calculated from the flame speed correlation developed earlier.

7.1 THE MATHEMATICAL MODEL

The problem can be stated as follows: given the state of the charge in the combustion chamber at crank angle A, calculate

the state at a subsequent crank angle B. The analysis involves continuous estimation of the energy changes in the working fluid. The total energy of the unburnt fraction is given by;

$$E_u(T) = \sum_{i=1}^{n} E_i(T) \qquad (1)$$

where $E_i(T)$ represents the energies of the individual elements comprising the mixture. The total energy of the burnt charge that has undergone a chemical reaction can be written as:

$$E_b(T,P) = \sum_{i=1}^{n} N_i e_i \qquad (2)$$

where e_i is the specific internal energy per mole of species i and N_i is the total number of moles of species i. Both e_i and N_i are functions of temperature and pressure. Over small ranges of temperature and pressure, the gas can be assumed to behave as a perfect gas. This is, in effect, a linearisation over small intervals by assuming that the energy changes are linear over the crank angle interval under consideration.

$$PV_b = \overline{R_b T_b} \qquad (3)$$

and

$$PV_u = R_u T_u \qquad (3)$$

The volume of the combustion chamber is given by:

$$V(\theta) = \int_0^{\alpha} V_b \, dx + \int_{\alpha}^{1} V_u \, dx \qquad (4)$$

and can also be expressed by the Slider Crank formula as:

$$V(\theta) = V_T \left[\frac{R_c - 1}{R_c} \left[\frac{1}{2}(1 - \cos\theta) \frac{L}{2R} \left(1 - \left(1 - \left(\frac{R}{L}\sin^2\theta\right)^2\right)^{1/2}\right)\right] + \frac{1}{R_c}\right] \qquad (5)$$

A first law energy balance on the total charge takes the form:

$$\frac{dE_T}{d\theta} = \frac{d\alpha}{d\theta} + \frac{dH}{d\theta} - \frac{P\,dV}{d\theta} \qquad (6)$$

In the above equations P is the pressure, v is the specific volume, R is the gas constant, T is the temperature, V_T is the total volume of the engine cylinder, α is the mass fraction engulfed by the combustion process (this includes the mass burnt but not the mass quenched on the cylinder walls), E_T is the total

energy, Q is the heat flow into the system. From Equations 1 and 2, Equation 6 can also be represented as:

$$E_T = M\left[\alpha \bar{e}_b + (1-\alpha) e_u\right] \tag{7}$$

where

$$\bar{e}_b = \frac{1}{M\alpha} \int_{m=0}^{\alpha} e_b \, dm.$$

With perfect gas behaviour over small ranges of temperature, it can be assumed that the specific heats are constant here:

$$\begin{aligned} e_u &= C_{vu} T_u \\ \bar{e}_b &= \overline{C_{vb}}\, T_b \end{aligned} \tag{8}$$

A final equation which fully describes the system can be obtained by assuming that the unburnt fraction is uniform in temperature and undergoes isentropic compression and expansion such that:

$$\frac{T_u(\theta)}{T_0} = \left[\frac{P(\theta)}{P_0}\right]^{\frac{\gamma_u - 1}{\gamma_u}} \tag{9}$$

where T_0 and P_0 are some reference values. γ is the ratio of the specific heats.

The above equations can now be solved to obtain the following first order differential equation for $P(\theta)$:

$$\frac{dP}{d\theta} = \frac{M \frac{d\alpha}{d\theta}\left[C_{vu} T_0 \left[\frac{P}{P_0}\right]^{\frac{\gamma_u - 1}{\gamma_u}} (\gamma_b - \gamma_u) - (a_b - a_u)(\gamma_b - 1)\right] - \gamma_b P \frac{dV}{d\theta} + (\gamma_b - 1)\left\{\frac{dQ}{d\theta} + \frac{dH}{d\theta}\right\}}{V + V_0\left[\left(\frac{\gamma_b - \gamma_u}{\gamma_u}\right)\left[\frac{P}{P_0}\right]^{\frac{\gamma_u - 1}{\gamma_u}}(1-\alpha)\right]} \tag{10}$$

In order completely to specify the temperature of each of the burnt elements as a function of crank angle the following relationships are used:

T_{bi} = Temperature of ith element at the instant of burning

T_{bin} = Temperature of the ith element at the instant when the nth element burns ($n > i$)

$$T_{bin} = T_{bi}\left[\frac{P_n}{P_i}\right]^{\frac{\gamma_b - 1}{\gamma_b}} \tag{11}$$

where

P_i = Pressure when ith element burns

P_n = Pressure when nth element burns.

The internal energy of the unburnt fraction at the instant when the nth element burns can be stated as:

$$E_n = M(1-\alpha_n)\left[C_{vu} T_o \left(\frac{P_u}{P_o}\right)^{\frac{\gamma_u - 1}{\gamma_u}}\right] \quad (12)$$

and the energy of the ith element when the nth element burns is:

$$E_i = M_i\left[C_{vb} T_{bi} \left(\frac{P_n}{P_i}\right)^{\frac{\gamma_b - 1}{\gamma_b}}\right] \quad (13)$$

The total internal energy of the burnt fraction E_b when the nth element burns is:

$$E_b = \sum_{i=1}^{n} M_i\left[C_{vb} T_{b(i)} \left(\frac{P_n}{P_i}\right)^{\frac{\gamma_b - 1}{\gamma_b}} \quad (14)$$

Substitution of Equations 13 and 14 into 11 produces the following:

$$E_o + Q_n - W_n = \sum_{i=1}^{n} M_i C_{vb} T_{bi}\left(\frac{P_n}{P_i}\right)^{\frac{\gamma_b - 1}{\gamma_b}} + M\left[1-\alpha_n\right]\left[C_{vu} T_o \left(\frac{P}{P_o}\right)^{\frac{\gamma_u - 1}{\gamma_u}}\right] \quad (15)$$

By a similar approach, the burning of the (n+1)th element will produce:

$$E + Q_{n+1} - W_{n+1} = \sum_{i=1}^{n} M_i C_{vb} T_{bi}\left(\frac{P_{n+1}}{P_i}\right)^{\frac{\gamma_b - 1}{\gamma_b}} + M_{(n+1)} C_{vb} T_{b(n-1)} \quad (16)$$

$$+ M\left[1-\alpha_{(n+1)}\right]\left[C_{vu} T_o \left(\frac{P_{(n+1)}}{P}\right)^{\frac{\gamma_u - 1}{\gamma_u}}\right.$$

If, during the compression process, heat transfer to the burnt element is assumed to be negligible, Equations 15 and 16 can be subtracted to produce

$$W_{n+1} - W_n = \sum_{i=1}^{n} M_i C_{vb}\left(T_{b(i)}\left(\frac{P_n}{P_i}\right)^{\frac{\gamma_b - 1}{\gamma_b}} - T_{b(i)}\left(\frac{P_{n+1}}{P_i}\right)^{\frac{\gamma_b - 1}{\gamma_b}}\right) \quad (17)$$

$$+ M\left[1-\alpha_n\right] C_{vu} T_o \left(\frac{P_u}{P_o}\right)^{\frac{\gamma_u - 1}{\gamma_u}} - M\left[1-\alpha_{n+1}\right]\left[C_{vu} T_o \left(\frac{P_{(n+1)}}{P_o}\right)^{\frac{\gamma_u - 1}{\gamma_u}}\right.$$

$$- M_{(n+1)} C_{vb} T_{b(n+1)}$$

$W_{n+1} - W_n$ represents the work done between the burning of the

nth and (n+1)th elements, which can be represented as:

$$W_{n+1} - W_n = \left(\frac{\rho_{n+1} + \rho_n}{2} \right)\left(V_{n+1} - V_n \right) \qquad (18)$$

7.1.1 Solution Procedure

Solution of Equation 10 takes the following form. The mass fraction burnt as a function of crank angle (θ) is obtained by application of Equation 26 obtained from the flame speed correlation equation. In this case, however, the area of the flame is reduced by the projected area of the quench layer as determined by Equation 25. The equilibrium concentration of the product species and the thermodynamic properties of the mixture are determined from the thermodynamic equilibrium model outlined in Chapter 5. After passage of the flame front, the quenched value is assumed to mixfully with the combustion products of the mass element from which it was derived and to attain the temperature of the burnt charge, but not to take part in post flame chemical reactions. This gives the values of $\overline{T_b}(\theta_i)$, $T_u(\theta)_i$, $\rho(\theta_i)$. Equation 10 is then solved for small movement of θ between θ_1 and θ_2. The computed values of $\overline{T_b}(\theta_2)$, $T_u(\theta_2)$ and $\rho(\theta_2)$ are checked against the estimated values and the constants C_{vu}, C_{vb}, a_u, and a_b are modified. The integration is repeated until the two values converge. This process produces the mean burnt gas temperature $\overline{T_b}$, the unburnt gas temperature T_u and the cylinder pressure as a function of crank angle. Consideration of the isentropic compression of the separate burnt element as the flame front progresses produces the variable temperature profiles across the burnt charge.

7.2 THE FORMATION OF NITRIC OXIDE

The variation of temperature and pressure for each of the burnt elements of the charge have been calculated, and from these data equilibrium concentrations of the combustion products can be established. The rates of energy-producing reactions for most of the elements of the exhaust products are sufficiently fast that

the burnt charge in the initial stages of expansion is close to thermodynamic equilibrium. As the reactions responsible for the formation of NO proceed relatively slowly the above condition does not apply to them. Very little NO is formed at the flame front. It is produced in post flame reactions after the burn up of the hydrocarbons. It can also be shown (Ref. 7.1) that NO freezes early in the expansion stroke before the other constituents of the exhaust gases depart appreciably from their equilibrium levels.

In order to calculate NO concentrations in each element of the burnt charge an extended Zeldovich reaction formula (Equations 19-21) was used. Equation 3 has been added to the Zeldovich mechanism to account for fuel-rich mixtures in which water is a major constituent (Ref. 7.5). The three equations are:

$$O + N_2 \rightleftharpoons NO + N \tag{19}$$

$$N + O_2 \rightleftharpoons NO + O \tag{20}$$

$$N + OH \rightleftharpoons NO + H \tag{21}$$

Equation 19 is endothermic left to right and relatively slow, whereas Equations 20 and 21 are exothermic and relatively fast.

The rate of change of NO concentration in a fluid element of volume V is:

$$\frac{1}{V}\frac{d[NO]V}{dt} = K_{19}[O][N_2] - K_{-19}[NO][N] + K_{20}[N][O_2] - K_{-20}[NO][O] + K_{21}[N][OH] - K_{-21}[NO][H] \tag{22}$$

where brackets denote concentration in g moles/cm^3 and $K_{\pm i}$ are the forward and reverse rates of the ith reaction. Before Equation 22 can be used to calculate NO formation rates, two questions must be resolved: the first, the method for calculating the Nitrogen atom concentration N, and second, the method for calculating O, O_2, OH and H. The N_2 concentration is essentially constant, since the N atom mole fraction is very small in comparison with the

species of interest, a steady state approximation can be made for N . With the steady state approximation, $\frac{1}{V}\frac{d[N]V}{dt}$ is set to zero, and thus:

$$K_{19}[O][N_2] - K_{-19}[NO][N]_s - K_{20}[N][O_2] + K_{-20}[NO][O] - K_{21}[N]_s[OH] + K_{-21}[NO][H] = 0 \quad (23)$$

where $[\ ]_s$ denotes a steady state concentration.

The second question, that of the radical and O_2 concentrations, is more complex. A model of the flame front in a spark ignition engine must be formalised before appropriate assumptions can be made. At the high temperatures found in spark ignition engines, the hydrocarbon (HC) oxidation reactions go rapidly to completion. The reaction zone itself is thin, although the turbulent flame front may extend across several burning eddies. It is therefore reasonable to assume that the species O, O_2, OH and H are in equilibrium in the burnt charge. Studies of the chemistry of the C-O-H system during the expansion stroke in a spark ignition engine (Ref. 7.6) show that O, O_2, OH and H equilibrium is maintained well into the expansion stroke, well beyond the point at which the NO chemistry freezes.

With this additional equilibrium assumption for O , O_2, OH, and H, Equations 22 and 23 can be rearranged to give:

$$\frac{d\{NO\}}{dt} = \frac{2M_{NO}}{\rho}\left[\frac{1 - (\{NO\}/\{NO\}_e)^2 R_{19}}{(1 + K\{NO\}/\{NO\}_e)}\right] \quad (24)$$

where $\{NO\}$ = NO mass fraction

M_{NO} = molecular weight of NO

ρ = gas density.

The one-way equilibrium reaction rate for Equation 19 is:

$$R_{19} = K_{19}[O]_e[N_2]_e = K_{-19}[N]_e[NO]_e$$

with subscript e denoting equilibrium concentration. Lastly,

$$K_{19} = R_{19}/(R_{20} + R_{21})$$

with R_2 and R_3 defined similarly to R_1, but for Equations 20 and 21.

Expressions for the forward rate constants for Equations 19 - 21, and values of R_i and K, for lean, stoichiometric and rich isooctane-air mixtures are listed in Table 7.1. In rich mixtures, it is R_3 rather than R_2 that determines the value of K. Omission of Equation 21 from the kinetic scheme causes underestimation of the NO formation and decomposition rates when

$$\{NO\}/\{NO\}_e \gtrsim 1$$

Equation 24 shows that $\frac{d\{NO\}}{dt}$ is a function of $\{NO\}$, pressure, temperature and equivalence ratio. The kinetic model must therefore be coupled with a thermodynamic model of the combustion process.

7.3 HYDROCARBON QUENCH LAYER THICKNESS

It is now well established that the formation of hydrocarbons in the exhaust gases of spark ignition engines is a result of flame quenching on the cylinder and piston surfaces and at the piston top land. The combustion chamber can then be looked upon as enclosing a bulk gas and unburnt gas in the quench layer, as shown in Figure 7.1.

The quench layer thickness has been the subject of much study and is a function of many variables including the charge pressure, temperature, the wall temperature and the equivalence ratio. The quench distance pressure dependence was obtained from Green and Agnew (7.7) and that for temperature from Friedman and Johnston (7.8). The one wall quench distance was assumed to be one third of the thickness of the two wall or parallel plate quench distance. The influence of wall temperature was taken from Wentworth (7.9).

The quench layer thickness can therefore be calculated from:

$$q = q_R \, 0.4 \left(\frac{4.052 \times 10^2}{P}\right)^a \left(\frac{373}{T_u}\right)^N \left(3 - 0.0056\, T_w\right) \quad (25)$$

where P is KN/m^2 and temperature is in $^\circ K$.

The quenching exponents are listed in Table 7.2. The incremental quench volume is then obtained from the quench layer thickness and the calculated flame movement during the increment. This can be calculated in the thermodynamic model prior to the

Reaction	Rate Constant (cm^3/mole s)	Ref.	R_i		
			= 0.8	= 1.0	= 1.2
1	$1.4 \times 10^{14} \exp(-75.400/RT)$	4	5.8×10^{-5}	2.8×10^{-5}	7.6×10^{-6}
2	$6.4 \times 10^{9} \exp(-6250/RT)$	4	4.8×10^{-5}	1.1×10^{-5}	8.3×10^{-7}
3	4.2×10^{13}	5	1.3×10^{-4}	9.7×10^{-5}	5.32×10^{-5}
$K = \frac{R_1}{R_2 + R_3}$			0.33	0.26	0.14

TABLE 7.1 VALUES OF RATE CONSTANTS AND ONE-WAY EQUILIBRIUM REACTION RATES FOR EXTENDED ZELDOVICH MECHANISM

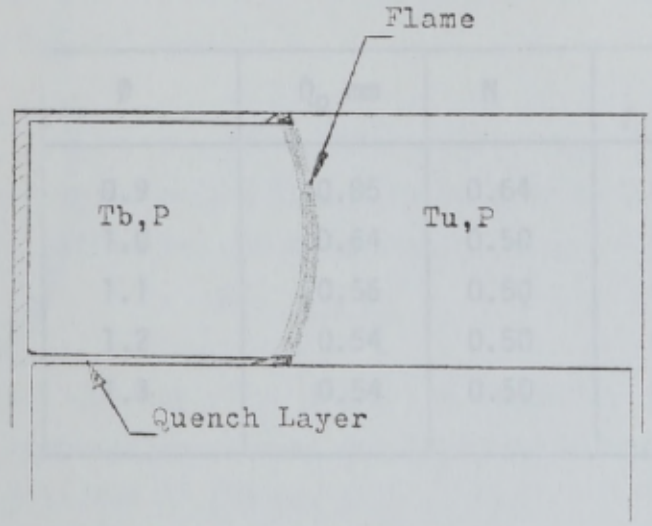

FIGURE 7.1 SCHEMATIC REPRESENTATION OF THE HYDROCARBON QUENCH LAYER

Ø	Q_R mm	N	a
0.9	0.85	0.64	0.53
1.0	0.64	0.50	0.52
1.1	0.56	0.50	0.62
1.2	0.54	0.50	0.66
1.3	0.54	0.50	0.66

TABLE 7.2 QUENCH LAYER PARAMETERS AS A FUNCTION OF EQUIVALENCE RATIO

calculation of the chemical composition of the burnt charge. The enthalpy of the unburnt charge is taken to leave the system during combustion.

7.4 HEAT TRANSFER

A considerable part of the heat transferred within the cylinder is transferred through the action of turbulent forced convection. Accurate calculation of the total heat quantity transferred depends therefore on precise calculation of the heat transfer coefficient.

Theoretical conditions require that determination of the heat transfer coefficient must be associated with the general relationship of turbulent forced convection. For air, assuming constant Prandtl number:

$$Nu = CRe^{n}$$

Substituting for Nu and Re and taking n to be 0.7, the heat transfer coefficient can be expressed as:

$$h = \frac{Ck\rho^{0.7} V_p^{0.7}}{\mu^{0.7} d^{0.3}}$$

The thermal conductivity k and the viscosity μ can be defined for general composition exhaust gas types as a function of temperature, following Sitkei (7.10) as:

$$k = 7.36 T_g \times 10^{5}$$

$$\mu = 3.3 T_g^{0.7} \times 10^{-8}$$

From the equation of state

$$\rho = P/RT$$

Thus the heat transfer coefficient becomes

$$h = \frac{CP^{0.7} V_p^{0.7}}{T_g^{0.2} d_e}$$

where d_e (the equivalent diameter) $= 4 \times \frac{\text{cylinder volume}}{\text{cylinder surface area}}$

$$= \frac{2Dh}{D + 2h}$$

Experimental evidence from Sitkei suggests that the above equation should take the form:

$$h = \frac{0.0428\ P^{0.7}\ Vp^{0.7}}{Tg^{0.2}\ de^{0.3}}$$

in which Tg is the momentary value of the mean gas temperature.

The quantity of heat transferred by convection is then calculated from the following equation:

$$Q = hA(Tg-Tw)d\theta$$

7.5 MASS BURNING RATE

The mass burning rate $\dot{M}b$ is calculated from the turbulent flame velocity correlation of Equation 9, Page 159, modified to account for the flame thickness and the area of the flame front occupied by the quench layers. The mass burning rate equation then becomes:

$$\dot{M}b = \rho u Afe Vt \qquad (26)$$

where Afe is the effective flame area, or, expressed in terms of the total mass in the combustion chamber: $\alpha = Mb/M$

$$\frac{d\alpha}{d\theta} = \frac{1}{M}\frac{dMb}{d\theta} = \left[\frac{\rho u Afe Vt}{\pi Rc^2 h \rho o}\right]\frac{dt}{d\theta}$$

At the beginning of combustion, the flame area is zero, thus:

$$\frac{d\alpha}{dt} = 0$$

An initial value is therefore needed to start the integration. It is assumed that, in the pre-propagation period, the flame front has not fully developed and the turbulent flame speed is constant. During the pre-propagation period 1% of the mass in the cylinder is burned. This occupies a hemispherical volume of radius R_I from the spark plug. The associated change in pressure in the combustion

chamber is very small, so that:

$$\frac{Vt}{Vl} \propto A\left(\frac{\rho u u'}{\mu}\right)^{0.77}$$

The time taken to burn the incremental value is thus:

$$Tb = Ri/Vt$$

and the rate of change of the burnt mass in the period is:

$$0.01MVt/\left(\frac{0.01M3}{\rho 02\pi}\right)^{1/3}$$

In the subsequent combustion process, the mean flame area over the crank angle interval is used in the calculation. The flame front area, as shown in Figure 5.14 ,is sufficiently well-behaved to allow this approximation to be made with little error, particularly near TDC.

As an extension to the work reported in this section, the effect on mass burning rates of changing u', the turbulence intensity was investigated. Turbulence intensity was increased by 50% and 100%, and the results are shown in Figure 7.2.

7.6 RESULTS OF THE CYCLE SYNTHESIS

Typical results of the cycle synthesis work are presented in Figures 7.3 -7.9. The graphs depict the exhaust emissions concentrations of NO and CO, and show the effect of the cyclical variation of the air-fuel ratio.

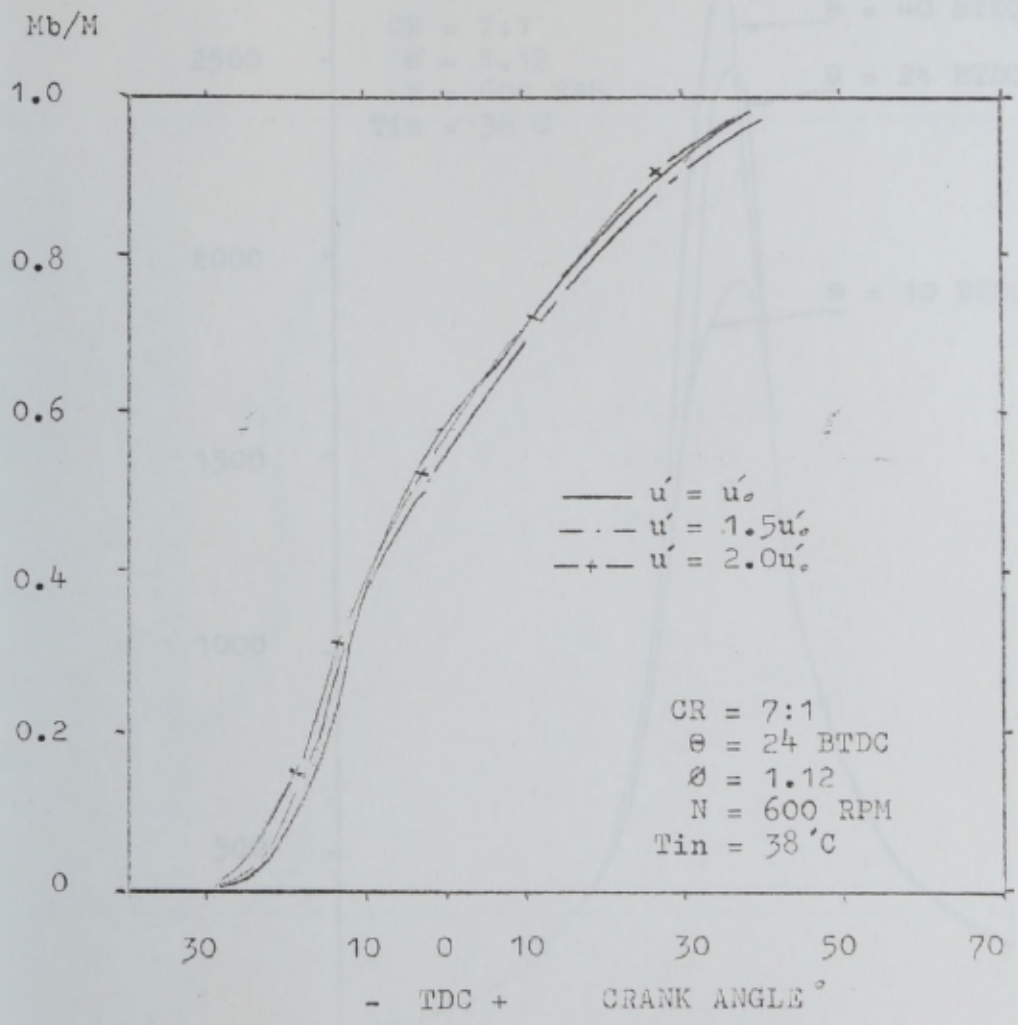

FIGURE 7.2 THE EFFECT OF CHANGES OF u' ON THE MASS FRACTION BURNT

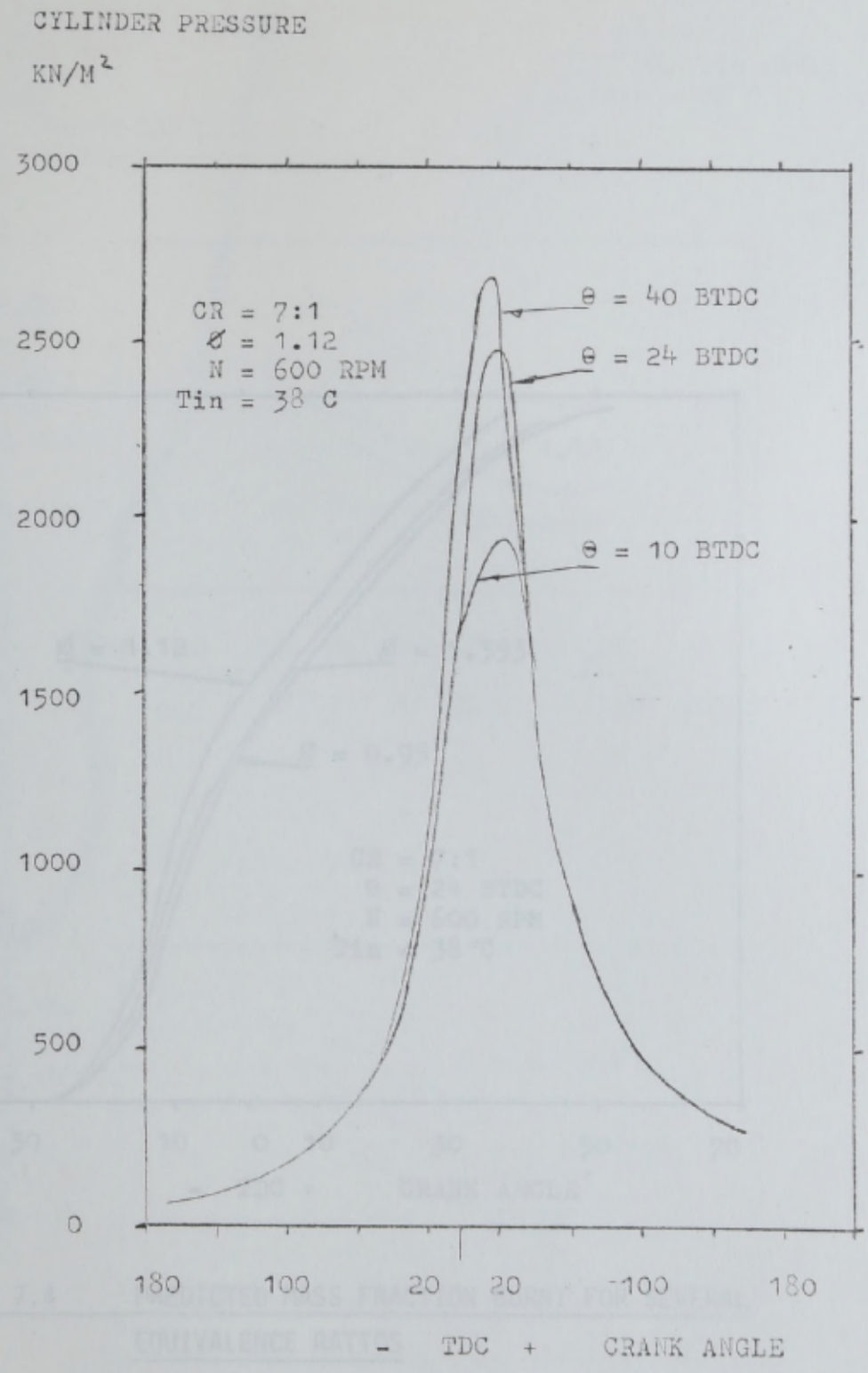

FIGURE 7.3 CYLINDER PRESSURE DIAGRAM

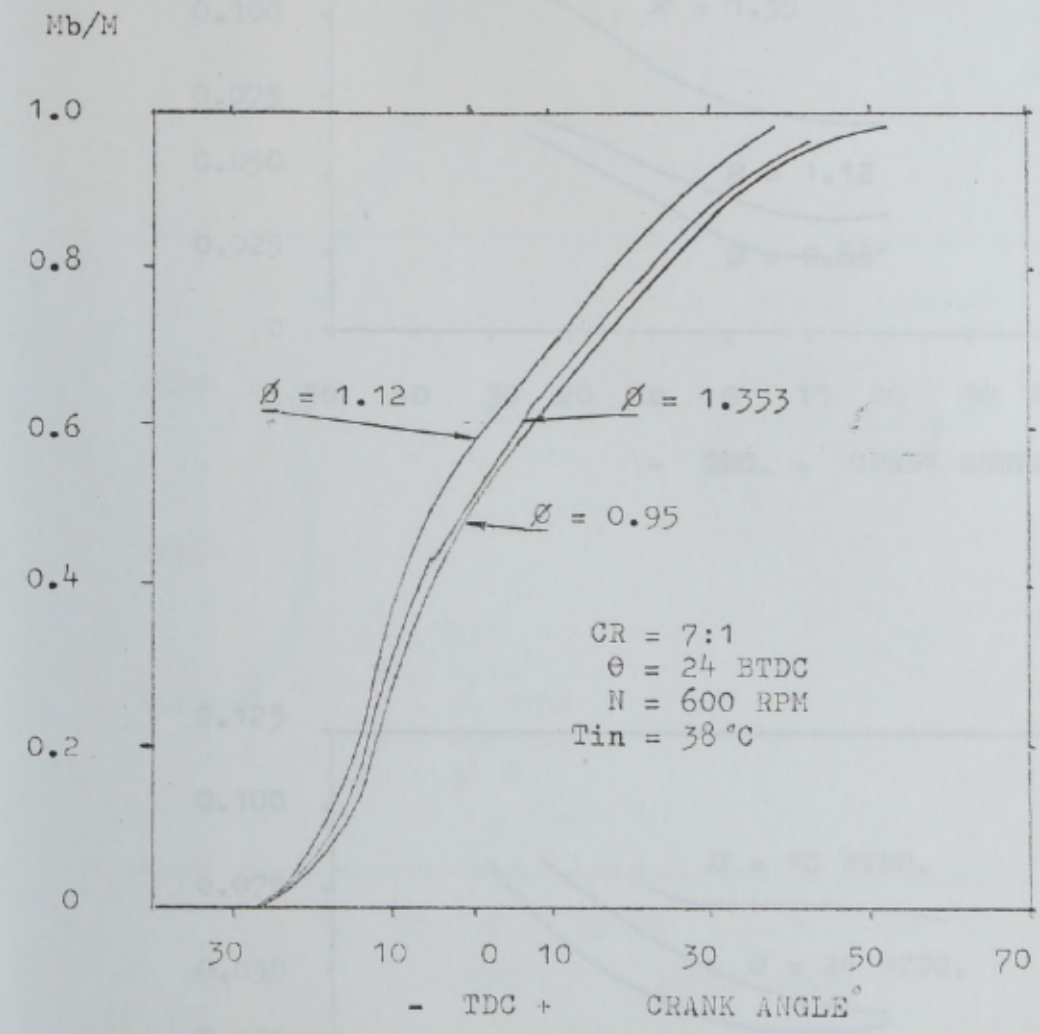

FIGURE 7.4 PREDICTED MASS FRACTION BURNT FOR SEVERAL EQUIVALENCE RATIOS

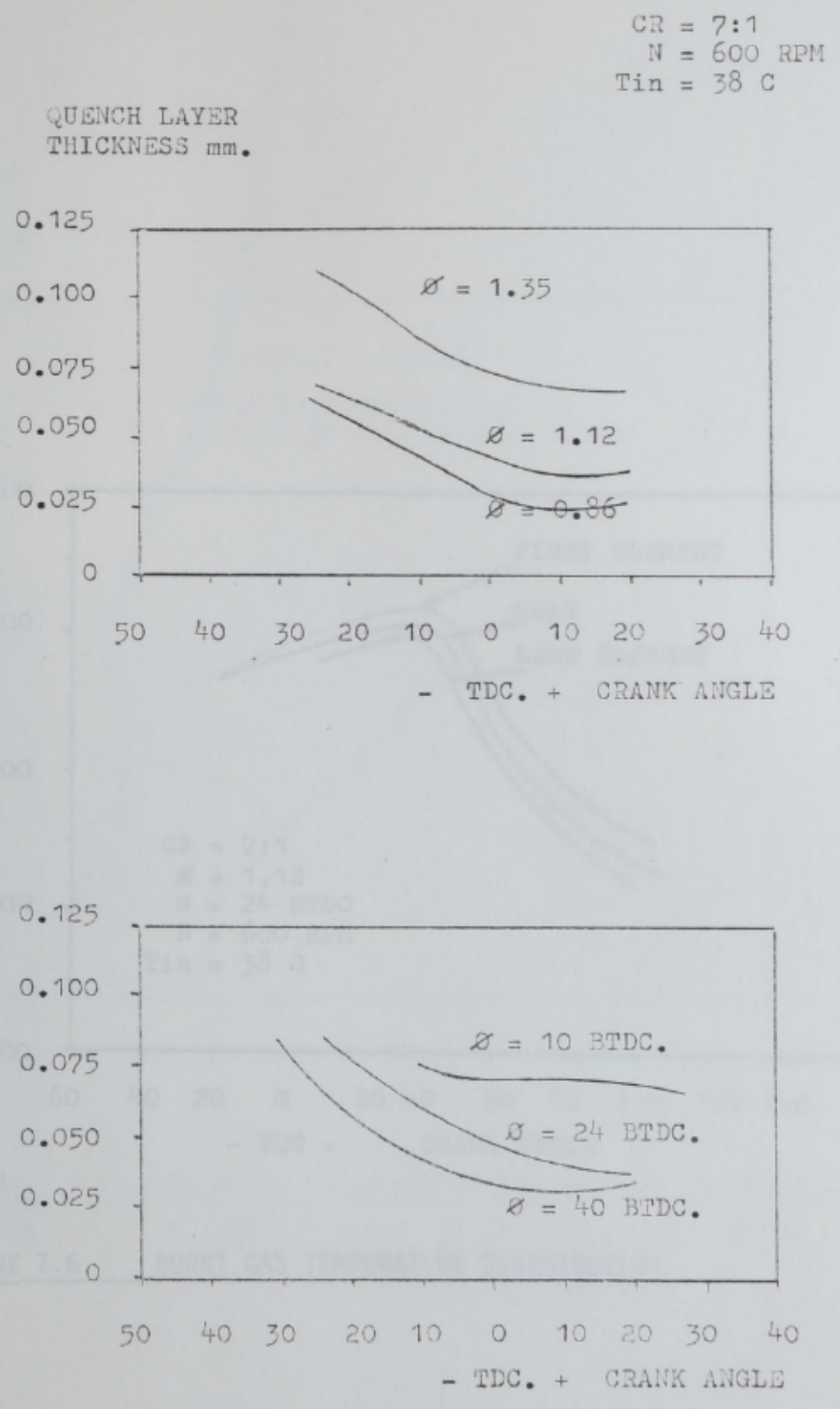

FIGURE 7.5 QUENCH LAYER THICKNESS FOR VARIOUS ENGINE CONDITIONS

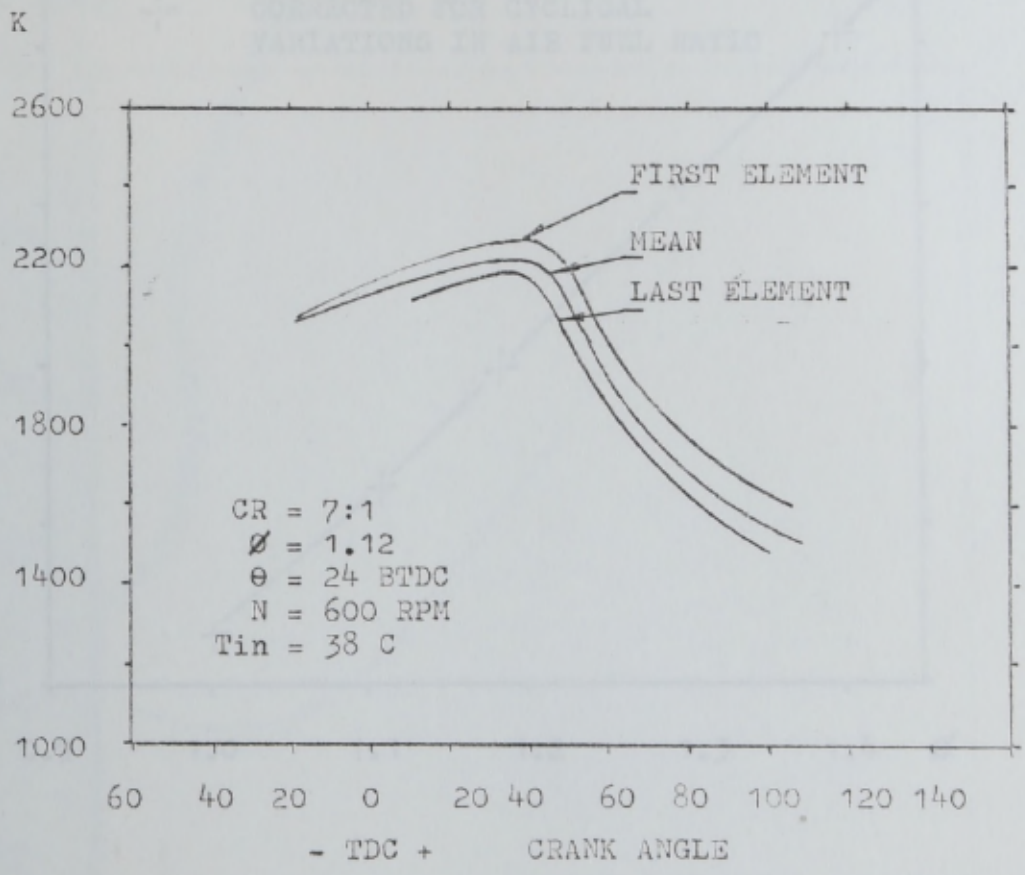

FIGURE 7.6 BURNT GAS TEMPERATURE DISTRIBUTION

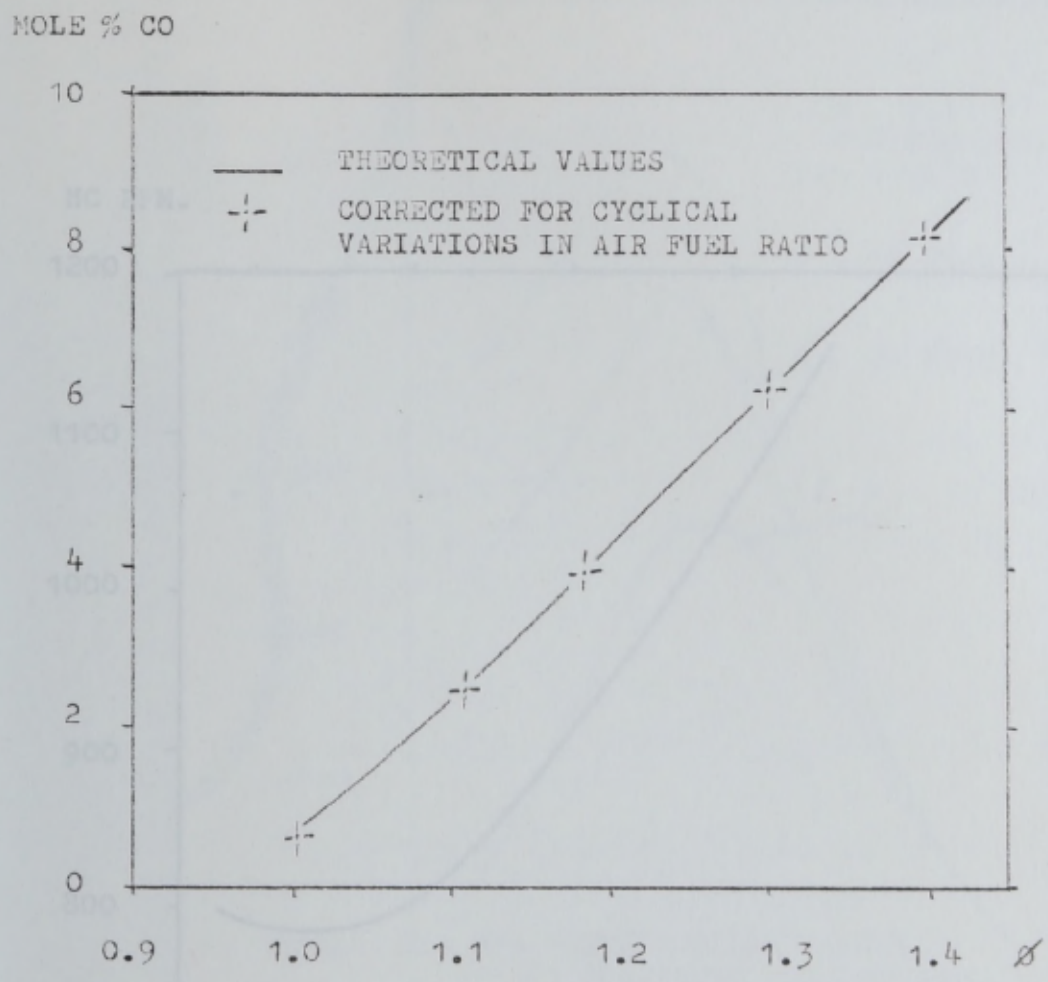

FIGURE 7.7 PREDICTED CO CONCENTRATION SHOWING THE EFFECT OF CYCLICAL VARIATION OF THE AIR-FUEL RATIO

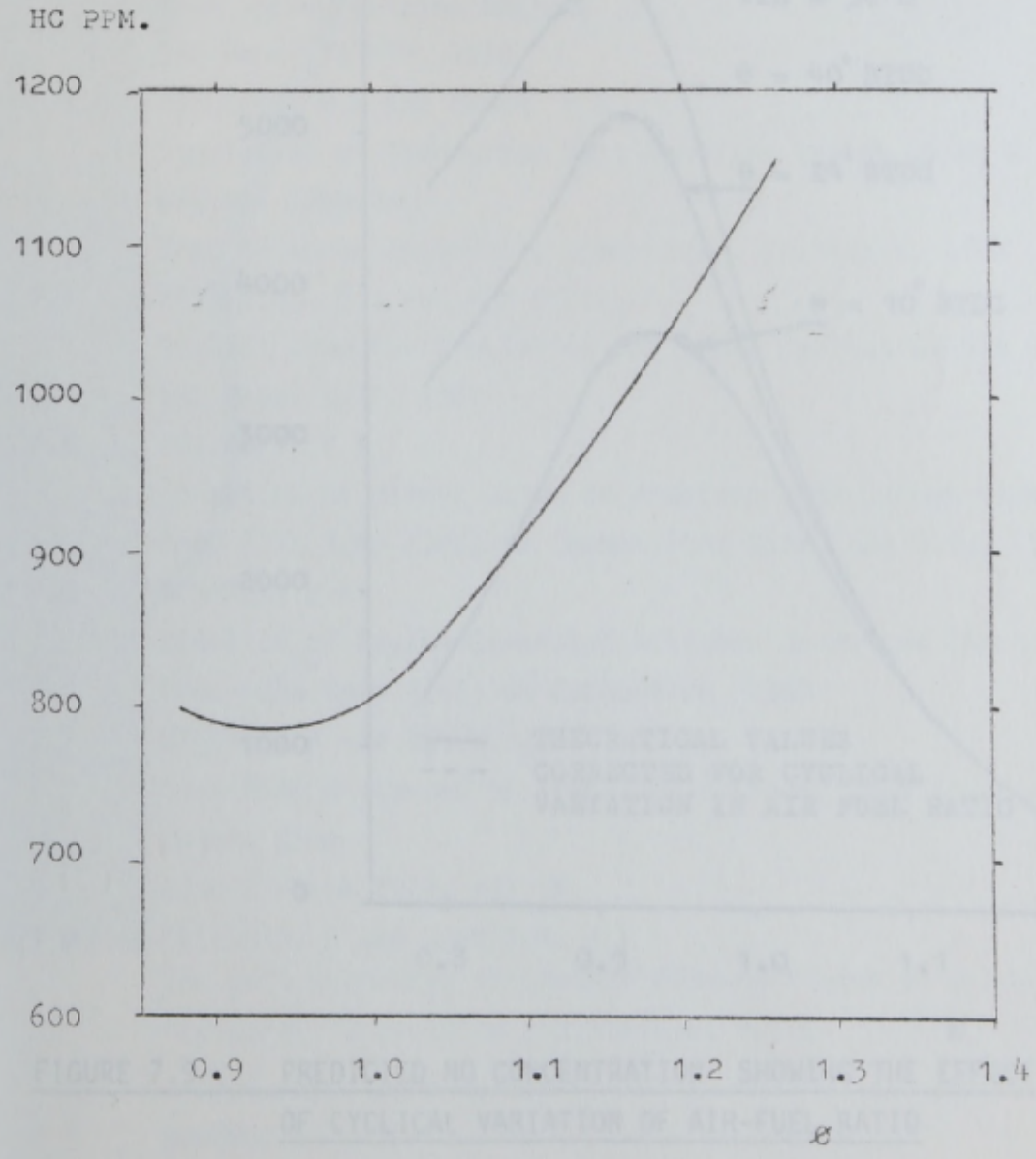

FIGURE 7.8 PREDICTED HYDROCARBON CONCENTRATION

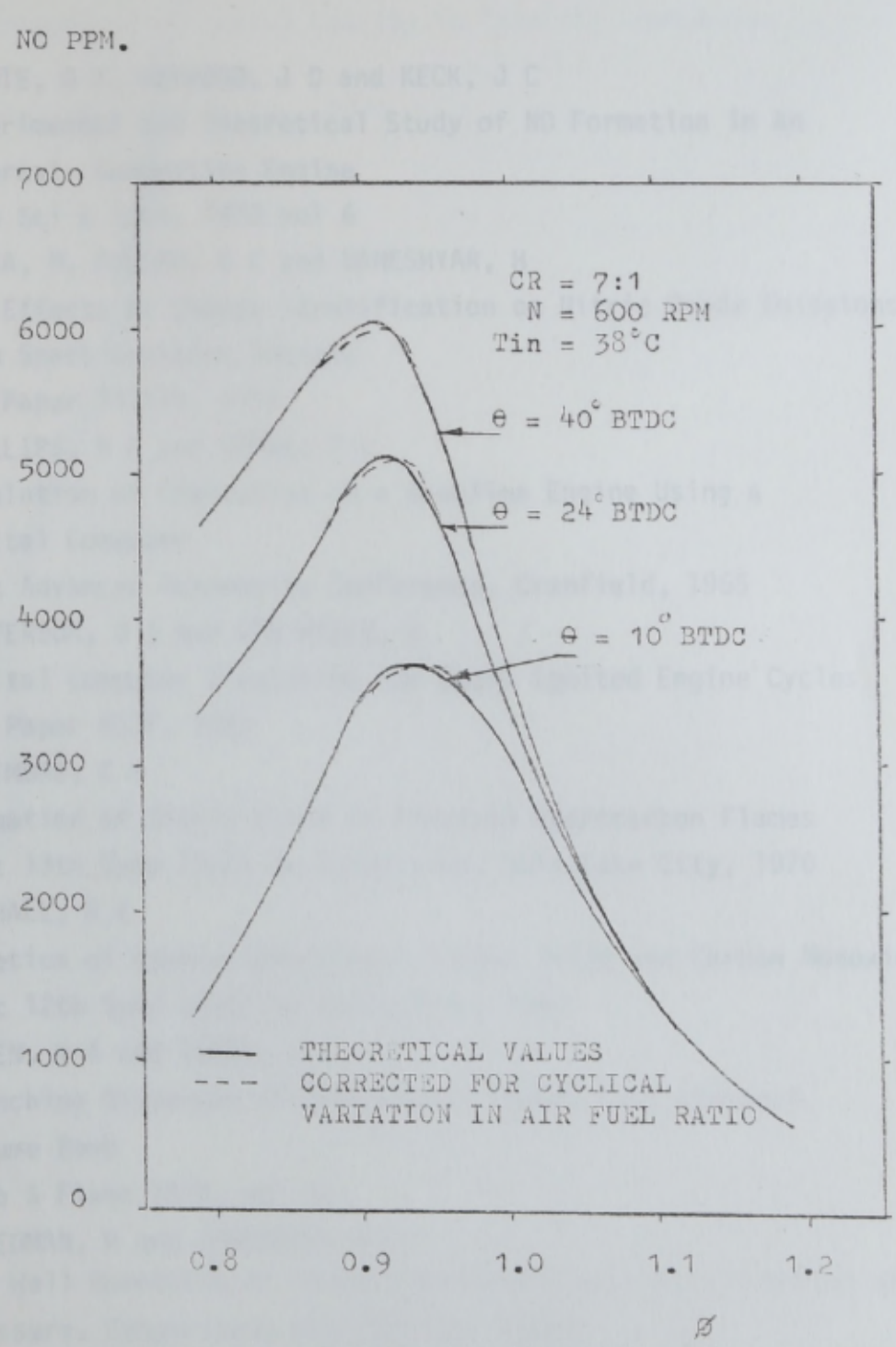

FIGURE 7.9 PREDICTED NO CONCENTRATION SHOWING THE EFFECT OF CYCLICAL VARIATION OF AIR-FUEL RATIO

REFERENCES

7.1 LAVOIE, G A, HEYWOOD, J D and KECK, J C
Experimental and Theoretical Study of NO Formation in an Internal Combustion Engine
Comb Sci & Tech, 1970 vol 6

7.2 WATFA, M, FULLER, D E and DANESHYAR, H
The Effects of Charge Stratification on Nitric Oxide Emissions from Spark Ignition Engines
SAE Paper 741175, 1974

7.3 PHILLIPS, R A and ORMAN, P L
Simulation of Combustion in a Gasoline Engine Using a Digital Computer
Proc Advanced Automobile Conference, Cranfield, 1965

7.4 PATTERSON, D J and VON WYLEN, G
Digital Computer Simulation for Spark Ignited Engine Cycles
SAE Paper 633F, 1963

7.5 FENIMORE, C P
Formation of Nitric Oxide in Premixed Hydrocarbon Flames
Proc 13th Symp (Int) on Combustion, Salt Lake City, 1970

7.6 NEWHALL, H K
Kinetics of Engine-Generated Nitrogen Oxide and Carbon Monoxide
Proc 12th Symp (Int) on Combustion, 1968

7.7 GREEN, K A and AGNEW, J T
Quenching Distances of Propane-Air Flames in a Constant Volume Bomb
Comb & Flame 1970, vol 15

7.8 FRIEDMAN, R and JOHNSTON, W C
The Wall Quenching of Laminar Propane Flames as a Function of Pressure, Temperature and Air-Fuel Ratio
J Appl Phys, 1950 vol 21

7.9 WENTWORTH, J T
Effect of Combustion Chamber Surface Temperature on Exhaust Hydrocarbon Concentration
SAE Paper 710587, 1971

7.10 SITKEI, G
Heat Transfer and Thermal Loading in Internal Combustion Engines
Akademiai Kiado, Budapest, 1974

CHAPTER 8 DISCUSSION OF THE EXPERIMENTAL AND THEORETICAL RESULTS AND CONCLUSIONS

INTRODUCTION

The experimental and theoretical results are discussed in this Chapter. The Chapter opens with an examination of the flame speed data obtained from the experimental work. The nature of the flame front propagation and the mechanism of cyclical variations of the air-fuel ratio are discussed. Next, the flame speed correlation is examined and suggestions are put forward for its use in cycle synthesis for unusual engine configurations or for the examination of alternative fuels. The role of turbulence is discussed with a view to reducing Hydrocarbon emissions in stratified charge engines, and the nature of the flame front in an IC engine and its effect on burning rates is also examined. The Chapter ends with consideration of the modelling of emissions, and it is suggested that post-flame reactions are responsible for the cyclical variations in cylinder pressure and temperature which produce cyclical variations in emissions concentrations.

8.1 FLAME FRONT BEHAVIOUR

The time taken for an expanding flame front to cross the combustion chamber in a CFR engine has been examined using two pure fuels, Benzine and Isooctane, and flame front travel time has been shown to depend upon fuel type, equivalence ratio and compression ratio under steady engine operating conditions. The difference in propagation times for the two fuel types was smaller than the effects of mixture strength and compression ratio but was large enough to affect the running of the engine. The cyclical variation of flame travel time was larger for the slower burning fuel, Isooctane and the largest cyclical variations occurred in weak mixtures. These findings reinforce the results of other research, suggesting not only that the results are correct, but that the experimental procedures adopted in this work were satisfactory.

A statistical analysis of the flame propagation times for each of the ion gaps in the cylinder head showed that the population distiributions of the flame travel times were not Normal, but had a tendency towards Poisson distributions. With a Normal distribution, the feature of interest can be readily expressed, as standard deviation and so attempts were made to normalise the flame travel times. This was achieved by making the variable of interest the flame propagation velocity, defined as

$$V_f = L_i / \tau_i$$

where L_i is the distance between the spark plug and the ion gap i. The distribution of the flame propagation velocity was found to be Normal, from which it was possible to define the mean flame velocity $\overline{V_f}$, the mean of the flame velocity and $\overline{\tau}$ defined as $L_i/\overline{V_f}$ and σ_f, the standard deviation of the flame velocity. The effect of various engine operating parameters on $\overline{V_f}$, σ_f and σ_f/V_f was then examined. The mean flame velocities were found to be dependent upon equivalence ratio, reaching a maximum at slightly rich mixtures. The standard deviation σ_f was practically constant. Increasing the compression ratio increased the flame velocity $\overline{V_f}$ and the standard deviation σ_f. The coefficient of variation was almost constant however, implying that σ_f is proportional to the mean flame velocity. The standard deviation of the flame velocity was seen to increase as the flame front progressed across the combustion chamber. It is generally accepted that the period following ignition is very important in the establishment of the expanding flame front. Cylinder pressure diagrams show a large degree of cycle-by-cycle variation in this region. The low σ_f at this region points to the existence of a weak relationship between flame propagation and energy release in the combustion process or an error in the instrumentation. This possibility will be examined in a later section.

As the standard deviation of the flame propagation velocity is the RMS of the deviation from its mean, it is mathematically analogous to the intensity of turbulence. An attempt was made to establish a relationship between σ_f and $\overline{V_f}$ similar to that

between u' and the turbulent flame speed. The turbulent flame is considered to have different structures depending on the scale of turbulence relative to the thickness of the laminar flame front. Karlovitz obtained analytically the relationship between u' and S_T as shown in Figure 6.11 for several values of turbulence intensity. On the basis of this figure, it was decided to plot $\overline{V_T}/V_L$ against δ/V_L for several engine operating conditions. The laminar flame speed V_L was varied in this case by changing the engine compression ratio. The outcome of this limited exercise showed an analogy between the CFR combustion and the case put forward by Karlovitz of a very weak turbulence intensity, ie

$$\frac{\overline{V_T}}{V_L} = 1 + u'/V_L$$

As it is possible that the intensity of the turbulence in the combustion chamber will change as combustion progresses, and since later results suggested that the turbulence in this instance was not weak, it was felt that the expression presented above could not adequately express the effect of turbulence on flame propagation. It was therefore decided to seek a correlation between $\overline{V_T}$ and u' of a much more general nature. The turbulent Reynolds number $R_{e\lambda}$ was chosen and the results will be discussed later in this Chapter.

A mechanism for cyclical variation of the flame velocity based on the joint effects of turbulence and the cyclical variation of the air-fuel ratio is suggested.The experimental results were examined according to this mechanism and proved to be in agreement. By assuming that the energy release was closely associated with the flame front movement, it should be possible, by recording simultaneous pressure traces and flame velocity data, to determine the frequency of occurrence of a given pressure diagram. Flame travel time and cylinder pressure data recorded simultaneously were examined for cyclical variations in pressure for the same flame travel times. The pressure variations were found to be too large, particularly at the intiation of combustion to be attributed to errors in the pressure measuring equipment. This suggested that the flame front is very distorted by turbulence and that the ion gaps were being triggered, in one instance by the

peaks of the flame wave, and in another, by the troughs. Alternatively, it might suggest that the energy release occurs in post-flame reactions which themselves follow a form of population distribution and are influenced by factors other than the movement of the flame front. Photographic recordings of flame fronts in internal combustion engines depict a flame front of finite thickness (several millimeters). Photographic evidence of flamesis always open to question as it is dependent on the sensitivity of the film, and it is not clear whether the photographs depict the flame thickness in turbulent flames or the extent of movement of a thin flame due to oscillations of the flame front during exposure of the film. As flame thickness can have an effect on the mass burning rates, it was decided to compare the value of the burnt charge as predicted from the mathematical model with that calculated from ion gap measurement for a particular cycle. The comparison inducated that, in this case, the flame front became fully established after travelling 30% of the full distance at a thickness of 5.1 mm. This was not an exhaustive test as the mass burning rate, as predicted by the mathematical model is dependent on the heat transferred from the charge to the chamber walls, and the heat tranfer process was modelled in a very basic fashion. Nonetheless, the analysis indicates the existence of a possible trend.

In conclusion, the evidence suggests that the wrinkled flame front hypothesis should be rejected in favour of the successive self ignition theory.

8.2 FLAME SPEED CORRELATION

Experimental evidence from non-engine data suggested the existence of a relationship between V_t/V_ℓ and the turbulent Reynolds number $R_{e_\lambda} = \rho u \lambda / \mu$. The experimental flame speed data were examined with the predicted value of the thermodynamic properties of the unburnt charge on this basis. Isotropic turbulence relationships coupled with the Rapid Distortion Theory were used to establish a correlation between V_t/V_ℓ and R_{e_λ} which took the form $V_t/V_\ell = A + B(C R_{e_\lambda})^n$

The best fit curve to the data points was obtained by choosing the exponent n to give the best fit. The scatter of the experimental points about the correlation was large but an examination of the data to determine further correlation between the ignition timing and the equivalence ratio was unsuccessful. The form of the correlation is useful as it will allow prediction of the mass burning rates in IC engines to be made for any fuel type based on knowledge of the thermodynamic properties of the unburnt charge, the geometric properties of the combustion chamber and the intensity of turbulence at the spark plug, all factors which are relatively easy to obtain. The application of the correlation to the prediction of mass burning rates in a two-zone model was reasonably successful. The predicted and measured properties of the charge in the combustion chamber were seen to match well.

However, the test of correlation was not particularly rigorous as the correlation was itself used to predict the data from which it was derived. The correlation should therefore be used to predict burning rates in different engines operating under different conditions to determine the extent of its validity.

The correlation is also weak in that it does not take into account, as a separate entity, the ignition delay period. Some insight into this phase of the combustion period can be gained however, by considering the ignition delay period to be proportional to the time taken for the flame front to engulf an eddy of characteristic size L' of mass $4/3\pi L'^3 \rho u$. This is given by the following equation, for which $(P/Po) = 1$:

$$Tb = \frac{CL'}{Vt} = \frac{CL'}{Vl(A+B(ho\rho uu'^{1.2})^{0.75})}$$

Assuming that the eddy size is related to the integral length scale the above equation becomes:

$$Tb \propto \frac{Cho}{Vl(A+B(\frac{ho\rho uu'^{1.2}}{\mu})^{0.75})}$$

Thus

$$Tb \propto \frac{ho^{0.27} u^{-0.97}}{Vl}$$

Increase in the turbulence intensity or the laminar flame speed will reduce the ignition delay time provided that eddy size is unaffected by the changes. In cases where the integral length scale and the turbulence intensity are linearly related, decreasing the turbulence intensity will increase the ignition delay period. The ignition delay period is therefore a very complex part of the combustion phase. It is related to the four fundamental quantities of turbulent combustion, the integral length scale L, turbulence intensity U', the Taylor microscale λ and the laminar flame speed V_l.

The correlation allows an estimate of the effect of charge turbulence in the fully developed combustion phase to be developed. As shown in the cycle synthesis work, increasing the turbulence intensity had a small effect on the mass burning rates. This can be explained as follows. After the ignition delay period, the increase of turbulence intensity will increase the mass burning rates, the cylinder pressure and the temperature of the unburnt charge relative to the initial turbulence levels. Increasing the unburnt charge temperature will increase the laminar flame speed and thus increase the mass burning rates. However, increasing the cylinder pressure will decrease the flame speed and thus reduce mass burning rates. The overall effect will therefore be a balance between these two opposing contributions. The results of this work indicate that provided the turbulence level is within the range to allow successful ignition of the charge, the subsequent propagation of the flame front is largely independent of the turbulence level. This suggests that flame-generated turbulence is of secondary importance.

It has been suggested that increasing turbulence levels will reduce the Hydrocarbon quench layer thickness. Stratified charge engines are poor in Hydrocarbon emissions compared with conventional enignes because of their large surface to volume ratio. This may be improved by increasing the turbulence in the main chamber to a higher level than that in the ignition chamber, to reduce the quench layer thickness. Once combustion has been initiated in the fuel-rich quiescent ignition chamber, which has been designed with a low surface to volume ratio, the flame will propagate into the highly

turbulent region of the main chamber.

Finally, the correlation allows the deigner to determine early in the design process, the effects that changes in the shape of the combustion chamber shape will have on the mass burning rates and the pressure diagram. It would be possible to tailor the shape of the cylinder pressure diagram to suit a particular application once the geometric parameters of the combustion chamber have been established, and the geometry of the flame front calculated. The level of charge turbulence at the point of ignition can be established from model testing using relatively inexpensive equipment. The correlation should also prove useful for modelling hybrid engines such as the paired cylinder Cranfield-Kushul engine for which empirical mass burning rate correlations are not available. It will also be of use in examining the suitability of alternative fuels for use in the spark ignition internal combustion engine.

The spherical flame approach of premixed combustion proved to be a useful approximation for combustion studies. The effect of flame thickness on mass burning rates was accounted for by reducing the flame radius by a flame thickness parameter. A better understanding of flame thickness, its effect on mass burning rates and its dependence on turbulence intensity, length scale and equivalence ratio should be developed and incorporated along with an analytical formulation of a thick flame zone.

8.3 EMISSIONS

The effect of the cyclical variation of the equivalence ratio on the concentration in the exhaust of, NO, HC and CO emissions was small. The cyclical variation of the equivalence ratio was small, and the requirement of a linear relationship between the flame speed and the air-fuel ratio limited the useful range of the corrections. Moreover, in the case of HC and CO, the relationship between the emission concentration and the equivalence ratio was very nearly linear, thus minimising the correction. For NO, where the equivalence ratio-emission concentration relationship is very non-linear, the effect is more noticeable. The discrepancy

the time-mean measurement concentrations and the predicted mean cycle concentration cannot be accounted for by the cyclical variation of the equivalence ratio. The formation of NO is obviously a very complicated process dependent on the temperature time-history of the burnt charge. If the extended Zeldovich mechanism is the correct mechanism to use to describe the chemical knietics of the formation process, the mechanism for generating the temperature time-history of the burnt charge would bear further investigation.

The spatial concentration of NO in the combustion chamber is highly temperature-dependent. Cyclical variations of the cylinder pressure will therefore produce large cycle-by-cycle variation in the NO concentrations. The cylinder pressure variations seem to be a product of post-flame reactions. In order to predict the formation of NO accurately, it is essential to understand the complex processes which take place at the flame front.

In this study, it was assumed that the quench layer mixed with the burnt charge after the passage of the flame front. The heat transfer from the burnt charge was therefore lost evenly from the entire mass equalising its temperature. If the quench layer remained on the cylinder walls to be removed by the outflow of burnt charge in the exhaust process, it would act as a thermal barrier between the bulk of the burnt charge and the cylinder walls. The heat transfer would then be drawn from a cooled quench layer with the bulk gas being compressed and expanded isentropically. The temperature of the burnt charge and the NO concentration would then be higher than that predicted here. Further error could be produced by the application of an overall heat transfer coefficient which did not take into account spatial variations. Further research in this area would be useful.

The predicted levels of Hydrocarbon emissions were in poor agreement with the experimentally measured concentrations. The modelling ignored the Hydrocarbons trapped in the piston crevices and the oxidation of Hydrocarbons in the post-flame reactions. The model is obviously oversimplified in this respect, but the quench layer thickness depicted in Chapter 7 is similar to those reported in the

literature. Since the usefulness of the flame speed correlation in determining the quench layer thickness has been demonstrated, a framework has been constructed within which further investigations might be pursued.

The levels of Carbon Monoxide concentrations predicted in the cycle synthesis were higher than the measured concentrations. This discrepancy casts doubt on the assumption of chemical equilibrium of the product species immediately after combustion. Further rate-controlled reactions, particularly with the Hydroxyl radical (OH) and possibly the Hydrogen atom (H) which are important species in the kinetics of formation and decomposition of NO and CO could occur in fuel rich mixtures.

8.4 EXPERIMENTAL METHOD

The method employed for measurement of the flame passage time was based on the assumption of a thin flame front propagating with little wrinkling and distortion, as the ion gaps were designed to produce an output voltage at the first passage of the flame front. If the flame front consists of successive eddies which would each trigger the ionisation sensor, then the combustion interval meter would react to the arrival of the first eddy only. The position of the probe in relation to the distortion of the flame front would then produce variations in the flame travel time. This suggests that the flame front must be examined using statistical techniques. The cyclical nature of the cylinder pressure diagrams suggests that the energy release in combustion occurs in post-flame reactions. The reaction zone would therefore be of a finite thickness. It is dubious in this case whether it is possible to predict mass burning rates accurately from flame motion, particularly at the beginning of combustion when the flame thickness is of the same order as the flame radius. These uncertainties make analysis of the prepropagation period more difficult.

The CFR engine proved, in this work, to be completely reliable. The Ellison warm-up procedure enabled repeatible running conditions to be established on different days. The piston crown temperature could be maintained at a pre-set level by adjusting the sump oil

temperature. The cylinder wall temperatures were adjusted by varying the flow rate of the cooling water. This would not be possible with a conventional engine in normal running conditions. It is possible that the cyclical variations of the flame travel time would, in the conventional engine, be influenced by the variation of the cylinder wall temperature in different engine conditions.

The choice of engine on which to conduct this work is open to the criticism that it is not typical of engines currently used in commercial units. The CFR engine is deficient in speed and power output and has geometric properties not found in commercial engines. It does however, have the stability and consistency of running essential to this type of work.

8.5 CONCLUSIONS

The conclusions which can be drawn from this work are summarised below:

1 The cyclical variation of the flame propagation velocity followed a normal distribution.

2 The standard deviation of the flame propagation velocity varied as the flame progressed across the combustion chamber. The smallest deviation was observed in the region of the spark plug. Large cycle-by-cycle variations in the combustion chamber pressure were observed as the flame front developed in the region of the spark plug. The pressure variations are therefore loosely connected with the flame front development in the intial stages of combustion.

3 For the experimental conditions examined, the flame propagation velocity correlated with the turbulent Reynolds number according to the equation:

$$\frac{V_T}{V_\ell} = 0.324\left[0.021\,\frac{\rho_o \rho_u u'^{1.33}}{\mu}\left(\frac{P_o}{P}\right)^{0.037}\right]^{0.73} - 4.581$$

4 The correlation, based upon turbulent burning data, presented in the literature dealing with non-engine flames is useful for predicting flame behaviour in an engine, with a quasi-dimensional, spherical-flame model

5 The scatter of the experimental points about the correlation

equation was large. The correlation should be examined in further work to determine whether ignition timing and equivalence ratio effects could reduce the scatter of the experimental points.

6 The quasi-dimensional, spherical-flame approach to predictive modelling of premixed engine combustion is a useful tool for combustion chamber design. To improve the accuracy of such models, a better understanding of flame front thickness and its dependence on turbulence intensity, length scale and mixture strength needs to be developed and incorporated in the models, along with an analytical formulation of a thick flame zone.

7 The application of the model as a predictive tool requires knowledge of the turbulence level in the combustion chamber. Experiments should be directed towards velocity turbulence levels, intake flow geometry and combustion chamber shape.

8 The role of turbulence in the combustion process is more important for the initiation of the combustion, rather than subsequent flame development. The flame development in this region is governed by thermodynamic considerations

9 The cyclical variation of the equivalence ratio had little effect on the predicted levels of NO, CO and HC in the exhaust gases. The spatial variation of NO in the combustion chamber is very temperature-sensitive and would therefore be more affected by cyclical variations in the combustion chamber pressures. The mechanism behind the cyclical variation of cylinder pressure should be the subject of further research.

10 The formation of the Hydrocarbon quench layer can be determined using the flame speed correlation but the role of this layer in the subsequent thermodynamic process in the combustion chamber has yet to be verified.

APPENDIX 1 EXPERIMENTAL EQUIPMENT

INTRODUCTION

This Appendix contains technical details of the equipment used in the experimental phase. A discussion of the pressure measurement technique is presented, followed by the calibrations of the pressure transducer and the thermocouples. The Appendix ends with a technical specification of the equipment used.

A1.1 MEASUREMENT OF THE COMBUSTION CHAMBER PRESSURE

The combustion chamber pressure is the prime variable from which the other thermodynamic and geometric properties of the burnt and unburnt charge are established. It is therefore essential that the measurement of the cylinder pressure is free of avoidable errors and that the measuring system chosen be the most suitable for the purpose. The criteria on which the choice might be based are discussed in the literature review in the next section.

A1.2 PROPERTIES OF TRANSDUCERS

For the purpose of measuring time-varying pressures, such as occur in internal combustion engines, quartz and semiconductor transducers are available with natural frequencies high in comparison with the fundamental frequency of the pressure fluctuations occurring in the combustion chamber. Table A1.1 presents a compilation of the essential properties and dimensions of some of the transducers which were considered for this application. According to the description of Brosh (A1.1) and Bynum et al (A1.2) these high frequency transducers can be regarded as practically undamped systems. This means that, for measuring purposes, only up to 30% of the natural frequency (depending on the form of the pressure behaviour) can be exploited without perceptible deterioration in the accuracy of measurement as a result of dynamic effects, for example, excessive oscillations. This upper limiting frequency is shown in Table A1.1, Column 5.

The quartz pressure transducer listed in Table A1.1 has a natural frequency of 65 KHz and an external diameter of 11mm. It is

MANU-FACTURER	TYPE	PRINCIPLE	FREQUENCIES		DIA/ LENGTH mm	RANGE Bar	ERROR %*	OSCILL-ATION SENSIT-IVITY Bar/g	TEMPER-ATURE SENSIT-IVITY %/K**	MAXIMUM OPERATING TEMPERATURE
			NATURAL KHz	USABLE KHz						
Kistler	701A	Quartz	65 plus	50	11.00/ 26.80	Vari-able to 250	±0.5	less than 10^{-4}	-0.01	510
Kulite	XQL-080	Semi-Conductor	100-150	30	2.10/ Vari-able	Vari-able to 8	±0.5	less than 10^{-7}	less than 0.05	370
SAI	SABJ-6M	Semi-Conductor	100	30	3.20/ 4.70	Vari-able to 70	±0.5	-	-0.05	430

TABLE A1.1 PROPERTIES AND DIMENSIONS OF SOME TRANSDUCERS WITH HIGH NATURAL FREQUENCY (VALUES QUOTED BY MANUFACTURERS)

*Combined Linearity and Hysteresis error, referred to as transducer measuring range

**expressed as a percentage of the measuring range

very well suited for the measurement of wall pressure fluctuations, although it cannot measure mean pressure level or static value at the same time as the magnitude of the pressure fluctuations.

Simpson and Gatley (A1.3) have investigated the sensitivity of various quartz transducers as a function of the frequency. They demonstrated the existence of variations in the calibration factor of some 1% of the static value over the frequency range up to 2.5Khz. The frequency behaviour above 2.5KHz of the transducer selected (the Kistler) could not be verified. However, it can be concluded, from its high natural frequency, that its sensitivity, even at high frequencies arouns 10KHz, can hardly deviate by more than 1% from the static value.

Terada and Kruggel (A1.4) reported on the variation with operating temperature of the sensitivity of various quartz transducers of the family to which the Kistler belongs. It was found to vary by some 1% up to 510 K. At higher temperatures, the transducer must be cooled to maintain accuracy of measurement and length of life. A water cooled adaptor was used in this work, housing the transducer as shown in Figure A1.1.

Some quartz transducers exhibit marked sensitivity to accelerations. Peters (A1.5) found that the use of acceleration compensation in transducers of type 603B led to significant improvement in sensitivity to oscillation. By employing adaptors or damping materials, such as Teflon or Delerin, the acceleration effect can be reduced still further. In some cases, a second transducer can be installed which is subject to the same installation conditions but not affected by pressure, sothat the effect of acceleration can be determined and then deducted from the signal received from the pressure transducer.

Semiconductor pressure transducers, for example, the Kulite type XQL-080 whose characteristic frequency is approximately 150 KHz, have some dimensions so small that they can be considered for installation in probes, and hence for the measurement of total pressures varying rapidly with time.

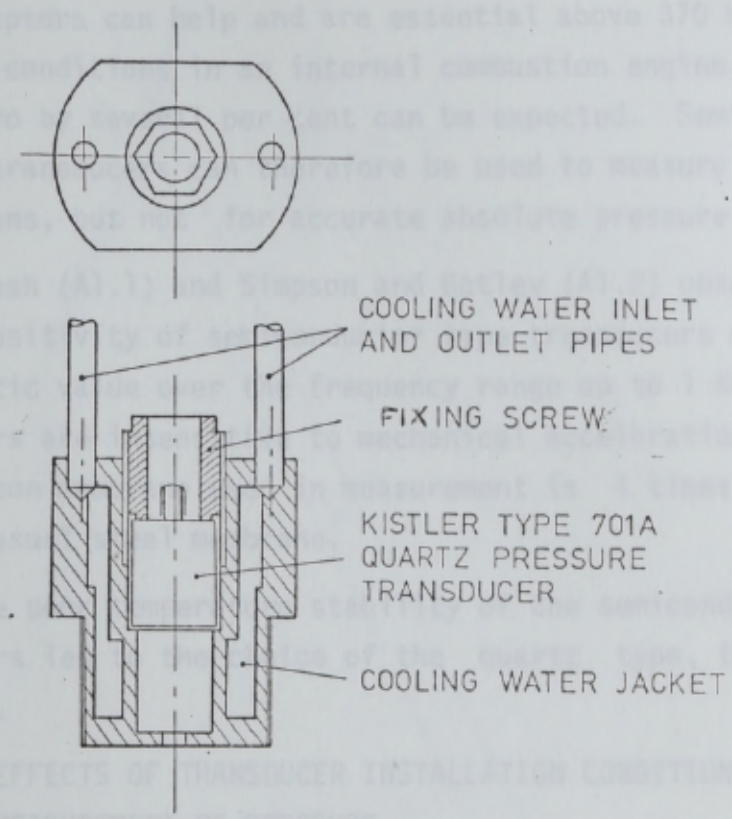

FIGURE A1.1 WATER COOLED MOUNTING ADAPTOR FOR QUARTZ PRESSURE TRANSDUCER

Pressure pickups, equipped with semiconductor strain guage bridges allow the measurement of absolute pressure fluctuations with time. Their disadvantage is their sensitivity to variations in the ambient temperature which manifests itself as a shift of the regulated transducer zero (Figure A1.2). A rise of 30 K in temperature can produce a zero drift of about 5% of the full scale range. Cooled adaptors can help and are essential above 370 K. Under the operating conditions in an internal combustion engine, a displacement of the zero by several per cent can be expected. Semiconductor pressure transducers can therefore be used to measure pressure fluctuations, but not for accurate absolute pressure measurement.

Brosh (A1.1) and Simpson and Gatley (A1.2) observed changes in the sensitivity of semiconductor type transducers of less than 1% of static value over the frequency range up to 1 KHz. The transducers are insensitive to mechanical acceleration as the very thin silicon membrane used in measurement is 4 times less dense than the usual steel membrane.

The poor temperature stability of the semiconductor type transducers led to the choice of the quartz type, the Kistler, in this work.

A1.3 EFFECTS OF TRANSDUCER INSTALLATION CONDITIONS ON THE MEASUREMENT OF PRESSURE

Only where the transducer can be installed so that the pulsating pressure operates immediately on its membrane can its dynamic properties be used as an aid in understanding the behaviour of rapid pressure fluctuations. For wall pressure measurements, this means that the transducer must be as flush as possible with the internal walls of the housing. Where the wave length of the transient pressure fluctuations normal to the transducer axis are no longer large in relation to the transducer diameter, for example, in detonation, the transducer cannot be installed directly at the measuring position, since it will only provide a summation of the pressure distribution momentarily immediately adjacent to its membrane (Figure A1.3). If the transducer is mounted away from the wall, but connected to the combustion chamber by a small diameter measuring bore, the frequency range for

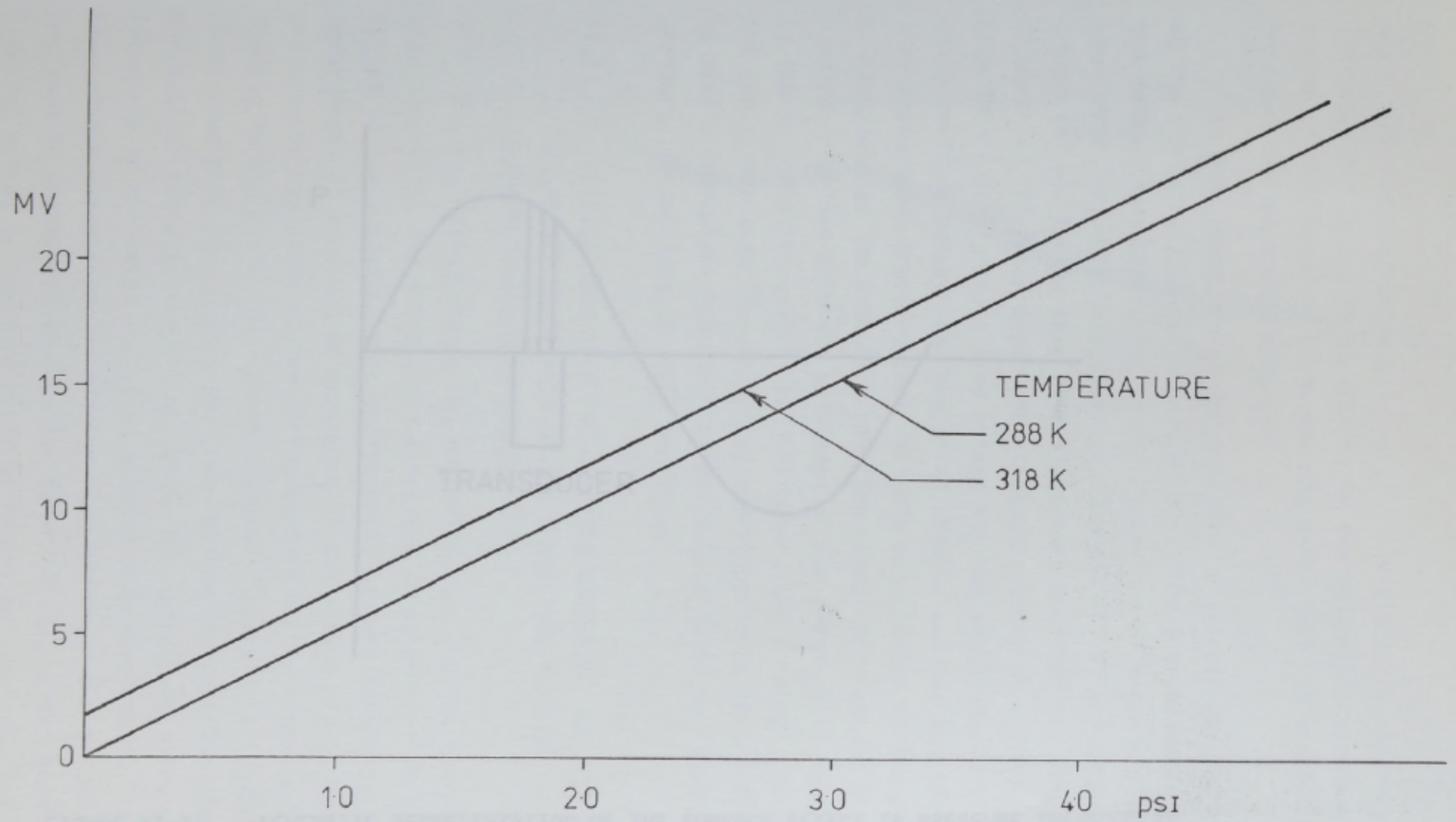

FIGURE A1.2 CALIBRATION CURVE OF A TYPE XQL-080 PRESSURE TRANSDUCER PLOTTED FOR DIFFERENT OPERATING TEMPERATURES (INPUT VOLTAGE 5V)

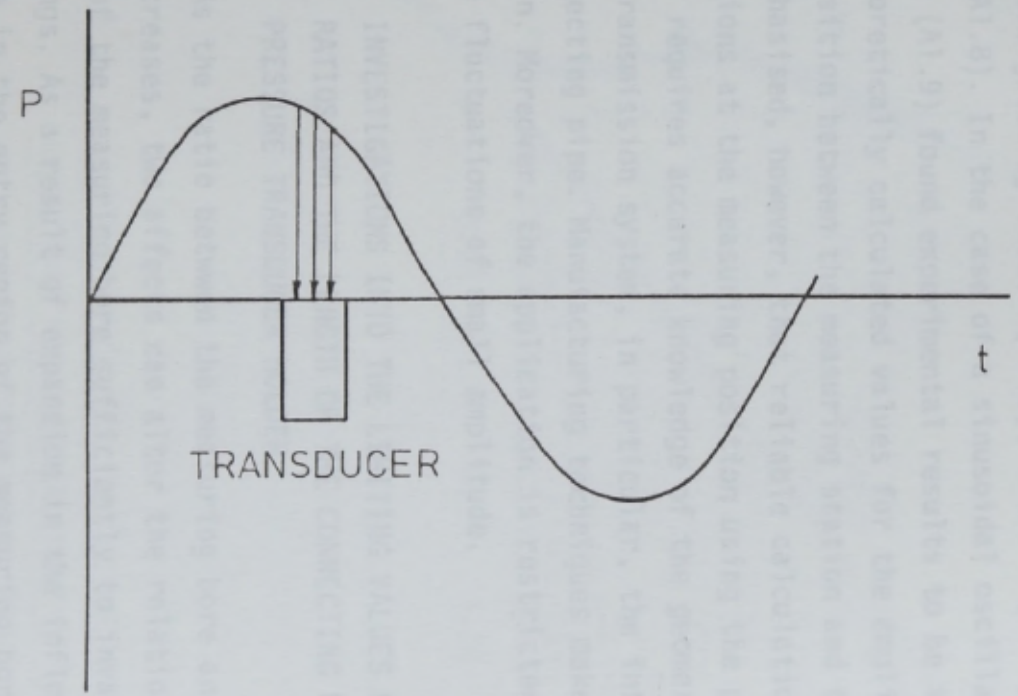

FIGURE A1.3 SCHEMATIC REPRESENTATION OF THE SURFACE EFFECT IN PRESSURE TRANSDUCERS (ON THE BASIS OF AN ARBITRARY LOCAL PRESSURE DISTRIBUTION)

which accurate pressure measurement is possible, is severely limited. This is due to throttling in the pneumatic transmission system of the measuring bore, and the unavoidable volume between the bore and the transducer membrane.

In many cases, it is not possible to install the transducer at the measuring station without a connecting tube between it and the combustion chamber. The dynamic behaviour of these systems has been investigated by Taback (A1.6), Iberall (A1.7) and Rohmann and Crogan (A1.8). In the case of a sinusoidal oscillation, Bergh and Tijdeman (A1.9) found experimental results to be in close agreement with theoretically calculated values for the amplitude ratio and phase position between the measuring station and the transducer. They emphasised, however, that reliable calculation of the pressure fluctuations at the measuring position using the pressure transducer readings requires accurate knowledge of the geometrical relationship in the transmission system, in particular, the internal radius of the connecting pipe. Manufacturing techniques make this difficult to obtain. Moreover, the application is restricted to sinusoidal pressure fluctuations of small amplitude.

A1.4 INVESTIGATIONS INTO THE LIMITING VALUES OF THE APERTURE RATIOS AND THE LENGTH OF THE CONNECTING PIPE OF THE PRESSURE TRANSDUCER HOLDER

As the ratio betwwen the measuring bore and the connecting pipe increases, two affects can alter the relationships in the region of the measuring bore sufficiently to invalidate pressure recordings. As a result of expansion in the inflow phase, the pressure in the entry region of the measuring bore rises and gas flowing in and out of the system produces fluctuations in the connecting pipe. The gas carries compression or expansion waves as a result of its displacement effect in the connecting pipe, and the intensity of the waves increases with the aperture ratio. Figure A1.4 shows these effects for an average Mach number of 0.5 assuming a rectangular pressure distribution. Werer (A1.10) investigated the limiting values of aperture ratio by measuring the relative deviation amounts for various fluctuation frequencies. From his

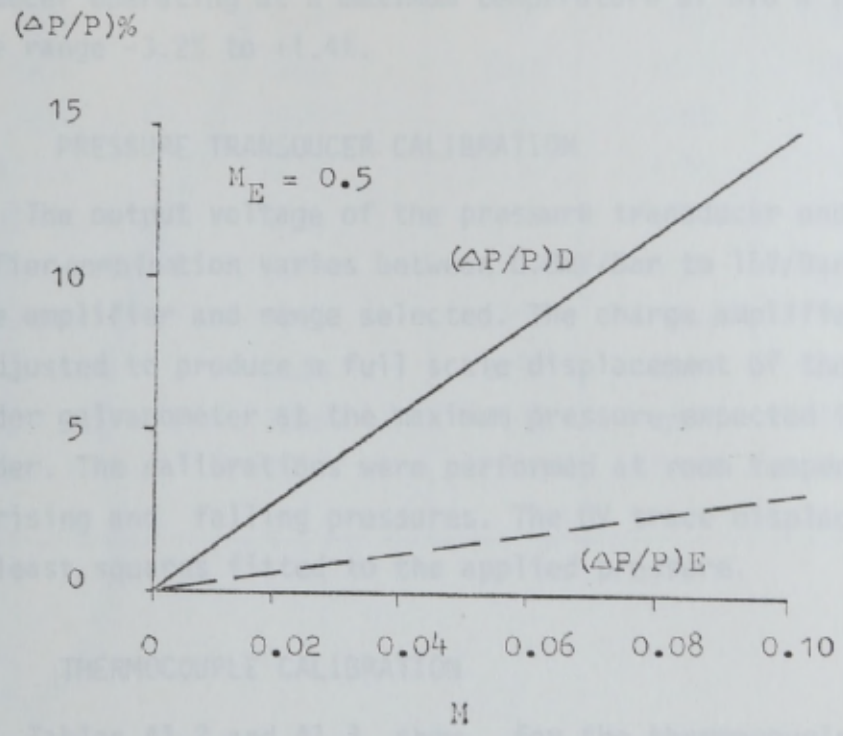

FIGURE A1.4 ORDER OF MAGNITUDE OF THE PRESSURE FLUCTUATION RESULTING FROM DISPLACEMENT EFFECT (ΔP/P)D AND OF THE CHANGE IN PRESSURE RESULTING FROM JET EXPANSION (ΔP/P)E, AS FUNCTIONS OF THE APERTURE RATIO M (SYMMETRICAL RECTANGULAR DISTRIBUTION)

observations, an upper limit for the sperture ratio of 0.020-0.025 was established. Below this ratio, the pressure indicated by the probe can be assumed to be within its normal accuracy.

On this basis, the diameter of the connecting passage of the mounting adaptor was 0.25mm. The error in the voltage output of the transducer operating at a maximum temperature of 510 K is therefore in the range -3.2% to +1.4%.

A1.5 PRESSURE TRANSDUCER CALIBRATION

The output voltage of the pressure transducer and charge amplifier combination varies between 0.8mV/Bar to 15V/Bar depending on the amplifier and range selected. The charge amplifier range was adjusted to produce a full scale displacement of the UV recorder galvanometer at the maximum pressure expected in the cylinder. The calibrations were performed at room temperature for both rising and falling pressures. The UV trace displacement was then least squares fitted to the applied pressure.

A1.6 THERMOCOUPLE CALIBRATION

Tables A1.2 and A1.3 show, for the thermocouples in the cylinder head and piston of the test engine, the temperature, the corresponding measured thermocouple output and the true output according to BS 4937 part 4, March 1973 reference tables. Figures A1.5 - A1.12 show the measured thermocouple output on the x axis, and on the y axis, the correction needed to align the thermocouples to the reference values.

The thermocouples were calibrated in a fluidised bed heat source against an NPL reference thermometer in 25°C steps to 250°C. The tail ends were connected to type K compensation leads immersed in oil and contained in along test tube immersed 10 in into correctly prepared melting ice, the zero centigrade reference. The type K thermocouple was expected to give a short term stability of $\pm$0.2°C over the temperature range considered.

TEMPERATURE °C	TRUE T/C O/P μV	ACTUAL T/C O/P μV			
		P_1	P_2	P_3	P_4
14.9	594	587	587	585	586
48.5	1960	1963	1962	1959	1960
75.4	3075	3086	3085	3075	3080
101.0	4135	4156	4156	4147	4147
124.9	5121	5152	5151	5138	5140
151.5	6196	6233	6233	6213	6214
173.5	7081	7107	7108	7084	7086
197.6	8039	8057	8057	8031	8033
222.4	9035	9048	9051	9022	9022
248.7	10097	10104	10106	10076	10077

TABLE A1.2 TEMPERATURE, MEASURED OUTPUT AND TRUE OUTPUT FOR PISTON THERMOCOUPLES

TEMPERATURE °C	TRUE T/C O/P μV	ACTUAL T/C O/P μV			
		W_1	W_2	W_3	W_4
16.2	645	641	642	640	641
48.4	1958	1956	1956	1955	1954
75.4	3074	3076	3075	3073	3071
101.1	4140	4147	4142	4140	4139
125.2	5130	5142	5144	5134	5131
151.5	6194	6207	6209	6194	6190
173.8	7089	7091	7093	7077	7074
197.6	8046	8038	8041	8025	8002
222.4	9040	9025	9027	9012	9009
248.7	10100	10076	10080	10066	10067

TABLE A1.3 TEMPERATURE, MEASURED OUTPUT AND TRUE OUTPUT FOR CYLINDER HEAD THERMOCOUPLES

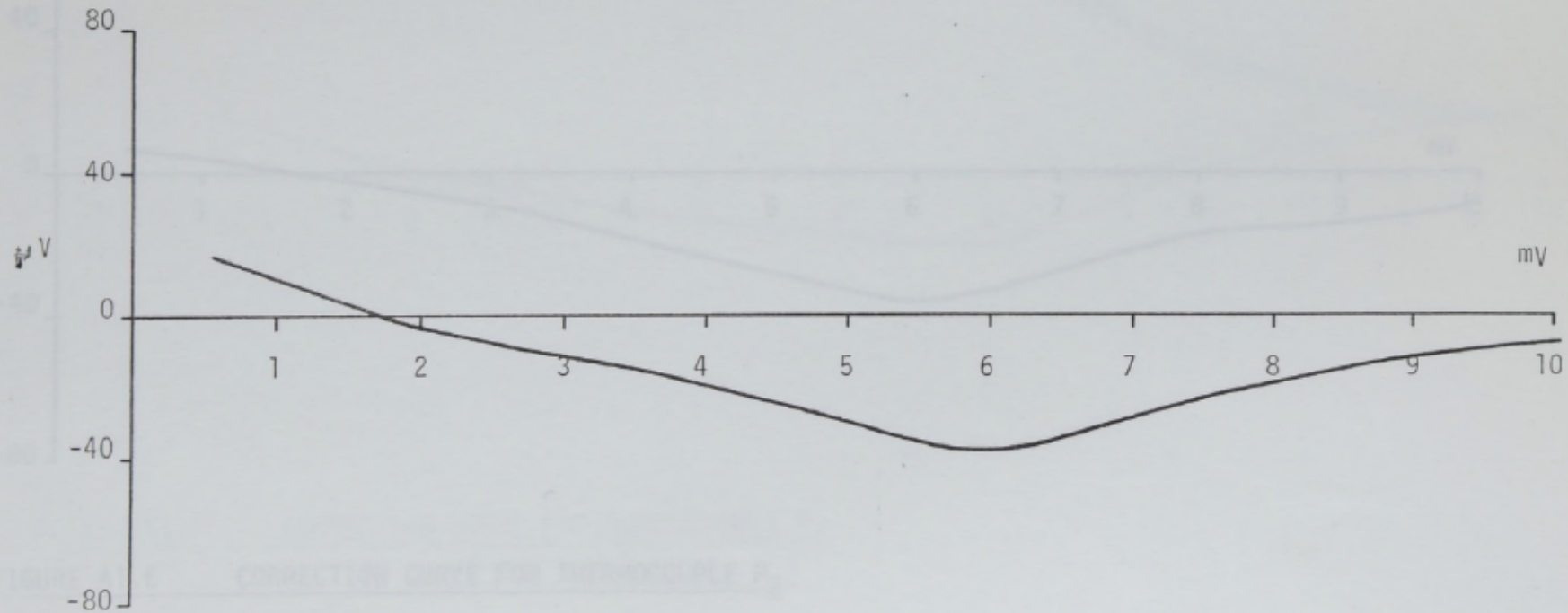

FIGURE A1.5 CORRECTION CURVE FOR THERMOCOUPLE P_1

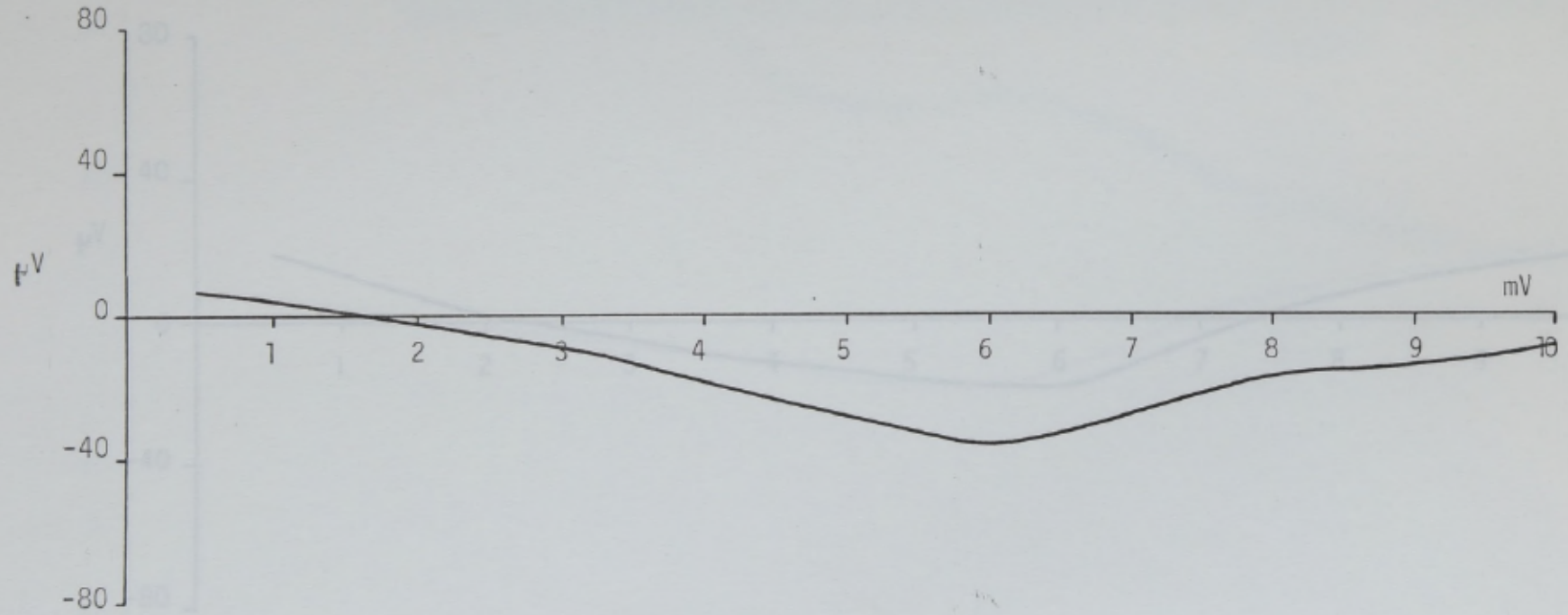

FIGURE A1.6 CORRECTION CURVE FOR THERMOCOUPLE P_2

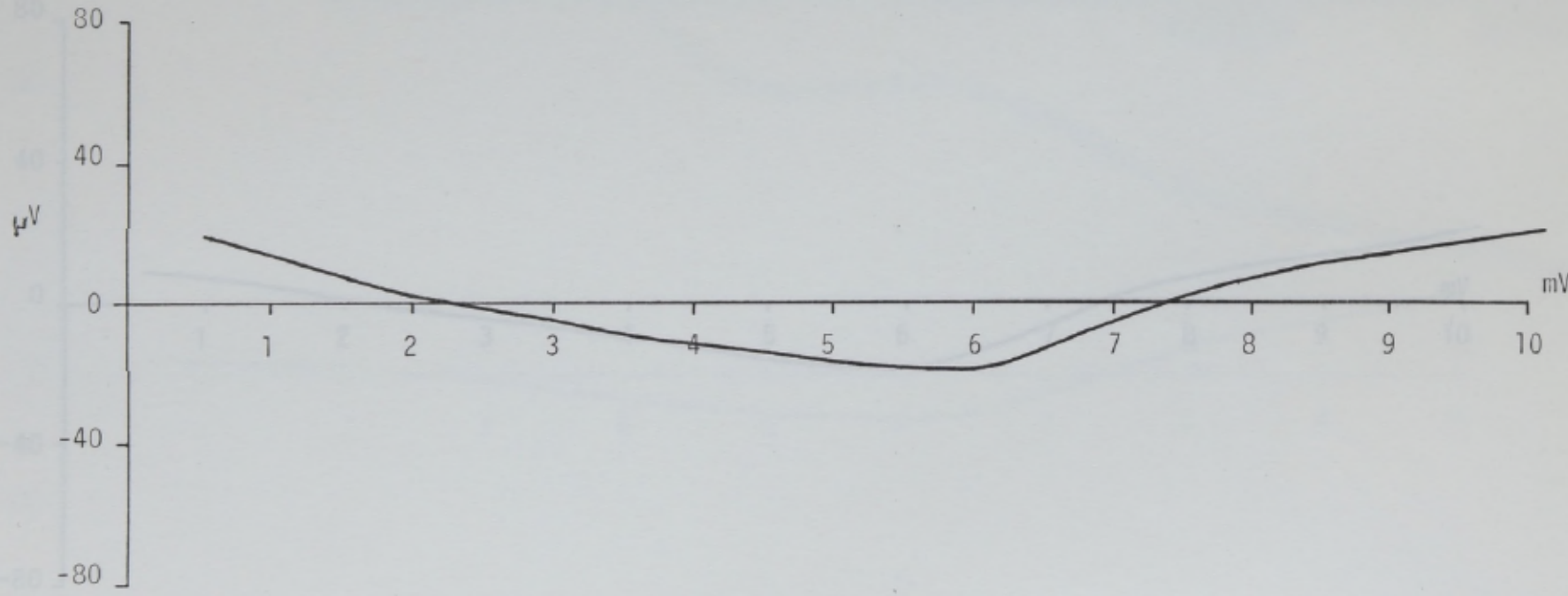

FIGURE A1.7 CORRECTION CURVE FOR THERMOCOUPLE P_3

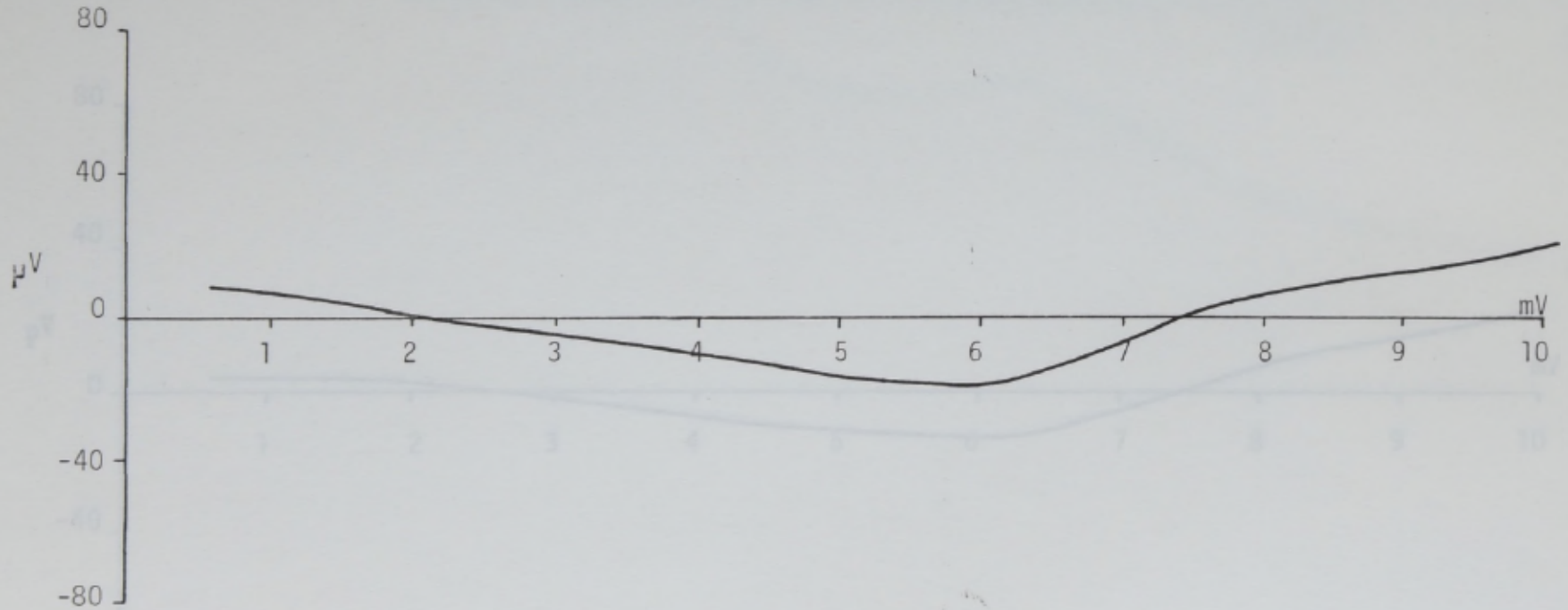

FIGURE A1.8 CORRECTION CURVE FOR THERMOCOUPLE P_4

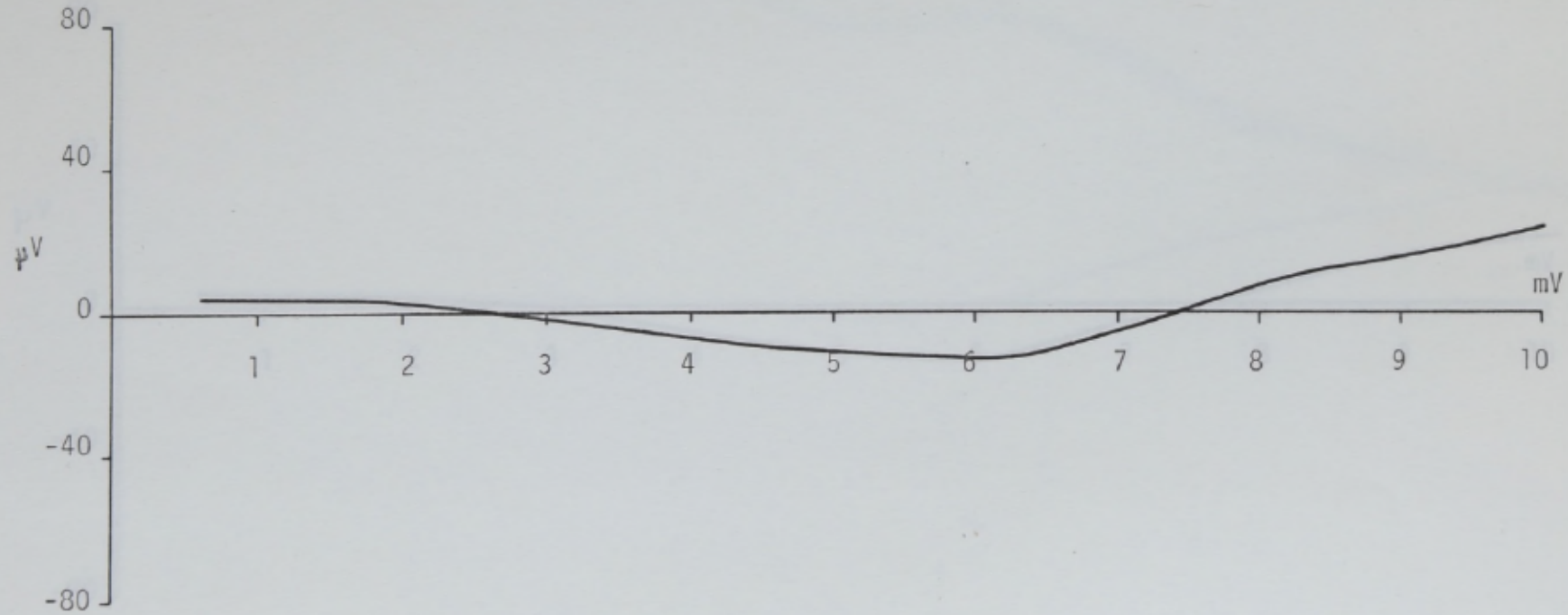

FIGURE A1.9 CORRECTION CURVE FOR THERMOCOUPLE W_7

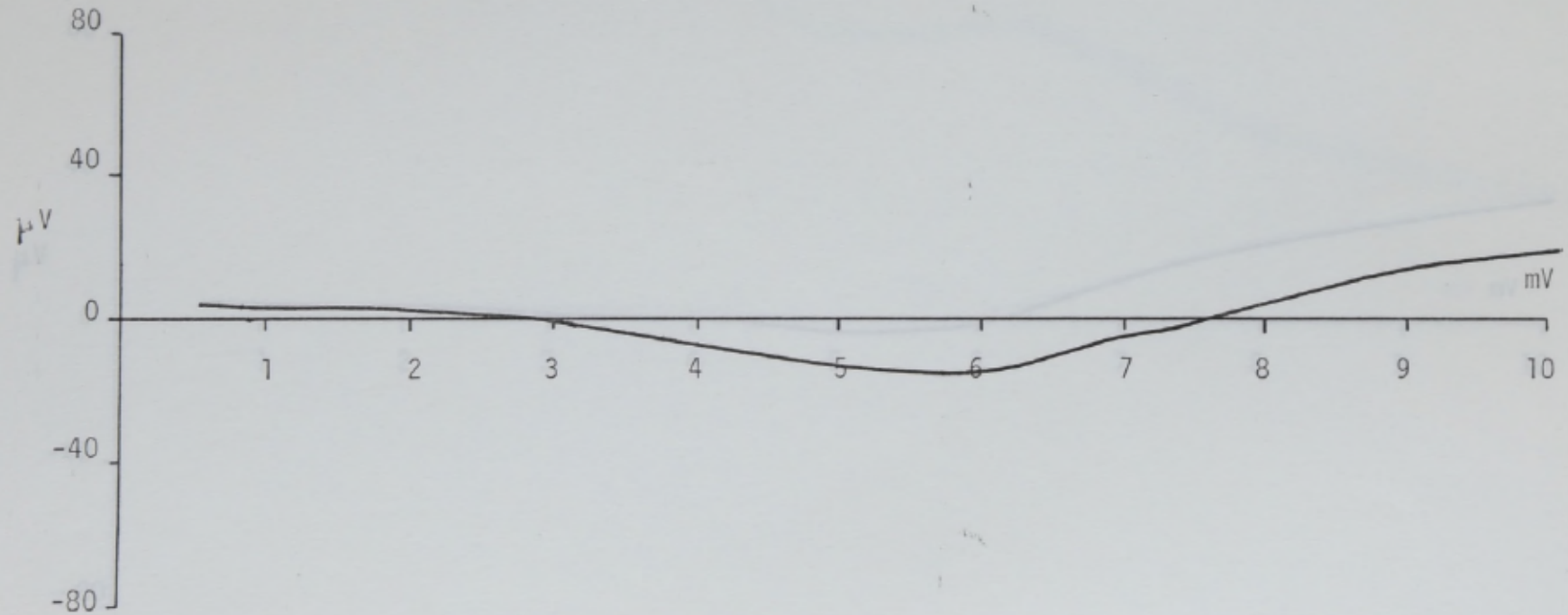

FIGURE A1.10 CORRECTION CURVE FOR THERMOCOUPLE W_2

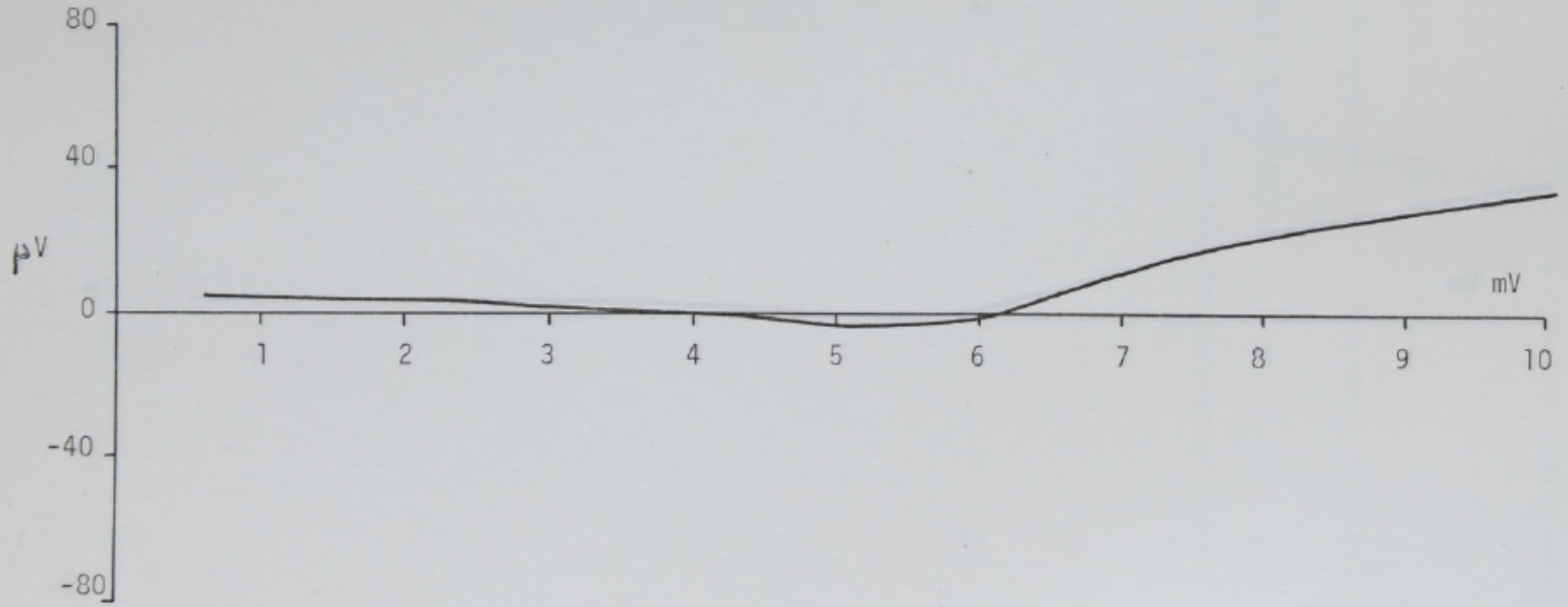

FIGURE A1.11 CORRECTION CURVE FOR THERMOCOUPLE W_3

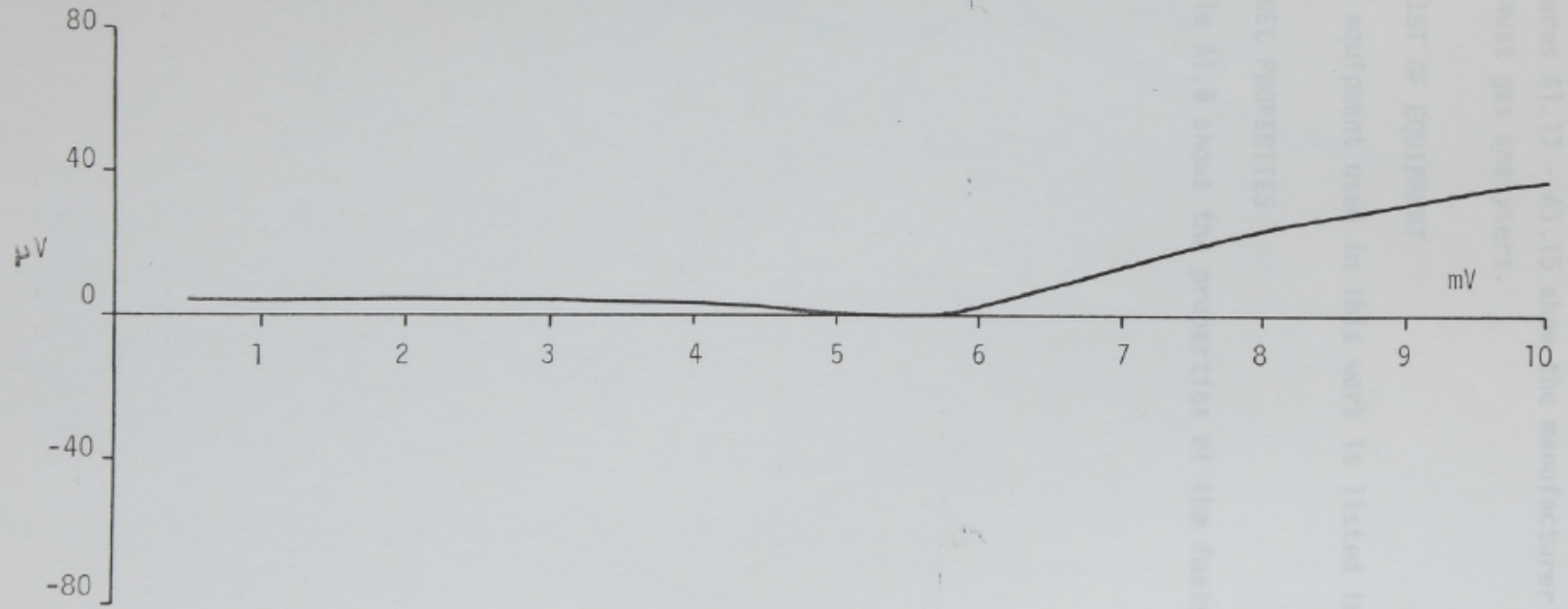

FIGURE A1.12 CORRECTION CURVE FOR THERMOCOUPLE W_4

A1.7 EXHAUST GAS ANALYSIS CALIBRATION

Figures A1.13 - A1.15 show the manufacturer's calibration of the exhaust gas analysers.

A1.8 LIST OF EQUIPMENT

The equipment used in this work is listed in Table A1.4.

A1.9 FUEL PROPERTIES

Table A1.5 shows the properties of the fuels used in this work.

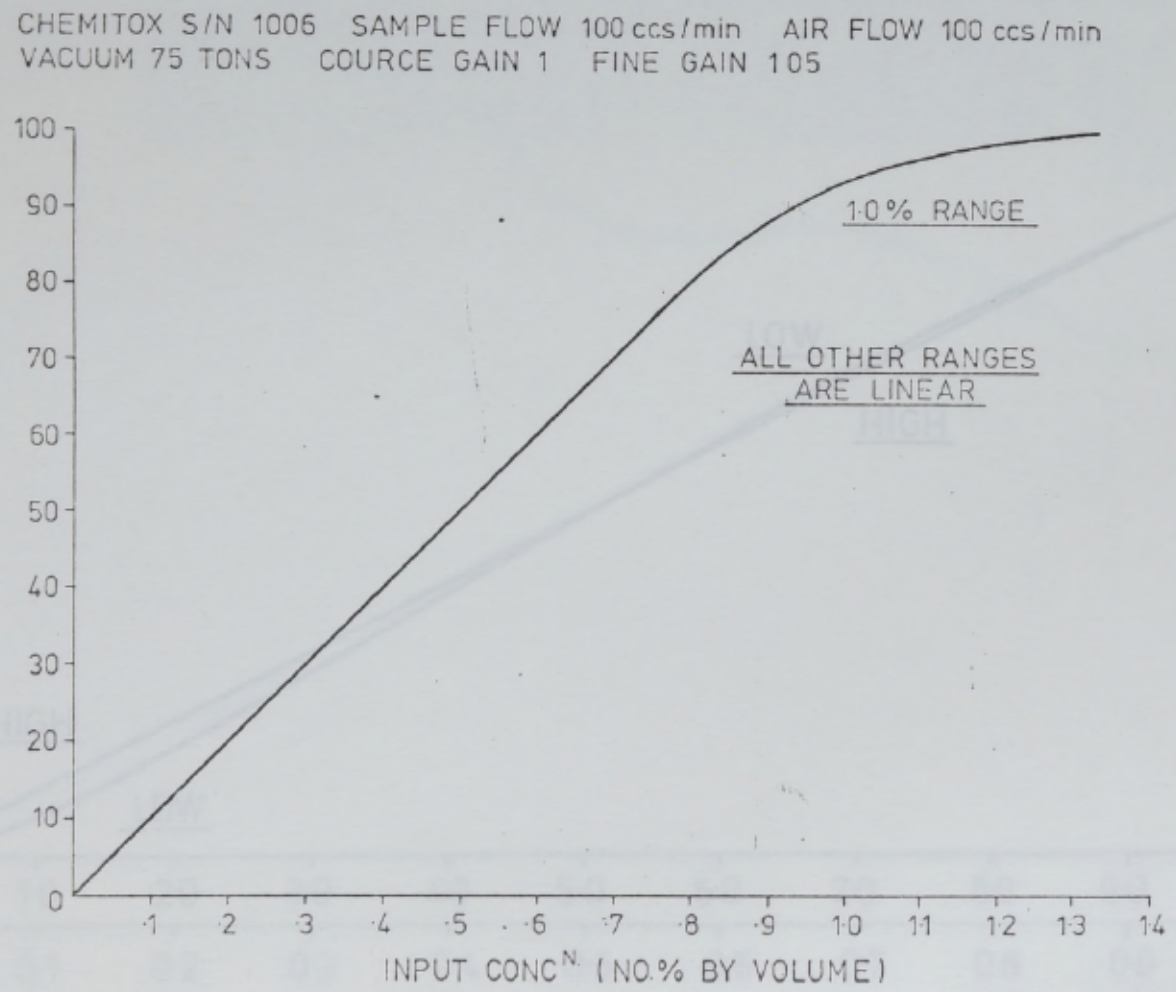

FIGURE A1.13 CALIBRATION CURVE FOR THE CHEMITOX GAS ANALYSER

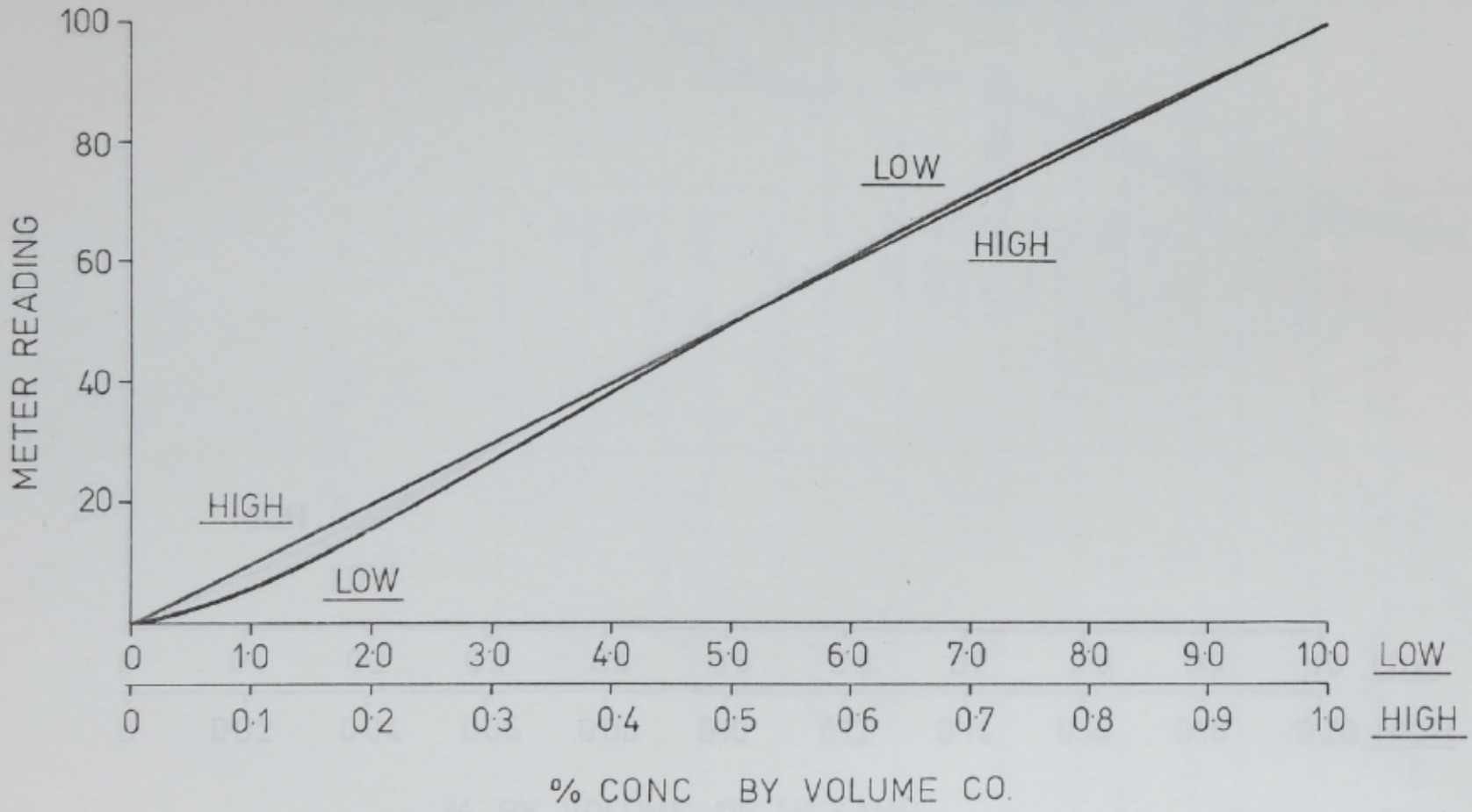

FIGURE A1.14 CALIBRATION CURVE FOR THE CO GAS ANALYSER

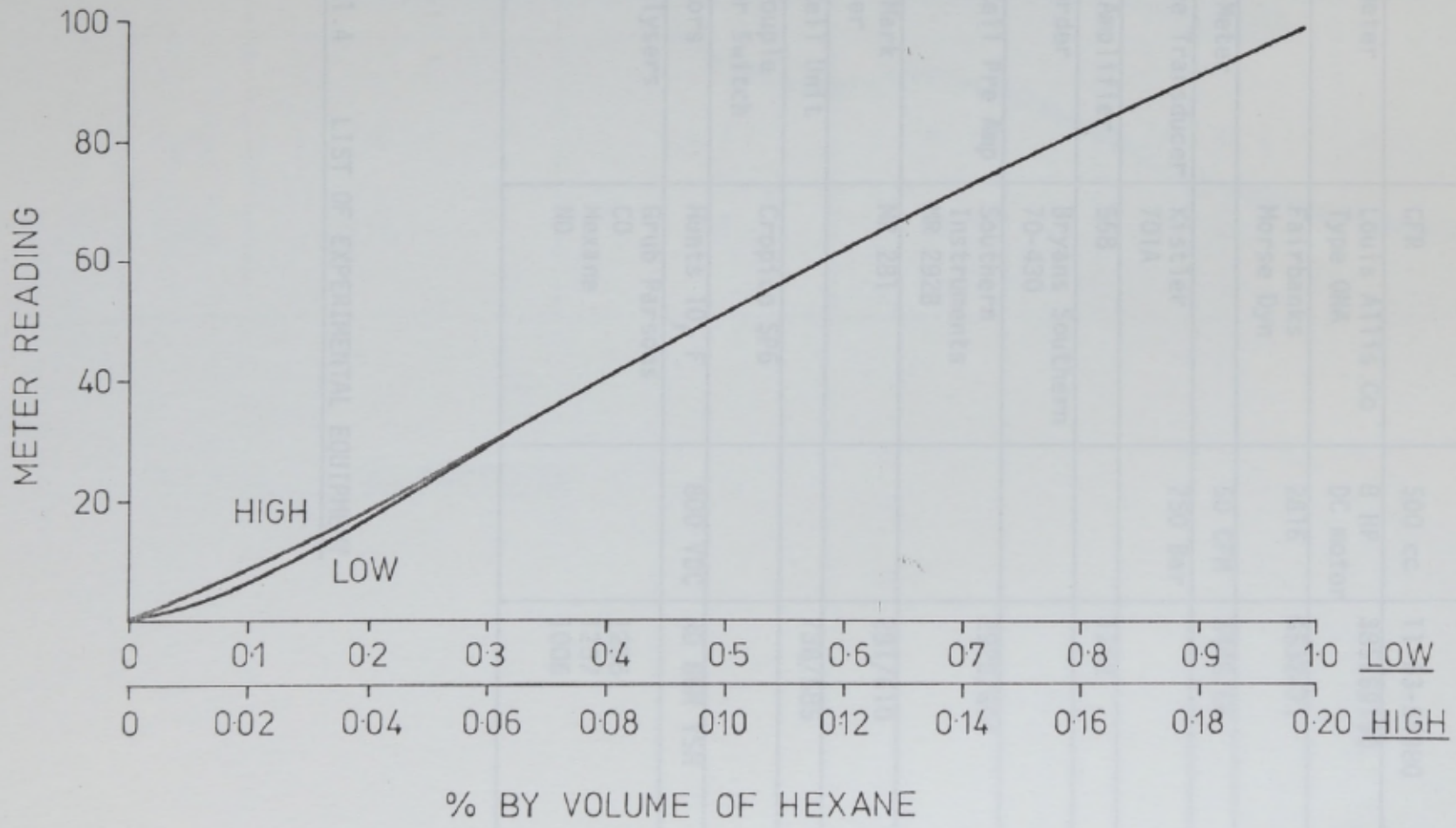

FIGURE A1.15 CALIBRATION CURVE FOR THE HEXANE GAS ANALYSER

EQUIPMENT	TYPE	RATING	SERIAL NUMBER
Engine	CFR	500 cc	11-63-54380
Dynamometer	Louis Allis Co Type ONA	8 HP DC motor	385769100
Scale	Fairbanks Morse Dyn	2816	G532471
Alcock Meter		50 CFM	3448/66
Pressure Transducer	Kistler 701A	250 Bar	
Charge Amplifier	568		1762
UV Recorder	Bryans Southern 70-430		
Photo Cell Pre Amp	Southern Instruments MR 292B		292B/604
Degree Mark Amplifier	MR 281		281/610
Photo Cell Unit			738/585
Thermocouple Selector Switch	Cropico SP6		
Capacitors	Hunts 10$_{\mu}$ F	800 VDC	RD 86M YSH
Gas Analysers	Grub Parsons CO Hexane NO		 1256 1257 1006

TABLE A1.4 LIST OF EXPERIMENTAL EQUIPMENT

FUEL	MOLECULAR WEIGHT	DENSITY g/cm^3 at 20 C	BOILING POINT °c	F/A Ø=1 %Vol	MINIMUM PURITY	SOURCE
C_6H_6	78.1	0.879	80-111	2.791	98.9	BDH
C_8H_{18}	114.2	0.692	99-222	1.674	99.6	BDH

TABLE A1.5 FUEL PROPERTIES

REFERENCES

A1.1 BROSH, A
Miniature Pressure Transducers for Wind Tunnel Models
Proc Instrument Society of America's International Aerospace Instrumentation Symp (17th), Las Vegas, 1971

A1.2 BYNUM, D, LEDFORD, R and SMOTHERMAN, W
Wind Tunnel Pressure Measuring Techniques
Agardograph No 145, 1970

A1.3 SIMPSON, J and GATLEY, W
Dynamic Calibration of Pressure Measuring Systems
Proc Instrument Society of America's International Aerospace Instrumentation Symp (16th), 1970

A1.4 TERADA, K and KRUGGEL, O
The Measurement of Rapidly Varying Pressures in Internal Combustion Engines Part II: Investigation into the Properties of Electrical Pressure Pickups under Static Loading (in German)
DFL Report No 194, 1963

A1.5 PETER, A
Measurement of Dynamic Pressures: Comparative Study of Standard Transducers. Practical Notes on the Technique of Measurement and Calibration (in French)
I SL Tech Note T 10/68, 1968

A1.6 TABACK, J
The Response of Pressure Measuring Systems to Oscillating Pressures
NACA TN 1819, 1949

A1.7 IBERALL, A
Attenuation of Oscillatory Pressures in Instrument Lines
NBS J Research RP2115, 1950 vol 45

A1.8 ROHMANN, C and CROGAN, E
On the Dynamics of Pneumatic Transmission Lines
ASME Paper 56-SA-1, 1956

A1.9 BERGH, H and TIJDEMAN, H
Theoretical and Experimental Results of the Dynamic Response of Pressure Measuring Systems
NLR TR, 1965

A1.10 WERER, H
Determination of the Time Averaged Pressure Fluctuating Flows, Especially in Turbomachines
RAE Library Translation No 1850, 1976

APPENDIX 2 COMPUTER PROGRAMS

INTRODUCTION

This Appendix contains listings of the programs developed as part of this research project. The SPSS package and the programs from the NAG library which were used in the mathematical analysis and the cycle synthesis work are not included. Listed are the combustion program, which was used to determine the equilibrium concentrations of the combustion products, the adiabatic flame temperature program and the program used to determine the geometric properties of the combustion chamber and the burnt charge.

The programs are listed separately but they can be used as subroutines in a larger program provided that they are supplied with the appropriate common block and data cards.

A2.1 THE COMBUSTION PROGRAM

The program is described briefly in this section and listed at the end of the Appendix. Exhaust species concentrations for the combustion of Isooctane and air mixtures are shown, together with the thermodynamic functions used in the cycle synthesis work.

The input data are supplied at section 1. The program can deal with any C, H, O, N fuel and air mixture within certain limits. The input requirements are:

C number of Carbon atoms in the fuel
H number of Hydrogen atoms in the fuel
O number of Oxygen atoms in the fuel
N number of Nitrogen atoms in the fuel
T_R reaction temperature °K
P reaction pressure lbf/in^2
PHI Equivalence Ratio.

The constants used in the routine are calculated in section 2 and section 3 includes the calculation of the Equilibrium constants. In section 4, the decision is made whether to make a new estimate of the concentration and go to section 5, or

to use the results of a previous computation as initial values. In section 6, the elements of the matrix of linearised equations are determined. The equations are solved by Gaussian Elimination in section 7. The estimate of the variables and the degree of convergence are checked in section 8, and the remaining mole fractions of the products are calculated in section 9.

The average molecular weight of the product species, the specific gas constant of the mixture, the specific enthalpy and the internal energy are calculated in section 10 from the relationships:

$$M = \sum_{i=1}^{11} x_i M_i$$

$$R = R_o/M$$

$$h = \sum_{i=1}^{11} x_i h_i/M$$

$$u = h-RT$$

The absolute enthalpy was defined as:

$$\text{absolute enthalpy} = \text{sensible heat at T above that at } T=0^oK = \text{heat of formation at } T=0^oK \text{ from the elements in the Standard Reference States at } T=0^oK$$

The values of the Specific Heats and the heats of formation were obtained from the Janaf Thermochemical Tables and were used in a matrix load up and linear interpolation routine. The results of the program are shown in Figures A2.1 - A2.14.

A2.2 ADIABATIC FLAME TEMPERATURE

This program requires as input, the reaction pressure P_R, an estimate of the reaction temperature T_r, the equivalence ratio PHI and the reactant enthalpy Ho. The program calls the combustion program to calculate the mole fractions of the exhaust constituents

and compares the reactant enthalpy with the enthalpy of the products in a convergence routine until convergence.

In section 1 the combustion program is called and R, H and U are calculated. The element of the matrix of partial differential equations are calculated. These are solved in section 2 using a Gaussian Elimination technique. The partial derivatives with respect to T of the products are calculated in section 3. Section 4 calculates the partial derivation of H for the products with T, and section 5 compares the enthalpy of the products and the reactants.

A2.3 CYLINDER AND FLAME GEOMETRY PROGRAM

This program provides the geometric properties of the burnt charge and the combustion chamber for specified flame radius and distance between the piston crown and the cylinder head for the CFR engine combustion chamber. For an input of RR, R and R_1, the program calculates SAF, SAP, SAH, SAW and V_b/V.

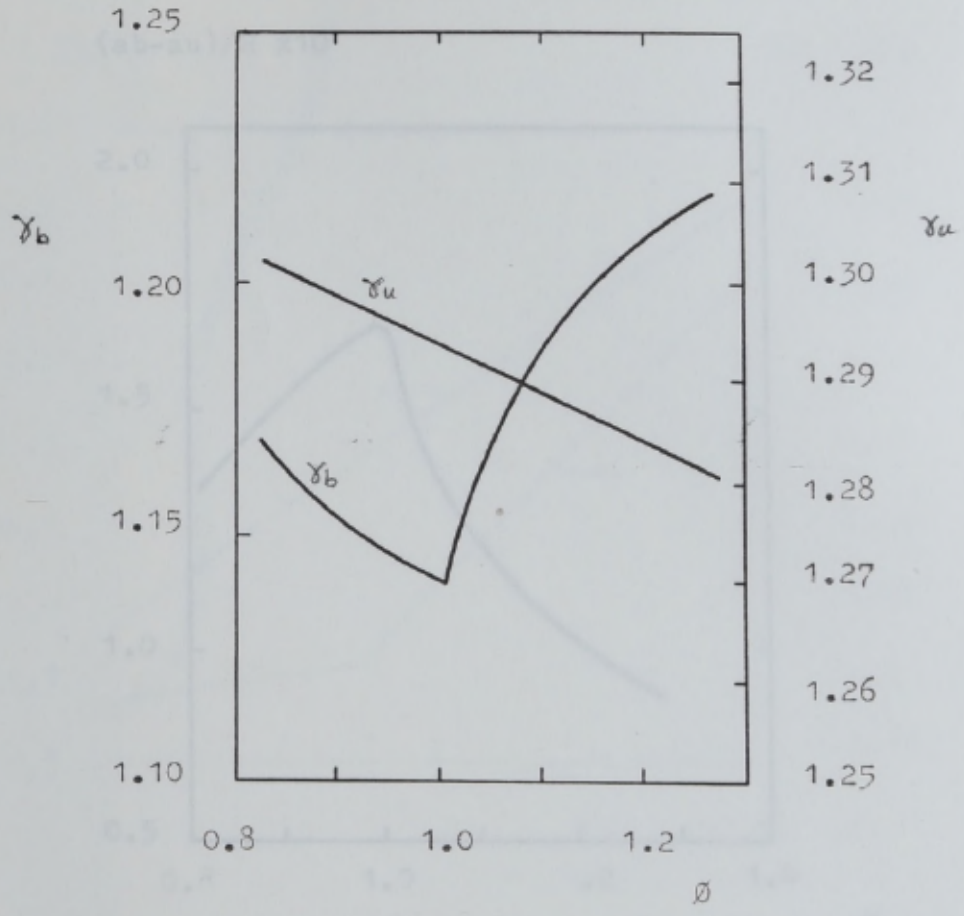

FIGURE A2.1 VALUES OF γ_b AND γ_u OBTAINED BY FITTING STRAIGHT LINES TO ENTHALPY TEMPERATURE PLOTS OF BURNT AND UNBURNT GAS MIXTURES OVER THE TEMPERATURE RANGE OF INTEREST

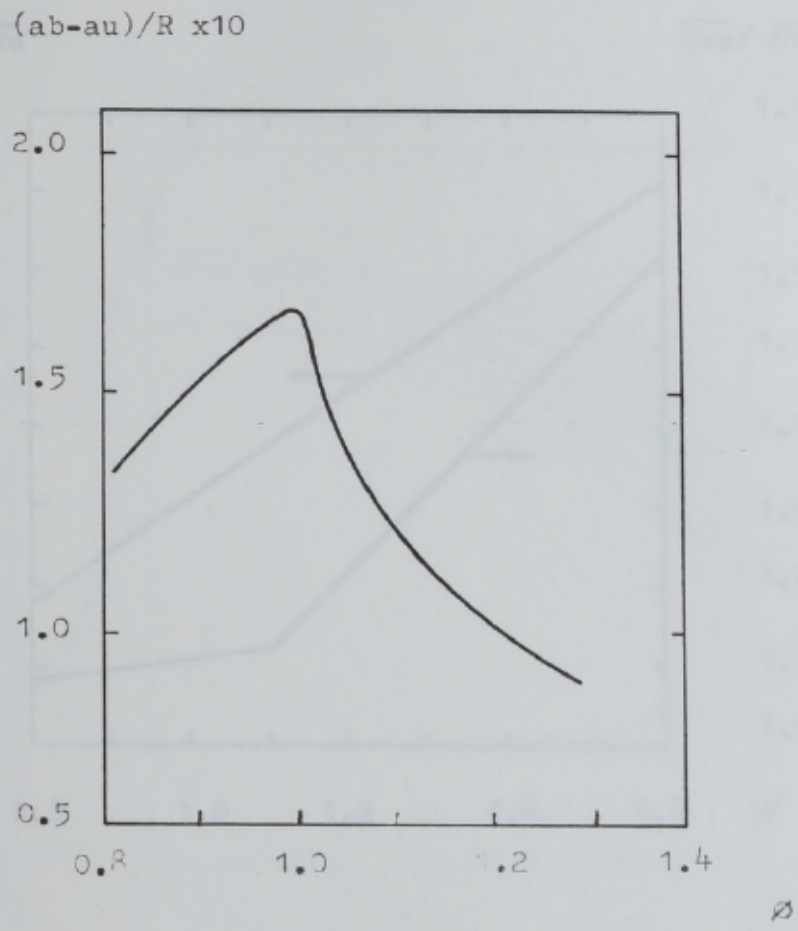

FIGURE A2.2 VALUES OF DIFFERENCE IN INTERCEPT OF STRAIGHT LINE FITS TO ENTHALPY TEMPERATURE PLOTS (ab - au) OF UNBURNT AND BURNT GAS MIXTURES AT T = 0°K

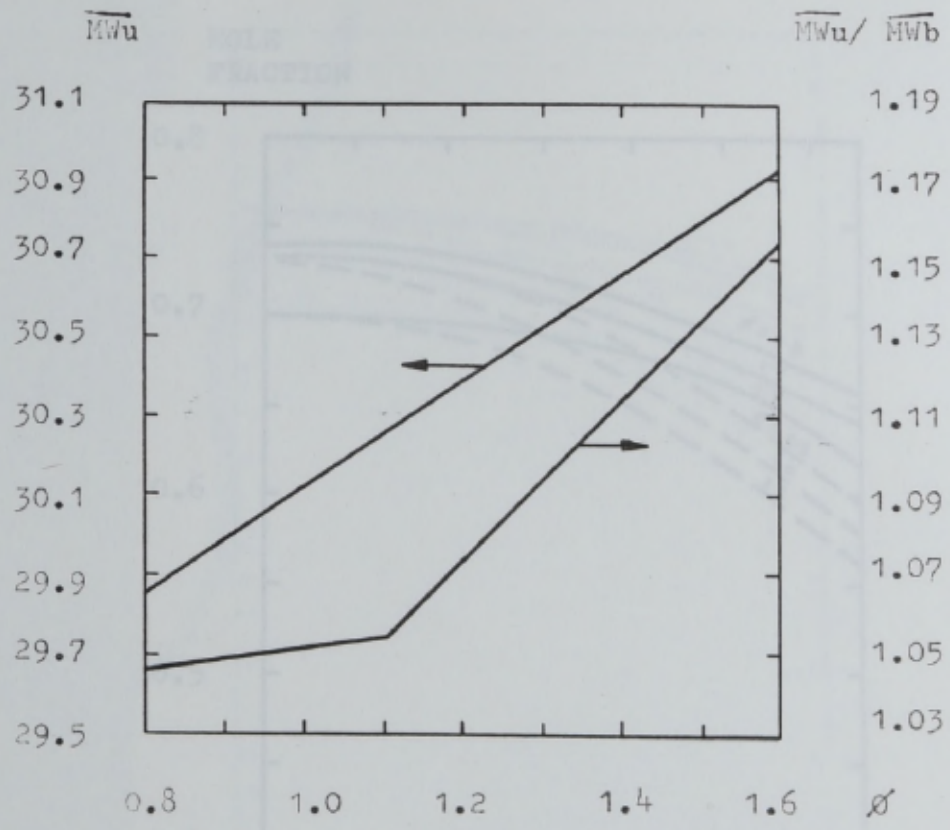

FIGURE A2.3 MOLECULAR WEIGHT OF BURNT AND UNBURNT ISOOCTANE-AIR GAS MIXTURES

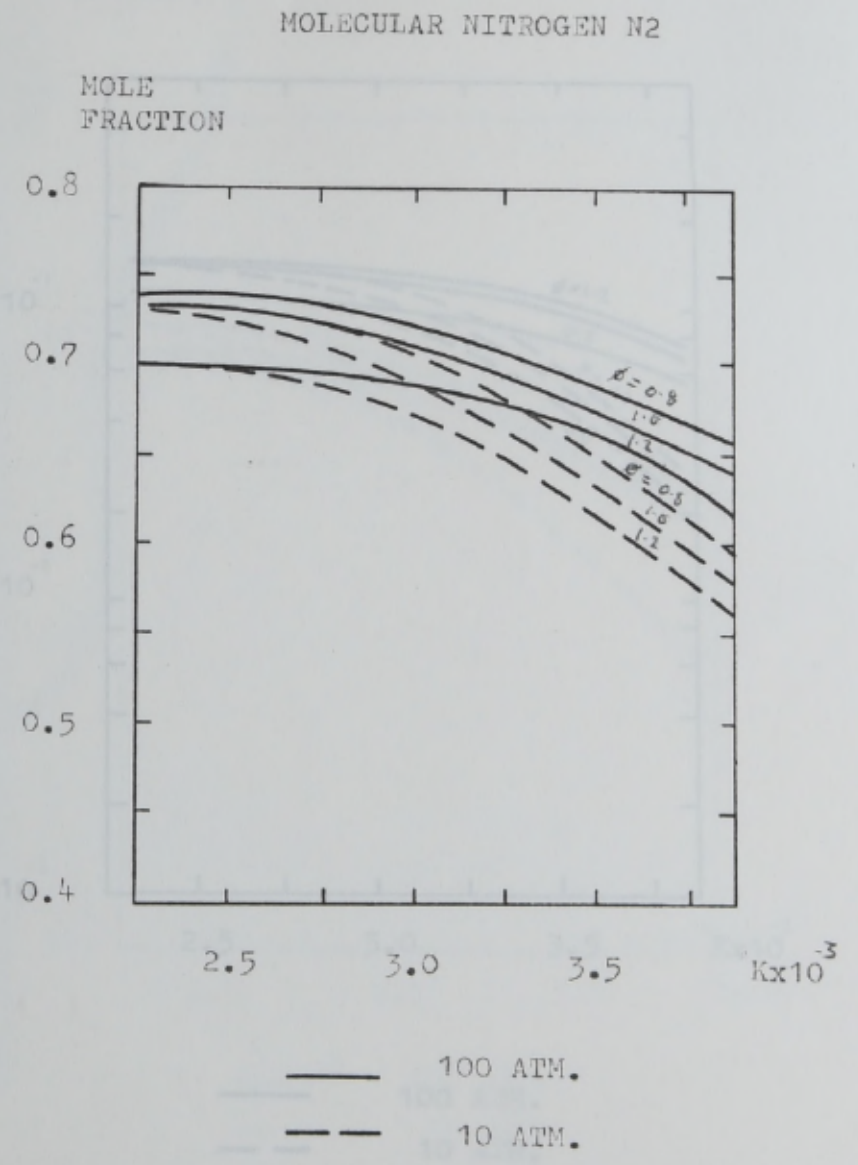

FIGURE A2.4 MOLE FRACTION AGAINST TEMPERATURE AND PRESSURE (N_2)

WATER H2O

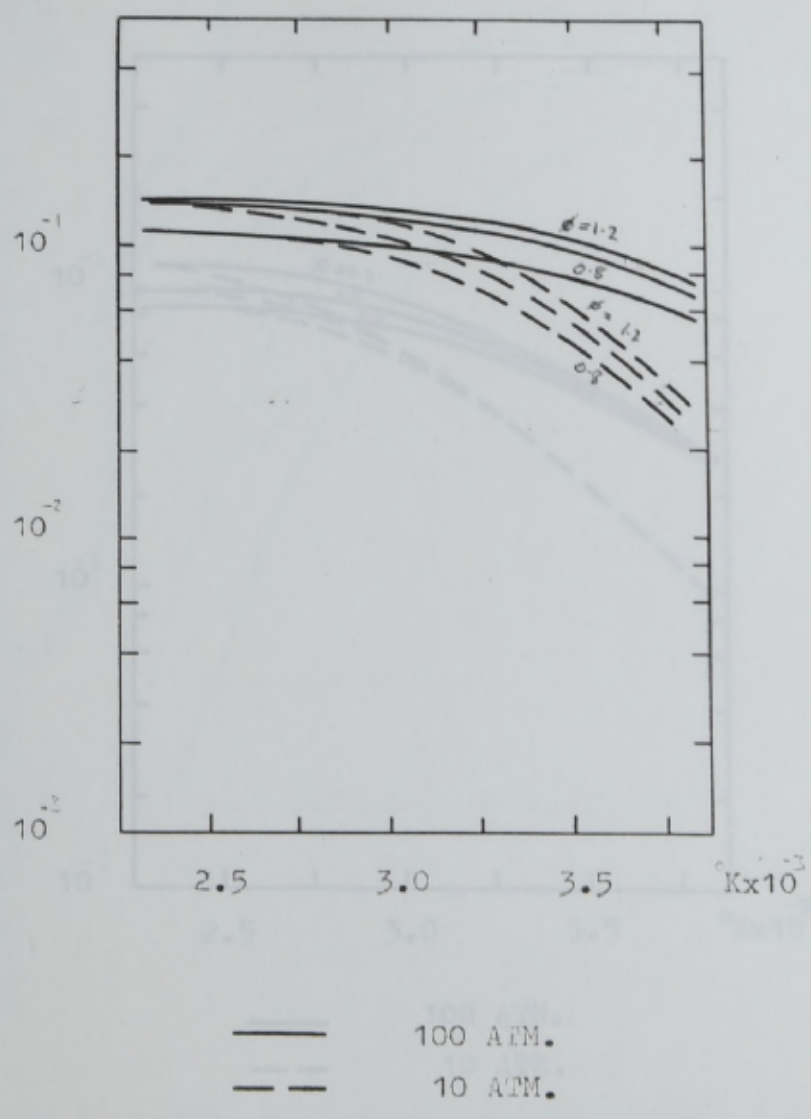

FIGURE A2.5 MOLE FRACTION AGAINST TEMPERATURE AND PRESSURE (H_2O)

CARBON DIOXIDE CO2

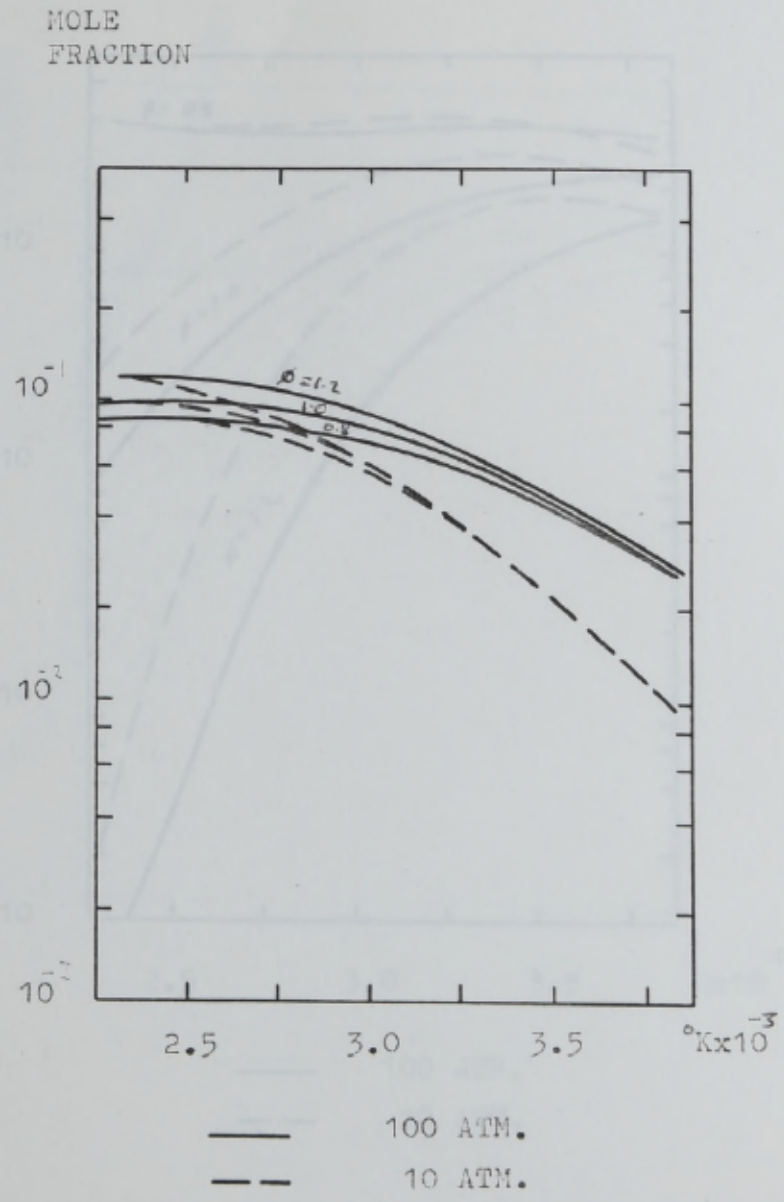

FIGURE A2.6 MOLE FRACTION AGAINST TEMPERATURE AND PRESSURE (CO_2)

MOLECULAR OXYGEN O2

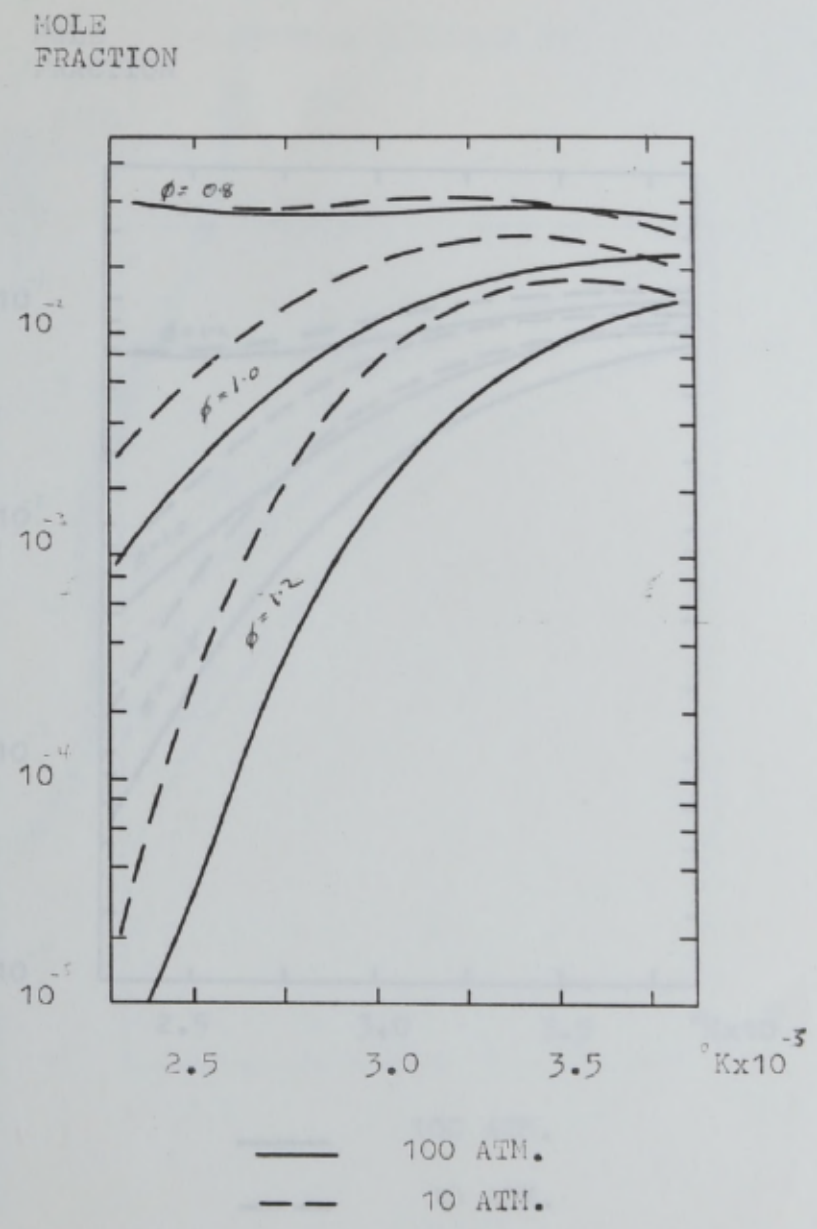

FIGURE A2.7 MOLE FRACTION AGAINST TEMPERATURE AND PRESSURE (O_2)

CARBON MONOXIDE CO

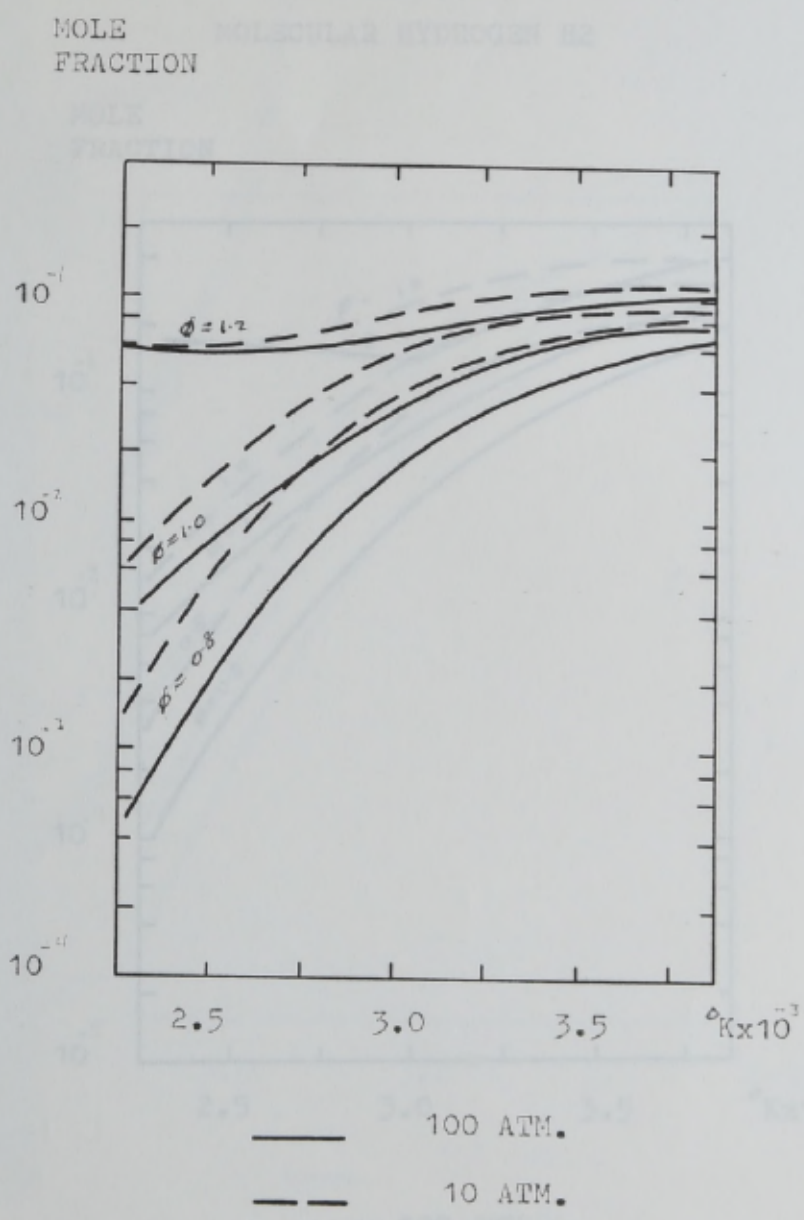

FIGURE A2.8 MOLE FRACTION AGAINST TEMPERATURE AND PRESSURE (CO)

MOLECULAR HYDROGEN H2

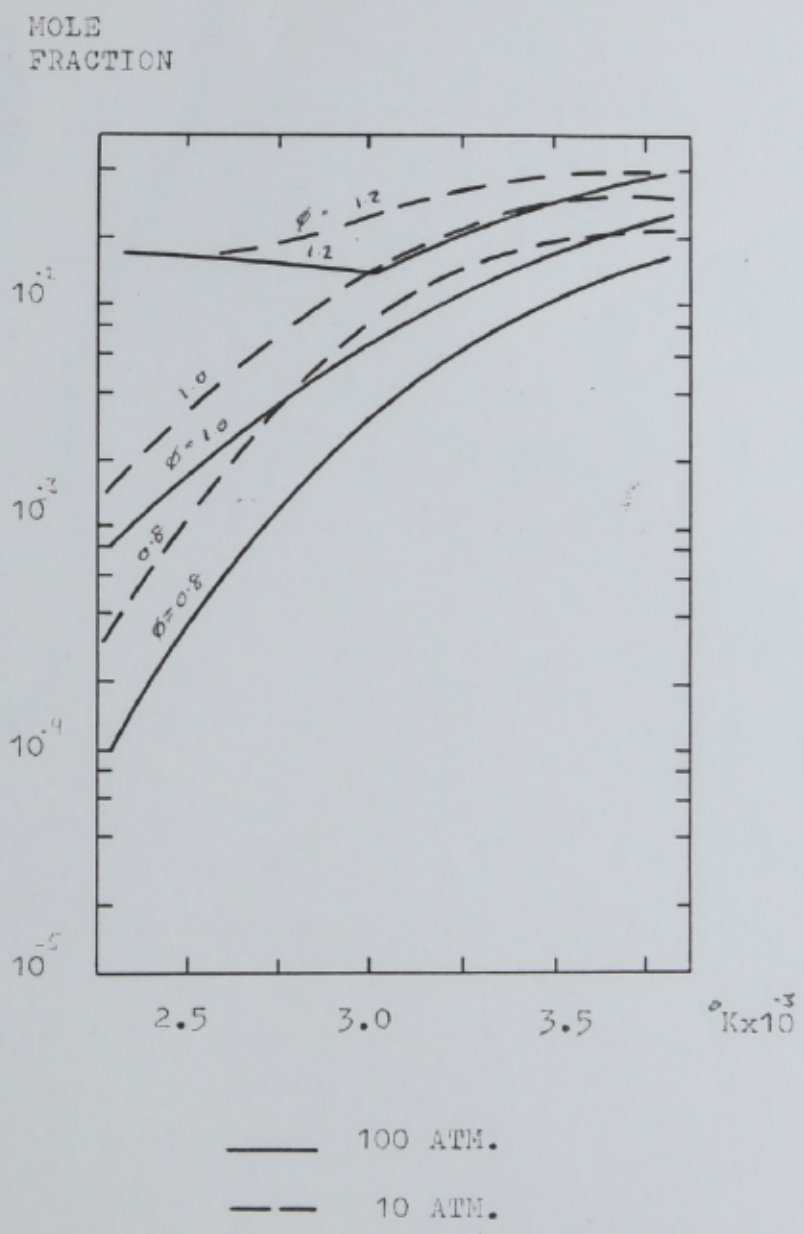

FIGURE A2.9 MOLE FRACTION AGAINST TEMPERATURE AND PRESSURE (H_2)

HYDROXYL OH

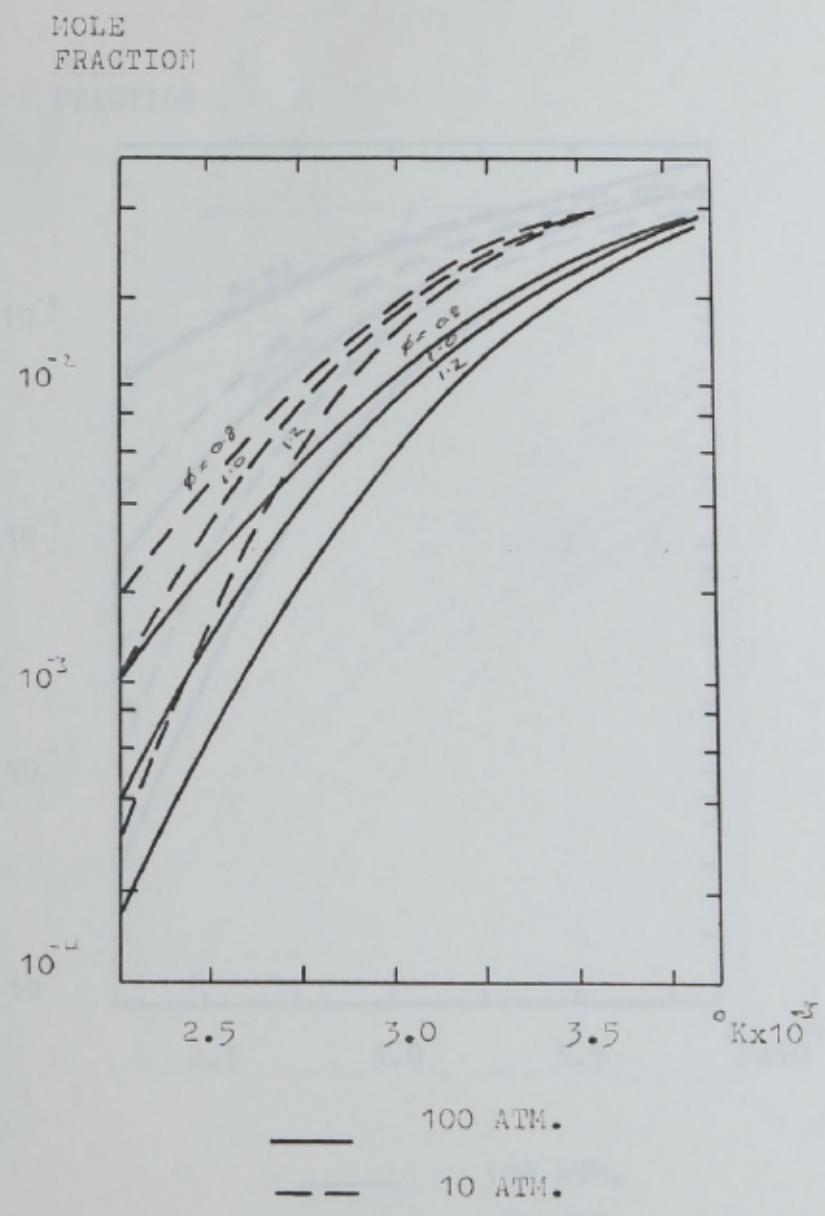

FIGURE A2.10 MOLE FRACTION AGAINST TEMPERATURE AND PRESSURE (OH)

NITRIC OXIDE NO

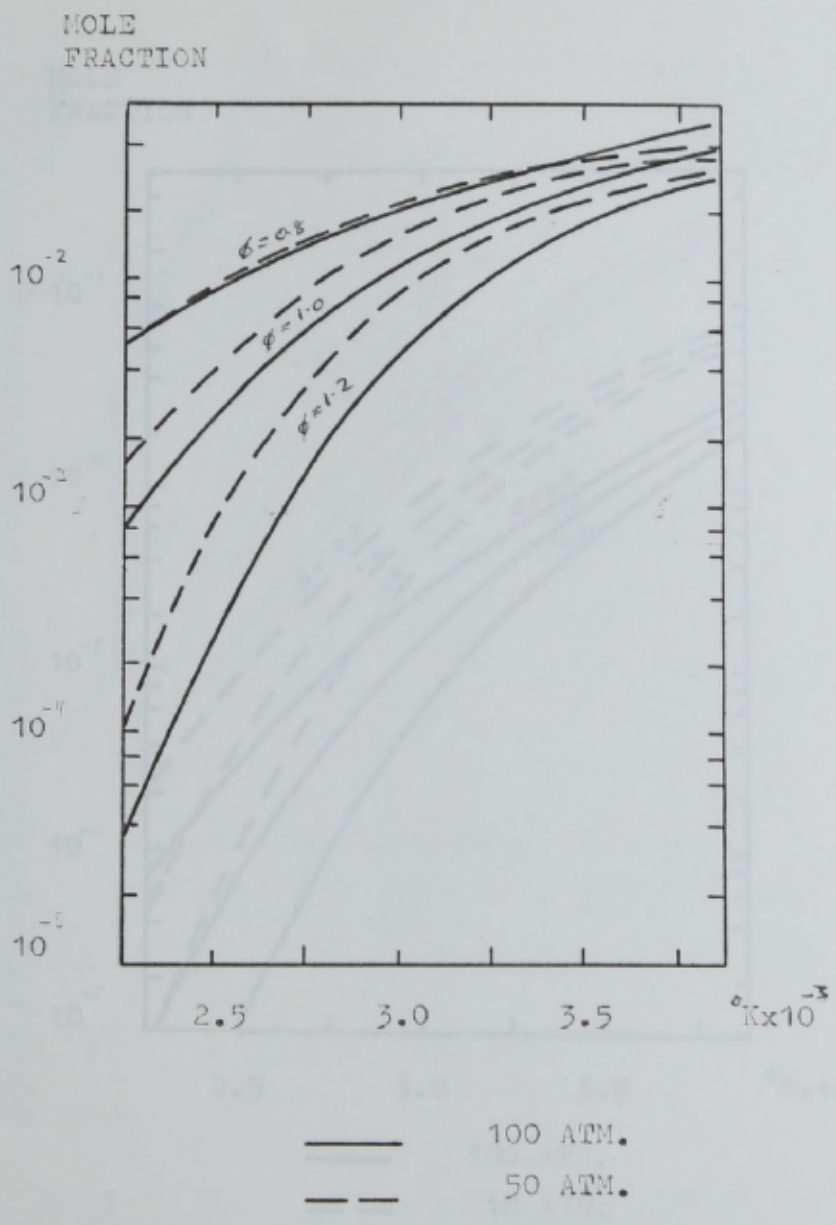

FIGURE A2.11 MOLE FRACTION AGAINST TEMPERATURE AND PRESSURE (NO)

ATOMIC OXYGEN O

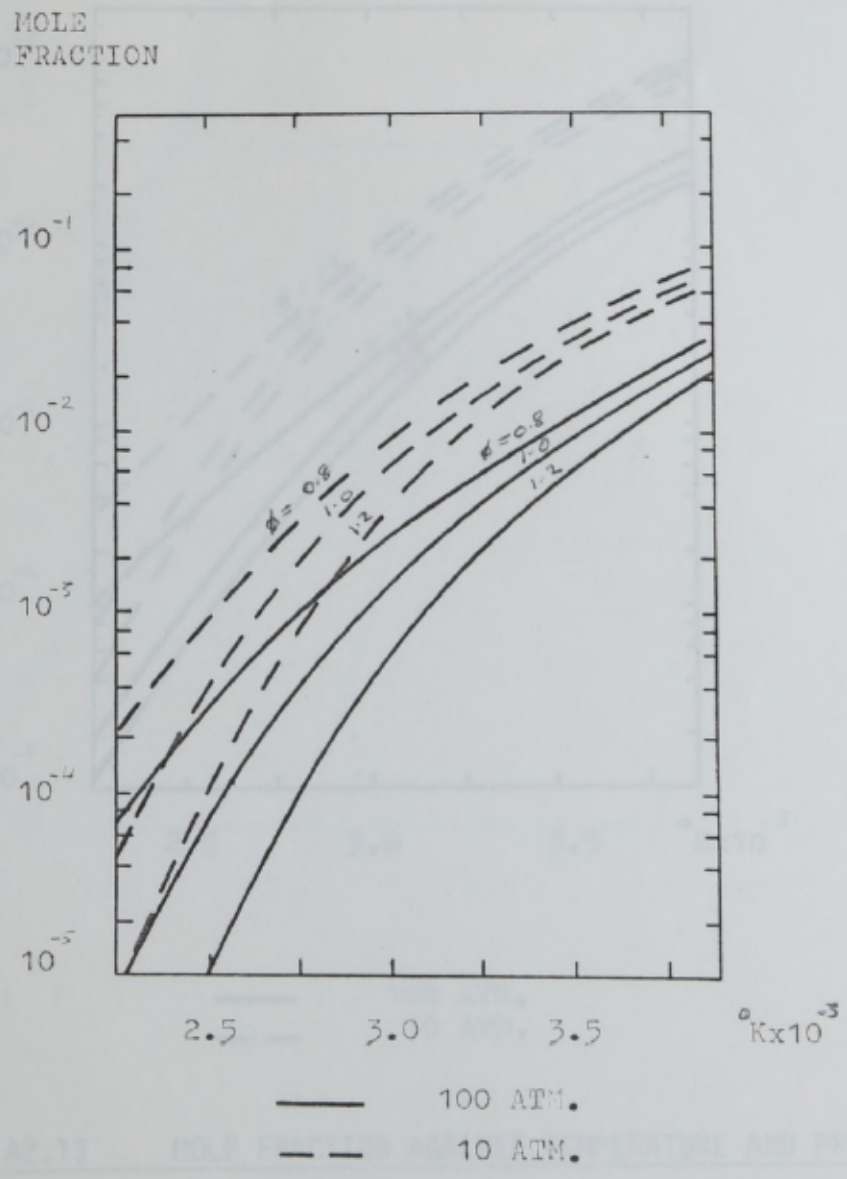

FIGURE A2.12 MOLE FRACTION AGAINST TEMPERATURE AND PRESSURE (O)

ATOMIC HYDROGEN H

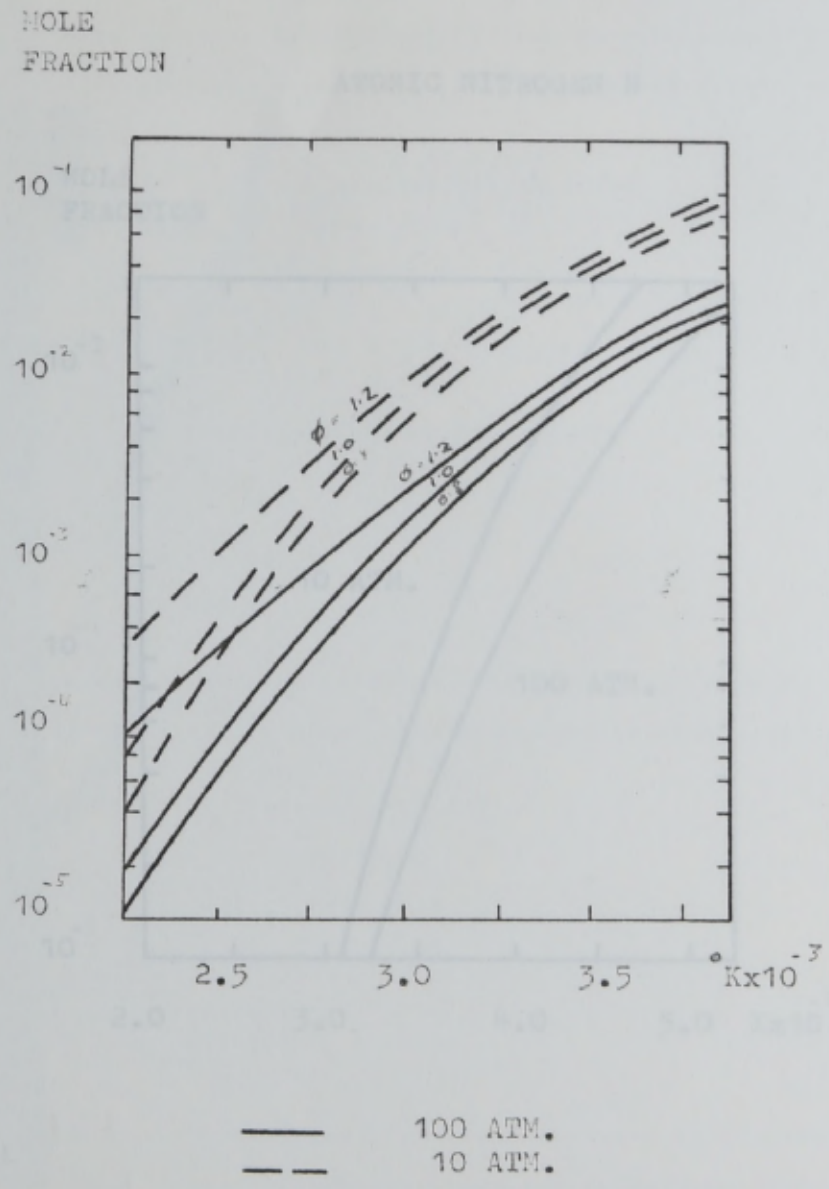

FIGURE A2.13 MOLE FRACTION AGAINST TEMPERATURE AND PRESSURE (H)

ATOMIC NITROGEN N

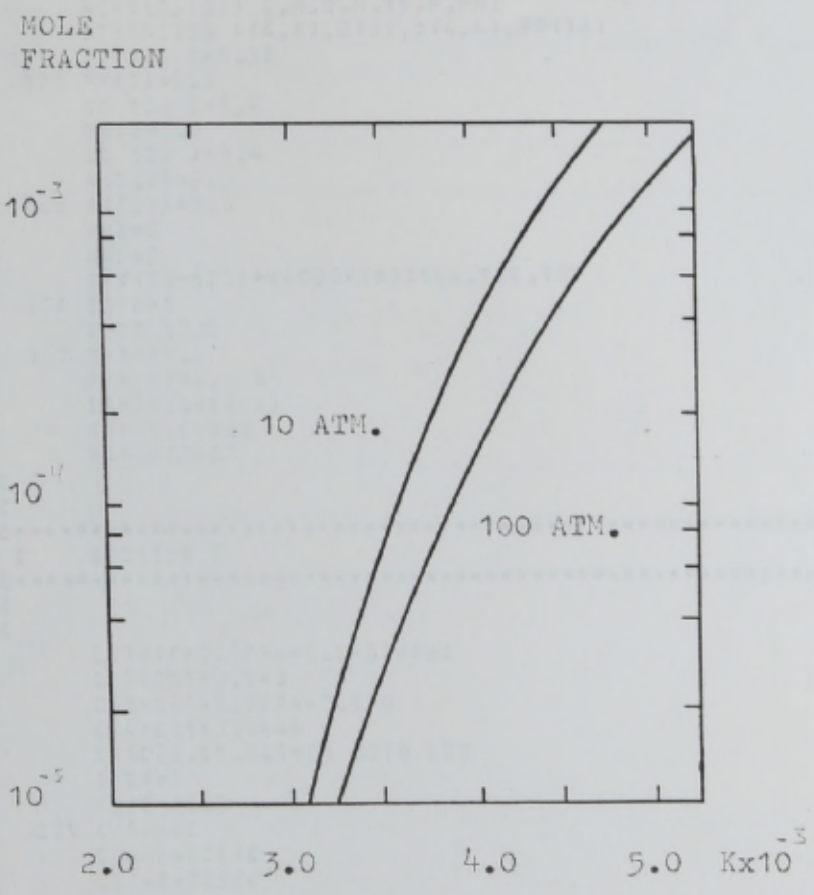

FIGURE A2.14 MOLE FRACTION AGAINST TEMPERATURE AND PRESSURE (N)

Computer program (p.288-298) has been removed for copyright reasons